SECTION A

JOURNAL OF RESEARCH

of the NATIONAL BUREAU OF STANDARDS

JNBAAR 78A(4) 447-554, July-Aug. 1974

U.S. DEPARTMENT OF COMMERCE / National Bureau of Standards

Physics and Chemistry

Journal of Research

of the

National Bureau of Standards

A. Physics and Chemistry

July–August • 1974

VOLUME • 78A

NUMBER • 4

Editor: C. W. Beckett

Associate Editor: D. D. Wagman

Publication dates:
Feb. 1, Apr. 1, June 1, Aug. 1, Oct. 1, Dec. 1, 1974

J. Res. Nat. Bur. Stand. (U.S.), A

JOURNAL OF RESEARCH

The National Bureau of Standards Journal of Research reports research and development in the fields of activity shown at right. Also included from time to time are survey articles on topics closely related to the Bureau's scientific and technical program.

The Journal is published in two separate sections as follows:

A. Physics and Chemistry

Contains papers of interest primarily to scientists working in these fields. Issued six times a year. Annual subscription: domestic, $17.00; foreign, $21.25. Single copy, varies.

B. Mathematical Sciences

Presents studies and compilations designed mainly for the mathematician and the theoretical physicist. Issued quarterly. Annual subscription: domestic, $9.00; foreign, $11.25. Single copy, $2.25.

The National Bureau of Standards[1] was established by an act of Congress March 3, 1901. The Bureau's overall goal is to strengthen and advance the Nation's science and technology and facilitate their effective application for public benefit. To this end, the Bureau conducts research and provides: (1) a basis for the Nation's physical measurement system, (2) scientific and technological services for industry and government, (3) a technical basis for equity in trade, and (4) technical services to promote public safety. The Bureau consists of the Institute for Basic Standards, the Institute for Materials Research, the Institute for Applied Technology, the Institute for Computer Sciences and Technology, and the Office for Information Programs.

THE INSTITUTE FOR BASIC STANDARDS provides the central basis within the United States of a complete and consistent system of physical measurement; coordinates that system with measurement systems of other nations; and furnishes essential services leading to accurate and uniform physical measurements throughout the Nation's scientific community, industry, and commerce. The Institute consists of a Center for Radiation Research, an Office of Measurement Services and the following divisions:

Applied Mathematics — Electricity — Mechanics — Heat — Optical Physics — Nuclear Sciences[2] — Applied Radiation[2] — Quantum Electronics[3] — Electromagnetics[3] — Time and Frequency[3] — Laboratory Astrophysics[3] — Cryogenics[3].

THE INSTITUTE FOR MATERIALS RESEARCH conducts materials research leading to improved methods of measurement, standards, and data on the properties of well-characterized materials needed by industry, commerce, educational institutions, and Government; provides advisory and research services to other Government agencies; and develops, produces, and distributes standard reference materials. The Institute consists of the Office of Standard Reference Materials and the following divisions:

Analytical Chemistry — Polymers — Metallurgy — Inorganic Materials — Reactor Radiation — Physical Chemistry.

THE INSTITUTE FOR APPLIED TECHNOLOGY provides technical services to promote the use of available technology and to facilitate technological innovation in industry and Government; cooperates with public and private organizations leading to the development of technological standards (including mandatory safety standards), codes and methods of test; and provides technical advice and services to Government agencies upon request. The Institute consists of a Center for Building Technology and the following divisions and offices:

Engineering and Product Standards — Weights and Measures — Invention and Innovation — Product Evaluation Technology — Electronic Technology — Technical Analysis — Measurement Engineering — Structures, Materials, and Life Safety[4] — Building Environment[4] — Technical Evaluation and Application[4] — Fire Technology.

THE INSTITUTE FOR COMPUTER SCIENCES AND TECHNOLOGY conducts research and provides technical services designed to aid Government agencies in improving cost effectiveness in the conduct of their programs through the selection, acquisition, and effective utilization of automatic data processing equipment; and serves as the principal focus within the executive branch for the development of Federal standards for automatic data processing equipment, techniques, and computer languages. The Institute consists of the following divisions:

Computer Services — Systems and Software — Computer Systems Engineering — Information Technology.

THE OFFICE FOR INFORMATION PROGRAMS promotes optimum dissemination and accessibility of scientific information generated within NBS and other agencies of the Federal Government; promotes the development of the National Standard Reference Data System and a system of information analysis centers dealing with the broader aspects of the National Measurement System; provides appropriate services to ensure that the NBS staff has optimum accessibility to the scientific information of the world. The Office consists of the following organizational units:

Office of Standard Reference Data — Office of Information Activities — Office of Technical Publications — Library — Office of International Relations.

---

[1] Headquarters and Laboratories at Gaithersburg, Maryland, unless otherwise noted; mailing address Washington, D.C. 20234.
[2] Part of the Center for Radiation Research.
[3] Located at Boulder, Colorado 80302.
[4] Part of the Center for Building Technology.

U.S. DEPARTMENT OF COMMERCE
Frederick B. Dent, Secretary
NATIONAL BUREAU OF STANDARDS
Richard W. Roberts, Director

Order all publications from the Superintendent of Documents
U.S. Government Printing Office, Washington, D.C. 20402

The Secretary of Commerce has determined that the publication of this periodical is necessary in the transaction of the public business required by law of this Department. Use of funds for printing this periodical has been approved by the Director of the Office of Management and Budget through June 30, 1976.

JOURNAL OF RESEARCH of the National Bureau of Standards—A. Physics and Chemistry
Vol. 78A, No. 4, July–August 1974

The Glass Transition Temperature of Monodispersed Polystyrenes and Their Binary Mixtures*

Leo A. Wall*

Institute for Materials Research, National Bureau of Standards, Washington, D.C. 20234

and

Roestamsjah * and Mary H. Aldridge**

The American University, Washington, D.C. 20016

(April 5, 1974)

Glass transition measurements on monodispersed polystyrenes of different molecular weight and their binary mixtures result in the following conclusions: (a) the effect of molecular weight on the glass transitions of monodispersed samples satisfies the Fox and Flory equation written as $T_g = T_{g\infty} - A/M_n$, with constant $A = 0.84 \times 10^{-5}$; (b) polymers of the same number average molecular weight with a broad distribution show lower glass transitions than the monodispersed; (c) the binary mixtures follow the Gordon-Taylor equation derived for copolymers, with constant k (experimental) 0.5.

Key words: Binary mixtures; glass transition temperature; monodispersed polystyrene.

1. Introduction

At the glass transition temperature, T_g, there is a discontinuity in both the thermal expansion coefficient and the heat capacity, which is characteristic of the given material [1]. Glass transition temperatures, therefore, can, in principle, be measured by dilatometry and differential thermal analysis. Extensive studies of the T_g of polystyrenes have been made [2, 3, 4]. The glass transition point is known to increase with molecular weight to a limiting value. For an extensive discussion of theoretical and experimental information on the glassy state, see the review article by Boyer [5].

The polystyrenes used in previous work [2, 3, 4][1] were whole polymers and fractionated samples prepared by free radical polymerization. In this study we have measured the glass transition temperature of anionically prepared monodispersed polystyrenes and their binary mixtures and compared our results with those obtained by the earlier workers [2, 3, 4]. The results of this investigation elucidate to a greater or lesser degree questions relating to the following points:

a. whether the more rapid DTA measurement procedures [6, 7] for T_g give results comparable to the dilatometric method;

b. whether the T_g of anionically prepared polymers differs from that of free radically prepared polymers;

c. whether the T_g of highly monodispersed polymers differs from that of fractions and whole polymers; and

d. the effect of molecular weight distribution.

2. Experimental Procedure

2.1. Glass Transition Temperature Measurement by DTA

The glass transition measurement of the samples was carried out with the Dupont 900 Differential Thermal Analyzer[2] using the standard cell. A 10 mg. sample was placed in the sample macrocell and glass beads were used as the reference. All samples were given the same thermal history, i.e., heating the sample at the rate of 20 °C/min from room temperature to

*Presented before the American Chemical Society 6th Middle Atlantic Regional Meeting, Baltimore, February 3–5, 1971. Based on thesis by Roestamsjah for Master of Science Degree.

**Deceased September 1972.

***National Chemical Institute, Council for Sciences of Indonesia, Bandung, Indonesia. Acknowledges support from the Agency for International Development, and Guest Worker privileges at the National Bureau of Standards.

[1]Figures in brackets indicate the literature references at the end of this paper.

[2]Certain commercial meterials and instruments are identified in this paper in order to adequately specify the experimental procedure. In no case does such identification imply recommendation or endorsement by the National Bureau of Standards, nor does it imply that the material or equipment identified is necessarily the best available for the purpose.

about 30 °C beyond the glass transition; examining the sample at this temperature to determine whether it needed a little pressing to make it compact, and then cooling to 0 °C at the same rate. The cooling was carried out using a constant flow of cold nitrogen gas obtained by boiling liquid nitrogen. During the experiments, a nitrogen flow of one standard cubic foot per hour was used. The heating rate chosen for this experiment was 20 °C/min and each sample was run at least three times. The reported values are the average of those which were obtained by the extrapolation method, i.e., by taking the intersection of the two straight lines drawn through the initial base line and the sloping portion of the thermogram. The reproducibility of T_g using this method is within ±1 °C. Some samples were also run at the rate of 10 °C/min and the glass transition temperature was slightly lower than that obtained at the rate of 20 °C/min (the difference being less than 1 °C). Although the "onset" temperature method of taking the T_g values may be closer to the reported values determined by the dilatometric method, unfortunately, it is much less reproducible.

2.2 Monodispersed Polystyrene Samples

The monodispersed polystyrene samples of different molecular weight were available in the Polymer Chemistry Section of the National Bureau of Standards as a result of recent work on polystyrene degradation [8]. Table 1 shows the molecular weights of the monodispersed samples used in this experiment as determined by different methods and also the glass transition temperatures measured by DTA. Also in column four are the $\bar{M}_n$ values used in the calculations and plots that are presented in the subsequent sections of this article.

2.3. Binary Mixtures of Monodispersed Polystyrene

Each binary mixture of monodispersed polystyrene was prepared by freeze-drying a dilute solution of the the binary mixture at the concentration of 0.1 g/100 cm³ using benzene as a solvent. After freeze-drying for 48 h with the use of an ordinary vacuum pump, the sample was then evacuated under high vacuum using an oil diffusion pump for 48 h at room temperature followed by 2 h heating at the temperature of boiling water. This procedure of taking the benzene out of the sample is sufficient for the purpose of this experiment, since several checks with the pure monodispersed samples show no change in the glass transition temperature measured before and after the freeze-drying.

3. Results

In figure 1, we present for comparison our experimentally measured glass transition temperatures and

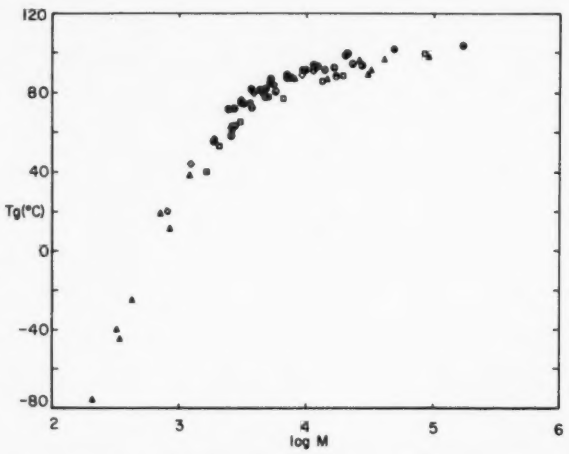

FIGURE 1. *The glass transition temperature of polystyrene as a function of number average molecular weight.*

The experimental results and the data from literature are represented by the following symbols: monodisperse polystyrene=●; binary mixtures of monodisperse (170,000)/(1,900)=◒, (170,000)/(2,450)=◓, (170,000)/(3,700)=◑, (20,000)/(2,450)=◐, (48,500)/(1,900)=⊕, (20,000)/(1,900)=⊖, (11,400)/(1,900)=○; Fox and Flory [2]=□; Ueberreiter and Kanig [3]=△; Schulz, Gunner, and Gerrens [4]=◇.

TABLE 1. *Molecular weight and the glass transition temperature of monodispersed polystyrenes*

$\bar{M}_n$				$\bar{M}_v$ Visc.	$\bar{M}_w$ G.P.C.	T_g(°C) by DTA at 20 °C/min
Chem. anionic	V.P.O.s	Mem.Os.	Value Used in Plots			
.....	1,900	.....	1,900	.....	.....	56.0
2,250	2,450	.....	2,450	.....	.....	72.0
3,900	3,700	.....	3,700	.....	.....	80.8
5,300	5,300	5,200	5,300	5,600	5,400	87.5
10,300	11,400	12,000	11,400	12,500	12,000	94.5
16,800	.....	22,000	20,000	20,000	22,000	99.2
20,800	.....	.....	22,500	22,500	.....	100.0
43,000	.....	49,000	48,500	48,500	50,000	102.0
.....	.....	170,000	170,000	180,000	.....	104.0

Note: V.P.O. = vapor phase osmometer; Mem.Os. = membrane osmometer; Visc. = viscometry; G.P.C. = gel permeation chromatography.

those of earlier investigations, plotted as a function of the logarithm of number average molecular weight. This plot shows in general the way the value for T_g increases with increasing molecular weight to a constant saturation value after which the T_g is independent of molecular weight.

One easily detects small but well defined trends in the results. The monodispersed polystyrenes tend to give values a few degrees higher than those reported earlier [2, 3, 4], while our binary mixtures show values that agree closely with the earlier data [2, 3, 4].

The differences between the T_g's of the monodispersed polystyrenes and those of the earlier workers are more discernible if one considers figure 2, in which the T_g is plotted as a function of the reciprocal number average molecular weight. A straight line can be drawn through the solid points for the monodispersed polystyrenes which differs somewhat from that drawn by previous workers [2]. These lines can be represented by the equation

$$T_g = T_{g\infty} - \frac{A}{\bar{M}_n}, \tag{1}$$

where $T_{g\infty}$ is the saturation value of T_g at higher molecular weight and the slope is A. For the monodispersed polystyrenes, $A = 0.84 \times 10^{-5}$ (see the full line in fig. 2) approximately the same as the value, 1×10^{-5}, found by Fox and Flory. The intercepts show a more definitive difference. Since the mixtures give values more in line with that for the dashed line, this difference is presumptively a result of differences in the molecular weight distributions.

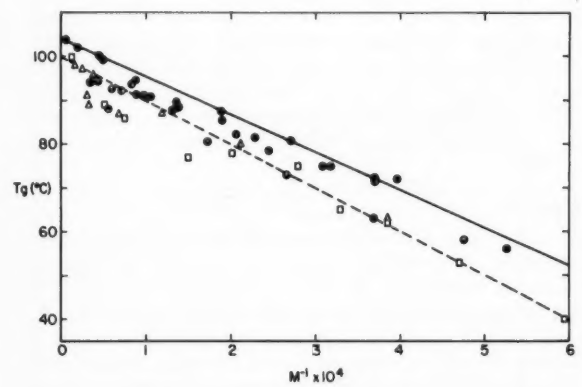

FIGURE 2. *Glass transition temperature as a function of the reciprocal of number average molecular weight.*

The solid line refers to the monodisperse polystyrene and the dashed line is the Fox-Flory line. Same symbols as in figure 1.

Bueche [9] has derived eq 1 using the free volume concept, in which the constant A has the following meaning:

$$A = \frac{2\rho N_{av}\theta}{\Delta\alpha}, \tag{2}$$

where ρ is the density of the polymer, N_{av} is the Avogadro number, 2θ is the excess free volume at T_g contributed by the chain ends, and $\Delta\alpha$ is the difference in the thermal expansion coefficient in the liquid or viscous state and the glassy state ($\Delta\alpha = \alpha_l - \alpha_g$).

The influence of the composition of the binary mixture on the glass transition temperature is shown in figure 3 in which the T_g is plotted as a function of weight percent of Polymer II.

The behavior of the binary mixtures was also examined using the Gordon-Taylor relation [10] derived for copolymers. This equation normally relates the glass transition temperature of homopolymers (T_{g_1} and T_{g_2}) and the weight fraction (w_1 and w_2). It can be expressed in two ways, as proposed by Wood [11]. By choosing $T_{g_1} > T_{g_2}$, the Gordon-Taylor equation may be written as

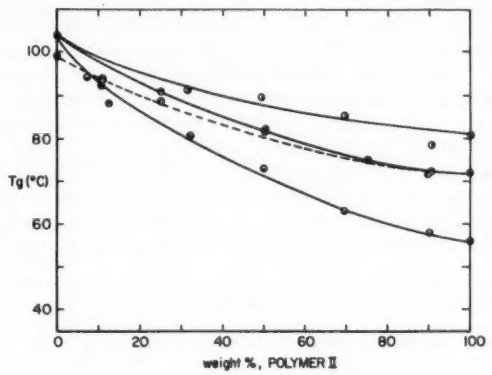

FIGURE 3. *Glass transition temperature of binary mixtures of polystyrenes as a function of composition expressed as weight percent.*

Same symbols as in figure 1.

$$T_g = T_{g_2} + k(T_{g_1} - T_g)\frac{w_1}{1 - w_1}, \tag{3}$$

or as

$$T_g = T_{g_1} - \frac{1}{k}(T_g - T_{g_2})\frac{1 - w_1}{w_1}. \tag{4}$$

It is seen that T_g varies nonlinearly with weight percent.

The constant k is defined by Gordon and Taylor as $k = (\Delta\alpha)_1/(\Delta\alpha)_2 = (\alpha_l - \alpha_g)_1/(\alpha_l - \alpha_g)_2$, where α_l, α_g are the coefficients of thermal expansion of the homopolymer in the liquid and glassy state. On the other hand, Wood [11] regarded k as a characteristic parameter for the particular system and not necessarily related to the individual properties of the particular homopolymers. Furthermore, Wood [11], on the basis of contrary experimental evidence, questioned the two chief assumptions of Gordon and Taylor, that the partial specific volumes were additive and that the thermal expansivities of the homopolymers remained the same in the copolymers as in the homopolymers themselves. In the equation then a formulation of k as a function of the ratio of $\Delta\alpha_1$ to $\Delta\alpha_2$ implies that the mixture behaves as an ideal solution, that is, partial volumes are additive [10] and that the co-

TABLE 2. *The experimental and the predicted values of constant* k *of the Gordon-Taylor expression applied to binary mixtures and mono-dispersed polystyrenes*

$\bar{M}_n(1)/\bar{M}_n(2)$	k (eq 3)	k (eq 4)	k (average)	k (calculated)	
				(eq 5)	(eqs 6 and 7)
(170,000)/(1,900)	0.51	0.57	0.53	0.87	0.94
(170,000)/(2,450)	.53	.57	.55	.91	.96
(20,000)/(2,450)	.58	.49	.53	.92	.96

efficients of expansion for the two components are also assumed to be the same in the mixture as in the homopolymers and are not functions of temperature.

Our experimental T_g's for mixtures (see legend fig. 1) gave quite linear fits to plots suggested by eqs (3) and (4), in which T_g is plotted against $(T_{g1}-T_g)w/(1-w_1)$ or against $(T_g-T_{g2})(1-w_2)/w_2$, respectively. However, the values of T_g for the monodispersed samples, determined from the intercepts, were several degrees lower than the values determined experimentally. A similar observation was reported [14] in a study of a system composed of compatible mixtures of poly-ϵ-caprolactone and polyvinyl chloride.

The values obtained for k from the above-mentioned plots are shown in table 2, together with the values calculated using eq (5), a general equation, derived by Simha and Boyer [12] and from eqs (6) and (7). [13]

$$\Delta\alpha \cdot T_g = \text{constant} = 0.113 \tag{5}$$

$$\alpha_g = 1.84 \times 10^{-4} + 224 \times 10^{-4}/\bar{M}_n \tag{6}$$

$$\alpha_l = 5.5 \times 10^{-4} + 643 \times 10^{-4}/\bar{M}_n. \tag{7}$$

Equations (6) and (7), experimentally determined equations, give the thermal expansion coefficients of the glassy and liquid polystyrenes as a function of number average molecular weight. The numerical constants are from references 5 (eq (6)) and 13 (eq (7)).

As can be seen in table 2, the predicted values of k are always greater than the experimental values. This indicates a failure of Gordon-Taylor additivity assumptions. For copolymers, Wood has pointed out similar results which indicate a deviation from the assumptions in the derivations.

4. Discussion

By assuming only that both mono- and polydisperse polystyrenes obey exactly eq (1), we can derive the Gordon-Taylor (GT) equation with $k = 1$ in the form:

$$T_g = T_{g_1} + w_2 (T_{g_2} - T_{g_1}). \tag{8}$$

Since the data on the binary mixtures shown in figure 2 and in figure 3 deviate from eq (1) in figure 2 and from eq (8) in figure 3, it is evident that while eq (1) may apply to the monodispersed samples, it fails or is only approximate for polydispersed mixtures. The values of the constants, $T_{g\infty}$ and A, in eq (1) are, of course, different for the polydispersed system and with the different values of the constants it follows that a somewhat different eq (1) applies to the polydispersed polymers.

In figure 4 we present again the experimental points for the binary mixture $\bar{M}_{n_1}$ (170,000)/$\bar{M}_{n_2}$ (1,900). It is seen that the points agree with minor scatter to the Gordon-Taylor relation with $k = 0.45$ and not when $k = 1.0$ or 0.9. Here the value of $k = 0.45$ was chosen on the best fit to the points in the mid composition range and is not based on plots suggested by eqs (3) and (4) that produced the values shown in table 2 and that failed to extrapolate to the exact value of the T_g for the monodispersed polymers.

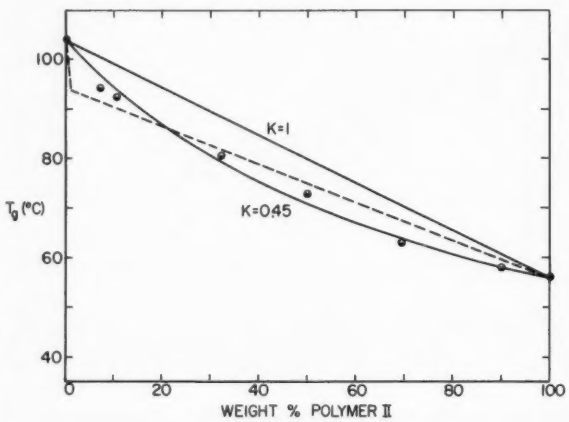

FIGURE 4. *Glass transition temperature of a binary mixture of monodisperse polystyrenes as a function of composition expressed as weight percent.*

The number average molecular weights of the two polymers are 170,000 and 1,900. Full lines Gordon-Taylor relation with $k = 1$ and 0.45. Dashed line entropy of mixing theoretical form.

One possible explanation of the observed data is on the basis of the entropy of mixing and the Gibbs-DiMarzio theory [15]. The entropy of mixing would operate to lower the glass transition and a maximum effect would occur at the composition of 0.5 mol or number fraction, which would correspond for the experimental system in figure 4 of 0.0111 weight fraction of polymer II (w_2). The dashed line then is the entropy of mixing effect normalized to the experimental points. It is seen that, while there may be some tendency towards the behavior of the dashed curve, the experi-

mental points are better fitted by the GT equation ($k = 0.45$). Theoretical calculation of the effect of the entropy of mixing involves knowledge of the exact number and distribution of the components in both substances mixed. A simple two-component mixing gives an entropy increase of 2 ln 0.5 = 1.4 cal/mol degree, in this case, mole of monomer units. This gives an estimated depression of the glass temperature of 0.32 °C at $w_2 = 0.0111$. Other entropic mixing effects may produce one or so degrees depression but it appears that the observed data are not readily accounted for in this way.

The relatively good fit to the GT eq ($k = 0.45$) suggests that an effect characteristic of the binary system is operating. At the moment several possible explanations of the observed results remain unexplored: a kinetic one, the observed T_g may approach more closely the Gibbs-DiMarzio T_2 [15] for a mixture than for a monodispersed material, or a thermodynamic one where a somewhat greater degree of order exists in the monodispersed polymers so that mixing produces a much greater increase in entropy. It should be added that Boyer's recent alternative treatment [16] likewise gives a satisfactory fit to the data.

5. Summary

Monodispersed polystyrene prepared anionically gives measurably higher glass transitions than fractionated or whole polymers prepared by free radical techniques. These monodispersed polystyrene data give an excellent correlation to the equation

$$T_g = T_{g\infty} - (8.4 \times 10^{-6})/\bar{M}_n.$$

Since mixtures of the monodispersed polymers also show lower values, the above difference is evidently an effect of distribution, that is, in binary mixtures low moleculas weight has a small plasticizing action on high molecular polymers of the same basic structure. Binary mixtures of low and high molecular weight monodispersed polystyrenes follow a Gordon-Taylor type relation having $k \cong 0.5$ which is lower than the value 0.9 estimated from either the Simha-Boyer equation or the Fox-Loshaek equation.

High and low molecular weight binary mixtures show T_g values which are smooth but nonlinear functions of the weight fraction. Their T_g's do not have the same proportionality with $1/\bar{M}_n$ as the monodispersed polystyrenes. Entropy of mixing does not appear to account for the lower T_g's of the binary mixtures.

The authors wish to express their appreciation to E. DiMarzio, L. A. Wood, R. Boyer, and R. Simha for helpful and enjoyable discussions of the glassy state, and to L. J. Fetters for certain osmotic and GPC molecular weight measurements.

6. References

[1] Kauzman, W., Chem. Rev. **43**, 219 (1948).
[2] Fox, T. G., and P. J. Flory, J. Polymer Sci. **14**, 315 (1954).
[3] Ueberreiter, K., and G. Kanig, J. Colloid Sci. **7**, 569 (1952).
[4] Schulz, G. V., K. von Gunner, and H. Gerrens, Z. Phys. Chem., N. F. **4**, 192 (1955).
[5] Boyer, R. F., Rubber Chem. and Technol. **36**, 1303 (1963).
[6] Keavney, J. J., and E. C. Eberlin, J. Appl. Polymer Sci. **7**, 47 (1960).
[7] David, D. J., in Techniques and Methods of Polymer Evaluation, Eds. P. E. Slade, Jr., and L. T. Jenkins, (Marcel Dekker, Inc., N.Y., Vol. I, 1966), p. 43.
[8] Wall, L. A., S. Straus, and L. J. Fetters, Polymer Preprints **10**, 1473 (1969).
[9] Bueche, F., Physical Properties of Polymers (Interscience, N.Y., 1962).
[10] Gordon, M., and J. S. Taylor, J. Appl. Chem. **2**, 493 (1952).
[11] Wood, L. A., J. Polymer Sci. **28**, 319 (1958).
[12] Simha, R., and R. F. Boyer, J. Chem. Phys. **37**, 1003 (1962).
[13] Fox, T. G., and S. Loshaek, J. Polymer Sci. **15**, 371 (1955).
[14] Koleske, J. V., and R. D. Lundberg, J. Polymer Sci. **A2**, 7, 795 (1969).
[15] Gibbs, J. H., and E. A. DiMarzio, J. Chem. Phys. **28**, 373 (1958).
[16] Boyer, R. F., Macromolecules **7**, 142 (1974).

(Paper 78A4–824)

JOURNAL OF RESEARCH of the National Bureau of Standards—A. Physics and Chemistry
Vol. 78A, No. 4, July–August 1974

A Method of Measuring the Solubilities of Hydrocarbons in Aqueous Solutions*

Robert L. Brown and Stanley P. Wasik

Institute for Materials Research, National Bureau of Standards, Washington, DC 20234

(December 7, 1973)

An apparatus is described which measures the equilibrium distribution of a hydrocarbon between a gas phase and a liquid water phase. The method involves a multiple equilibration procedure which requires the analysis of only the gas phase. Gas-liquid chromatography was used for the hydrocarbon analysis because of its high sensitivity and selectivity. Supplemented by vapor pressure data, the observed distribution can be used to calculate the solubility of the hydrocarbon in the liquid phase. This was done for benzene, toluene, and ethylbenzene in distilled water over the temperature range 5 to 20 °C and in an artificial seawater over the temperature range 0 to 20 °C. The various factors affecting the accuracy of the results are discussed in detail.

Key words: Aqueous solutions; benzene solubility; hydrocarbons; partition coefficients; seawater.

1. Introduction

A knowledge of the equilibrium properties of aqueous hydrocarbon solutions is valuable in several fields. In water pollution control such information is helpful in devising abatement processes [1],[1] in modeling natural water systems [2], in designing toxicity experiments, and in developing analytical techniques. In petroleum research it is useful for understanding how hydrocarbons migrate and accumulate to form oil fields [3]. In biology a knowledge of how hydrocarbons behave in water is important for understanding the effects of hydration on the configuration of biopolymers [4]. And in chemistry, experimental data on these solutions are needed for testing models of water and aqueous solutions [5].

These aqueous solutions can be characterized by determining the concentration of a particular hydrocarbon in both the solution and in the vapor above the solution. The ratio of its concentration in the two phases is an equilibrium constant called the partition coefficient. The solubility of a hydrocarbon is the maximum concentration it can have at equilibrium in the solvent at a given temperature and can be determined from the values of the partition coefficient and the vapor pressure of the pure liquid hydrocarbon at that temperature.

Although there have been many measurements of hydrocarbon solubilities in water, most have been done at only one temperature. Furthermore, there have been very few measurements on hydrocarbons in seawater. Because of the increasing need for information about these systems we have undertaken a program of measuring partition coefficients and their temperature dependence for a variety of hydrocarbons in aqueous solution. Our method involves a procedure which requires analysis of only the vapor phase. The analytical technique used is called headspace gas analysis [6]. This is widely used for determining the volatile constituents of biological fluids. We used gas-liquid chromatography for the hydrocarbon analysis because of its high sensitivity and selectivity for these compounds. The hydrocarbons are introduced into the apparatus as vapors to avoid the danger of emulsion formation [7], which arises when liquid hydrocarbons are mixed with water. In this report we describe the apparatus and discuss the various factors affecting the precision and accuracy of the partition coefficients.

The apparatus in its present configuration is best suited for measuring partition coefficients whose values lie in the range 1 to 10. The partition coefficients of many aromatic hydrocarbons fall in this range. Our method has a number of advantages over the spectrophotometric techniques that have been widely employed in the past for solubility measurements on these compounds. Because of the selectivity of the chromatographic analysis, compound purity is not a critical factor. This selectivity also means that several compounds can be studied at the same time. To accomplish this, high sensitivity is also necessary. A hydrogen flame detector was used and its high sensitivity for hydrocarbons made it possible to work at low concentrations where interactions between compounds are negligible. The spectrophotometric method is limited to compounds having high solubilities or large absorption coefficients. On the other hand, the high

* This work was supported by the Office of Marine Technology, Maritime Administration.
[1] Figures in brackets indicate the literature references at the end of this paper.

sensitivity of the flame detector allows one to study a much larger number of compounds. Furthermore, absolute calibration of the detector is not necessary. Only its linearity need be established and the apparatus itself can be used to do this.

To test the method, we measured the solubilities of benzene, toluene, and ethylbenzene in distilled water. These compounds have been examined extensively by several investigators using ultraviolet absorption spectroscopy to measure the hydrocarbon concentration in the liquid phase. Because of their relatively high solubilities and toxicity to marine organisms [8], these hydrocarbons may be significant factors in the oil spill problem. For this reason we also used this apparatus to measure their solubilities in seawater. Partition coefficients for the compounds in distilled water were measured over the temperature range 5 to 20 °C. The partition coefficients in an artificial seawater were measured over the temperature range 0 to 20 °C. Solubilities were then determined from the partition coefficients and vapor pressure data.

2. Description of the Apparatus and Experiments

2.1. Principle of the Experimental Methods Used

In this section we give a simplified analysis of the experimental procedures. A detailed analysis of how the partition coefficients were evaluated from the observed relative hydrocarbon concentrations is given in the Appendix.

1. Determination of Absolute Partition Coefficients

The equilibrium distribution of a solute between two phases can be determined by measuring its relative concentration in only one phase [9]. Consider a system composed of (1) a gas phase and (2) a liquid phase, having volumes V_1 and V_2, into which we introduce some hydrocarbon solute molecules. (Our particular system contains a gas phase consisting of helium with a little water and hydrocarbon vapor, and a liquid phase consisting of distilled water or seawater and a small amount of dissolved helium and hydrocarbon.) Let the equilibrium concentrations of the hydrocarbon solute in the gaseous and liquid phases be C_1 and C_2, respectively, and let the partition coefficient K be defined as the ratio C_2/C_1. We assume that the solute concentration is sufficiently low in each phase so that there will be no interactions between solute molecules; i.e., K will not depend on C_1 and C_2. The total number of moles N of solute in the system at equilibrium is $C_1(V_1+KV_2)$. Suppose we now remove a fraction α of the solute molecules from the gas phase and allow the system to equilibrate again. (In our system, the hydrocarbon molecules are removed simply by discarding a known portion of the gas phase and replacing it with pure helium.) Let C_1' be the gas phase concentration of the solute at equilibrium after the extraction of αC_1V_1 moles of solute. The total number of moles of solute in the system is now

$$N'=C_1'(V_1+KV_2)=N-\alpha C_1V_1=C_1[(1-\alpha)V_1+KV_2]. \tag{1}$$

We define the extraction factor F by

$$F\equiv C_1'/C_1 \tag{2}$$

From eq (1), we see that the gas phase concentration ratio F is related to K by the expression

$$K=(V_1/V_2)(F+\alpha-1)(1-F)^{-1}. \tag{3}$$

Using this procedure, one can determine K from a knowledge of the volumes of the phases and the observed relative solute concentrations in one phase. We shall refer to this procedure as an extraction experiment.

b. Partition Coefficients at Different Temperatures

The temperature dependence of the partition coefficients can be determined by doing extraction experiments at different temperatures. It is possible, however, without removing any of the hydrocarbon from the system, to obtain the partition coefficient at various temperatures in terms of its value at some reference temperature T_R. This can be done simply by measuring the relative hydrocarbon concentration in the gas phase as the temperature of the system is changed. Consider the system described in the preceding paragraph. Suppose the total number of moles of solute in the system at equilibrium is $N=C_1(V_1+KV_2)$. As the temperature of the liquid phase changes, N remains constant, and the volumes V_1 and V_2 also remain approximately constant. Let K and K_R be the values of the partition coefficient, and C_1 and C_{1R} be the corresponding solute concentrations in the gas phase at the liquid phase temperatures T and T_R, respectively. Also, we define a concentration ratio G,

$$G\equiv C_1/C_{1R}. \tag{4}$$

Then K can be expressed in terms of G and K_R;

$$K=(V_1/V_2)(1-G)G^{-1}+K_R/G. \tag{5}$$

This procedure will be referred to as a *nonextraction* experiment.

2.2. Apparatus

A schematic diagram of our apparatus is shown in figure 1. It consists of two major parts:

(1) A glass equilibration cell of volume V_0 (≈ 75 cm^3), which contains a volume V_1 (≈ 45 cm^3) of the aqueous solution. It also contains a small amount of the gas phase of volume $V_a=V_0-V_L$.

(2) A gas container of volume V_p (≈ 160 cm^3), also made of glass. The gas in this container is that portion of the gas phase which is removed and replaced with pure helium during an experiment.

These two containers are connected by a system of

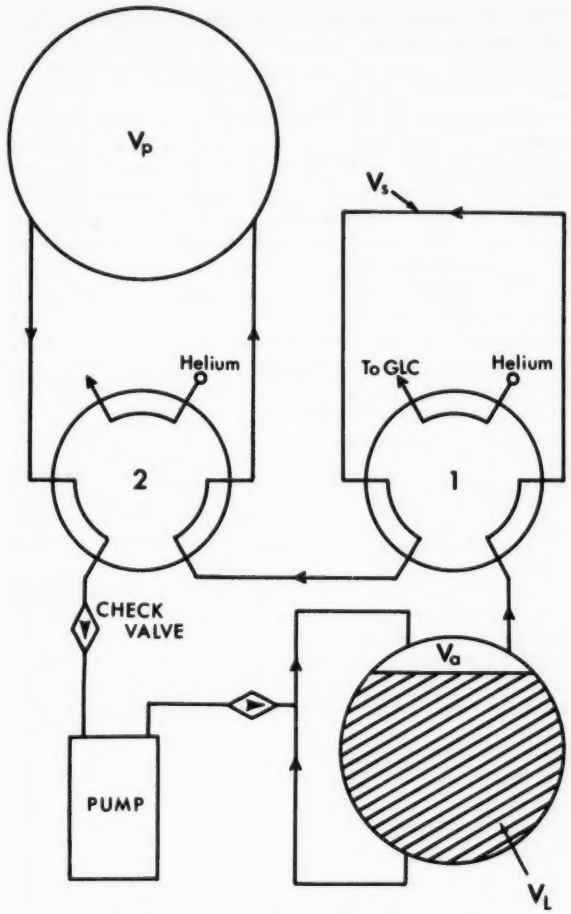

FIGURE 1. *Schematic diagram of the apparatus.*

The total volume of the present apparatus is about 265 cm³; $V_p \approx 160$ cm³ and $V_L \approx 45$ cm³. The remaining volume is about 60 cm³; this arises almost entirely from the volume of gas in the equilibration cell and from the volume in the pump.

stainless-steel tubing through which helium carrier gas circulates. The volume of the connecting tubing is considerably smaller than the combined volume of the equilibration cell and the gas volume V_p.

Helium carrier gas is continuously pumped from the gas container containing volume V_p, through the equilibration cell, and then returned to V_p. The pump is a metal bellows having a displacement of 2 cm³ and was built by the NBS shops. It runs at about 100 strokes per minute. The helium enters the equilibration cell through a liquid-filled side-arm. It enters the side-arm below the surface of the liquid, and as it rises, moves liquid from the cell up the side-arm and back into the cell. In the cell, a liquid surface area of approximately 40 cm² is exposed to the gas phase. At the pumping rates used, a liquid volume equal to the total volume of liquid in the cell circulates through the side-arm every 1.5 min. This arrangement has the advantage that a single pump circulates both gas and liquid.

After leaving the equilibration cell, the helium passes through the first of two 6-port gas sampling valves. By switching this valve, a small sample ($V_s \approx 0.25$ cm³) of the hydrocarbon-containing carrier gas can be sent to the chromatograph for analysis without interrupting the circulation. The carrier then passes to the second valve and through V_p. Switching this second valve allows the gas in V_p to be purged and replaced with pure helium at atmospheric pressure. From V_p the gas returns to the pump. It completes one circuit through the apparatus in slightly less than a minute.

Before assembly, the metal portions of the apparatus were cleaned with trichloroethylene; the glass parts were washed with 10 percent by weight aqueous HF and rinsed several times with distilled water.

The equilibration cell is contained in a water bath whose temperature is controlled to within 0.01 °C. The rest of the system is enclosed by an air bath held at 100 ± 0.05 °C.

The chromatographic column was a 1/8-in by 6-ft piece of stainless-steel tubing packed with 10 percent w/w silicone gum rubber (methyl vinyl) on Chromosorb W–AW–DMCS 80–100 mesh, kept at 100 °C. Peak areas were measured with an electronic integrator.

The helium used for the carrier gas had a purity of 99.999 volume percent. The benzene, toluene, and ethylbenzene were of 99.99 mole percent purity. Distilled water from the laboratory supply was used without any purification except prolonged extraction with the helium carrier. The sea water was artificial. It was prepared according to a recipe given by Sverdrup et al. [10], and had a chlorinity value of 19.00‰. (The chlorinity is the total amount of chlorine, bromine, and iodine in grams contained in 1 kg of seawater assuming that the bromine and the iodine have been replaced by chlorine. [10])

2.3. Experimental Procedures

To begin a determination of the absolute partition coefficients by the extraction procedure, the entire apparatus including the liquid was first purged with helium. Then, a gaseous mixture containing benzene, toluene, and ethylbenzene was introduced into the apparatus. This was done by putting value number two (see fig. 1) in the purge position and replacing the pure helium in V_p with helium which had passed through a saturator containing a mixture of liquid hydrocarbons. This valve was then switched back to the position shown in figure 1, and the gas mixture was circulated through the apparatus and allowed to equilibrate for at least 1/2 h with the liquid phase. The pressures of the hydrocarbons initially in V_p were adjusted so that their pressures in the circulating carrier gas were always considerably below their vapor pressures at the temperature of the equilibration cell. Periodic measurements of the relative hydrocarbon concentrations in the circulating carrier showed no further change 10 min after their introduction. The equilibration time was thus quite short. After the first equilibration, the hydrocarbon molecules in V_p were removed by switching V_p out of the circulating part of the

apparatus and purging it with pure helium. V_p was then switched back to the circulating part of the apparatus and the gas in it was allowed to equilibrate a second time with the liquid phase.

An extraction experiment was normally followed by the nonextraction procedure. This was done by varying the temperature of the equilibration cell while measuring the gas phase solute concentrations. After each temperature change, 45 min was allowed for the phases to equilibrate.

3. Results

We have described two types of experiments:

(1) The extraction procedure utilizes the concentration ratio F. This is the ratio of the equilibrium gas phase concentration of a particular hydrocarbon before and after extraction of a known fraction of the gas phase. The absolute value of the partition coefficient K is obtained from F through use of eq (3). (This is analogous to eq (A2) in the appendix.) These K values become the reference values K_R for use in the nonextraction procedure.

(2) The nonextraction procedure utilizes the concentration ratio G and combines this with a reference K_R determined from an extraction experiment. The quantity G is the ratio of the observed gas phase concentration of a particular hydrocarbon at the temperature at which K_R was determined, to its concentration observed at some other temperature. In this procedure, no gas is removed from the apparatus. Absolute K values are determined from K_R and G through use of eq (5) (eq (A3), appendix).

Our observed values of the partition coefficients of benzene, toluene, and ethylbenzene in distilled water water are given in table 1. Absolute values were determined from extraction experiments performed at two temperatures, 11.75 and 20.06 °C. The values shown are averages of several determinations at each temperature. Partition coefficients at the other temperatures listed in the table were obtained from nonextraction experiments. For each compound, the value at 7.06 °C was determined using the average value of K at 11.75 °C as the reference partition coefficient K_R. The values at the remaining temperatures were determined using the average value of K at 20.06 °C as the reference partition coefficient.

Next to each K value listed in table 1, there are two numbers in parentheses. The first is the standard deviation of the K values determined from the nonextraction experiments. It reflects the dispersion observed in the concentration ratios G. It gives an estimate of the dispersion encountered in determining K values *relative* to the appropriate reference values K_R. The second number in parentheses is the standard deviation for the absolute K values. For K values determined by the extraction procedure it is simply the observed standard deviation of the K values determined from the ratio F through use of eq (3) (eq (A2)). It reflects the dispersion in the ratio F. The standard deviation for the absolute K values determined from the nonextraction experiments and the K_R values was calculated by combining the observed standard deviations of G and K_R through the use of eq (5) (eq (A3)). Formulas for the calculation of error propogation were obtained from reference [11].

The main cause of the dispersion in the K values arises from the dispersion in the relative concentration measurements. This, in turn, arises for the most part from the variation in sample size caused by the pressure pulsations in the sample loop V_s produced by the action of the pump. Separate experiments were conducted to estimate the dispersion involved in making the relative concentration measurements. Let us define an observation as one measurement of the relative concentration of one particular component in one sample of volume V_s of the circulating gas. Repeated observations are considered to correspond to repeated injections of samples of the circulating gas into the chromatograph under the same experimental conditions. (A small portion of the gas, $\approx 0.1\%$, is removed from the apparatus each time a sample is taken, and the observations are corrected for this.) A group of 60 observations of relative benzene concentrations was found to have a coefficient of variation of 0.75 percent. For gas samples taken at constant pressure,

TABLE 1. *Averaged values of determined partition coefficients of benzene, toluene, and ethylbenzene in distilled water*

Temp. (°C)	Number of observations	Partition coefficients K						Predicted deviations standard	
		Benzene		Toluene		Ethylbenzene			
4.50	3	12.33(0.14) [a]	(0.24) [b]	12.92(0.13) [a]	(0.23) [b]	12.31(0.12) [a]	(0.23) [b]	(0.13) [a]	(0.22) [b]
6.33	3	11.10(0.04)	(0.18)	11.42(0.04)	(0.18)	10.70(0.04)	(0.18)	(0.12)	(0.20)
7.06	3	10.45(0.11)	(0.19)	10.68(0.10)	(0.18)	9.91(0.08)	(0.17)	(0.12)	(0.32)
8.96	3	9.52(0.11)	(0.19)	9.61(0.11)	(0.19)	8.82(0.09)	(0.18)	(0.11)	(0.18)
11.75 [c]	6	8.17(0.00)	(0.10)	8.05(0.00)	(0.10)	7.20(0.00)	(0.09)	(0.00)	(0.19)
12.10	3	8.03(0.07)	(0.16)	7.92(0.07)	(0.16)	7.11(0.06)	(0.15)	(0.10)	(0.16)
15.10	3	6.91(0.09)	(0.16)	6.68(0.09)	(0.16)	5.85(0.08)	(0.15)	(0.09)	(0.15)
17.93	3	6.18(0.04)	(0.12)	5.85(0.04)	(0.12)	5.04(0.04)	(0.12)	(0.08)	(0.13)
20.06 [c]	4	5.51(0.00)	(0.11)	5.14(0.00)	(0.11)	4.36(0.00)	(0.12)	(0.00)	(0.10)

[a] This number is the standard deviation of the K values determined from the nonextraction experiments. It is an estimate of the dispersion found in determining K values relative to the appropriate reference values K_R.

[b] This number is the standard deviation for the absolute K values.

[c] The value of K determined at this temperature was used as the reference value K_R.

[d] From propogation of error formula (p. 459 in text).

TABLE 2. *Averaged values of determined partition coefficients of benzene, toluene, and ethylbenzene in artificial seawater*

Temp.	Number of observations	Partition coefficients K						Predicted standard deviations	
		Benzene		Toluene		Ethylbenzene			
0.19	3	12.17(0.18)[a]	(0.25)[b]	12.58(0.18)[a]	(0.25)[b]	12.12(0.17)[a]	(0.24)[b]	(0.11)[a]	(0.16)[b]
5.32	3	8.96(0.08)	(0.16)	8.88(0.07)	(0.15)	8.16(0.06)	(0.15)	(0.10)	(0.14)
10.05	3	6.91(0.12)	(0.17)	6.59(0.12)	(0.17)	5.83(0.11)	(0.16)	(0.09)	(0.12)
14.96	3	5.35(0.06)	(0.11)	4.92(0.06)	(0.11)	4.19(0.06)	(0.11)	(0.07)	(0.10)
20.04[c]	3	4.18(0.00)	(0.11)	3.70(0.00)	(0.10)	3.05(0.00)	(0.10)	(0.00)	(0.07)

[a] This number is the standard deviation of the K values determined from the nonextraction experiments. It is an estimate of the dispersion found in determining K values relative to the appropriate reference values K_R.
[b] This number is the standard deviation for the absolute K values.
[c] The value of K determined at this temperature was used as the reference value K_R.

on the other hand, the coefficient of variation was only 0.15 percent. This represents the reproducibility of the detection system.

With 0.75 percent as the coefficient of variation for relative concentration measurements, it was possible to calculate the dispersions to be expected in determining F and G, and, through eqs (3) and (5) (eqs (A2) and (A3)), in the derived K values. The standard deviation determined for K in this fashion is shown in the last column in table 1. As before, the first number in parenthesis is the standard deviation of the K values relative to the reference K values K_R at 11.75 and 20.06 °C. The agreement of these calculated standard deviations with those determined from the measurements shown in the table is satisfactory.

We believe that the standard deviations shown in table 1 give a good estimate of the uncertainty in the absolute K values. As mentioned earlier, essentially all of the error in these experiments arises from the concentration measurements. The errors involved in measuring the other parameters—(pressures, volumes, and temperatures)—in eqs (A2) and (A3) are negligible by comparison.

With regard to systematic errors, our major concern is that a significant fraction of the hydrocarbon could be adsorbed on the surface of the apparatus rather than in the gas phase. To check for such effects, the extraction factor for the dry apparatus was examined for a mixture of benzene, toluene, and ethylbenzene and found to be the same for all the compounds and also equal to the calculated value. In another experiment with the dry apparatus, the surface-to-volume ratio of the volume V_p was increased by a factor of four. The compounds again exhibited the calculated extraction factor. These experiments indicated that surface adsorption was a negligible factor in these measurements.

Lack of detector linearity would consitute another source of systematic error. The apparatus itself can be used to check the response of the detector. If there is no liquid water in the apparatus, each time the gas in V_p is removed and replaced with pure helium, a constant, known fraction of the hydrocarbon is removed from the apparbtus. The linearity of the detector for benzene, toluene, and ethylbenzene was confirmed over a 100-fold concentration range by repeatedly extracting the gas in V_p. Two such experiments done at different air bath temperatures gave values of F that were within 0.4 percent of the value calculated for the dry system.

Our results for the partition coefficients of benzene, toluene, and ethylbenzene in the artificial sea water are shown in table 2. Absolute values were determined from extraction experiments at 20.06 °C. The values at the other temperatures were determined from nonextraction experiments using the average value of

TABLE 3. *Solubility of benzene in distilled water*

Temp. (°C)	Solubility S(wt. percent)		Ref. [14]
	Present work	Ref. [13]	
4.5	0.184(0.0033)[a]	0.172(0.0024)[a]	
4.9		.177(0.0034)	
5.0		.174(0.0024)	
5.2			0.181.
6.3	.185(0.0033)		
6.7		.174(0.0019)	
7.1	.181(0.0055)		
9.0	.181(0.0034)	.173(0.0031)	
10.0			.180(0.0006).
11.8	.177(0.0041)		
12.1	.177(0.0035)		
12.5		.172(0.0002)	
14.9			.177(0.0016).
15.0		.173(0.0026)	
15.1	.179(0.0038)		
17.9	.179(0.0038)		
20.0		.171(0.0021)	
20.1	.176(0.0032)		
20.6		.172(0.0020)	
21.0			.179.
24.8		.171(0.0034)	
24.9		.174(0.0024)	
25.6			.179(0.0002).

Other values

9.8	0.176 Ref. [15].
10.0	.175 Ref. [16].
15.0	.150 Ref. [17].
17.0	.171(0.0008) Ref. [18].
20.0	.139 Ref. [19].
24.0	.172(0.0008) Ref. [18].
25.0	.140 Ref. [20]; 0.178 Ref. [15]; 0.180 Ref. [19]; 0.186 Ref. [16]; 0.172(0.001) Ref. [21]; 0.189 Ref. [22]; 0.178(0.0045) Ref. [23]; 0.176 (0.03) Ref. [24]; 0.174 Ref. [25].

[a] The numbers in parentheses are standard deviations.

K at 20.06 °C as the reference partition coefficient K_R. The standard deviations shown in parentheses have the same meaning as in table 1.

To convert the partition coefficients to solubilities, it is necessary to use vapor pressure data. Our partition coefficients were measured at hydrocarbon pressures of the order of 1–5 percent of their vapor pressures at any particular temperature. Under such dilute conditions the activity of the hydrocarbon in either the vapor or the liquid is proportional to its concentration. We shall assume that the proportionality holds in the liquid phase for all concentrations up to a saturated solution. In the gas phase, however, a very small correction must be made for the departure of the hydrocarbon vapor from ideal gas behavior. One can show that the weight percent S of a hydrocarbon in an aqueous solution in equilibrium with a liquid hydrocarbon can be written as

$$S=(M/\rho_L)(p/RT)K(1+2Bp/RT)(100) \qquad (6)$$

where M is the molecular weight of the hydrocarbon, ρ_L is the density of the liquid solution, K is the partition coefficient measured at low hydrocarbon pressures, p is the vapor pressures of the hydrocarbon at the temperature T, R is the gas constant, and B is the second virial coefficient for hydrocarbon-hydrocarbon interactions. When liquid hydrocarbon is present at equilibrium, it will dissolve some water. The amount dissolved is so small, however, that no correction was made for its effect on the hydrocarbon vapor pressures [12]. Also, no correction was made for the contribution of hydrocarbon-water interactions to the second virial coefficients.

Our results for the solubility of benzene at different temperatures in distilled water are given in table 3 along with literature values. When available, standard deviations are listed in parentheses after each S value. In this temperature region there have been only two other extensive sets of measurements; those of Arnold et al. [13], and those of Bohon and Clussen [14]. Both groups used spectrophotometric analytical techniques. Our results agree satisfactorily with those of Bohon and Claussen over the whole temperature range, but are systematically higher than those of Arnold et al., by about 4 percent over most of the range.

Our results for the solubilities of toluene and ethylbenzene in distilled water are shown in tables

TABLE 4. *Solubility of toluene in distilled water*

Temp. (°C)	Solubility S (wt. percent)	
	Present work	Ref. [14]
0.4		0.0658(0.0007) [a]
3.6		.0646(0.0004)
4.5	0.0612(0.0010) [a]	
6.3	.0601(0.0011)	
7.1	.0586(0.0018)	
9.0	.0587(0.0011)	
10.0		.0628
11.2		.0624(0.0000)
11.8	.0573(0.0014)	
12.1	.0575(0.0012)	
14.9		.0622(0.0003)
15.1	.0569(0.0013)	
15.9		.0620(0.0000)
17.9	.0577(0.0013)	
20.1	.0566(0.0011)	
25.6		.0623(0.0004)
Other values		
16.0	0.047 Ref. [26]	
25.0	.0536(0.0003) Ref. [21]; 0.053 Ref. [25]; .0515(0.0017) Ref. [23]	

[a] The numbers in parentheses are standard deviations.

TABLE 5. *Solubility of ethylbenzene in distilled water*

Temp. (°C)	Solubility S (wt. percent)	
	Present work	Ref. [14]
0.4		0.0219(0.0003)
4.5	0.0196(0.0004) [a]	
5.2		.0213(0.0001)
6.3	.0192(0.0004)	
7.1	.0186(0.0006)	
9.0	.0187(0.0004)	
11.8	.0181(0.0005)	
12.1	.0183(0.0004)	
15.1	.0180(0.0005)	
17.9	.0184(0.0005)	
20.1	.018 ;(0.0004)	
20.7		.0207
21.2		.0207
25.6		.0208(0.0002)
Other values		
15.0	0.014 Ref [26]	
25.0	.0165(0.0002) Ref. [21]; 0.0168 Ref. [27]; .0152(0.0008) Ref. [23].	

[a] The numbers in parenthesis are standard deviations.

TABLE 6. *Solubilities of benzene, toluene, and ethylbenzene in an artificial seawater having a chlorinity[a] value of 19.00 percent*

Temp.	Number of observations	Solubility S (wt. percent)		
		Benzene	Toluene	Ethylbenzene
0.19	4	0.1323(0.0017) [b]	0.0449(0.0006) [b]	0.0140(0.0002) [b]
5.32	4	.1376(0.0022)	.0429(0.0007)	.0133(0.0003)
10.05	4	.1347(0.0023)	.0416(0.0008)	.0129(0.0003)
14.96	4	.1318(0.0025)	.0405(0.0008)	.0125(0.0003)
20.04	4	.1296(0.0022)	.0397(0.0008)	.0122(0.0003)

[a] See Ref. [10] for definition of chlorinity.
[b] The numbers in parentheses are standard deviations for the absolute K values.

4, 5, and 6, respectively. For these compounds, the only extensive data in our temperature range are those of Bohon and Claussen [14]; our results are systematically lower than theirs by roughly 8 percent over the whole temperature range.

4. Appendix: Detailed Analysis of the Apparatus and Experimental procedures

4.1. Determination of Absolute Partition Coefficients

The area under the chromatographic peak is proportional to the hydrocarbon concentration in the sample volume V_s (see fig. 1). One must relate measurements of peak areas after successive equilibrations to the partition coefficient. The general way this is done was outlined in section 2.1a. In the detailed analysis we take into account the fact that different parts of the apparatus are at different temperatures, and also different pressures because of the viscous drag on the circulating carrier gas. For completeness we also consider effects arising from nonideal gas behavior even though they happen to be too small to be important in the measurements on benzene, toluene, and ethylbenzene. (They are important, however, in relating the partition coefficients to solubilities.)

The analysis is based on the assumption that thermal diffusion effects will be negligible because of the thorough mixing resulting from the carrier circulation. Thus, the composition of the gas phase will be the same in all parts of the apparatus. It is convenient to divide the gaseous portion of the apparatus into several parts which may differ in temperature and total pressure. Let V_i be the volume of the ith part, and T_i and P_i be its temperature and pressure. Let $C_{\alpha i}$ be the concentration of the component α in the volume V_i. $X_\alpha = C_{\alpha i}\bar{V}_i$ is the mole fraction of α in the mixture, and $\bar{V}_i$ is the volume of 1 mol of the mixture at the temperature and pressure T_i and P_i. The mole fraction x_α is assumed to be the same for all the V_i. Let us define a factor $R_{ij} = C_{\alpha i}/C_{\alpha j}$. This is the ratio of the steady-state concentration of α in V_i to its concentration in V_j. The volume $\bar{V}_i$ can be expressed in terms of the virial equation of state [28],

$$\bar{V}_i = RT_i/P_i + B_i$$

where R is the gas constant, and B_i is the second virial coefficient for the mixture in the volume V_i; it is a function of the temperature and composition of the mixture. Since the product $C_{\alpha i}\bar{V}_i$ is the same for all V_i, one has the relation

$$R_{ij} = (P_iT_j)(P_jT_i)^{-1}[1 + (P_jB_j/T_j - P_iB_i/T_i)/R]. \quad \text{(A1)}$$

Only terms to first order in the B_i have been considered. This expression enables us to relate the concentration of α in different parts of the apparatus to $C_{\alpha s}$, its concentration in the sample loop V_s. Let us now consider how the partition coefficient can be gotten from measurements of the relative values of $C_{\alpha s}$.

We define an extraction factor $F_\alpha = C'_{\alpha s}/C_{\alpha s}$, where $C_{\alpha s}$ is the concentration in V_s during the first equilibration with the liquid phase; $C'_{\alpha s}$ is the concentration after purging V_p with pure helium and allowing a second equilibration. By the same arguments presented in section 2.1a, we can show that

$$K_\alpha = \left(F_\alpha \sum_i R_{is}V_i - \sum_i R'_{is}V_i + R_{ps}V_p \right) [V_L(R_{\alpha s} - F_\alpha R'_{\alpha s})]^{-1} \quad \text{(A2)}$$

where K_α is the partition coefficient, i.e., the ratio $C_{\alpha a}/C_{\alpha L}$. $C_{\alpha a}$ is the equilibrium concentration of α in the gas volume V_a located just above the liquid in the equilibration cell and $C_{\alpha L}$ is its corresponding concentration in the liquid. V_L is the volume of the liquid phase. The summations are over all the volumes in the gas phase portion of the apparatus. The parameter R'_{ij} is very slightly different from R_{ij} because of the effect of the composition change on the virial coefficients B_i and B_j. In our experiments the concentrations of the hydrocarbons were so low that the contribution of the B_i to the R_{ij} could be neglected. R'_{ij} could thus be set equal to R_{ij}. Repeated purges of V_p under these conditions, followed by equilibration will thus produce the same fractional decrease in $C_{\alpha s}$.

The different volumes V_i were measured in various ways. Some were determined by filling with water and weighing. Others were determined by pressurizing and measuring the volume of gas released when V_i was opened to the atmosphere. Several cylindrical volumes were measured directly. The temperatures T_i were measured with mercury thermometers. The various pressures P_i in the apparatus were estimated by means of the Poiseuille equation. The average pressure drop across the pump was about 2 percent of the total pressure in the system.

4.2. Determination of the Temperature Dependence of K_α

The temperature dependence of the partition coefficient can be determined by repeating the above extraction experiment at a different temperature. It is convenient, however, not to extract the hydrocarbon, but simply to observe its relative gas phase concentration at different equilibration cell temperatures. This temperature is the same as that of V_a, the gas volume just above the liquid in the equilibration cell. The concentration $C_{\alpha s}$ of α in the sample loop depends on the temperature T_a of the equilibration cell in the following way,

$$C_{\alpha s}(T_a) = N_\alpha \left\{ R_{\alpha s}(T_a)[V_a(T_a) + K_\alpha(T_a)V_L(T_a)] + \sum_{i \neq a} R_{is}V_i \right\}^{-1}. \quad \text{(A3)}$$

The temperature dependences of V_a and V_L are very

small and can be easily calculated. That of R_{as} is given by eq (A1). The quantity N_α is the total number of moles of the species α in the system and is constant. Let T_{aR} be some reference temperature. We define the ratio $G_\alpha = G_{\alpha S}(T_a)/C_{\alpha S}(T_{aR})$. One can use eq (A3) to calculate $K_\alpha(T_a)$ from the observed values of G_α and the value of $K_\alpha(T_{aR})$ determined at T_{aR} by an extraction experiment.

5. References

[1] Tsonopoulos, C. and Prausnitz, J. M., Ind. Eng. Chem. Fundam. **10,** 593 (1971).
[2] LeFeuvre, A. R., Water and Water Pollution Handbook, Vol. **1,** L. L. Ciaccio, Ed. (Marcel Dekker, Inc., New York, 1971), p. 263.
[3] Peak, E. and Hodgson, G. W., J. Amer. Oil Chemists Soc. **4,** 215 (1966).
[4] Ben-Naim, A. J. Chem. Phys. **57,** 5257 (1972).
[5] Ben-Naim, A., Water and Aqueous Solutions, R. A. Horne, Ed. (Wiley, New York, 1972), p. 425.
[6] Luckey, M. J., J. Forensic Sciences **16,** 120 (1971).
[7] Peake, E. and Hodgson, G. W., J. Amer. Oil Chemists Soc. **44,** 696 (1967).
[8] Blumer, M., Environmental affairs **1,** 54 (1971).
[9] McAuliffe, C., Chemical Technology, January 1971, (American Chemical Soc., Washington, DC), p. 46.
[10] Sverdrup, H. U., Johnson, M. W., and Fleming, R. H., The Oceans, (Prentice-Hall, Inc., Englewood Cliffs, New Jersey, 1942), p. 186, formula of Brujewicz (Subow, 1931).
[11] Wilson, E. B., Jr., An Introduction to Scientific Research, (McGraw-Hill, New York, 1952), p. 272.
[12] Black, C., Joris, G. G., and Taylor, H. S., J. Chem. Phys. **16,** 537 (1948).
[13] Arnold, D. S., Plank, C. A., and Erickson, E. E., Chem. Eng. Data Ser. **3,** 253 (1958).
[14] Bohon, R. L. and Claussen, W. F., J. Amer. Chem. Soc. **73,** 1571 (1951).
[15] Vermillion, H. E., Ph.D. thesis, 1939, Duke University, Durham, NC.
[16] Stearns, R. S., Oppenheimer, H., Simon, E., and Harkins, W. D., J. Chem. Phys. **15,** 496 (1947).
[17] Hill, A. E., J. Amer. Chem. Soc. **44,** 1163 (1922).
[18] Franks, F., Gent, M., and Johnson, H. H., J. Chem. Soc. 2716 (1963).
[19] Hayashi, M., and Sasaki, T., Bull. Chem. Soc. Japan **29,** 857 (1956).
[20] Booth, H. S. and Everson, H. E., Ind. Eng. Che. **40,** 1491 (1948); **41,** 2627 (1949).
[21] Morrison, T. J., and Billett, F., J. Chem. Soc. 3819 (1952).
[22] Horiba, S., Mem. Coll. Eng., Kyoto Imp. Univ. **1,** 49 (1914).
[23] McAuliffe, C., J. Phys. Chem. **70,** 1267 (1966).
[24] Brady, A. P., and Huff, H., J. Phys. Chem. **62,** 644 (1958).
[25] Andrews, L. J., and Keefer, R. M., J. Am. Chem. Soc. **71,** 3644 (1949).
[26] Führer, H., Chem. Ber. **57,** 510 (1924).
[27] Andrews, L. J., and Keefer, R. M., J. Am. Chem. Soc. **72,** 5034 (1950).
[28] Hirschfelder, J. O., Curtiss, C. F., and Bird, R. B., Molecular Theory of Gases and Liquids (Wiley, New York, 1954).

(Paper 78A4–825)

JOURNAL OF RESEARCH of the National Bureau of Standards—A. Physics and Chemistry
Vol. 78A, No. 4, July–August 1974

Theoretical and Experimental Compton Scattering Cross Sections at 1.12 MeV in the Case of Strongly Bound *K*-Shell Electrons*

P. N. Baba Prasad and P. P. Kane****

(March 4, 1974)

Measurements are reported for the differential cross sections for Compton scattering of 1.12 MeV gamma rays by the *K*-shell electrons of tin, tantalum, gold, and thorium. A few discrepancies between approximate theoretical calculations and the experimental results for different energies are pointed out. The need for an exact relativistic calculation is indicated.

Key words: Compton scattering; differential cross section; electron binding; gamma rays; *K*-shell; photons.

The Compton scattering of gamma rays by strongly bound atomic *K*-shell electrons has been studied experimentally at 0.279 MeV [1],[1] at 0.320 MeV [2], very intensively at 0.662 MeV [3 . . . 11] and at an average energy of 1.002 MeV [12]. We have given preliminary reports on similar measurements made with a zinc-65 source at an energy of 1.12 MeV [13].

Motz and Missoni [3] suggested that the results for large momentum transfers can be understood within the framework of an impulse approximation. Recently, a justification [14] of this approximation within the framework of nonrelativistic quantum mechanics has been given. If the target electron momentum $\mathbf{p}$ makes angles α and α' with the momenta $\boldsymbol{\eta}$ and $\boldsymbol{\eta}'$ of the incident and the scattered photons respectively, the energy k of the photon scattered through an angle θ is given by eq (1).

$$\frac{k}{k_0}=\frac{1-\beta\cos\alpha}{k_0E^{-1}(1-\cos\theta)+(1-\beta\cos\alpha')} \tag{1}$$

where k_0 is the incident photon energy, β is the ratio of the initial electron velocity to the velocity of light and E is the sum of the rest energy and the kinetic energy T of the target electron. In view of the virial theorem, a convenient measure of T is taken[2] to be the binding energy of the electron. Unfortunately, in the work of Jauch and Rohrlich [15], there was a misprint so that α appeared in the denominator instead of α'. The final result for the cross section $\left(\frac{d\sigma_K}{d\Omega}\right)_{\text{Imp.}}$ is obtained in terms of an average, as in eq. (2).

$$\left(\frac{d\sigma_K}{d\Omega}\right)_{\text{Imp.}}=\frac{\int_{-1}^{+1}\int_{-1}^{+1}\left(\frac{d\sigma}{d\Omega}\right)d(\cos\alpha)\,d(\cos\phi)}{\int_{-1}^{+1}\int_{-1}^{+1}d(\cos\alpha)\,d(\cos\phi)} \tag{2}$$

where ϕ is the angle between the planes formed by the pairs of vectors $(\boldsymbol{\eta}, \mathbf{p})$ and $(\boldsymbol{\eta}', \mathbf{p})$ and the relativistic expression for $d\sigma/d\Omega$ in the case of a free but fast electron has been given by Jauch and Rohrlich.

In the calculation of Motz and Missoni for 0.662 MeV, the misprinted formula with α instead of α' was used and so the average over ϕ was not evaluated. On the basis of the correct eq (2), Shimizu et al. [7] proceeded to derive an extremely complicated expression in closed form. A graphical integration of (2) was performed by Ramalinga Reddy et al. [2, 12] for 0.320 MeV and 1.002 MeV gamma rays. However, on the basis of a repetition of their calculations, it appears to us that they might have used the misprinted formula. Pingot [9] evaluated the averages for 0.662 MeV by a numerical integration procedure. His theoretical values for gold were in disagreement with the experimental data and with the first two calculations.

In a few recent reports [1, 9, 10], an attempt has been made to compare the experimental results for $d\sigma_K/d\sigma_{KN}$ at all angles with the calculated values of the incoherent scattering function S_K for *K*-shell electrons. Here, $d\sigma_K/d\sigma_{KN}$ is the ratio R of the scatter-

*Work supported in part by a grant from the National Bureau of Standards, Washington, D.C. under the PL–480 programme.

**Present address: Physics Department, Indian Institute of Technology, Powai, Bombay–76, India.

[1] Figures in brackets indicate the literature references at the end of this paper.

[2] According to the virial theorem, the average kinetic energy of an electron bound by the attractive Coulomb potential in an atom turns out to be equal to the negative of half the average potential energy. Therefore, the average kinetic energy is the negative of the sum of the potential and the kinetic energies. Thus, the kinetic energy may be put equal to the binding energy of the electron.

ing cross section of an electron bound in the K-shell to the Klein-Nishina prediction for an electron initially free and at rest.[3] On the basis of a nonrelativistic treatment and the incoherent scattering function approximation, Shimizu et al. [7] have given an analytical expression for S_K, which should be really valid only for small momentum transfers. But the same expression was used in the above-mentioned reports even at large scattering angles. The resulting S_K values for gold at 0.279 MeV and 0.662 MeV were in approximate agreement with the measured values of the ratio R. However, on the other hand, the data for lead at 0.662 MeV do not agree well with the S_K values computed in this way or according to an earlier relativistic treatment [4].

We have repeated the numerical evaluation associated with eq 2 and with the well-known Klein-Nishina formula for $\frac{d\sigma_{KN}}{d\Omega}$, for five gamma energies including 1.12 MeV. The resulting estimates for the ratio $R_{\text{Imp.}}$ are less than unity at all angles and are in disagreement with several experimental values of R at 0.279 MeV, 0.320 MeV, 0.662 MeV, and 1.002 MeV. Some of the new experimental results for R at 1.12 MeV, outlined briefly in the following paragraph, are also in disagreement with the theoretical estimates of $R_{\text{Imp.}}$. Our estimates for a gold scatterer and 0.662 MeV gamma rays agree extremely well with those reported by Pingot and thus confirm the correctness of the estimation procedure.

The experimental results at 1.12 MeV were obtained in a conventional coincidence experiment with 14.9 mg/cm² thorium, 12.9 mg/cm² gold, 22.1 mg/cm² tantalum and 18.8 mg/cm² tin scatterers. The bias level in the gamma channel was chosen to correspond to about one third of the photon energy calculated for the Compton scattering from a free and stationary electron. However, an additional consideration determined the final choice. It was desirable to keep the bias substantially above the target atom K_α x-ray energy in order to minimize the spurious coincidences arising from K x-rays registering in the gamma detector and the scattered gamma rays simultaneously registering in the thin x-ray detector. The final bias values were 0.300 MeV, 0.165 MeV, 0.165 MeV, and 0.100 MeV in the case of measurements made at scattering angles of 25, 60, 90, and 120° respectively except that for thorium at 120°, the bias was 0.165 MeV. Measurements of random coincidences were made as usual. In addition, counts due to the natural radioactivity of the thorium foil were determined in an auxiliary experiment. The experimental results obtained by us are summarized in the third column of table 1. The values estimated according to impulse approximation mentioned above are listed in the fourth column. S_K values calculated according to the formula of Shimizu et al. are tabulated in the last column. It should be noted that several $S_{K\,(\text{Shimizu})}$ values are larger than unity and much larger than the

TABLE 1. *Experimental and theoretical values of* $R=\frac{d\sigma_K}{d\sigma_{KN}}$ *for 1.12 MeV gamma rays from a zinc-65 source*

Element	θ	$R_{\text{expt.}}$	$R_{\text{Imp.}}$[a]	$S_{K\,(\text{Shimizu})}$[b]
Thorium 14.9 mg/cm²	25°	0.39 ± 0.13	0.896	0.420
	60°	.96 ± 0.13	.918	1.149
	90°	1.35 ± 0.13	.934	1.489
	120°	0.92 ± 0.18	.869	1.655
Gold 12.9 mg/cm²	25°	.67 ± 0.09	.925	0.560
	60°	.82 ± 0.12	.937	1.575
	90°	1.39 ± 0.12	.952	2.046
	120°	1.07 ± 0.16	.898	2.277
Tantalum 22.1 mg/cm²	120°	0.96 ± 0.26	.914	2.735
Tin 18.8 mg/cm²	25°	.78 ± 0.07	.967	1.491
	60°	.97 ± 0.08	.975	4.406
	90°	1.09 ± 0.09	.985	5.765

[a] The values of $R_{\text{Imp.}}$ are estimated for K-shell electrons on the basis of eqs (1) and (2) in the text, and the Klein-Nishina formula.

[b] S_K is computed from an equation given by Shimizu et al (reference [7]). In their equation, b and not b^2 should be put equal to $Z\frac{\hbar}{a_0}$.

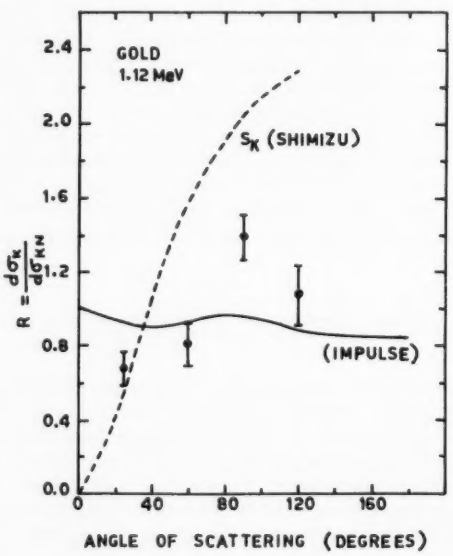

FIGURE 1. *Angular distribution of the cross section ratio* $R=\frac{d\sigma_K}{d\sigma_{KN}}$.

ϕ – Present experimental results at 1.12 MeV for a gold scatterer.
..... S_K calculated according to the formula of Shimizu et al.
——— = The theoretical values of $R_{\text{Imp.}}$ calculated according to eqs (1) and (2), and the Klein-Nishina formula.
As pointed out in the text, the impulse approximation is expected to be valid for large transfers; whereas the $S_{K\,(\text{Shimizu})}$ formula has been derived in a nonrelativistic treatment and for small momentum transfers.

[3] The two symbols R and S_K are introduced, for the purposes of this paper, to distinguish between (1) an operational definition of the ratio R of bound-electron incoherent scattering to free-electron (Klein-Nishina) scattering obtained either from (a) experiment or (b) a theoretical model not restricted to small scattering angles, and (2) $S(q,Z)$ (here S_K for K-shell electrons only), the same ratio, but defined as the probability of atomic excitation or ionization resulting from any impulsive action imparting a recoil momentum q to an atomic electron (see, e.g., Grodstein [16], Evans [17], Davisson [18], Hubbell [19], or Storm and Israel [20]), calculated up to now from models claiming validity only for applications to small angles.

corresponding experimental values of R. In figure 1, the experimental results for a gold scatterer are compared with the theoretical values computed according to the above mentioned approximations.

The detailed spectral distributions of 1.12 MeV photons Compton scattered by the K-shell electrons of different atoms are being determined at present. The results of this study will be reported in a later communication.

For 0.662 MeV gamma rays, a relativistic calculation [16] employing Dirac eigenfunctions for the initial and final electron states and the bound electron propagator for intermediate states has been done. It is clearly necessary to extend this type of calculation to other gamma ray energies. A similar suggestion has been made recently by other workers [17].

References

[1] Pingot, O., Nucl. Phys. **A** 133, 334 (1969).
[2] Ramalinga Reddy, A., Lakshminarayana, V., and Jnanananda, S., Proc. Phys. Soc. (Lond.) **91**, 71 (1967).
[3] Motz, J. W., and Missoni, G., Phys. Rev. **124**, 1458 (1961).
[4] Sujkowski, Z., and Nagel, B., Arkiv Fys. **20**, 323 (1961).
[5] Varma, J., and Eswaran, M. A., Phys. Rev. **127**, 1197 (1962).
[6] Missoni, G., and Di Lazzaro, M. A., Istituto Superiore Di Sanita Reports, ISS–63/7, 63/8, 66/6, 66/7, and 66/8 (1963) and (1966).
[7] Shimizu, S., Nakayama, Y., and Mukoyama, T., Phys. Rev. **140A**, 806 (1965).
[8] Ramalinga Reddy, A., Lakshminarayana, V., and Jnanananda, S., Ind. J. Pure and Appl. Phys. **4**, 371 (1966).
[9] Pingot, O., Nucl. Phys. **A119**, 667 (1968).
[10] Krishna Reddy, D. V., Narasimhacharyulu E., and Murthy, D. S. R., Proc. of the Nuclear and Solid State Physics Symposium, Roorkee (1969) 84 and ibid. Madurai (1970), p. 177.
[11] East, L. V., and Lewis, E. R., Physica **44**, 595 (1969).
[12] Ramalinga Reddy, A., Parthasaradhi, K., Lakshminarayana, V., and Jnanananda, S., Ind. J. Pure and Appl. Phys. **6**, 255 (1968).
[13] Baba Prasad, P. N., and Kane, P. P., Proc. of the Nuclear and Solid State Physics Symposium, Roorkee, (1969) 81 and ibid. Madurai (1970), p. 187.
[14] Eisenberger, P., and Platzman, P. M., Phys. Rev. **A2**, (1970) 415.
[15] Jauch, J. M., and Rohrlich, F., The Theory of Photons and Electrons (Addison Wesley Publishing Co.; 1955) p. 230, eq 11–8.
[16] Grodstein, G. W., Nat. Bur. Stand. (U.S.), Circ. 583, 54 pages (1957).
[17] Evans, R. D., Encycl. Phys. (Springer-Verlag, Berlin), S. Flügge, Ed., **34** (1958), p. 218.
[18] Davisson, C. M., in Alpha- , Beta- , and Gamma-Ray Spectroscopy (North-Holland, K. Siegbahn, Ed.; 1965), p. 57.
[19] Hubbell, J. H., Nat. Stand. Ref. Data Ser., Nat. Bur. Stand. (U.S.), 29, 85 pages (Aug. 1969).
[20] Storm, E., and Israel, H. I., Nucl. Data Tables **A7**, 565 (1970).
[21] Whittingham, I. B., J. Phys. A. (Gen. Phys.) **4**, 21 (1971).
[22] Tseng, H. K., Gavrila, M., and Pratt, R. H., Report No. 2 (1973), unpublished.

(Paper 78A4–826)

538-709 OL - 74 - 2

JOURNAL OF RESEARCH of the National Bureau of Standards—A. Physics and Chemistry
Vol. 78A, No. 4, July–August 1974

Standardization of ^{60}Co and ^{137}Cs Gamma-Ray Beams in Terms of Exposure*

T. P. Loftus and J. T. Weaver

Institute for Basic Standards, National Bureau of Standards, Washington, D.C. 20234

(April 19, 1974)

At the National Bureau of Standards (NBS), the exposure-rate standards for ^{60}Co and ^{137}Cs gamma rays were based for a number of years on a weighted average of measurements using a cylindrical ionization chamber and a group of small spherical chambers. Complex setup conditions for the cylindrical chamber, differences between the cylindrical and spherical chamber data, and recognition that the institution of this weighted average exposure-rate standard increased the difference between free-air-chamber and cavity-chamber measurements, led to the development of new spherical chambers. All correction factors for exposure-rate measurements were investigated and updated. Excellent agreement was achieved between independent exposure-rate measurements for six spherical chambers and, as of May 1, 1972, the exposure standards were reduced 0.7 percent for ^{60}Co and 0.6 percent for ^{137}Cs gamma rays. Recalculation of correction factors since that time indicates that the standard ^{137}Cs should be further reduced by 0.2 percent, and this adjustment was made on July 1, 1974.

The uncertainties associated with each of the quantities entering into the determination of exposure rate were tabulated and the overall uncertainty of the exposure rates used for instrument calibrations at NBS was found to be about 0.7 percent for addition in quadrature.

Key words: Cavity ionization chamber; exposure; gamma rays; ^{60}Co; ^{137}Cs; standards.

1. Introduction

The standard instrument employed for exposure measurements, for x-rays generated by potentials from ten up to a few hundred kilovolts, is the free-air ionization chamber [1, 2, 3].[1] Experimental difficulties encountered with this instrument at high energies, in fulfilling the requirement that all ionizing particles be stopped in air, cause standards laboratories to have recourse to another method of standardization. This alternate method, which obviates the necessity of a free-air chamber operated at high pressure, or with large plate spacing, employs cavity ionization chambers and relies on the principles of the Bragg-Gray theory [4] for its validity.

The exposure, X, is the quotient of dQ by dm where dQ is the absolute value of the total charge of the ions of one sign produced in air when all electrons liberated by photons in a volume element of air having mass dm are completely stopped in air [5]. The special unit of exposure is the roentgen which is equal to 2.58×10^{-4} $C \cdot kg^{-1}$.

During 1959, Wyckoff [6] measured a ^{60}Co source and a ^{137}Cs source, in roentgens, using a pressurized free-air chamber. For comparison, the exposure rates were also measured using the cylindrical cavity ionization chamber of Attix [7]. The cavity-chamber measurements were performed in an open-air geometry and corrected for room scattering. Good agreement was achieved between the two methods of measurement although the cavity-chamber measurement of the ^{137}Cs source appeared low (see table 1, column 2).

The activity of the ^{60}Co source was determined from calorimetric measurements in 1961 by Myers [8] who calculated[2] $\bar{W}_{air}$ by combining the activity and free-air-chamber data. His value of 33.84 eV per ion pair is in good agreement with the presently accepted value of 33.73 eV [9], thus indicating consistency of the free-air-chamber measurements of exposure with other physical measurements.

The apparent good agreement between the free-air-chamber and cavity-chamber measurements was to some extent fortuitous, since subsequent comparisons between the cylindrical chamber and a group of spherical chambers showed that the cylindrical chamber response decreased, in relation to the spherical chambers, with increasing distance from the source. This characteristic of the cylindrical chamber had been observed by Attix [7] who hypothesized that the reduction was due to attenuation in the chamber end walls and who avoided the effect by orienting the axis of the chamber at an angle to the direction of the incident radiation.

The calibration of the NBS collimated gamma-ray

*This work was supported in part by the Defense Civil Preparedness Agency by Work Order DCPA 01-74-C-0034.

[1] Figures in brackets indicate the literature references at the end of this paper.

[2] The value of μ_{en} used to compute $\bar{W}_{air}$ is not given in Myers' report. If the data of Hubbell [10] are used, the authors compute $\bar{W}_{air} = 33.71$ eV, which is in excellent agreement with the accepted value.

TABLE 1. *Relationship of cavity-chamber and free-air-chamber source measurements, and ratios of collimated beam calibrations*

Ratios of cavity-chamber exposure rate to free-air-chamber exposure rate. ^{60}Co and ^{137}Cs source measurements.			Ratio of weighted mean exposure rate to exposure rate based on cylindrical chamber measurements with radiation incident ⊥ to chamber axis. Calibration change in 1961.	Ratio of new weighted mean exposure rate, based on measurements with six spherical chambers, to 1961 weighted mean. Calibration change in	
Source	Cylindrical chamber. Radiation incident ⊥ to chamber axis. (1959)	Weighted mean of cylindrical and small spherical chamber data. Cylindrical chamber axis at 45° to incident radiation. (1961)		May 1972	July 1974*
^{60}Co	1.003	1.019	1.016	0.993	0.993
^{137}Cs	0.984	0.994	1.010	0.994	0.992
(1)	(2)	(3)	(4)	(5)	(6)

*All new data provided in this publication reflect the July 1974 values.

beams, at the time of the free-air-chamber and cavity-chamber comparison, was based on measurements with the cylindrical chamber with its axis perpendicular to the direction of the incident radiation. To eliminate the distance effect in measurements with this chamber, the gamma-ray beams were recalibrated in 1961 with the chamber axis at an angle of 45° to the beam direction. At the same time, the beams were also calibrated with a small spherical chamber. The beam calibrations were then adjusted to a weighted mean of these two sets of measurements. The effect of this change on the free-air-chamber, cavity-chamber comparison is shown in table 1, column 3, and the effect on the calibrated beams is shown in table 1, column 4. The comparison of these measurements assumes that the ratios established for the directional dependence of the cylindrical chamber in a collimated beam are applicable to the open-air calibrations. All data in table 1 are for source-to-chamber distances comparable to those used in the open-air-geometry source measurements (0.8 m).

While the cavity-chamber and free-air-chamber measurements of exposure rate for high-energy gamma rays agreed to about 2 percent, the difference was still sufficiently large as to indicate that the corrections for the cavity chamber could be improved. The procedure of angling the cylindrical chamber in the beam to remove the distance effect, not only caused a divergence of the cavity-chamber, free-air-chamber exposure measurements,[3] but added complexity to setup conditions for beam measurements. These difficulties prompted the development of new chambers which would not be critically directional dependent (and therefore easily set up), would allow investigation of possible variation of chamber response with chamber size, and eventually lead to the establishment of a standard based on a group of chambers of homogeneous geometry. The new chambers would also allow studies of chamber wall corrections, with the goal of improving agreement between the free-air-chamber and cavity-chamber exposure-rate measurements. To accomplish these goals, a group of eight spherical chambers was assembled. The chambers are fabricated from high-purity graphite and had special, closely fitting shells for wall-absorption measurements. The group of chambers and shells makes possible six [4] determinations of exposure rate. The results of the measurements with these chambers, as well as some updating of calculated corrections, indicate that the exposure rates used at NBS since 1961 were too high by approximately 0.7 percent for ^{60}Co and 0.6 percent for ^{137}Cs gamma rays. The gamma-ray beams used for instrument calibrations were recalibrated on this basis as of May 1, 1972 (table 1, column 5). The adjustment in the gamma-ray standards is in a direction to improve the free-air chamber and the cavity chamber agreement for ^{60}Co, although it appears there is still a difference[5] of about 1.2 percent.

The preceding discussion is based on ratios of chamber readings at different times in different radiation fields. The percentage difference between the free-air chamber and the cavity chamber for these gamma-ray energies should be considered as an estimate. Since the high-pressure free-air chamber is no longer available, confidence in the validity of the cavity-chamber determinations of exposure rate is derived from intercomparisons with other standards [12] and comparisons of cavity-chamber ionization measurements with other physical measurements such as source power [13]. Such comparisons have shown agreement in exposure-rate determinations to within several tenths percent.

2. Relationship Between Cavity Ionization and Exposure

The work of Gray was concerned with the measurement of gamma-ray energy absorbed in a small volume of material. His derivations and experiments led to the

[3] This statement pertains only to the ^{60}Co data since the angulation procedure improves the agreement for ^{137}Cs. However, examination of the 1959–1961 data for the ^{137}Cs measurements shows that the room scatter correction is 1.6 percent, roughly four times the correction used for ^{60}Co. Later calculations for similar measurement conditions [11] indicate the correction should have been about 0.5 percent.

[4] The wall correction for one of the 50-cm³ chambers is determined by utilizing three chambers as a group while the corrections for the other two of the chambers are determined by addition of shells. Although the aforementioned chamber does not therefore provide an entirely independent measurement of X, it is treated as such in the calculations.

[5] The difference in the measurements for ^{60}Co is only about 0.8 percent if consistent constants are used, e.g., the 1961 data incorporated a correction for relative humidity which is not now applied [14] and the value used for the ratio of the mean collision stopping powers of carbon to air was ≃ 1.003. As presently calculated, this correction is ≃ 1.006.

familiar expression

$$ {}_mE_w = J_g \bar{W}_g \frac{{}_mS_w}{{}_mS_g} \quad (1) $$

where ${}_mE_w$ is the energy absorbed per unit mass of the medium, J_g is the number of ion pairs formed per unit mass of gas in a cavity in the medium, $\bar{W}_g$ is the average energy required to form an ion pair in the gas and ${}_mS_w/{}_mS_g$ is the ratio of the mass collision stopping power for electrons in the medium, to that in the gas. A condition for the validity of eq (1) is that all electrons producing ionization in the cavity gas are generated in the wall of the cavity, and that the cavity does not disturb the electron flux.

For measurement of exposure, the medium in eq (1) is the wall of a cavity chamber with sufficient thickness to exclude electrons generated in other media. Any wall material and any gas can be used, provided the stopping-power ratio and the average energy required to form an ion pair in the gas are known. If the chamber wall is carbon, the energy absorbed per unit mass of air is

$$ {}_mE_{\text{air}} = {}_mE_c \frac{(m\mu_{en})_{\text{air}}}{(m\mu_{en})_c} \quad (2) $$

where ${}_m\mu_{en}$ is the mass energy-absorption coefficient, and

$$ {}_mE_{\text{air}} = J_g \bar{W}_g \frac{{}_mS_c}{{}_mS_g} \frac{(m\mu_{en})_{\text{air}}}{(m\mu_{en})_c}. \quad (3) $$

If the gas in the cavity is air, the subscript g represents air. The equation for exposure computations derived from eq (3) is:

$$ X = \frac{1}{2.58 \times 10^{-4}} \frac{Q_{\text{air}}}{v\rho} \frac{{}_mS_c}{{}_mS_{\text{air}}} \frac{(m\mu_{en})_{\text{air}}}{(m\mu_{en})_c} \prod k_i \quad (4) $$

where 2.58×10^{-4} is the number of coulombs per kilogram of air produced by one roentgen, Q_{air} is the measured charge (in coulombs), v is the chamber volume (in m^3) and ρ is the density (in kg/m^3). $\prod k_i$ is the product of all the factors required to correct the measured charge for experimental conditions. These are:

- k_h the correction for water vapor in the air.
- k_s the correction for loss of ionization due to recombination.
- k_{st} the correction for chamber stem scatter.
- k_w the correction to zero wall thickness.
- k_{CEP} the reduction in the wall correction k_w, taking into account the mean center of electron production.

Other corrections are required for specific experimental conditions.

3. Cavity-Chamber Description

The cavity chambers, used for studies leading to the revised (May 1, 1972) ^{60}Co and ^{137}Cs exposure-rate standards, were fabricated from reactor-grade, high-purity graphite, following the design of Wyckoff [15]. The spherical shape was chosen in order to allow the standards to be based on a homogeneous group of chambers of different volumes, to avoid the distance effect and the complexity of set up in measurements with the cylindrical chamber, and to present a uniform, symmetrical, chamber aspect to the source.

The dimensions of the spherical chambers are given in table 2. The three small-volume chambers, identified as 0.5, 1, and 2, were designed to be used as a group to determine a wall correction and provide one measurement of gamma-ray exposure. These chambers have the same nominal outside diameter but different wall thicknesses and thereby different cavity volumes. They were fabricated using ball end-mills of diameters 3/8, 1/2, and 5/8 in. The wall-thickness values given for these three chambers were derived from measurements of outside diameters and the diameters of the end-mills used in their fabrication.

The net volumes given in table 2 are the differences between the cavity volumes and the volumes of the collection electrodes. The electrode diameter for the 50-cm^3 chambers is nominally 0.3 cm but for all other chambers it is nominally 0.1 cm.

The 50-cm^3 chambers have the same nominal cavity size but different wall thicknesses and can be used as a group to determine the wall correction. The wall correction can also be determined by the addition of closely fitting shells to two of the chambers. With the two methods of wall-absorption measurement available, each of the 50-cm^3 chambers can be considered

TABLE 2. *Dimensions of spherical graphite ionization chambers*

Nominal volume	Volume	Net volume	Outside diameter	Graphite density	Radial Wall Thickness	
(cm^3)	(cm^3)	(cm^3)	(cm)	($g \cdot cm^{-3}$)	(cm)	($g \cdot cm^{-2}$)
0.5	0.440	0.431	2.078	1.72	0.563	0.968
1	1.140	1.131	2.065	1.73	.398	.688
2	2.029	2.019	2.080	1.74	.246	.428
10	10.088	10.069	3.428	1.72	.3755	.647
30	30.262	30.24	4.607	1.74	.3751	.653
50–1	51.943	51.634	5.34	1.73	.3652	.632
50–2	50.425	50.089	5.58	1.73	.5085	.880
50–3	50.460	50.155	5.80	1.73	.6129	1.060

to provide an independent measurement of exposure.

Of all the spherical chambers, the 50-cm³ chambers are of the highest quality, great care having gone into their fabrication to insure close tolerances in all dimensions. Measurements of wall thickness at many locations on the periphery of both halves of each 50-cm³ chamber show that the range of the wall thickness variation is less than 0.025 $g \cdot cm^{-2}$ and the largest difference between average values for the two halves is 0.016 $g \cdot cm^{-2}$.

The fabrication of the 10-cm³ and 30-cm³ chambers was performed with less restriction on the variation of chamber wall thickness with the result that the average wall thicknesses for the two halves differ by 0.016 cm (0.025$g \cdot cm^{-2}$) for the 10-cm³ chamber and 0.052 cm (0.089$g \cdot cm^{-2}$) for the 30-cm³ chamber. Although these differences seem to infer uncertainties in the chamber wall correction of up to 0.3 percent, in fact the chamber response is related to the average wall thickness and the average is used in plotting the chamber response versus wall thickness to determine the wall correction. The wall thicknesses given in table 2 for these two chambers are the overall averages for measurements in a radial direction at a number of positions (see fig. 1), and the corrections are determined for the chambers by the addition of closely fitting spherical shells to the chamber walls.

The densities for the 0.5-cm³ and 2-cm³ chambers were measured using the principle of Archimedes, while density for the 1-cm³ chamber was inferred from measurements of another chamber fabricated from the same material. The densities for the 50-cm³ chambers were determined from a cylindrical block machined from the same material. The densities for the 10-cm³ and 30-cm³ chambers were determined using differential weighings in and out of distilled water. The differential weighing method, and mechanical measurement of dimensions and weighing of the same graphite block give densities which differ by only 0.01$g \cdot cm^{-3}$.

4. Wall Corrections and Volume Measurements

Ideally, the measurement of high-energy gamma radiation, in terms of exposure, should be made by sampling the ionization per unit mass of air, in a small volume surrounded by enough air to establish secondary-particle equilibrium, and removed from other sources of secondary-particle radiation. In practical situations, these conditions seldom can be met, necessitating the use of thick-walled ionization chambers.

The material chosen for the chamber wall should be sufficiently like air, with respect to its interaction with the radiation of interest that, with small corrections, the chamber wall can be considered nearly equivalent to air with a greater-than-normal density. Chambers are actually designed to have walls thick enough to exclude the highest energy secondary particles produced by interaction of the radiation with other media and this thickness is more than sufficient to achieve secondary-particle transient equilibrium [16]. Chamber ionization measurements can be plotted versus cham-

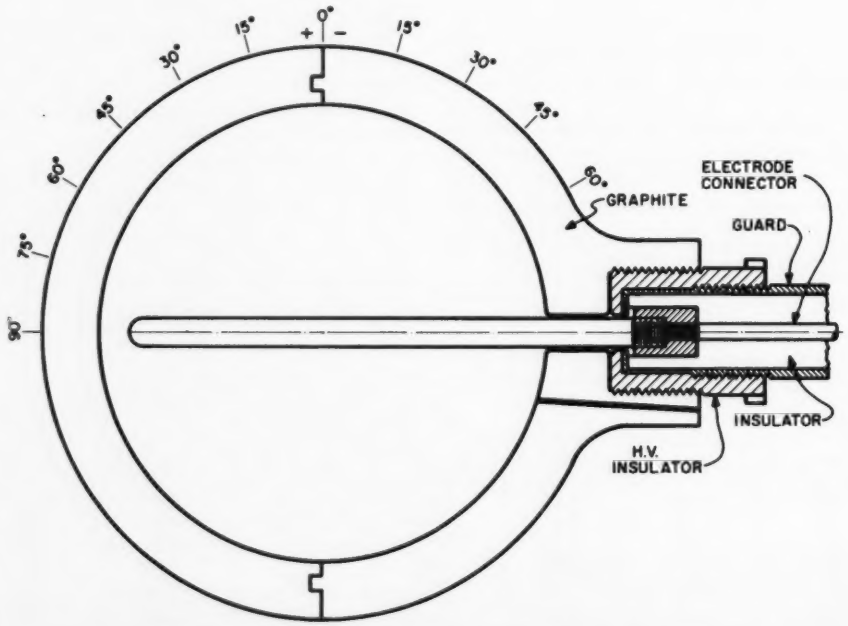

FIGURE 1. *Cavity chamber design and location of wall thickness measurements.*

ber wall thickness to allow extrapolation of transient-equilibrium readings to zero wall. This procedure provides an over-estimate of the corrected chamber reading as shown by Whyte [17]. The zero-wall chamber data must be reduced to account for the fact that the ionization in the chamber is being produced by electrons which are generated at some depth in the chamber wall and to bring the data into agreement with the zero-wall value for equilibrium conditions.

The amount by which the zero-wall correction for cavity chambers should be reduced can be estimated from the work of Wyckoff [6] who used, for photon attenuation corrections in a free-air chamber, a distance from the defining diaphragm to the mean position of origin of electrons producing ionization in the collecting plate region. The mean position of origin of the ionizing electrons was determined by Roesch [18] to be 0.3 times the practical electron range (350 cm-atm for ^{60}Co and 90 cm-atm for ^{137}Cs). Thus the total air path, between diaphragm and collection region, used to compute the air attenuation correction, was reduced by 105 cm-atm and 27 cm-atm for ^{60}Co and ^{137}Cs gamma rays, respectively. Since carbon and air are nearly alike as to interactions with gamma rays and electrons, the same thicknesses of material can be used for these energies. The fractional reduction calculated from the expression $1-(\mu/\rho)(\rho x)$ is 0.995 for ^{60}Co and 0.999 for ^{137}Cs gamma rays. The values for μ/ρ (0.033 and 0.040 cm^2/g) are averages from the data given in table 3. Since the correction is small, considerable latitude is allowable in each of the factors before the correction changes by 0.1 percent. This correction has been identified as k_{CEP} since the extrapolation of the wall-absorption data is effectively carried out only to the mean center of electron production.

The wall corrections for ^{60}Co were determined by the addition of spherical graphite shells, for all chambers, and by combining data for groups of chambers designed as a set in the case of the three small-volume chambers and the three 50-cm^3 chambers. The agreement between the two methods is excellent for the 50-cm^3 chambers and the data are shown in figure 2. As a consequence of the close agreement between the two absorption methods, it was only necessary to use the 50-cm^3 chambers as a group to determine the wall correction for ^{137}Cs gamma rays. These data are also shown in figure 2.

The averages of several sets of measurements of chamber reading versus wall thickness for the 10- and 30-cm^3 chambers are plotted in figures 3 and 4. The lines drawn through the points are least-squares regressions giving equal weight to each point. The wall-absorption corrections for all the chambers are summarized in table 3.

Determination of the appropriate wall-absorption correction for the set of small-volume chambers presents difficulties which are not present for the other chambers. The small chambers differ considerably in volume and when operated at the same collection potential have different field strengths. It is necessary, therefore, to apply corrections for recombination, determined for each chamber, for the exposure rate used in the experiment. An additional difficulty, and one which exacerbates the situation, is the relatively large uncertainty

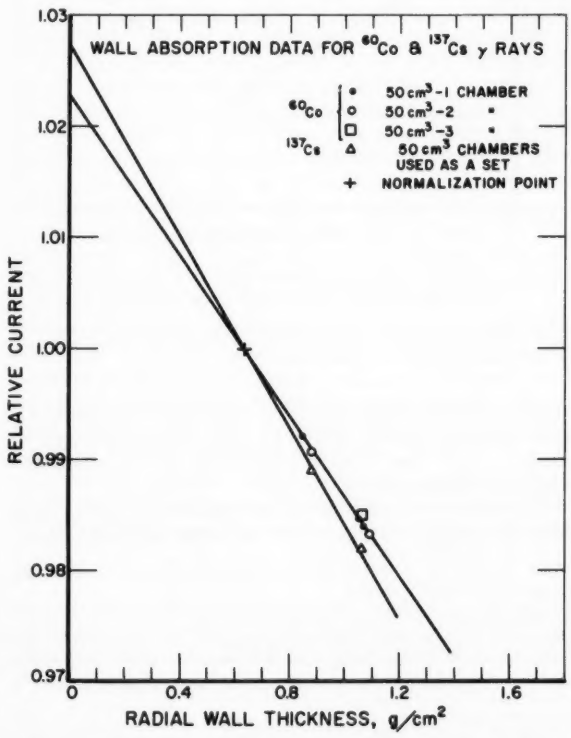

FIGURE 2. *All 50-cm^3 chamber absorption data for ^{60}Co gamma rays are combined by normalization to the data for 50–1 chamber.*

The chamber group and shell addition data are shown to be consistent. The line drawn through the points was calculated using the least squares method with the data weighted according to the number of determinations for each point. The line through the points for ^{137}Cs gamma rays is also based on the least squares method.

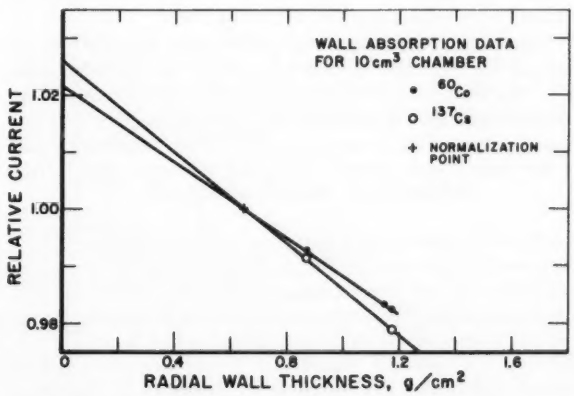

FIGURE 3. *Relative ionization currents produced in the 10-cm^3 chamber by ^{60}Co and ^{137}Cs gamma rays as the wall thickness is increased by the addition of graphite shells to front and back of the chamber.*

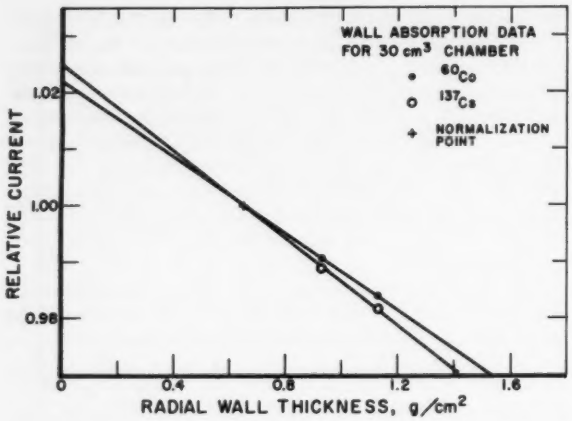

FIGURE 4. *Relative ionization currents produced in the 30-cm³ chamber by ^{60}Co and ^{137}Cs gamma rays as the wall thickness is increased by the addition of graphite shells to front and back of the chamber.*

in the determination of the volumes for these small chambers. The differential weighing technique, i.e., weighing the chambers with and without the cavity filled with distilled water, provides volume measurements for all the large chambers with a range of only 0.02 cm³. If this range is used as a measure of the imprecision of the technique, it is obvious that for small-volume chambers such as the 0.5, 1, 2 group, the uncertainty in the volume determination can be large. Analysis of the measurements for these chambers reveals that the average volumes have the statistical parameters given in table 4. Since the confidence interval increases as the chamber volume decreases, the data for the small chambers cannot be considered to be of equal value. Weighting factors of 1, 3, and 4, based on the inverse of the 95 percent confidence intervals are therefore assigned to 0.5, 1, and 2 chambers, respectively, in the calculation of regression lines for wall absorption. The data for both gamma-ray energies are shown in figure 5 where the lines drawn through the points are determined by least squares.

The wall correction for the small-chamber set is based on the use of the chambers in combination, i.e., the current per unit volume for each chamber was plotted against chamber radial wall thickness and the data extrapolated to zero-wall. The resulting wall correction, the 1-cm³ chamber volume and other required corrections produce exposure-rate data for this chamber group which is only about 0.3 percent higher than that calculated from other spherical-chamber measurements.

Experiments designed to determine wall corrections for the small chambers, by addition of close-fitting

TABLE 4. *Statistical parameters associated with volume determinations for 0.5, 1, and 2 chambers*

Chamber	Average volume (cm³)	Number of measurements	Standard deviation of the mean (percent)	Weights based on 95% confidence interval
2	2.029	2	[a] 0.00	4
1	1.140	5	.07	3
0.5	0.440	7	.2	1

[a] A series of three sets of weighings were performed for 2 and then the chamber halves were separated for inspection. The relative standard deviation of the mean, for these first weighings, is 0.035 percent. The chamber was reassembled and two more sets of weighings were performed. There was no difference (to 0.01 mg) between the last two weighings. Because the chamber halves were separated between the weighings, the volume resulting from only the last two measurements is used, however the relative standard deviation of the mean for the first series is utilized to develop weights for regression analysis.

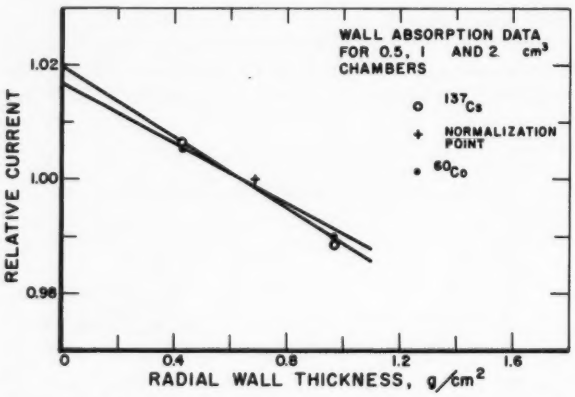

FIGURE 5. *Relative ionization current per unit volume for the small chambers plotted against radial wall thickness.*

Due to the different internal chamber dimensions, each measurement must be corrected for recombination. The data are weighted as described in the text and the line drawn is the regression line based on the weighted data.

TABLE 3. *Summary of wall-absorption correction factors*

Chamber	Radial wall thickness ($g \cdot cm^{-2}$)	Correction to zero wall		Correction per unit thickness ($\% \cdot g^{-1} \cdot cm^2$)	
		^{60}Co	^{137}Cs	^{60}Co	^{137}Cs
50–1	0.632	1.0227	1.0272	3.59	4.30
50–2	.880	1.0319	1.0384	3.63	4.36
50–3	1.060	1.0387	1.0467	3.65	4.40
30	0.653	1.0220	1.0249	3.37	3.81
10	.647	1.0216	1.0260	3.34	4.02
1	.688	1.0168	1.0199	2.44	2.89

shells to each of the chambers, show that the slopes of the chamber reading versus wall thickness curves for these chambers are consistent with those determined for the larger chambers, but greater than the slope determined by using the small chambers as a group. Since the chamber halves are joined by the tongue-in-groove method, with the juncture around the chamber middle (opposite a large fraction of the volume for the small chambers), it appears appropriate to use the chambers as a group to determine a wall correction. In this way, the effect of structural features on the small chamber exposure determinations will be minimized.

5. Recombination Corrections

For accurate measurement of gamma-ray beams with ionization chambers, it is required that all the charge produced in the chamber volume be collected and measured. This ideal is approached closely by the spherical chambers even though the geometry of the combined cylindrical electrode and spherical chamber produces nonuniform electric field strengths within the chamber volume. Tests for recombination of ions, at a particular exposure rate, are carried out by increasing the chamber collection potential until the current measured for potential V is at most only a few tenths percent greater than the current measured for $V/2$. Methods of treating ionization data have been developed which take into consideration the recombination mechanisms involved and which make possible the estimation of corrections in a consistent manner. Analysis of recombination characteristics for a particular chamber may be facilitated by plotting the reciprocal of the ion currents against the negative powers of the collecting potentials V^{-1} or V^{-2} [19]. Neither provides straight-line extrapolation if small corrections, e.g., of the order of tenths of one percent, are being sought and it is often necessary to estimate the correction by extrapolating a curve. If sufficient data are available, recombination corrections for a particular operating potential can be estimated and tabulated as a function of exposure rate $\dot{X}$. These data can then be used to determine constants for an equation which includes $\dot{X}$ explicitly.

In theory, columnar and volume recombination vary as V^{-1} and V^{-2} respectively. Both effects being present, and each being small, the total correction can be considered to be the product $\left(1+\frac{C}{V}\right)\left(1+\frac{A\dot{X}}{V^2}\right)$ with only volume recombination dependent on $\dot{X}$. The values of the constants for the 50-cm³ chambers which have inside diameters of about 4.6 cm and collection electrodes 4 cm in length and 0.3 cm in diameter, are:

$$A = 7200\mathrm{V}^2\mathrm{R}^{-1}\mathrm{s}$$

$$C = 0.66\mathrm{V}.$$

Recombination corrections for all other chambers were determined as required, by graphical extrapolation of reciprocal current versus reciprocal collection-potential curves, where intercomparisons of exposure-rate data were of interest; however, general relationships were not established as in the case of the 50-cm³ chambers. In all cases, the chambers were operated with sufficiently high collection potentials so as to make the saturation corrections not greater than a few tenths percent.

The corrections for recombination are based on the averages of chamber currents measured for both polarities of collection potential. This procedure was observed in obtaining all measurements in order to eliminate the contribution of extra-cameral ionization to the chamber ionization current.

6. Stem Leakage and Scatter Corrections

In the ideal case, the current measured by the electrometer system is generated exclusively by the electrons which ionize the gas in the chamber cavity. This ideal is not quite realized in practice since the radiation induces leakage currents in the supporting stem, and scatter from the stem adds to the chamber reading. Both of these effects are small. Studies using test stems show that induced stem-leakage currents, for the range of exposure rates used in these standardization measurements, are less than 0.1 percent of the chamber current and negligible where measurements are averaged for both positive and negative collection potentials.

The effect of stem scatter on the chamber readings is measured by using an identical stem in contact with the chamber on the side opposite the supporting stem. The stem-scatter corrections determined for all chambers are given in table 5. The corrections are small but tend to increase as the chamber size decreases. This is expected since the material immediately adjacent to the chamber is most important for this effect and the relative size and the proximity of the scatterer are greater for the smaller chambers.

TABLE 5. *Stem-scatter corrections for ^{137}Cs and ^{60}Co gamma rays*

Chamber	^{137}Cs	^{60}Co
1	0.996	0.998
10	.998	.999
30 and 50	.999	.999

7. Stopping-Power Corrections

The stopping-power correction required is the ratio of the weighted mean stopping powers for carbon and for air where the weights are based on the slowing-down electron spectrum generated by the gamma rays. The value of the stopping power depends, among other things, on the mean excitation energy, I, for the material of interest. Ratios of the weighted mean stopping-power of carbon to that of air, $1/\bar{f}$, provided by Boutillon [20][6] are used at this time at NBS. In

[6] Details regarding the calculation of $\bar{f}$ are given by Boutillon in [30] where different mean excitation energies for carbon and air are used.

the calculation of $\bar{f}$, $I_c = 78$eV and $I_{air} = 86.8$ eV [21], and the stopping powers used in the weighting procedure are restricted to those for electrons with energies exceeding some energy limit Δ. The limiting energy is related to the cavity chamber dimensions. The energy limits were computed at NBS using the average linear intercepts [22], $\bar{L} = 4/3\ r$, for chambers with radii r, and the assumption that the projected range is about 75 percent of the "continuous-slowing-down-approximation" path length [21] for electrons in air at standard temperature and pressure. The stopping-power ratios are given in table 6 along with a value of Δ for each chamber.

TABLE 6. *Mass stopping-power ratios of carbon to air, $1/\bar{f}$, with $I_c = 78$ eV and $I_{air} = 86.8$ eV*

Chamber	Δ (keV)	Stopping power ratio [a]	
		^{60}Co	^{137}Cs
1	24	1.007	1.014
10	37	1.006	1.014
30	46	1.006	1.013
50	50	1.006	1.013

[a] The stopping-power ratios used prior to May 1, 1972 were about 0.3 percent and 0.6 percent lower for ^{60}Co and ^{137}Cs respectively. The values of I used were $I_c = 76.4$ eV and $I_{air} = 80.5$ eV.

8. Mass Energy-Absorption Coefficient Ratio

The energy-absorption coefficient ratio converts data for photon energy absorbed in carbon to photon energy absorbed in air. The latest data published by Hubbell for $_m\mu_{en}$ [10] tabulates coefficients with three significant figures for carbon and for air, starting at 0.6 MeV. The ratio of the coefficients is within 0.1 percent of unity over the tabulated energy range of 0.6 to 2.0 MeV. The constancy of this ratio is, of course, one of the reasons for choosing carbon as the wall material for the cavity chamber. However, the spectra in the ^{60}Co and ^{137}Cs gamma-ray beams include energies below the minimum tabulated energy and, especially in the case of ^{137}Cs, weighting of $_m\mu_{en}$ in accord with the beam spectra could not be carried out. A special calculation, performed by Hubbell, extending the energy range down to 10 keV and increasing the number of significant figures for the coefficients, made it possible to take the entire spectrum into consideration for both ^{60}Co and ^{137}Cs. The data of Costrell [23, 24] most representative of the NBS beam spectra were used to determine weighted mean values of $_m\mu_{en}$ with the weighting performed in accord with the energy-fluence distribution of the photon beams. The ratios of the weighted means are 0.9995 for ^{60}Co and 0.9997 for ^{137}Cs. Hubbell's ratios, in the energy region of interest, are given in table 7. The ratios are believed to be known only to 0.5 percent in the region from 10 keV to 100 keV while they are believed to be known to 0.1 percent or better in the region from 0.1 MeV through 1.33 MeV. Since only a negligible fraction of the total energy in the beams is below 0.1 MeV, the uncertainty for the ratios of the weighted mean energy-absorption coefficients, for ^{137}Cs and ^{60}Co gamma rays, is taken as 0.1 percent.

TABLE 7. *Mass energy-absorption coefficient ratio, air to carbon*

Photon energy (MeV)	$\frac{(_m\mu_{en})_{air}}{(_m\mu_{en})_c}$
0.05	1.7415
.10	1.0847
.15	1.0199
.20	1.0069
.30	1.0014
.40	1.0000
.50	0.9998
.662	.9995
1.00	.9994
1.17	.9994
1.33	.9994

9. Measurements

Although beam measurements with the chambers were carried out at various times and at various source-to-chamber distances in the course of establishing the corrections required, the data which form the basis for the ^{60}Co and ^{137}Cs exposure standards were taken at 2 m from the sources.

The intercomparison of the cavity chambers was carried out under measurement conditions which minimized disturbing influences to the greatest possible extent. The beams used were uniform across the chamber dimensions to within the accuracy of careful densitometric measurement. The average film density over the smallest and largest chamber diameters was found to differ by less than 0.1 percent. The inverse square nonuniformity for the largest chamber (radius about 2.5 cm) at the measurement distance of 2 m was less than 0.02 percent in the direction perpendicular to the beam. In the direction parallel to the beam, the difference between the chamber response for a nonuniform beam (inverse square), and the chamber response assuming uniform irradiation, is 0.005 percent as calculated from the Spiers equation [25].

Although the variation of beam intensity over the range of chamber sizes is unimportant according to the criteria established above, the influence of source-chamber distance was investigated by comparing two chambers with inside diameters of 16 mm and 46 mm (2 and 50–1, respectively) at three distances from a ^{60}Co source. The distances chosen bracket the position used for the chamber intercomparison. The data given in table 8 show excellent agreement in the ratios of chamber readings, indicating there is no significant distance dependence due to chamber size for source-chamber distances of interest in these investigations. The geometrical center was taken as the position of the chamber for all measurements.

Two sets of intercomparisons of the six chambers were carried out in the ^{60}Co beam. Each was performed within one day on two separate occasions. The largest difference, 0.1 percent, between the two measurements was for the smallest-volume chamber. Intercomparisons

TABLE 8. *Ratios of currents for 46-mm and 16-mm diameter chambers*

Distance (cm)	Current ratios	Ratio corrected for recombination
75	25.17	25.20
150	25.19	25.20
300	25.19	25.20

of the chambers for ^{137}Cs gamma rays were carried out in the same manner as for ^{60}Co but the measurements occupied a longer period of time since the corrections for each chamber were determined at the same time. The longer half-life for ^{137}Cs reduces the importance of concurrent measurements for the intercomparison of the chambers and only small decay corrections were required. The largest difference between the two sets of ^{137}Cs gamma-ray measurements for each chamber was 0.06 percent.

A summary of the correction factors pertinent to each chamber for the two gamma-ray beams is given in table 9. The last column in the table is the product of all the corrections for a particular chamber. The measurements at 2 m from the sources and utilization of these factors produce exposure-rate data which are in excellent agreement as shown in table 10 where the result for each chamber is compared to the mean.

If the data from each of the chambers were considered to be equally uncertain, the inverse of the ratios given in table 10 could be used as a small additional correction to bring the data for each chamber into agreement with the mean value. Since this is not the case, it appears that a weighting procedure based on the magnitude of the uncertainty for each chamber is appropriate.

An effort to quantify these uncertainties has been made by estimating upper limits for nonstatistical quantities and combining them with uncertainties based on standard deviations of the mean for data which can be treated statistically. The upper limits assigned to the uncertainties are, in most cases, arbitrary and are based on the judgment of the authors.

TABLE 10. *Ratios of exposure rates, as determined with each ionization chamber, to the unweighted mean exposure rate* ($7 \times 10^{-3} R \cdot s^{-1}$)

Chamber	^{137}Cs	^{60}Co
1	1.0033	1.0025
10	.9998	.9998
30	.9973	.9990
50–1	.9999	.9994
50–2	.9999	.9995
50–3	1.0000	.9998

The factors considered, and the related estimated uncertainties, are listed in table 11 where Δt and ΔV

TABLE 11. *Uncertainties, S, in percent, for all factors in the intercomparison of the six NBS cavity ionization chambers. The uncertainties for* Δt *and* v *are based on standard deviations of the means brought to a 95 percent confidence level. The uncertainty for the stopping-power ratio takes into consideration only the variation with chamber size and this and all other uncertainties are estimated upper limits*

	Ionization chamber					
Factor	1	10	30	50–1	50–2	50–3
ΔV	0.020	0.020	0.020	0.020	0.020	0.020
Δt	.056	.021	.027	.011	.015	.014
v	.200	.327	.043	.017	.052	.064
T	.03	.03	.03	.03	.03	.03
P	.01	.01	.01	.01	.01	.01
k_w	.30	.10	.10	.10	.10	.10
Δk_{sp}	.04	.04	.04	.04	.04	.04
k_e	.02	.02	.02	.02	.02	.02
k_{ss}	.02	.02	.02	.02	.02	.02
k_a	.03	.03	.03	.03	.03	.03
k_R	.00	.00	.00	.01	.01	.01

are the time and potential changes for the Townsend balance measurements. P and T are the pressures and temperatures during the measurements, v represents the chamber volumes, and the next four factors are corrections for the wall effect, stopping power, recombination and stem scatter. The last two factors are

TABLE 9. *Summary of correction factors for each ionization chamber*

Chamber	Wall absorption	Stopping-power ratio	Energy-absorption coefficient ratio	Stem scatter	k_{CEP}	Product of correction factors
			^{137}Cs gamma rays			
1	1.0199	1.0143	0.9997	0.9964	0.9990	1.0294
10	1.0260	1.0138	.9997	.9979	.9990	1.0366
30	1.0249	1.0135	.9997	.9992	.9990	1.0365
50–1	1.0272	1.0133	.9997	.9987	.9990	1.0382
50–2	1.0384	1.0133	.9997	.9987	.9990	1.0495
50–3	1.0467	1.0133	.9997	.9987	.9990	1.0578
			^{60}Co gamma rays			
1	1.0168	1.0069	0.9995	0.9982	0.9950	1.0164
10	1.0216	1.0064	.9995	.9992	.9950	1.0217
30	1.0220	1.0062	.9995	.9992	.9950	1.0219
50–1	1.0227	1.0061	.9995	.9990	.9950	1.0223
50–2	1.0319	1.0061	.9995	.9990	.9950	1.0315
50–3	1.0387	1.0061	.9995	.9990	.9950	1.0383

corrections for lack of reproducibility of chamber position in the direction of the beam, k_a, and for nonuniformity of the beam in a radial direction, k_R.

The uncertainties listed in table 11 were added in quadrature, and the reciprocals of these sums were used as relative weighting factors to compute a weighted mean exposure rate, $\bar{X}$, at the chamber intercomparison position. The values of the relative weighting factors are given in table 12. The ratio of

TABLE 12. *Sums of the squares of the uncertainties in table 11, and the weighting factors, w_j, for each ionization chamber*

Chamber	ΣS_j^2	w_j
1	0.1378	0.02928
10	.1221	.03304
30	.01728	.2335
50–1	.01521	.2653
50–2	.01773	.2276
50–3	.01909	.2114

TABLE 13. *Chamber correction k_{std} required to bring exposure-rate measurements for each chamber into agreement with the weighted mean exposure rate $\bar{X}$.*

Chamber	^{60}Co	^{137}Cs
1	0.9970	0.9962
10	.9997	.9997
30	1.0005	1.0022
50–1	1.0002	0.9996
50–2	1.0003	.9996
50–3	0.9998	.9995

the weighted mean exposure rate to the exposure rate determined with a particular chamber, j, provides a correction factor, ${}_jk_{std}$, for that chamber to the weighted mean thus,

$$ {}_jk_{std} = \frac{\sum w_i \dot{X}_i}{\dot{X}_j}. $$

Values of ${}_jk_{std}$ are given in table 13.

The product of the chamber corrections given in table 9, the correction to the weighted mean exposure rate given in table 13, and a recombination correction provide a total correction factor for each chamber. This factor, when used with measurement data, allows use of any of the above chambers to standardize a ^{60}Co or ^{137}Cs gamma-ray beam. The recombination correction, of course, may be rate dependent and then must be determined at the time of measurement or from previous data.

10. Accuracy

As stated above, an attempt was made to optimize all conditions which would influence the measurements. The degree of success can in part be judged by the agreement to within 0.1 percent of two sets of measurements at different times for several chambers.

Estimates of the uncertainties associated with each chamber are given in table 11 from which weights were computed based on those factors affecting the relationship of one chamber to another. Not included in this tabulation are uncertainties for factors common to all chambers such as the mass energy-absorption coefficient ratio, the reduction in the wall-absorption correction to account for the CEP effect, and the uncertainty in the stopping-power ratio, since only the uncertainty in the restricted ratio due to variation in chamber size was considered. The uncertainty for k_{std} must also be included in estimating the accuracy of an exposure-rate determination when any one of the chambers is used since

$$ \bar{\dot{X}} = {}_j\dot{X}_j k_{std} $$

where the subscript j indicates a particular chamber. The uncertainty for ${}_jk_{std}$ can be computed using the usual rule for the propagation of error and the relation

$$ {}_jk_{std} = \sum_i w_i x_i / x_j $$

where the x_i are proportional to the exposure rates as determined using each of the chambers. The x_i are independent and uncorrelated and $\sum_i w_i = 1$. The general equation for the uncertainty in ${}_jk_{std}$ is

$$ {}_jS\ (k_{std}) = \left[(1 - w_j)^2 S_j^2 + \sum_i{}' \ w_i^2 S_i^2 \right]^{1/2} $$

where the prime on the summation sign means the sum is taken over all i except $i = j$. The values for S and w given in table 12 were used to compute the uncertainties for k_{std} given in table 14.

TABLE 14. *Uncertainty of k_{std} for each ionization chamber*

Chamber	$S(k_{std})$
1	0.37
10	.34
30	.12
50–1	.11
50–2	.12
50–3	.12

At the present time the correction for the effect of moisture in the air in the cavity chamber is considered to be equal to unity [14]. However, the work of Niatel [26] and Guiho [27] both indicate the relative humidity affects the ionization measurements. An estimate of the upper limit uncertainty for this effect is taken to be 0.3 percent.

The uncertainty in the unrestricted stopping power is estimated by Berger [21] to not exceed 2 percent. This estimate is based on a wide range of materials and energies, and the use of certain I values and a

theoretical equation. Agreement between theoretical and experimentally determined stopping-power ratios is given as 0.1 percent [28] but the experimental uncertainty is given as 0.5 percent. It seems, therefore, that a conservative estimate for the upper limit of the uncertainty for the mass stopping-power ratio is 0.5 percent when the cavity gas is air and the wall material is nearly air-equivalent.

The uncertainty in the ratio of the mass energy-absorption coefficient has been estimated by Hubbell [29] to be less than 0.05 percent. His estimate is based on the difference between the coefficients calculated by the Klein-Nishina equation with and without corrections for electron binding and bremstrahlung losses. An uncertainty of 0.1 percent is arbitrarily assigned to this ratio.

The overall uncertainty in the NBS measurement of ^{137}Cs or ^{60}Co gamma radiation in terms of exposure is computed by adding in quadrature the upper limits of the non-statistical uncertainties with the standard deviations of the means of the statistical uncertainties brought to a 95 percent confidence level. The data used for this computation is given in table 15 with the statistical uncertainty for Δt taken from the data resulting from the intercomparison of the six chambers (table 11). The uncertainty for the recombination correction is for the exposure rate used in the intercomparison. The uncertainties for the chamber volumes, zero-wall corrections and stem-scatter corrections are included in the uncertainty for k_{std} for each chamber (values given in table 14).

TABLE 15. *Uncertainties in the determination of NBS exposure rates* ($\dot{X}$)

Quantity or factor	Percent uncertainty (S)
Potential	0.02
Capacitance	.02
Temperature	.03
Pressure	.10
Relative humidity	.30
Stopping-power ratio	.50
Mass energy-absorption coefficient	.10
CEP correction	.20
Distance (axial)	.03
Recombination	.02
Time	(see table 11)
k_{std}	(see table 14)

The overall uncertainty for measurement of NBS exposure rates is determined from the data in table 15 added in quadrature. These sums are given for each chamber in table 16.

It should be pointed out that the overall uncertainty data in table 16 have been computed using statistics derived from measurements at an exposure rate of about 7×10^{-3} R · s^{-1}. For other exposure-rate conditions, where the statistics for time measurement (Δt), or the uncertainty for recombination loss differs significantly from the values used, recalculation of the uncertainties might be necessary.

TABLE 16. *Overall uncertainty for NBS exposure rates*

Chamber	Uncertainty (percent)
1	0.74
10	.72
30	.65
50–1	.64
50–2	.65
50–3	.65

11. Summary and Conclusions

The foregoing provides a complete description of the cavity ionization chambers, their relationship to one another and to the weighted average of their exposure-rate data which is taken as the NBS standard. Once the correction to the standard has been established for each chamber, any of the chambers can be used to calibrate a ^{60}Co or ^{137}Cs gamma-ray beam.

The uncertainties associated with each of the factors entering into the determination of exposure rates, for ^{60}Co and ^{137}Cs gamma-ray beams, are given and the total estimated uncertainty for measurements with each of the chambers is computed for representative measurement conditions.

The ratio of the cavity-chamber to free-air-chamber exposure-rate determinations for ^{60}Co gamma rays may be $(1.019)(0.993) = 1.012$ if the ratios of measurement data given in table 1 hold. The difference of 1.2 percent is just a little less than the sum of the uncertainties for each method of measurement. A correction to the cavity chamber data for scattering in the chamber walls would reduce the cavity-chamber, free-air-chamber difference but would increase the differences between other, more recent, comparisons.

The difficulties experienced with the large cylindrical chamber have been more circumvented than solved, however the close agreement between the six spherical chambers of greatly different size gives good confidence in the new exposure standard. Moreover, the agreement of the new exposure standard for ^{60}Co with other standards [12] and other physical measurements [13] is within 0.4 percent.

12. Appendix

The procedure in standardizing a gamma-ray beam at NBS is to calibrate the beam at several distances from the source and then fit the data to a suitable function which will allow accurate computation of exposure rates at selected distances, or of distances for selected exposure rates. The equation used for this purpose is derived by using the inverse square law with corrections for air attenuation and buildup. A cubic equation has been found adequate for the correction terms, giving an equation of the form

$$\dot{X}\, D^2 = K_1 \left[1 + K_2 D + K_3 D^2 + K_4 D^3\right]$$

where $D = S + S_0$. The distances read on the scale,

S, are adjusted by the term S_0 to make D the distance from a point in the beam to an effective center of the source.

The values of S_0 and the K_i were determined for each calibration range using a computer program for non-linear least-squares function fitting (SAAM) developed by Berman and Weiss.[7] The constants for each of the sources are given in table 17.

TABLE 17. *Constants for exposure-rate versus distance equation for five calibration ranges as of December 31, 1973*

Source	S_0 (cm)	K_1 ($mR \cdot s^{-1} \cdot m^2$)	10^3K_2 (m^{-1})	10^3K_3 (m^{-2})	10^3K_4 (m^{-3})
B036 – ^{137}Cs	27.91	97.572	46.23	−26.05	4.898
B015A – ^{137}Cs	−0.71	2.6495	−8.945	0.8528	0
B021A – ^{137}Cs	−.41	25.328	−3.889	−.1139	0
B015B – ^{60}Co	−.14	2.5178	−2.804	−.2278	0
B021B – ^{60}Co	−.53	22.387	−0.9036	−1.279	0

Using the constants given in table 17, the agreement between exposure rates determined from the equation and the measured exposure rates is, on the average, 0.01 percent.

The authors wish to acknowledge that they have benefitted greatly from the thoughtful and detailed comments of H. O. Wyckoff, Robert Loevinger, and W. B. Mann in the preparation of this paper.

13. References

[1] Design of free-air ionization chambers, Nat. Bur. Stand. (U.S.), Handb. 64, 16 pages (Revised July 1969).
[2] Ritz, V. H., Standard free-air chamber for the measurement of low energy x-rays (20 to 100 kilovolts-constant-potential), J. Res. Nat. Bur. Stand. (U.S.), **64C** (Eng. and Instr.), No. 1, 49–53 (Jan.–Mar. 1960).
[3] Lamperti, P. J. and Wyckoff, H. O., NBS free-air chamber for measurement of 10 to 60 kV x-rays, J. Res. Nat. Bur. Stand. (U.S.), **69C** (Eng. and Instr.), No. 1, 39–47 (Jan.–Mar. 1965).
[4] Gray, L. H., An ionization method for absolute measurement of gamma-ray energy, Proc. Roy. Soc. **A156**, 578 (1936).
[5] International Commission on Radiological Units, Report 19, Radiation Quantities and Units, Issued July 1, 1971, p. 8.

[7] The program was developed by M. Berman and M. F. Weiss of the National Cancer Institute, National Institutes of Health, Bethesda, Md. The program is stored in the NBS computer and was made available to the authors for these computations.

[6] Wyckoff, H. O., Measurement of cobalt-60 and cesium-137 gamma rays with a free-air chamber, J. Res. Nat. Bur. Stand. (U.S.), **64C** (Eng. and Instr.), No. 2, 87–97 (April–June 1960).
[7] Attix, F. H. and Ritz, V. H., A determination of the gamma-ray emission of radium, J. Res. Nat. Bur. Stand. (U.S.), **59**, 293–305 (Nov. 1957) RP2801.
[8] Myers, I. T., LeBlanc, W. H., Fleming, D. M., and Wyckoff, H. O., An Adiabatic Calorimeter for High Precision Source Standardization and Determination of $\bar{W}$ (Air). Document HW–SA–2165, Hanford Atomic Products Operation, Richland, Washington, March 1, 1961.
[9] National Bureau of Standards Handbook 85, Physical Aspects of Irradiation. Page 11, March 31, 1964.
[10] Hubbell, J. H., Photon cross sections, attenuation coefficients and energy absorption coefficients from 10 keV to 100 GeV, Nat. Stand. Ref. Data Ser. 29, Nat. Bur. Stand. (U.S.), 85 pages (August 1969).
[11] Loftus, T. P., Standardization of cesium-137 gamma-ray sources in terms of exposure units (Roentgens), J. Res. Nat. Bur. Stand. (U.S.) **74A** (Phys. and Chem.), No. 1. (Jan.–Feb. 1970).
[12] Niatel, M. T., and Loftus, T. P., to be published.
[13] Petree, B., Humphreys, J. C., Lamperti, P. J., Loftus, T. P., and Weaver, J. T., to be published.
[14] Loftus, T. P., Petree, B. and Weaver, J. T., Radiology, **86**, 1966, p. 149.
[15] Report of the International Commission on Radiological Units and Measurements (ICRU), Nat. Bur. Stand. (U.S.), Handb. 78, 99 pages (Jan. 1959), p. 19.
[16] National Bureau of Standards Handbook 85, Physical Aspects of Irradiation, page 2 (March 31, 1964).
[17] Whyte, G. N., Principles of Radiation Dosimetry (John Wiley and Sons, Inc. New York, 1959), p. 64.
[18] Roesch, W. C., Dose for nonelectronic equilibrium conditions, Radiation Research, **9**, 399 (1958).
[19] Boag, J. W., Radiation Dosimetry (Academic Press, New York, 1966, Vol. II, Chap. 9), pp. 12 and 22.
[20] Boutillon, M., Bureau International des Poids et Mesures, 92310 Sevres, France, private communication.
[21] Berger, M. J., and Seltzer, S. M., Tables of Energy Losses and Ranges of Electrons and Positrons. NASA SP–3012, 1964 (Available from the Clearinghouse for Scientific and Technical Information, Springfield, Va.)
[22] Tomkieff, S. I., Nature **155**, 24 (1945).
[23] Costrell, L., Scattered radiation from large ^{60}Co calibration sources, Health Phys. **8**, 261 (1962).
[24] Costrell, L., Scattered radiation from large ^{137}Cs sources, Health Phys. **8**, 491 (1962).
[25] Spiers, F. W., British Journal of Radiology, **14**, 147 (1941).
[26] Niatel, M. T., C. R. Acad. Sci. Paris, **268**, 1650–1653, Series B, June 22, 1969.
[27] Guiho, J. P., Pavlicsek, I., Ostrowsky, A., et Goenvec, H., Influence de l'état hygrometrique de l'air sur l'ionization produite par les rayonnements X ou γ. C. R. Acad. Sci. Paris, t.278 (14 janvier 1974), Série B–69.
[28] NCRP, Stopping powers for use with cavity chambers, Nat. Bur. Stand. (U.S.) Handb. 79 (Sept. 1961).
[29] Hubbell, J. H., private communication.
[30] Boutillon, M., and Niatel, M. T., A study of a graphite cavity chamber for absolute exposure measurements of ^{60}Co gamma rays, Metrologia **9**, 139–146 (1973).

(Paper 78A4–827)

JOURNAL OF RESEARCH of the National Bureau of Standards—A. Physics and Chemistry
Vol. 78A, No. 4, July–August 1974

Investigation of Freezing Temperatures of National Bureau of Standards Aluminum Standards*

George T. Furukawa

Institute for Basic Standards, National Bureau of Standards, Washington, D.C. 20234

(March 29, 1974)

The design of a high-precision furnace for investigating the freezing points of metals up to 700 °C or higher is described. The freezing points of aluminum samples of nominally 99.999 percent purity from two batches were compared in terms of the ratio $R(\mathrm{Al})/R(\mathrm{TP})$, the ratio of the resistance of the platinum resistance thermometer at the aluminum freezing point to that at the triple point of water. The average standard deviation of measurements of the ratio $R(\mathrm{Al})/R(\mathrm{TP})$ obtained on six specimens corresponds to ± 0.40 mK, while the average standard deviations of $R(\mathrm{Al})$ and $R(\mathrm{TP})$ correspond to ± 0.17 mK and ± 0.14 mK, respectively. (The variations in the measurements of $R(\mathrm{TP})$ are amplified by 3.4 in the ratio $R(\mathrm{Al})/R(\mathrm{TP})$.) The spread of the mean $R(\mathrm{Al})/R(\mathrm{TP})$ obtained for five out of the six specimens corresponds to 0.51 mK; the deviation of the mean $R(\mathrm{Al})/R(\mathrm{TP})$ of the sixth specimen from the mean $R(\mathrm{Al})/R(\mathrm{TP})$ of the five specimens corresponds to -1.31 mK. (The sixth specimen may have been contaminated during the assembly of the freezing-point cell or the original sample bar was inhomogeneous.) The results show that aluminum can provide a freezing point (near 660 °C) that is at least as reproducible as the freezing point of antimony (near 631 °C)

Key words: A–C bridge; aluminum; aluminum point; fixed point; freezing point; IPTS–68; platinum resistance thermometer.

1. Introduction

The upper temperature limit of the platinum resistance thermometer (prt) range of the International Practical Temperature Scale of 1968 (IPTS–68) [27][1] is 630.74 °C and one of the reference temperatures for calibrating a standard platinum-rhodium alloy and platinum thermocouple that extends the temperature scale upward on the IPTS–68 is 630.74 °C, as determined by a prt. When no allowance is made for loss of insulation in the standard prt with mica insulation, the spread among the prt's at 630.74 °C could be 0.01 K or more [19]. In addition, the calibration of the prt is based on the measurements at the triple point of water (TP) and the freezing points of tin and zinc; any error in calibration of the prt would be greatly amplified by the extrapolation to 630.74 °C [23]. This uncertainty could be reduced by including a fixed point at the upper temperature limit of the prt range in the definition of the temperature scale for prt's. Furthermore, the quality of reproducibility of the IPTS–68 in the region of the upper temperature limit of the prt range can be better evaluated by employing highly reproducible fixed points in conjunction with prt's constructed of insulators better than mica, which begins to liberate a significant amount of water starting from about 500 °C. With prt's insulated with mica the lower reproducibility of the IPTS–68 at the higher temperatures could be principally from the loss of electrical insulation and to a lesser degree from changes in the platinum [1].

The freezing point of aluminum, a secondary reference point which is assigned 660.37 °C on the IPTS–68, has been used for many years in calibrating thermocouples [24]. The freezing point of antimony, another secondary reference point which is assigned 630.74 °C on the IPTS–68, is also used for calibrating thermocouples. Thus, the freezing point of antimony is very close and that of aluminum is not far from the junction of the prt and thermocouples ranges of the IPTS–68. As a part of the effort at the National Bureau of Standards (NBS) to maintain and develop the IPTS–68, a series of experimental studies is in progress to determine the reproducibility of the IPTS–68 and to find better means to define temperature scales. This paper presents the investigation of the reproducibility of the freezing point of aluminum. The investigation of the reproducibility of prt's in the region of the aluminum point will be a topic for future work; better prt's must be constructed first.

Aluminum was selected first for the investigation because it was considered superior to antimony for a number of reasons. Aluminum is much more abundant than antimony and, because of the greater technologic importance of aluminum, it is available in greater amounts at high purity and at lower cost. At the

*This work was supported in part by the Office of Standard Reference Materials, Institute of Materials Research, National Bureau of Standards.

[1] Figures in brackets indicate the literature references at the end of this paper.

freezing point the vapor pressure of aluminum is about 2×10^{-8} torr whereas that of antimony is about 0.2 torr [21], and aluminum is less toxic than antimony. The thermal diffusivity of liquid and solid aluminum at its freezing point was estimated to be many times greater than that of liquid and solid antimony at its freezing point [2, 6, 9, 22]. Liquid aluminum supercools 1 or 2 K, while liquid antimony can supercool more than 20 K [18]; therefore, the preparation required to realize the freezing point of aluminum should be simpler than that of antimony.

2. Samples

The freezing-point investigations were conducted on aluminum samples from two batches. The samples as originally received at the Office of Standard Reference Materials (OSRM) of the NBS from the supplier were in the form of cylindrical rods about 91 cm long. Sample bars of batch 1558 were 3.2 cm diam; sample bars of batch 2571 were 3.8 cm diam. The samples had been purified by zone refining techniques and homogenized by melting together the different zone refined units. Bars of batch 1558 were made by casting in graphite molds, while those of batch 2571 were made by casting in alumina molds. The specimens of batch 1558 that were received for the freezing-point studies appeared to have in them specks of graphite. The specimens of batch 2571 appeared to contain a number of voids that were absent in specimens of batch 1558. The information supplied with batch 2571 suggests that the voids were caused by hydrogen that was dissolved in the liquid aluminum which on solidification expelled the hydrogen. The solubility of hydrogen at 1 atm pressure in aluminum at the freezing point is about 0.5 to 0.8 cm^3 per 100 g of the liquid and about 0.04 to 0.05 cm^3 per 100 g of the solid [2]. The solubility of hydrogen in solid aluminum is apparently less at the lower temperatures, the reported solubilities at 400 °C being about 0.003 to 0.004 cm^3 per 100 g [2]. (The above volumes of hydrogen are in terms of the gas at 1 atm pressure and at 20 °C.)

The chemical analyses given in the assay certificates that accompanied the samples from the supplier are summarized in table 1. The assay is based on spectrochemical analysis. Except for Fe, the analyses of the supplier for the two batches of aluminum are about the same. The mass spectrometric analysis of batch 2571 by P. J. Paulsen of the Analytical Mass Spectrometry Section of the Bureau, summarized also in table 1, shows that Fe and Zn are present in relatively high concentrations. The spectrochemical analysis apparently also did not detect the 0.2 ppm of Na that was detected by the mass spectrometric method. No element of mass greater than zinc was detected in the aluminum by the mass spectrometric analysis; the limit of detection by the method of some of the elements are listed in table 1.

If the worst case is considered, the analysis given in table 1 indicates that the aluminum of batch 2571 could be about 99.9993 percent pure. The analysis on batch 1558 indicates that the material to be 99.9998 percent pure; however, the analysis on batch 1558 is not as extensive as that on batch 2571. Other impurities not detected by the spectrochemical method may be present. These SRM samples are undergoing other analyses of chemical composition and measurements of physical properties. The presence of other impurities or the presence of certain impurities in greater amounts than indicated in table 1 may be revealed by these investigations.

TABLE 1. *Chemical analysis of the aluminum samples and the estimated depression of the freezing point by the impurities*

Element	Batch 1558	Batch 2571		Estimated effect from each impurity[d]
	Supplier ppm[a]	Supplier ppm[a]	NBS ppm[b]	mK/ppm
Ca	0.2	0.2		−0.6
Fe	0.5	0.1	1.4	−0.3
Mg	< 0.1	0.1	0.2	−0.6
Mn	0.1	0.2	[c] ≤ 0.3	−0.1
Si	0.3	0.3		−0.7
Cr	0.2		≤ 0.04	+0.2
Cu	0.2	0.1	≤ 0.1	−0.3
Ni			≤ 0.2	
Ti			≤ 0.05	
V			≤ 0.04	
Na			0.2	−0.7
Ga			≤ 0.06	
Zn			5	−0.2
Estimate of total effect of impurities	−0.57 mK	−0.47 mK	−1.7 mK	

[a] Based on spectrochemical analysis.
[b] Mass spectrometric analysis by P. J. Paulsen, Analytical Mass Spectrometry Section, NBS.
[c] The values preceded by the symbol ≤ indicate the upper limit of the elements not detected. These values were not included in determining the total change in the freezing point from the impurities.
[d] Estimated from phase diagram data [11].

M. B. Kasen of the Cryogenics Division of the NBS at Boulder, Colorado, determined the residual resistivity ratios (ratio of the resistance at 0 °C to that at 4.2 K) of samples taken from the ends, middle, and outer surfaces of the aluminum bars of batch 2571 [12]. Of the total of 45 specimens from 17 bars that were examined, only two specimens were not within the residual resistivity ratio (*RRR*) 5000 ± 250. These two specimens were found to have scattered porosity. The *RRR* measurements indicate that the aluminum sample bars of batch 2571 are fairly uniform. The ultra-purity aluminum samples (SRM–RM–1R and SRM–RM–1C) have the *RRR* values of about 16200 or 16600 [13], which suggests that the aluminum samples used in the present freezing-point measurements could be of somewhat lower purity.

Most phase diagrams in the vicinity of the pure components are based on extrapolation of observations at relatively high impurity concentrations and, in many cases, the undetected impurity may have been the

predominant source of the observed effect. Nevertheless, an attempt was made employing phase diagrams to estimate the possible effect of the impurities that were reported in the analyses of the two batches of aluminum. In estimating the effect, the effect of each impurity was assumed to be independent of the presence of the other impurities. The effect in mK/ppm of an impurity was estimated from the phase diagram data [11]. Table 1 summarizes the estimate of the freezing-point depression based on the spectrochemical analyses furnished by the supplier and on the mass spectrometric analysis. The values preceded by the symbol ≤ indicate in principle the sensitivity of the mass spectrometric method for the given element; the effect of the impurities at these values were not considered in the depression of the freezing point. The results of the estimate suggests that the freezing points of the two batches of aluminum samples could be 2 mK lower than the freezing point of pure aluminum. (The elements Na and Zn not detected by spectrochemical analysis in the sample from batch 1558 were assumed to be present to the same degree as found in the sample from batch 2571.)

3. Preparation and Assembly of the Aluminum-Point Cells

Figures 1, 2, and 3 show schematic drawings of three aluminum freezing-point cells that were assembled for the investigations described in this paper. Special precautions were observed in the handling of the aluminum samples to avoid contamination or altering their purity. High-purity graphite components were employed in containing the samples. The samples, each about 358 g, were received from the Office of the Standard Reference Materials of the NBS in the form of cylindrical rods enclosed in polyethylene bags. The samples of 3.2 cm diam were about 16.7 cm long; the samples of 3.8 cm diam were about 11.4 cm long. These samples had been cut from bars that were about 91 cm long with a carbide tipped tool and etched in a solution at a temperature of 190 to 200 °C consisting (by volume) of reagent grade phosphoric acid (15 parts), sulfuric acid (5 parts), and nitric acid (1 part). The samples were not identified with respect to the bars from which they were cut; therefore, the samples from different bars were considered identical for the present work.

The freezing-point cells were assembled as follows. The 3.2 cm diam samples were of convenient size such that they could be inserted directly in the crucible and the lid attached snugly at the top of the crucible. The graphite thermometer well, which was designed to slide slowly, under its own weight, through the central hole in the lid, was inserted by melting the sample by induction heating under vacuum. Figure 4 shows schemetically the arrangement for melting and inserting the thermometer well. The system was continuously pumped at high vacuum while gradually increasing stepwise the induction heating power. The pumping system was trapped with liquid nitrogen. The heating power was maintained constant with the crucible tem-

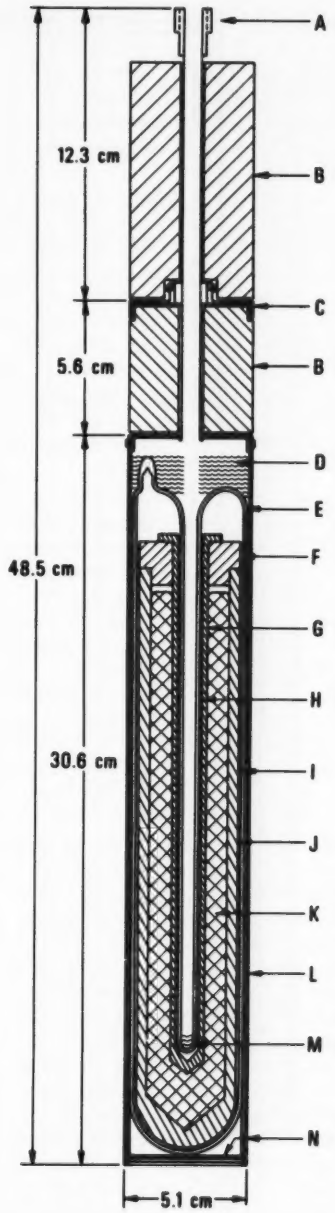

FIGURE 1. *Sealed aluminum-point cell (Type 1 cell).*

A. Thermometer guide tube (Inconel, 7.94 mm o.d. × 0.13 mm wall) with an adapter at the top for attaching a handle for lifting or lowering the cell into the furnace well.
B. Magnesia (MgO) block insulation.
C. Heat shunts (Inconel flange).
D. Fiberfrax insulation.
E. Fused quartz outer envelope (48 mm o.d. × 1.5 mm wall).
F. Graphite lid.
G. Graphite thermometer well.
H. Fused quartz thermometer well (precision bore (7.94 mm i.d.) and continuous with the outer envelope).
I. Fused quartz fiber, woven tape for cushioning.
J. Graphite crucible.
K. Aluminum sample.
L. Inconel case.
M. Fused quartz fiber pad for cushioning the thermometer.
N. Fiberfrax paper liner.

538-709 OL - 74 - 3

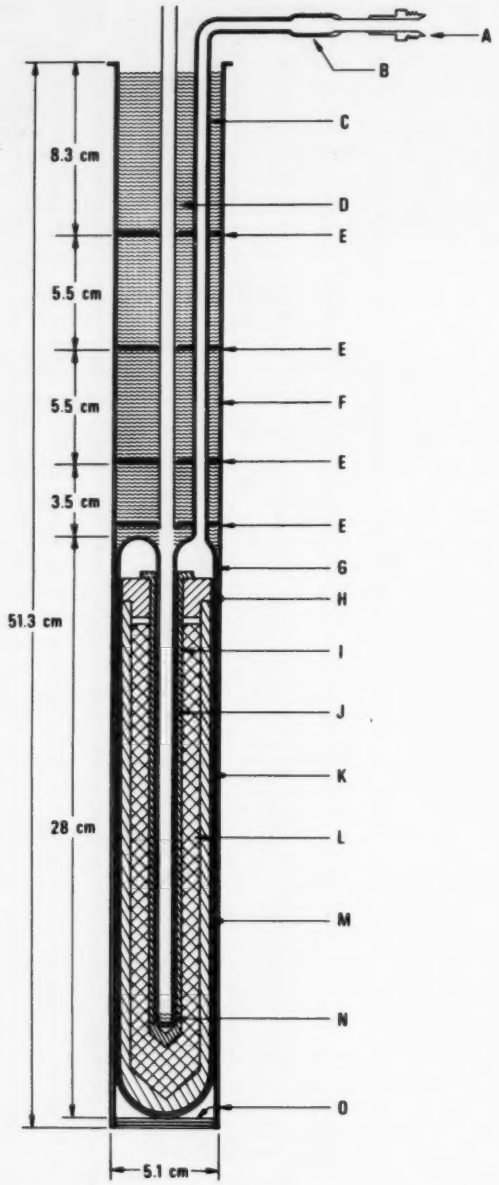

FIGURE 2. *Fused quartz aluminum-point cell with Inconel casing (Type 2 cell).*

A. Connection to high vacuum, purified argon gas source, and manometer (see fig. 5).
B. Fused quartz-to-Kover graded seal.
C. Fused quartz connecting tube (7.4 mm o.d. × 1 mm wall), outer surface matte finished to minimize radiation piping.
D. Thermometer guide tube (Inconel, 7.94 mm o.d. × 0.13 mm wall).
E. Heat shunts (Inconel disks).
F. Insulation, cut from Fiberfrax blanket.
G. Fused quartz outer envelope (48 o.d. × 1.5 mm wall).
H. Graphite lid.
I. Graphite thermometer well.
J. Fused quartz thermometer well (precision bore (7.94 mm i.d.) and continuous with the outer envelope).
K. Fused quartz fiber, woven tape for cushioning.
L. Aluminum sample.
M. Graphite crucible.
N. Fused quartz fiber pad for cushioning the thermometer.
O. Fiberfrax paper liner.

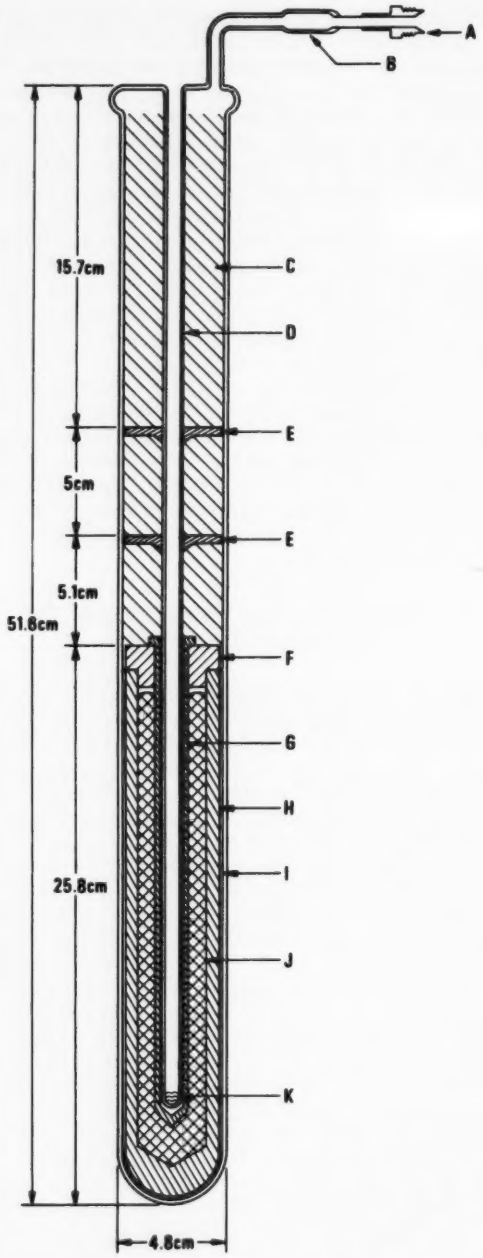

FIGURE 3. *Aluminum-point cell with fused quartz casing (Type 3 cell).*

A. Connection to high vacuum, purified argon gas source, and manometer (see fig. 5).
B. Fused quartz-to-Kovar graded seal.
C. Insulation, fused quartz wool.
D. Fused quartz thermometer well (precision bore 7.94 mm i.d. and continuous with the outer fused quartz envelope), outer surface matte finished to minimize radiation piping.
E. Heat shunts, graphite disks.
F. Graphite lid.
G. Graphite thermometer well.
H. Graphite crucible.
I. Fused quartz fiber, woven tape for cushioning.
J. Aluminum sample.
K. Fused quartz fiber pad for cushioning the thermometer.

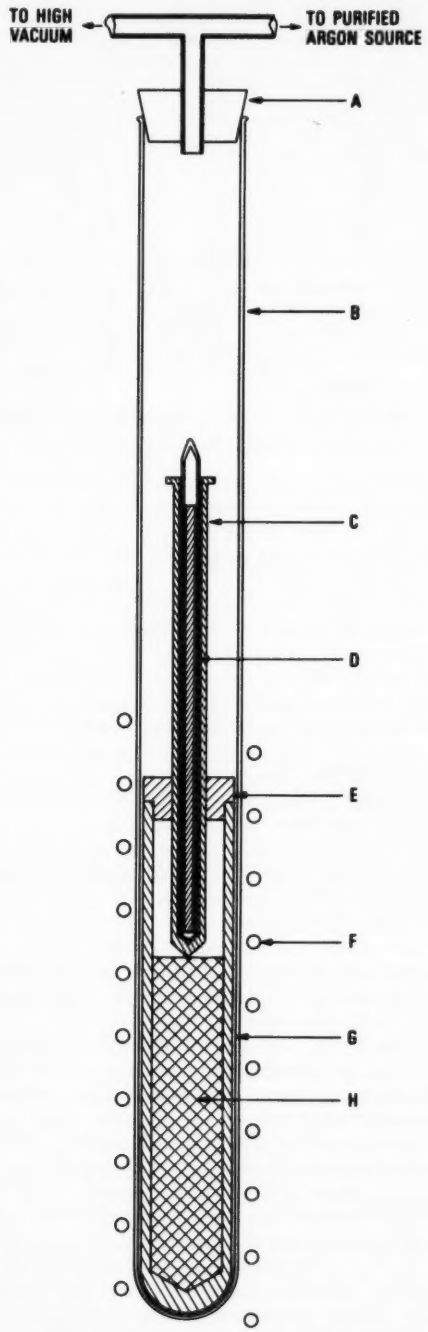

FIGURE 4. *Apparatus for inserting graphite thermometer well in the graphite crucible containing the molten aluminum sample.*

A. Silicone elastomer cap.
B. Fused quartz tube.
C. Graphite thermometer well.
D. Tungsten rod sealed in fused quartz tube.
E. Graphite lid.
F. Induction heater coils.
G. Graphite crucible.
H. Aluminum sample.

perature at approximately 600 °C (a slight red glow in the graphite crucible) for about 1 h at a pressure of about 0.01 torr or lower (1 torr = 1 mm Hg at 0 °C and at the standard gravity = 133.322 N/m² [20].) The heating power was then gradually raised stepwise until the aluminum sample began to melt and the thermometer well began to "sink" into the crucible. The buoyant force of the liquid aluminum was offset by the weight of the tungsten rod, sealed in fused quartz tubing, placed in the graphite thermometer well (see D, fig. 4). After the sample started to melt, the thermometer well sank into the desired position in the crucible within about 30 min. The heating power was then turned off, the sample allowed to cool, and the crucible and its contents were removed from the assembly after filling the apparatus with dried pure argon gas. The argon gas employed was 99.999 percent (5N) pure and was dried by passing through a trap cooled to the temperature of boiling oxygen.

The 3.8 cm diam aluminum samples were too large in diameter to be inserted directly into the crucible. The samples were melted into the crucibles from a high-purity graphite funnel following a vacuum pumping and induction heating procedure similar to that outlined above for inserting the thermometer well into the crucible containing the aluminum sample. (The apparatus and procedure for filling the crucible with the aluminum samples through a graphite funnel were the same as those employed previously with tin and zinc samples [8, 23].) After the crucible was filled with the aluminum sample, it was first cooled and the thermometer well was inserted by the procedure outlined earlier for the 3.2 cm diam samples.

For protection of the samples and ease of handling, the graphite crucibles containing the samples were enclosed in three types of fused quartz cells shown in figures 1, 2, and 3. The assembly procedure was as follows. (Henceforth, for convenience these cells will be referred to as types 1, 2, and 3, respectively.) The fused quartz envelope, with the central thermometer well of precision bore fused quartz, was made first to fit the graphite crucible as closely as possible. The outer tube was sawed apart near the top. The graphite crucible was then inserted using woven fused quartz fiber tape as a cushion between the crucible and the outer fused quartz envelope. Before the outer tube was resealed, either the fused quartz thermometer well or the outer tube was shortened so that when assembled the bottom of the fused quartz thermometer well would be about 3 mm above the bottom of the graphite thermometer well. (When the aluminum is melted the buoyant force of liquid aluminum causes the bottom of the graphite thermometer well to rest against the bottom of the fused quartz well so that during operation of the cell the thermal resistance of of the 3 mm gap will no longer exist.) The above allowance for the graphite thermometer well to rise 3 mm was made to compensate for any unknown differences in the thermal expansion of the graphite used to fabricate the thermometer well and the crucible.

The completely sealed type 1 cell shown in figure 1 had the same configuration as that of type 2 cell of figure 2 when the outer tube was sealed at the sawed junction. After pumping at high vacuum (10^{-5} torr near the diffusion pump; see figure 5 for the general arrangement of pumping and gas handling system) for three days with the cell at 670 to 675 °C, the cell was filled with purified argon gas and maintained at slightly above atmospheric pressure until the cell cooled to the ambient temperature. The cell was then immersed in an insulated container of water at a known temperature. After the cell reached an equilibrium temperature, the argon pressure in the cell was adjusted so that its pressure would be 1 atm when heated to the melting point of aluminum; the cell was then sealed at the location shown in figure 1. These type 1 cells were employed during the initial preliminary freezing-point experiments to gain experience and to determine the best operating conditions. Because of the uncertainty of the actual pressure at the freezing point, these cells were subsequently converted to the type 2 cell configuration shown in figure 2. (Although the effect of the pressure on the freezing point is expected to be relatively small, the temperature uncertainty due to the inability to determine the actual pressure was thought unnecessary.)

The completely sealed type 1 cell was inserted in an Inconel[2] tube (5.08 cm o.d. × 0.25 mm wall) using Fiberfrax paper strips for cushioning and for alining with respect to the thermometer guide tube that is shown in figure 1. Magnesia block insulation was machined to fit around the thermometer guide tube and to fit inside the furnace well.

The type 2 cell of figure 2, similar to that of type 1 cell, is mounted inside an Inconel (5.08 cm o.d. × 0.25 mm wall) tube. The thermometer guide tube (D) is also Inconel (7.94 mm o.d. × 0.13 mm wall). Pairs of Inconel disks spaced along the assembly served as heat shunts to help temper the prt and improve its immersion characteristics [23]. One of the disks fits closely with the inside wall of the outer tube but fits rather loosely with the inner thermometer guide tube; the other disk fits closely with the thermometer guide tube but fits loosely with the outer tube. The thermometer guide tube and the fused quartz thermometer well must be assembled axially alined in the 5.08 cm o.d. Inconel case. The above design of the shunts makes allowances for any small relative misalinement of the Inconel thermometer guide tube and the fused quartz thermometer well with respect to the outer Inconel case and at the same time provides for the desired heat path between the outer and inner Inconel tubes. The disks are slotted to accommodate the cell tube (C). During assembly the disks were positioned to be in mechanical contact with the cell tube so that the tube would also be tempered. The cell tube was given a matte finish by "sand blasting" to reduce the light (heat) piping from the aluminum-point cell [17]. The space between the Inconel disks and the tubes was filled with layers of insulation (disks cut from 1.3 cm thick Fiberfrax blanket).

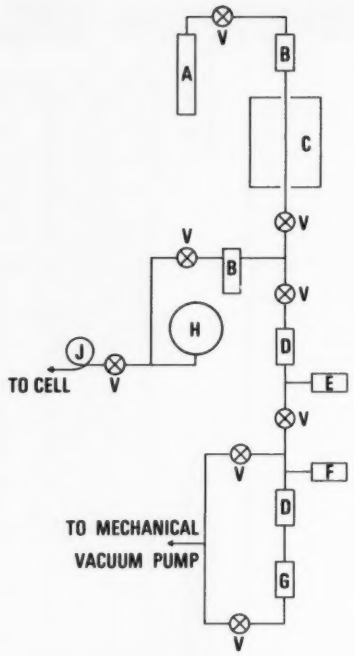

FIGURE 5. *Schematic arrangement of the high vacuum, argon gas purification and handling, and pressure measurement system.*

A. High-purity argon gas supply cylinder.
B. Cryogenic traps, liquid oxygen.
C. Inconel tube (packed with copper metal and with copper oxide) in furnace.
D. Cryogenic traps, liquid nitrogen.
E. Vacuum gauge, cold cathode type.
F. Vacuum gauge, thermocouple type.
G. Oil diffusion pump.
H. Dial type manometer, lowest subdivision of scale: 1 mm Hg (torr).
J. Flexible loop of tubing (Inconel, 3.18 mm o.d. × 0.20 mm wall) for connecting to the aluminum-point cell.
V. Valve, bellows type.

The type 3 cell is shown in figure 3. As described in type 1 and type 2 cells, the fused quartz envelope was also made first and sawed apart at the top. Adjustments were made to the outer fused quartz tube or to the thermometer well so that when assembled the bottom of the thermometer well would be about 3 mm above the bottom of the graphite thermometer well. Both the outer fused quartz tube and the thermometer well were sand blasted to obtain a matte finish to reduce light (heat) piping [17] from the aluminum-point cell. Fused quartz fiber tape was employed to cushion the graphite crucible inside the fused quartz envelope. Graphite disks (E) served as heat shunts between the outer tube and the inner thermometer well. Fused quartz wool was used for insulation in the space above the graphite crucible. The final seal at the top was made after "packing" the cell as shown in figure 3.

Table 2 lists the aluminum samples, the cell design, and the laboratory designation of the aluminum-point cells that were assembled.

[2] Certain commercial materials are identified in this paper in order to simplify the description of the apparatus or procedure. Such identification does not imply recommendation or endorsement by the National Bureau of Standards.

TABLE 2. *Identification of aluminum samples, cell design and designation of aluminum-point cells*

Cell designation	Cell type	Sample batch No.
A–1[a]	[a]1 and 2	2571
A–2[a]	[a]1 and 2	1558
A–3	3	1558
A–4	3	2571
A–5	2	2571
A–6	2	1558

[a] During preliminary experiments to determine the best procedure to conduct the investigations on the reproducibility of the aluminum-point cells, the samples were assembled in type 1 cells. They were later converted to type 2 cells for the measurements shown in table 3 and in figure 11.

4. Vacuum, Argon Gas Handling, and Pressure Measurement System

Figure 5 shows schematically the vacuum, argon gas handling, and pressure measurement system. The vacuum pumping system consisted of the usual mechanical and oil diffusion pumps preceded by two liquid nitrogen traps (D) in series. All valves (V) preceding these two liquid nitrogen traps were packless, bellows sealed types; all connecting lines were principally stainless steel. The only component that was not stainless steel was the flexible loop of Inconel tubing (J) (3.18 mm o.d. × 0.20 mm wall) that connected the valve to the aluminum-point cell.

The argon gas that was employed to pressurize the aluminum-point cells (all three types of cells) was first purified. The 5N purity argon gas from the cylinder (A) was first passed through a trap (B) cooled to the oxygen boiling point to remove water and other condensable substances. This gas was then passed through a tube (C) containing, successively, finely divided copper metal and cupric oxide held at about 700 °C. The purpose of the copper metal was to remove any oxygen from the argon; the cupric oxide should oxidize any hydrocarbons or other organic impurities and hydrogen. Another trap (B) held at the oxygen boiling point condensed any carbon dioxide and water that may have been formed.

The argon gas pressure was determined by employing a dial type manometer (H) with a differential pressure range of 0 to 760 torr. Each division of the dial scale corresponded to 1 torr. The manometer was actuated by a sensitive bellows. The uncertainty of the pressure measurement with the dial manometer, based on comparison with a mercury U-tube manometer, was estimated to be ± 0.5 torr.

5. Furnace

The furnace that was employed in the freezing-point investigation is shown schematically in figure 6. The furnace is similar in design to those used in the investigation of National Bureau of Standards–Standard Reference Material (NBS–SRM) tin standards [8]. However, there are a number of basic differences in the design. The furnace consists of an axially located Inconel alloy well (C) for the freezing-point cells. The bottom end of the Inconel well was sealed by "heliarc" welding an Inconel disk (S). An Inconel flange (B) was heliarc welded to the top end of the Inconel well. This Inconel well assembly and the furnace shell (Q) form a vacuum tight enclosure which protects the stack of four cylindrical coaxial blocks of copper (top (H), end (J), center (O), and bottom (U)) from oxidation. The space surrounding the copper blocks was packed with Fiberfrax insulation. The space was evacuated and purged with pure argon gas several times and filled with the gas at a pressure slightly above atmospheric. The four copper blocks were suspended by the Inconel well; however, the weight is partially supported by the Fiberfrax insulation at the bottom. Eight Inconel tubes (F) (3.97 mm o.d. × 0.20 mm wall), sealed at the bottom end and equally spaced on 6.668 cm diam, extend from the top of the Inconel flange (B) to the bottom of the bottom copper block (U). Small silicone elastomer "O" rings make a vacuum tight seal between these tubes and the Inconel flange. These tubes serve to contain thermocouples for controlling the furnace temperature and to contain resistance thermometers or thermocouples for determining the vertical temperature distribution of the furnace core under a given furnace control condition.

The center copper block (O) was constructed from two cylinders which were assembled by precooling the inner cylinder in liquid nitrogen and quickly inserting it inside the preheated outer cylinder. Before the cylinders were "shrunk together" eight grooves that closely fit the eight 3.97 mm o.d. Inconel tubes (F) were milled on the outside of the inner cylinder. The assembled center copper block was shrunk onto the lower end of the central Inconel tube by a process similar to that employed in assembling the block from two copper cylinders.

The top (H) and end (J) copper blocks contain circularly arranged holes (G and K) for separate control heaters. They contain also holes to accommodate the eight 3.97 mm o.d. Inconel tubes (F). The control heaters were assembled by inserting each arm of "U" shaped loops of 1.30 mm diameter nickel-chromium alloy wire in each of two adjacent round twin-bore alumina tubes (G and K). The lower portions of the "U" shaped loops were insulated with several short segments of single-bore alumina tubes. These elements were assembled successively and inserted in the holes provided in the copper blocks (G and K). The elements were heliarc welded in series to form the control heaters. These two copper blocks were also shrunk onto the central Inconel well. The wall thicknesses of the two segments of the Inconel well that separate the center, end, and top copper blocks have been reduced (to 0.8 mm) so that the temperature controls of the blocks would not interact excessively. The wall thickness of the Inconel well between the top copper block and the Inconel flange was also reduced (to 0.4 mm) to minimize the heat leak at the top of the furnace.

The bottom copper block is suspended by means of Inconel screws from the copper end plate (T) attached

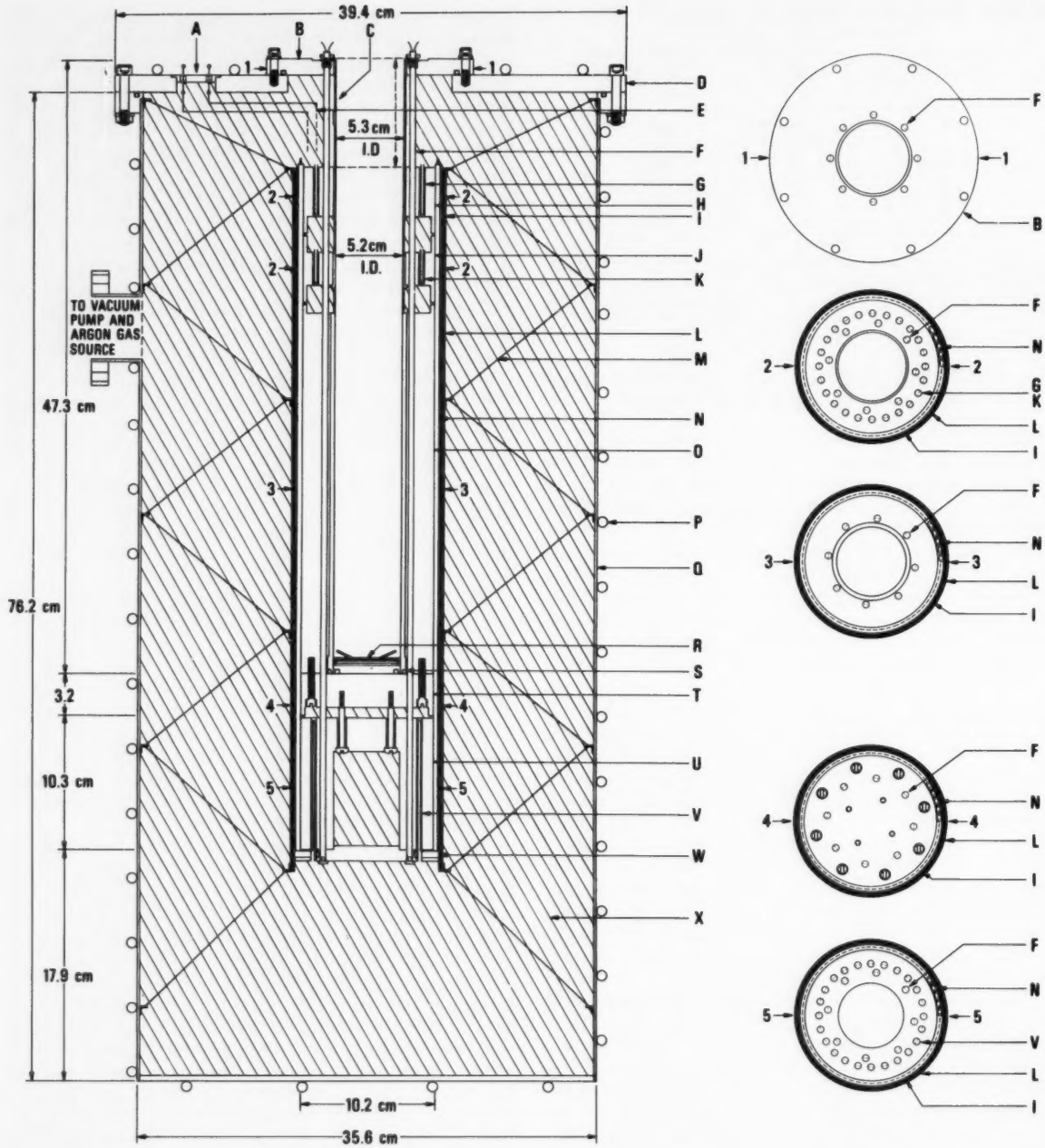

FIGURE 6. *Schematic of furnace core and body.*

A. Hermetic insulated posts for electric leads.
B. Inconel flange welded to tube C.
C. Inconel tube furnace core.
D. Brass cover plate.
E. Electric leads (8) to control heaters.
F. Inconel tubes (8, 3.97 mm o.d. × 0.20 mm wall) with thermocouples for temperature control or for monitoring the furnace temperature.
G. Heater for the top core block.
H. Top core block.
I. Copper cylinder for holding the main heater M tightly against the copper blocks H, J, O, and U.
J. End core block.
K. Heater for the end core block.
L. Axially centered copper cylinder for receiving the furnace core.
M. Nickel-chromium alloy wire for suspending and centering copper cylinder L.
N. Main heater.
O. Center core block.
P. Coil for circulating cooling water.
Q. Stainless steel furnace shell.
R. Inconel "spider" for centering the quartz glass cell (type 3 cell) shown in figure 3.
S. Inconel disk welded to tube C.
T. End plate for the center core block.
U. Bottom core block.
V. Heater for the bottom core block.
W. Fused quartz ring for supporting the main heater N.
X. Fiberfrax insulation.

to the center copper block. The bottom block also contains circularly arranged holes (V) for control heaters and holes to accommodate the eight 3.97 mm o.d. Inconel tubes (F). The control heater for the bottom block was assembled from "U" shaped loops of nickel-chromium alloy wire in a manner similar to those used in assembling the control heaters for the end and top copper blocks.

The main heater (N) extends the whole length of the four copper blocks. It was constructed in a manner similar to the control heaters for the end, top, and bottom copper blocks from "U" shaped loops of 1.30 mm diam nickel-chromium alloy wire and oval-shaped twin-bore alumina tubes (4.8 × 6.4 mm o.d.). These elements were assembled tightly spaced around the four copper blocks and the "U" shaped loops were heliarc welded in series to form a cylindrical heater. A tightly fitting copper cylinder (I) was slipped over the "cylinder" of alumina tubes to hold them in place against the copper blocks. The main heater assembly rests on a fused quartz ring (W) at the bottom.

The "furnace core" comprises the central Inconel well assembly, the copper blocks, the control heaters, and the tightly fitting copper cylinder that holds the main heater in place. This core was assembled on a larger brass cover plate (D) which contains electrically insulated, hermetically sealed connectors for gold lead wires (E) to the main heater and to the heaters on the end, top, and bottom copper blocks. Before the furnace core which was assembled on the brass cover plate was lowered into the furnace shell (Q), the interior of the shell was packed with Fiberfrax around an axially centered copper cylinder (L). The inside diameter of this cylinder is about 0.8 mm larger than the outside diameter of the copper cylinder that held the main heaters around the copper blocks so that the furnace core would slide smoothly in place and at the same time leave relatively little space for undesirable heat convection currents.

The temperature control of the parts of the furnace was achieved by utilizing Chromel-P/Alumel thermocouples and control components similar to those previously described [23]. The furnace control system is shown schematically in figure 7. The control thermocouple located at the middle of the center copper block was referenced to a large aluminum block held at a constant temperature and was connected to a 10-Ω standard resistor $R_1(S)$. The furnace control temperature was selected by adjusting the current from a pair of mercury cell batteries BA(Hg) through this standard resistor. The voltage drop across the 10-Ω standard resistor $R_1(S)$ was accurately monitored by observing the voltage drop across a second standard resistor $R_2(S)$, in series with the first, by means of a potentiometer. The control of the furnace temperature was monitored by observing the voltage of a

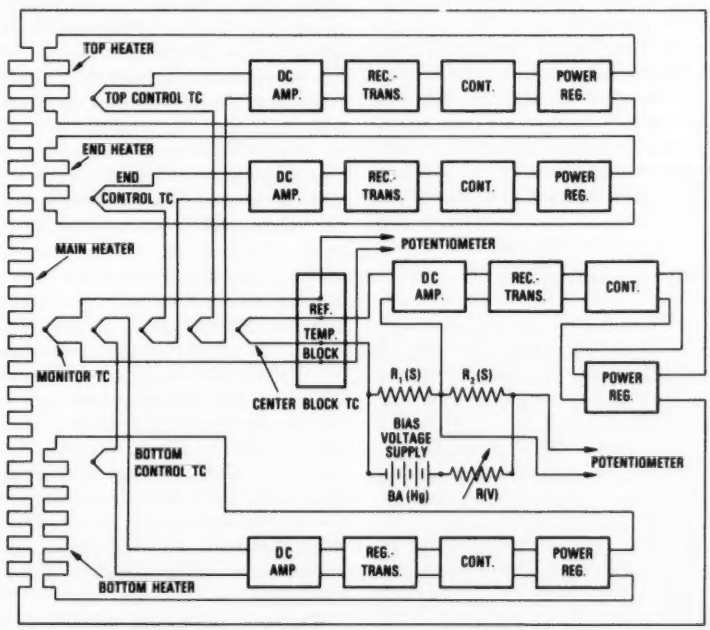

FIGURE 7. *Schematic block diagram of the furnace control system.*

TC: Chromel-P/Alumel thermocouple
DC AMP: Chopper type d-c amplifier.
REC-TRANS: Strip chart recorder plus transmitting variable resistor.
CONT: Three-mode controller.
POWER REG: Solid-solid gate drive, full-wave silicon-controlled rectifier, plus transformer package.
$R_1(S)$: Standard resistor (10 Ω) for bias voltage source.
$R_2(S)$: Standard resistor (10 Ω) for monitoring bias voltage source.
R(V): Variable resistor for adjusting bias voltage.
BA(Hg): Mercury cells.

separate thermocouple referenced to the previously mentioned aluminum block that was held at a constant temperature.

The control thermocouples for the end, top, and bottom copper blocks were of the differential type; their reference junctions were located at the middle of the center block and their control junctions were located about 1 cm within the respective blocks from the center block.

The voltage output of each control thermocouple was amplified by a chopper type d-c amplifier and this output was connected to a strip-chart recorder. A "transmitting variable resistor," coupled mechanically to the recorder indicator, operated a "three-mode" controller which, in turn, operated a "solid-state gate drive" for a full-wave silicon-controlled rectifier. The rectifiers controlled the a-c power to each of the heaters. The a-c power supplies were transformers with voltage outputs and power capacities appropriate to the heaters. The total power required to hold the furnace at 660 °C was about 300 W.

The thermocouple that was employed to monitor the temperature control showed the center copper block to be stable to ± 0.01 K for several hours. No miniaturized resistance thermometer suitable for use at 660 °C was available to accurately probe the vertical profile of the furnace under operating conditions. However, on the bases of the experiences with furnaces of similar design that are used at the zinc and tin points [8, 23], of the improvements in the present design to reduce heat leaks and temperature gradients, and of the results of differential thermocouples that were used to probe temperature differences in the furnace, the uniformity of the center copper block temperature is expected to be within ± 0.05 K at 660 °C. (The uniformity of the center block of the furnace used with tin-point cells is shown in reference [8] to be about ± 0.01 K.)

6. Thermometry

The work of Berry [1] showed that commercially available prt's containing mica (muscovite or phlogopite) insulation begin to exhibit electrical leakage when used at temperatures above about 500 °C because of the accumulation of moisture that is liberated from the mica, the moisture being liberated faster the higher the temperature. Mica contains as a part of its chemical structure hydroxyl (OH) radicals which at high temperatures decompose irreversibly to water. The total amount of water that can theoretically be liberated on the basis of the chemical formula is about five weight-percent. As a consequence of the liberation of water mica undergoes mechanical deterioration, such as swelling and disintegration into small flakes (exfoliation). The electrical leakage of the prt becomes excessive when relatively little water is liberated from the mica; hence, the prt loses its insulation considerably before the mica begins to exhibit mechanical deterioration. The prt which has lost its insulation can be "rejuvenated" by removing the moist air in the thermometer envelope by pumping at about 200 °C (where the rate of liberation of water from the mica is negligible) and replacing with dry air. The "lifetime" of the prt, before it is necessary to replace again the moist air with dry air, is shorter the higher the temperature the prt is used. Continuous pumping of the prt envelope at the higher temperatures, where the "vapor pressure" of water of the mica is high, can cause the mica to exfoliate excessively. The results of the investigation by Berry [1] on the useful lifetimes of the gas fillings of prt's suggest that when commercial prt's with phlogopite mica insulation are used at the aluminum point they should be pumped and refilled with dry air whenever the accumulated exposure to the temperature reaches about one week, or even less, if high precision measurements are to be performed.

To avoid the periodic pumping and filling with dry air a "birdcage" type prt (laboratory designation: HTSS–15) with synthetic sapphire insulation [4] was obtained on loan from Sharrill D. Wood of the Temperature Section of the Bureau. The prt resistor had been assembled by threading platinum wires through holes in sapphire disks and welding them in series. The thermometer leads were also separated by sapphire disks and between the disks were sapphire rod spacers 1.3 cm long. At the upper end of the prt where the temperature would be close to the room temperature, high-purity alumina (Al_2O_3) was used instead of sapphire for lead insulation. The sheath was fused quartz. The thermometer, i.e., the platinum wire, did not contact the sheath at any point. This prt was used earlier by Mrs. Wood at temperatures up to 1100 °C and had been at temperatures in the vicinity of 1065 to 1100 °C for over 300 h [28]. For the application to the present work the external leads and thermometer "head" were replaced with another thermometer head containing BNC connectors so that the prt could be used with an a-c bridge which operated at 400 Hz [3, 23]. The two leads from one end of the prt sensor were the center terminals of the two BNC receptacles; the two leads from the other end of the prt sensor were the outer or the shield terminals of the receptacles. The prt resistance, which was nominally 0.26983 Ω, was considered somewhat low for best measurements, but no other prt that could endure the repeated use at the aluminum point was immediately available. The outer surface of the fused quartz sheath of the prt had bands of matte finish, starting from about 5.5 cm from the thermometer tip, to reduce radiation piping [17]. The matte finish had been obtained by blowing at high velocity fine particles of alumina abrasive against the surface.

The work of Evans and Wood [5] suggested that the birdcage type prt requires relatively greater depth of immersion before its indication would correspond to the equilibrium temperature of the fixed-point cell. Therefore, special precautions were taken in the design of the aluminum-point cell to temper the section of the prt well above the graphite crucible that contains the aluminum sample (see figs. 1, 2, and 3). The

thermometer guide tubes were made as close fitting as practical to minimize the thermal resistance to the prt. Heat shunts were provided between these tubes and the furnace wall or the outer Inconel case.

An aluminum sleeve is generally employed in the thermometer well of the triple-point-of-water (TP) cell to improve the thermal contact of the prt with the cell [23]. With the birdcage type prt, because of the effect of inductive interaction with the sleeve, the a-c bridge method consistently yielded results that were higher with the aluminum sleeve than without the sleeve. The observed resistance at the TP was equivalent to 4.9 mK higher with one sleeve of 5.1 cm length and 3.6 mK higher with another sleeve of 4.4 cm length and slightly looser fit with the prt. The a-c bridge measurements at the TP of "standard" commercial prt's (the platinum coil helically wound on mica crosses and with an electrical resistance of 0 °C of 25.5 Ω) with and without the aluminum sleeve have been found to be different by only 0.1 mK or less. In a similar comparison at the TP, the apparent resistance of a prt with a helically wound coil and with a resistance at 0 °C of 0.23 Ω measured with sleeve correspond to about 0.2 mK higher than without the sleeve. In the results reported in this work no aluminum sleeve was employed in the measurements with the TP cell. All a-c bridge measurements (at both the TP and the aluminum point) were performed at 3.54 and 5.00 mA currents and the resistance values were calculated for zero thermometer current. All references to values of $R(\mathrm{Al})$ or $R(\mathrm{TP})$ are at zero thermometer current. A strip-chart recorder was employed with the a-c bridge so that the freezing temperatures could be automatically recorded with the prt. The gains of the amplifiers of the bridge and of the recorder were adjusted so that, with a thermometer current of 3.54 mA, 1.2 mm on the recorder chart corresponded to 0.1 μΩ (or about 0.1 mK for the prt employed in this work).

The a-c bridge that was employed in this work measures the ratio of the prt resistance to that of the reference resistor. The reference was a 10-Ω resistor wound on a card and hermetically sealed in a rectangular metal case with a silicone compound to aid in the dissipation of heat that is generated in the resistor during use. The resistor case was placed in good thermal contact with an aluminum block and placed in an aluminum box thermostated at 28 °C. The variation in temperature of the aluminum block was less than 2 mK. The temperature coefficient of resistance of the resistor at 28 °C is smaller than 1 ppm per °C. The resistance of the 10-Ω reference is within about 2×10^{-5} of the nominal value. Since relative values of resistances and the resistance ratios $R(\mathrm{Al})/R(\mathrm{TP})$ of the aluminum-point cells are being compared, the real value of the reference resistor was not considered in the results presented in this work. The reference resistor was taken to be exactly 10 Ω.

In the aluminum point cell the prt was necessarily surrounded by solid and liquid aluminum. The freezing-point experiments, to be described later, required a mantle of solid aluminum to be immediately adjacent to the graphite thermometer well. However, in every case the prt and the aluminum were separated by 1 mm of fused quartz and 2.3 mm of graphite (see figs. 1, 2, and 3). The inside diameters of the aluminum sleeves mentioned earlier that were employed with the TP cell differed by 0.3 mm; this relatively small difference in separation of the prt and the sleeve plus the difference in the length of the sleeve of 6.4 mm caused a change in the thermometer resistance corresponding to about 1.3 mK. To test the effect of any inductive interaction in the aluminum-point cell a TP cell of large inner diameter was employed to simulate the conditions. A graphite well of the same dimensions as used in the aluminum-point cell was closely fitted inside a closed-end aluminum sleeve. A closed-end fused quartz tube corresponding to the thermometer well of the fused quartz envelope was placed inside the graphite tube. The resistances observed with the above assembly inside the TP cell correspond to a temperature 2.9 mK higher than that observed without the assembly. The effect of the inductive interaction in the aluminum-point cell would probably be of this order. (The electrical conductivity of graphite at the aluminum point is, depending upon the type of graphite, two to three times that at the TP; on the other hand, the electrical conductivity of solid aluminum is approximately five times smaller at the aluminum point than at the TP [10]. Also, the electrical conductivity of graphite is about 100 to 1000 times smaller than that of aluminum at these temperatures [10]). However, in the experiments described in this paper the reproducibility of the aluminum point was to be investigated and one of the requirements was that the effect of the inductive interaction on the prt be the same among the aluminum-point cells. Since the geometry of all three types of cells was the same in the neighborhood of the aluminum sample, the effect of the inductive interaction was expected to be the same in all the cells as long as the "freezes" in the cells were prepared in the same way. (This assumption is supported somewhat by the reproducibility of the freezing points that were obtained with the aluminum-point cells, although a portion of the small deviations in the freezing points could have come from small differences in the effect of inductive interaction.)

The d-c resistance measurements employing the Mueller bridge (G–3) that was available with the prt ($R(0\ ^\circ\mathrm{C})=0.26\ \Omega$) were considered unwieldy and to lack the precision that is possible with the a-c bridge method. If a prt with the resistance of 2.6 or 5 Ω were available, d-c resistance measurements would have been practical for the investigations presented in this paper.

7. Experimental procedures

7.1. Freezing procedures

The aluminum liquid was found to supercool about 0.4 to 1.5 K before the nucleation of the solid started.

Usually the liquid supercooled about 0.4 to 0.6 K. Several freezing procedures were tried to obtain information on the "thermal behavior" of the aluminum freezing-point cell.

To avoid quenching in defects in the prt wire by cooling rapidly from the aluminum point, it was found necessary to withdraw the prt from the aluminum-point cell in steps over a period of 30 min. Then, following the procedure described by McLaren [19], the prt was annealed at 480 °C in a tube furnace for 30 min and removed to cool at room temperature. This treatment was found to yield resistance readings at the TP that were repeatable to ± 0.1 mK or better.

With the type 1 cell the freeze was initiated by withdrawing the cell from the furnace and quickly re-inserting it in the furnace when the prt indicated the onset of recalescence [8, 16]. Before the cell was withdrawn from the furnace, the furnace was set to control 1 K below the freezing point. The cell was withdrawn as soon as its temperature had decreased close to the freezing point; meanwhile, the furnace temperature continued to decrease to the lower "control point". However, in most cases the furnace temperature was not at the control point when the cell was about to be re-inserted. The insertion of the cooled cell (outer parts) helped to lower the furnace temperature; the recalescence raised the temperature of the aluminum sample to its melting point. The input power to the furnace was sufficient to quickly compensate for any excessive cooling of the furnace by the cooled cell. (The furnace was designed to be well insulated so that relatively low input power could maintain it at any desired temperature; as a consequence, the cooling rate of the furnace was relatively slow. On the other hand, for heating a wide range of input power was readily available.) Since the presence of a mantle of solid aluminum around the thermometer well was considered essential to precision measurements, a cold fused quartz rod or a cold prt was also inserted in the thermometer well in these experiments before any temperature measurements were made. (No effort was made to determine the course of the freezing temperatures without first inducing a freeze around the thermometer well. To introduce a preheated prt into the aluminum-point cell without freezing or without changing the amount of solid aluminum around the thermometer well would require slow insertion of the prt into the cell in such a manner that the prt is preheated to the aluminum point in the thermometer guide tube.)

When a mantle of solid aluminum was frozen around the thermometer well, the freezing temperatures obtained with the freeze first induced by withdrawing the cell from the furnace were essentially the same as those obtained by a procedure, which was adopted in the experiments described in this paper, in which the freeze was initiated in the furnace without any handling of the cell. (The procedure will be described in the following paragraphs.) There was a certain degree of danger in withdrawing the hot cell from the furnace and there was always, during this operation, some "tapping" of the cell against the furnace well. (There was, in addition to possible personal injury, the danger of breaking the prt.) The type 2 and type 3 cells, which were the cell designs selected for the present investigation, could not be conveniently withdrawn from the furnace because of the connection to the gas handling system.

Since the aluminum did not supercool excessively, such as with tin [8, 16] or antimony [18], the freezing procedure that was adopted was to allow the freeze to start in the furnace in a manner similar to that employed with zinc [15, 23] which supercools only about 0.06 K. The procedure for initiating the freeze, without disturbing the cell in the furnace, was to start with the melt 4 to 6 K above the freezing point and then to reduce the furnace temperature to about 1 or 2 K, depending upon the degree of supercool, below the freezing temperature. The furnace was usually at the new "control temperature" within 15 to 20 min after the furnace controls were set to the lower temperature. Usually within the following 10 to 15 min the aluminum liquid was at the bottom of its "supercool" and in the next 5 min the temperature of the sample rose to within about 0.1 K of the freezing temperature. Although the initial temperature increase was rapid immediately after the start of recalescence, the subsequent temperature rise was slower; even after 1 h the temperature was lower by about 0.5 mK than the value that was obtained after a freeze was induced around the thermometer well by inserting a cold fused quartz rod or a cold prt.

As mentioned earlier, it was necessary to withdraw the prt from the cell in steps over a period of 30 min to avoid quenching in lattice defects and, in addition, to anneal the prt at 480 °C for 30 min. Only one suitable prt was available for these experiments. Therefore, to conserve experimental time, the time required for the sample, after the start of cooling, to go through the supercool and then recover to about 0.1 K of the freezing point was estimated from the results of preliminary experiments. At about the time when the temperature of the cell had recovered to about 0.1 K of the freezing point two fused quartz rods were successively inserted for a period of about 5 min each to induce a freeze around the thermometer well. Also, at this time, if the furnace was set to control at 2 K below the freezing point, it was raised to control at 1 K below. (Meanwhile the prt, which had previously been withdrawn from the cell, was annealed and its resistance at the TP was determined.) The rod was then removed and the cold prt inserted. About 15 to 20 min were required after insertion of the prt to be certain that the prt had come to an equilibrium temperature. The freezing temperatures were usually observed over the next 40 to 50 min, after which the sample was completely remelted for the next freeze. When the sample was allowed to freeze only for a period of time as outlined above, about 1 hour was required to melt what was frozen. However, two hours of heating were allowed before the next freeze was started. During the melting period, the prt was slowly withdrawn from the cell and annealed and its resistance at the TP was measured. Two freezes were obtained during a normal

day. Usually after the second freeze, the sample was allowed to melt and remain melted overnight. In the morning, during the period of time at which the sample was cooled to initiate the freeze and later while the two fused quartz rods were inserted in the cell to freeze aluminum around the thermometer well, the prt was annealed (or annealed again depending upon whether the resistance of the prt at the TP was determined last on the previous day) and its resistance at the TP was determined.

On the basis of the results of a series of preliminary freezing experiments and the time required to prepare a cell for the experiments, it was decided to investigate the six aluminum samples successively one cell per week. Either a type 2 or a type 3 cell was investigated during the week. The schedule for the week was as follows: (Some repetition of previous descriptions are included for clarity.) On Monday, except for the first cell, the cell from the previous week was disconnected from the gas handling system and removed from the furnace. The new cell was then inserted in the furnace and connected to the gas handling system. After pumping the cell to a high vacuum, the electric power to the furnace heaters was switched on and the furnace was set to control at a temperature 4 or 6 K above the freezing point to melt the sample over night. The furnace reached the control point about 5 h after the heaters were turned on. Meanwhile the pumping of the cell at high vacuum was continued. The TP cell was also prepared on Monday. On Tuesday morning the aluminum-point cell was slowly filled (in order that impurities are reacted in the copper metal-copper oxide furnace and collected in the cold traps) to 1 atm pressure of purified argon gas and in the meantime the prt was placed in the annealing furnace at 480 °C for 30 min prior to the measurement of its resistance at the TP. After the cell was filled with argon gas to 1 atm pressure, the furnace temperature was set to cool and control at a temperature 2 K below the freezing point. Later at an appropriate time, the time at which the aluminum sample was estimated to have recovered to within about 0.1 K of the freezing point, the first fused quartz rod was inserted in the thermometer well to induce freezing around the well and the furnace temperature control was reset to control at a temperature 1 K below the freezing point. After about 5 min the first rod was removed and a second rod was inserted. Meanwhile the resistance of the prt at the TP was determined. After the second rod had been in the cell for 5 min, it was removed and the prt inserted in the cell. The measurements of the freezing point and the remelting of the aluminum sample were described earlier. By Friday, the desired number of "freezes" usually would have been obtained and on Friday afternoon the furnace and the cell were allowed to cool over the weekend.

7.2. Measurement Procedure

The intercomparison of the freezing temperatures of the aluminum samples was based on the analysis of the prt resistance ratios $R(\mathrm{Al})/R(\mathrm{TP})$, the ratio of the resistance observed with the freezing aluminum sample to the resistance observed with a TP cell, reduced to zero thermometer current. The values of $R(\mathrm{Al})$ were adjusted to 1 atm pressure on the liquid aluminum surface and to a common depth of immersion of the prt in the aluminum-point cell (16.7 cm from the liquid aluminum surface to the middle of the prt sensor). (The depth of immersion of the prt in the aluminum-point cell was estimated from the mass of the sample and the geometry of the graphite cell, assuming that 20 percent of the sample was solid.) The values of $R(\mathrm{TP})$ were at a fixed depth of immersion in a TP cell (27.5 cm from the water surface to the middle of the prt sensor). Measurements of the resistance of the prt were made at the TP before and after each measurement in the aluminum-point cell and, except for two cases, the average $R(\mathrm{TP})$ was used to determine the $R(\mathrm{Al})/R(\mathrm{TP})$ ratios. The values of $R(\mathrm{Al})$ were observed at two currents (3.54 and 5.00 mA) over a period of 40 to 50 min after the prt readings indicated that it was at an equilibrium temperature. Figure 8 shows results of experiments in which the complete freezing of the samples were recorded. (No freezing curve is shown for cell A−6; the graphite crucible containing the sample broke soon after the freezing data given in table 3 were taken.) As shown by the figure, the temperature of the aluminum-point cell changed by less than 0.1 mK during the usual 40- to 50-min period when the observations were taken. A change of 1 mK in the freezing point occurred only after over one-half (over 6 or 8 h of recorded data) of the sample was frozen.

8. Results

8.1. Effect of Pressure on the Freezing Temperature

The effect of argon gas pressure on the freezing point of aluminum was investigated over the range 0.3 to 2 atm pressure. Since the differential pressure dial manometer had the range of only 0 to 760 torr, the pressure measurements above 1 atm were performed with the manometer open to the ambient atmospheric pressure (i.e., the pressure measurements were relative to the atmospheric pressure). An auxiliary dial manometer was employed to determine the atmospheric pressure. The results of the measurements are shown in figure 9. The increase in the freezing temperature of aluminum was calculated from the results to be 7.1 mK/atm. The estimated uncertainty of the value is ±0.3 mK/atm. McAllan and Ammar [14] list 6.1 mK/atm as the increase in the freezing temperature with increase in pressure.

The pressure effect on the freezing temperature was also calculated employing the Clapeyron relation

$$dT/dp = \frac{T_f(V_l - V_s)}{L}, \qquad (1)$$

where V_l and V_s are the specific volumes of the liquid and solid aluminum, respectively; T_f is the freezing

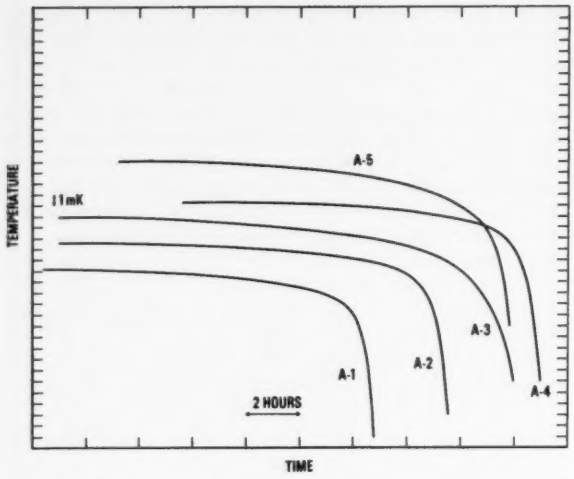

FIGURE 8. *Typical freezing curves of the aluminum samples recorded starting approximately fifteen minutes after the insertion of the platinum resistance thermometer in the cell.*

The curves are displaced both vertically and horizontally; they are meant to show only the relative temperatures within the individual freezing curves.

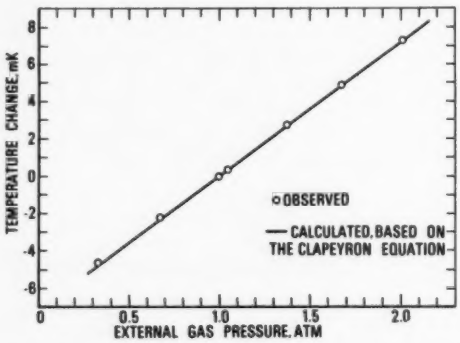

FIGURE 9. *Effect of the pressure of argon gas on the freezing temperature of aluminum.*

The solid linear curve, based on the Clapeyron equation, is normalized to the freezing temperature at 1 atm pressure.

temperature; L is the latent heat of fusion; and dT/dp is the pressure coefficient of T_f. Using 933 K (660 °C) for T_f, 10.7 kJ/mol for L reported by Stull and Prophet [26], and the densities 2.368 and 2.55 g/cm³ for the liquid and solid aluminum, respectively, given by Brandt [2], the calculated pressure coefficient of the freezing temperature becomes 7.18 mK/atm, which is close to the experimentally observed value.

Using 7.1 mK/atm as the pressure coefficient of the freezing temperature and 2.368 g/cm³ for the density of liquid aluminum, the expected variation in the observed freezing point with the depth of immersion of the prt becomes 0.016 mK per cm of liquid aluminum. To check the adequacy of immersion of the prt, the freezing temperatures at various depths of immersion were measured for the three types of cells. The results are shown in figure 10. The solid line is the expected variation in temperature with immersion. The results show that the immersion of the prt is more than adequate for the three types of cells when the prt is fully immersed in the cell. On the basis of the results obtained with cells of type 1 and type 2, the immersion characteristics of the prt in type 3 cell can be improved by introducing better heat shunts between central thermometer guide tube and the outer case.

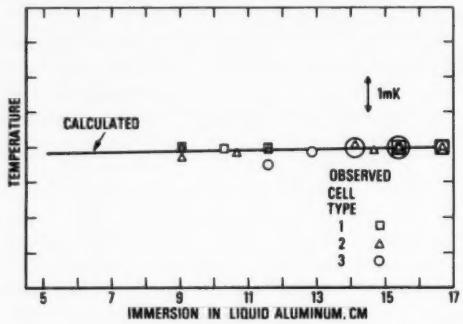

FIGURE 10. *Immersion characteristics of the platinum resistance thermometer in the aluminum point cells and the effects of the hydrostatic pressure of liquid aluminum on the vertical temperature distribution of the cell.*

(The depth of immersion was estimated as the distance from the top surface of the aluminum in the cell to the mid-point of the thermometer coil. The calculated curve (straight line) is based on the Clapeyron equation. It is normalized to the reading at approximately 16.7 cm immersion when the thermometer is touching the bottom of the thermometer well of the aluminum-point cell.)

8.2. Comparison of the Freezing Temperatures

The observed values of $R(\mathrm{Al})$ and $R(\mathrm{TP})$ and the calculated values of the ratio $R(\mathrm{Al})/R(\mathrm{TP})$ are summarized in table 3 and are also plotted chronologically in figure 11. In the figure, the tick marks along the abscissa indicate the occurrences of the observation of either $R(\mathrm{Al})$ or $R(\mathrm{TP})$. The ratios $R(\mathrm{Al})/R(\mathrm{TP})$ are plotted where the observation of $R(\mathrm{Al})$ occurred.

Except in the measurements of series 4 (cell A–4), the mean $R(\mathrm{TP})$ of each series of measurements tended to increase; however, there is a value (0.269833218 Ω) among those in the third series that is close to the highest value (0.269833245 Ω) of the sixth or the last series of measurements. Nevertheless, the spread of the mean $R(\mathrm{TP})$ corresponds to only 0.31 mK, which shows that the overall change in the mean $R(\mathrm{TP})$ was still relatively small in spite of the prt being subjected to the temperature of the aluminum point before the observations of $R(\mathrm{TP})$. The average standard deviation of the six series of measurements of $R(\mathrm{TP})$ corresponds to ± 0.14 mK. The spread of all values (58 observations) of $R(\mathrm{TP})$ is 0.81 mK. The two relatively low values of $R(\mathrm{TP})$ found in the measurements of series 1 (cell A–6) and series 2 (cell A–5), without any accompanying decrease in the value of $R(\mathrm{Al})$, were attributed to the ice mantle of the triple-point of water cell possibly not being completely "free" from the thermometer well. In the later measurements starting with those of series 3,

TABLE 3. *Observed thermometer resistance at the triple point of water and at the freezing points of the aluminum samples and the values of the ratios of the resistances*

Cell A–6 (Series 1)

Date	R(Al) or R(TP) Ohms	R(TP), mean Ohms	R(Al)/R(TP)
9–25–73	[a,b]0.269832809		
	[b]0.269832825		
9–26–73	0.269832718		
	0.910413896	0.269832708	3.37399385
	0.269832699		
	0.910414003	0.269832725	3.37399403
	0.269832751		
	0.910413852	0.269832780	3.37399278
	0.269832810		
9–27–73	0.269832621		
	0.910413816	0.269832508	3.37399605
	0.269832394		
	0.910413882	0.269832630	3.37399477
9–28–73	0.269832867		
	0.910414020	0.269832852	3.37399250
	0.269832836		
	0.910413930	0.269832896	3.37399162
10–2–73	0.269832955		
Mean R(TP)	0.269832739	Mean 3.37399366	
Std. Dev.[c]	$\pm 163 \times 10^{-9}$	Std. Dev. $\pm 149 \times 10^{-8}$	
	± 0.15 mK	± 0.46 mK	
Mean R(Al)	0.910413914		
Std. Dev.	$\pm 76 \times 10^{-9}$	Spread 443×10^{-8}	
	± 0.09 mK	1.38 mK	
Mean R(Al) / Mean R(TP)	3.37399352	Deviation from the mean of five cells[d]	-24×10^{-8} -0.07 mK

Cell A–5 (Series 2)

Date	R(Al) or R(TP) Ohms	R(TP), mean Ohms	R(Al)/R(TP)
10–2–73	0.269832955		
	0.910413819	0.269832995	3.37398997
	0.269833035		
	0.910414069	0.269833021	3.37399057
10–3–73	0.269833007		
	0.910413922	0.269832878	3.37399182
	0.269832749		
	0.910413979	0.269832758	3.37399353
	0.269832768		
	0.910413887	0.269832749	3.37399330
10–4–73	0.269832730		
	0.910413864	0.269832674	3.37399415
	0.269832618		
	0.910414088	0.269832497	3.37399720
10–5–73	0.269832376		
	0.910414091	0.269832624	3.37399562
	0.269832871		
Mean R(TP)	0.269832790	Mean 3.37399327	
Std. Dev.	$\pm 208 \times 10^{-9}$	Std. Dev. $\pm 245 \times 10^{-8}$	
	± 0.19 mK	± 0.76 mK	
Mean R(Al)	0.910413965		
Std. Dev.	$\pm 109 \times 10^{-9}$	Spread 723×10^{-8}	
	± 0.12 mK	2.25 mK	
Mean R(Al) / Mean R(TP)	3.37399308	Deviation from the mean of five cells[d]	-63×10^{-8} -0.20 mK

TABLE 3. *Observed thermometer resistance at the triple point of water and at the freezing points of the aluminum samples and the values of the ratios of the resistances*—Continued

Cell A–3 (Series 3)

Date	R(Al) or R(TP) Ohms	R(TP), mean Ohms	R(Al)/R(TP)
10–10–73	0.269832746		
	0.910413453	0.269832848	3.37399045
	0.269832951		
	0.910413741	0.269832924	3.37399057
	0.269832897		
	0.910413590	0.269833058	3.37398833
	0.269833218		
	0.910413735	0.269832991	3.37398971
10–11–73	0.269832764		
	0.910413534	0.269832912	3.37398995
	0.269833060		
	0.910413475	0.269832954	3.37398921
	0.269832848		
Mean R(TP)	0.269832926	Mean 3.37398970	
Std. Dev.	$\pm 168 \times 10^{-9}$	Std. Dev. $\pm 81 \times 10^{-8}$	
	± 0.16 mK	± 0.25 mK	
Mean R(Al)	0.910413588		
Std. Dev.	$\pm 126 \times 10^{-9}$	Spread 224×10^{-8}	
	± 0.15 mK	0.70 mK	
Mean R(Al) / Mean R(TP)	3.37398998	Deviation from the mean of five cells[d]	-420×10^{-8} -1.31 mK

Cell A–4 (Series 4)

Date	R(Al) or R(TP) Ohms	R(TP), mean Ohms	R(Al)/R(TP)
10–15–73	[b]0.269832848		
10–16–73	0.269832782		
	0.910413955	0.269832820	3.37399266
	0.269832859		
	0.910413957	0.269832856	3.37399222
	0.269832854		
10–17–73	0.269832767		
	0.910413715	0.269832756	3.37399257
	0.269832746		
	0.910414340	0.269832782	3.37399457
	0.269832819		
	0.910414699	0.269832858	3.37399495
	0.269832898		
	0.910414060	0.269832829	3.37399294
10–18–73	0.269832760		
	0.910413952	0.269832676	3.37399445
	0.269832592		
	0.910414115	0.269832684	3.37399496
10–19–73	0.269832775		
	0.910414074	0.269832662	3.37399508
	0.269832548		
	0.910414112	0.269832776	3.37399380
10–23–73	0.269833004		
Mean R(TP)	0.269832784	Mean 3.37399382	
Std. Dev.	$\pm 124 \times 10^{-9}$	Std. Dev. $\pm 112 \times 10^{-8}$	
	± 0.12 mK	± 0.35 mK	
Mean R(Al)	0.910414098		
Std. Dev.	$\pm 265 \times 10^{-9}$	Spread 286×10^{-8}	
	± 0.31 mK	0.89 mK	
Mean R(Al) / Mean R(TP)	3.37399364	Deviation from the mean of five cells[d]	-8×10^{-8} -0.02 mK

TABLE 3. *Observed thermometer resistance at the triple point of water and at the freezing points of the aluminum samples and the values of the ratios of the resistances*—Continued

Cell A–2 (Series 5)

Date	R(Al) or R(TP) Ohms	R(TP), mean Ohms	R(Al)/R(TP)
10–24–73	0.269832938		
	0.910414732	0.269832953	3.37399388
	0.269832968		
	0.910414712	0.269833026	3.37399289
	0.269833085		
	0.910414876	0.269832969	3.37399421
	0.269832853		
10–25–73	0.269832758		
	0.910414659	0.269832791	3.37399563
10–26–73	0.269832824		
	0.910414540	0.269833010	3.37399246
	0.269833196		
	0.910414860	0.269833048	3.37399317
	0.269832900		
10–27–73	0.269832854		
	0.910414727	0.269832955	3.37399384
	0.269833056		
	0.910414960	0.269832953	3.37399472
	0.269832850		
Mean R(TP)	0.269832935	Mean	3.37399385
Std. Dev.	$\pm 131 \times 10^{-9}$		$\pm 103 \times 10^{-8}$
	± 0.12 mK		± 0.32 mK
Mean R(Al)	0.910414758		
Std. Dev.	$\pm 134 \times 10^{-9}$	Spread	317×10^{-8}
	± 0.16 mK		0.99 mK
Mean R(Al) / Mean R(TP)	3.37399420	Deviation from the mean of five cells[d]	-5×10^{-8} -0.02 mK

Cell A–1 (Series 6)

Date	R(Al) or R(TP) Ohms	R(TP), mean Ohms	R(Al)/R(TP)
10–30–73	0.269832882		
	0.910415384	0.269833042	3.37399518
	0.269833203		
	0.910415347	0.269833124	3.37399402
10–31–73	0.269833044		
	0.910415434	0.269833064	3.37399509
	0.269833085		
	0.910415206	0.269833022	3.37399477
	0.269832958		
	0.910415621	0.269833081	3.37399557
	0.269833204		
	[e]0.910417677	[f]0.269833722	3.37399518
11–1–73	[b,f]0.269833722		
	[e]0.910417552	[f]0.269833722	3.37399472
	0.269833132		
	0.910415657	0.269833188	3.37399437
11–2–73	0.269833245		
	0.910415425	0.269833161	3.37399385
	0.269833077		
	0.910415514	0.269832988	3.37399634
	0.269832898		
Mean R(TP)	0.269833073	Mean	3.37399491
Std. Dev.	$\pm 128 \times 10^{-9}$	Std. Dev.	$\pm 74 \times 10^{-8}$
	± 0.12 mK		± 0.23 mK
Mean R(Al)	0.910415448		
Std. Dev.	$\pm 147 \times 10^{-9}$	Spread	249×10^{-8}
	± 0.17 mK		0.78 mK

TABLE 3. *Observed thermometer resistance at the triple point of water and at the freezing points of the aluminum samples and the values of the ratios of the resistances*—Continued

Cell A–1 (Series 6)

Date	R(Al) or R(TP) Ohms	R(TP), mean Ohms	
Mean R(Al) / Mean R(TP)	3.37399503	Deviation from the mean of five cells[d]	$+101 \times 10^{-8}$ $+0.31$ mK
Average Std. Dev. of R(TP)			$\pm 154 \times 10^{-9}\Omega$ $\sim \pm 0.14$ mK
Spread of the mean R(TP) among the six series of observations			$334 \times 10^{-9}\Omega$ ~ 0.31 mK
Average Std. Dev. of R(Al)			$\pm 143 \times 10^{-9}\Omega$ $\sim \pm 0.17$ mK
Spread of the mean R(Al) of the six cells			$1860 \times 10^{-9}\Omega$ ~ 2.15 mK
Average Std. Dev. of R(Al)/R(TP)			$\pm 127 \times 10^{-8}$ $\sim \pm 0.40$ mK
Spread of the mean R(Al)/R(TP) of the six cells			521×10^{-8} ~ 1.62 mK
Mean of the mean R(Al)/R(TP) of the six cells			3.37399320
Spread of the mean R(Al)/R(TP) of five cells (excluding cell A–3)			164×10^{-8} ~ 0.51 mK
Mean of the mean R(Al)/R(TP) of five cells (excluding cell A–3)			3.37399390

[a] The last two figures were obtained by interpolation in the strip-chart record. On the bases of the sensitivity of the measurement system and the "noise" in the strip-chart record, the *accuracy of the interpolation* is estimated to be about ± 3 (approximately ± 0.3 mm on the chart) in the next to the last figure given. The extra figure was carried to retain an over-all consistency in the calculations.

[b] This observation was not included in computing the mean R(TP) of this series of measurements.

[c] Standard deviation is defined here as $[\Sigma d^2/n-1)]^{1/2}$, where d is the deviation of the individual values from the mean and n is the number of observations.

[d] Cell A–3 was excluded from the mean.

[e] This observation was not included in computing the mean R(Al) for this cell, but was included in computing R(Al)/R(TP).

[f] This rather high value of R(TP) was considered to be more consistent with the two adjacent exceptionally high values of R(Al) and, therefore, was employed in computing the R(Al)/R(TP) for these two values of R(Al).

the "inner melt" of the TP cell was made slightly thicker and was checked immediately before use to make certain that the ice mantle was completely free. This procedure seems to have eliminated low values of R(TP).

Except for cell A–3, the mean R(Al) also tended to increase similar to the mean R(TP) with each series of measurements. If the results on cell A–3 are included, the spread of the mean R(Al) and the average standard deviation correspond to 2.15 mK and ± 0.17 mK, respectively. On the other hand, if cell A–3 is ex-

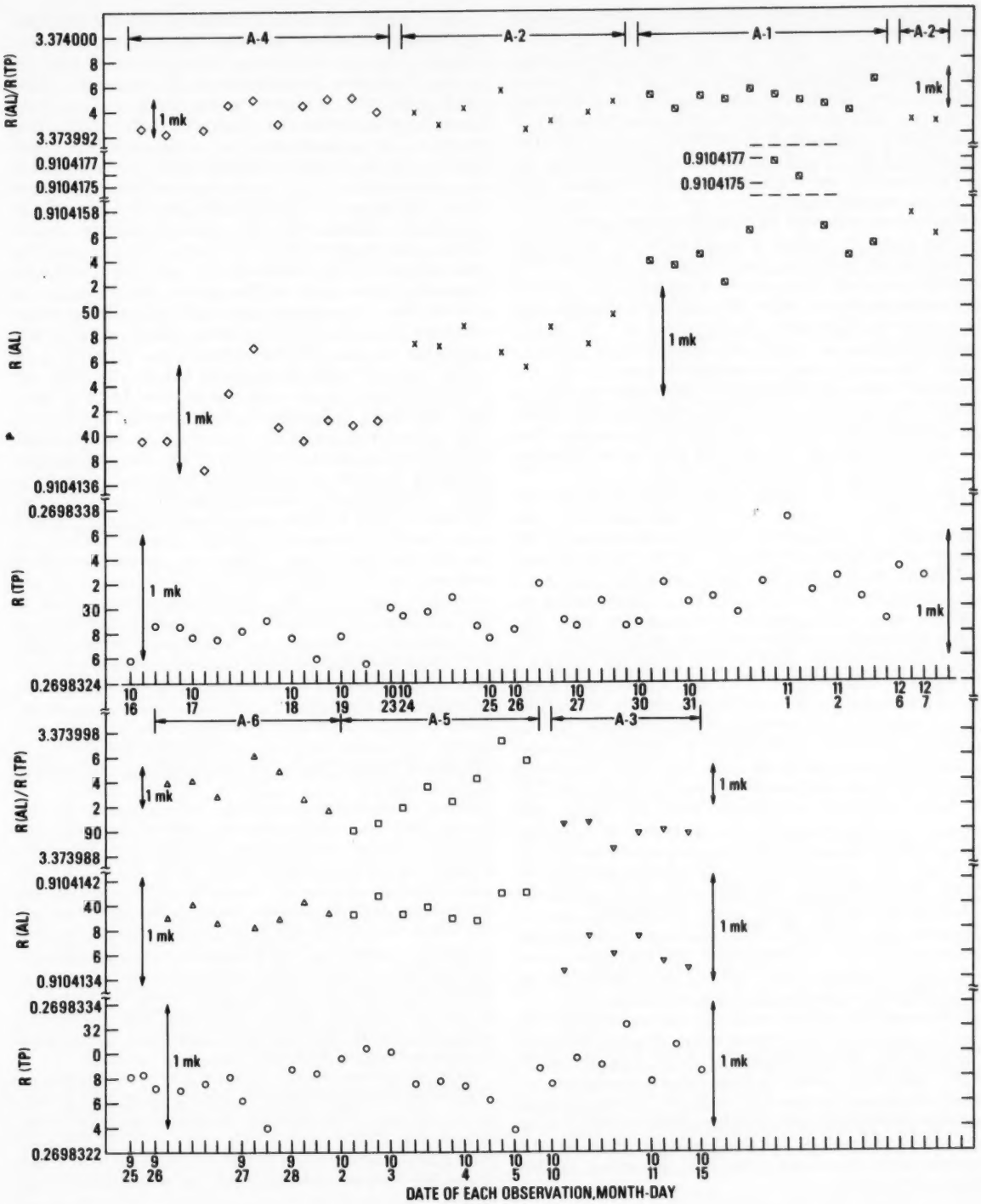

FIGURE 11. *Sequence of observed resistances (at "zero current") of the platinum resistance thermometer (HTSS–15) at the triple point of water and in the various aluminum-point cells.*

The ratios of the resistances $R(\mathrm{Al})/R(\mathrm{TP})$ are plotted at the location (abscissa) corresponding to the observed value of $R(\mathrm{Al})$.

cluded, the spread of the mean R(Al) and the average standard deviation correspond to 1.77 mK and ±0.17 mK, respectively, which are not very different from the values obtained including cell A–3 in the group. Actually, the difference between the lowest mean R(Al) (i.e., cell A–3) and the next lowest mean R(Al) (cell A–6) is smaller than the differences between the highest (cell A–1) and the second highest (cell A–2), and between the second highest and third highest (cell A–4) values of mean R(Al)'s.

The values of mean R(Al)/R(TP) seem to be more random than the values of mean R(TP) or the values of mean R(Al). If the average of the mean R(Al)/R(TP)'s of cells A–6, A–5, A–4, and A–2, which have a spread that corresponds to only 0.18 mK, is compared with the values obtained with cells A–3 and A–1, the deviations correspond to −1.23 mK and +0.39 mK, respectively. However, the standard deviations of the observed values of R(Al)/R(TP) are large enough to include the results on cell A–1 with the four cells. On the other hand, the results on cell A–3 suggest that the aluminum sample in the cell may be of different purity from those of the other five cells.

The standard deviations of the values of R(TP) and R(Al) obtained for each series of measurements are considerably less than the standard deviations of the values of R(Al)/R(TP) (except in the case of cell A–4 where the standard deviations of R(Al) and of the ratio R(Al)/R(TP) are close). This deterioration in precision arises from the amplification (by about 3.4) of the variations in R(TP) when the ratio R(Al)/R(TP) is computed. In the case of cell A–4, the standard deviation (±0.31 mK) of R(Al) was sufficiently large that the deviation in R(TP) (standard deviation: ±0.12 mK) did not contribute significantly to the standard deviation of R(Al)/R(TP). When the ratio R(Al)/R(TP) was computed from the mean R(Al) and mean R(TP) and compared with the mean R(Al)/R(TP) for each cell, the maximum deviation (0.11 mK) occurred in the measurements with cell A–2. In the case of cell A–5, where the standard deviation (±0.76 mK) and the spread (2.25 mK) of the R(Al)/R(TP) values are the largest, the difference between [mean R(Al)]/[mean R(TP)] and mean R(Al)/R(TP) corresponds to only 0.06 mK. This close agreement in the values of [mean R(Al)]/[mean R(TP)] and mean R(Al)/R(TP) indicate there are no gross errors in the computations employing the observed data.

Following the above sets of measurements the freezing points of two freezes were obtained with cell A–2 (see fig. 11 at 12–6 and 12–7). The values of R(TP) and R(Al) seem to follow the general upward trend; the values of the ratio R(Al)/R(TP) are in good agreement with the earlier values. These values were not included among the earlier data used in the analysis and discussion that are presented in this paper.

9. Discussion and Conclusions

The results of the freezing-point investigations on two batches of aluminum samples of nominally 99.999 percent purity show that within the precision of the experimental method presented in this paper the two samples can not be distinguished by their freezing points. However, one specimen of batch No. 1558, which cell A–3 contains, seems to have a slightly lower freezing point than the other specimens; this suggests the possibility that contamination could have occurred during preparation of the cell or that the sample bars are not homogeneous. When the mean values of the ratio R(Al)/R(TP) for five out of the six cells (excluding cell A–3) are compared, the spread of the ratio corresponds to 0.51 mK. The mean of the ratio R(Al)/R(TP) obtained for cell A–3 deviates from the mean ratio of the above five cells by an amount that corresponds to −1.31 mK. The average standard deviation of the ratios R(Al)/R(TP) obtained for the six cells corresponds to ±0.40 mK.

The experimental procedures that have been developed in the present work and the results that have been obtained demonstrate that aluminum can provide a freezing-point that is at least as reproducible as the freezing point of antimony [19]. Since aluminum is highly reactive chemically it must be isolated in inert surroundings. Although graphite (carbon) and aluminum form a stable compound (Al_4C_3) [7], aluminum can be contained in a graphite crucible without excessive reaction, if any. Either the aluminum-carbon reaction is slow even near the temperature of the aluminum point or the aluminum carbide that is formed adheres strongly to the graphite crucible and is relatively insoluble in aluminum. (Microscopic investigations of Al_4C_3 have been reported on samples that were formed when aluminum was cast in graphite crucibles under vacuum and at temperatures above 1000 °C [25]. The Al_4C_3 crystallites that were formed in that case apparently rose to the surface of the liquid aluminum where they were observed after the sample was solidified.)

Since aluminum supercools only about 1 K, the freezing of the aluminum can be initiated in the furnace without withdrawing the hot cell from the furnace as is customarily done with antimony [18], which usually supercools over 10 or 20 K, to initiate the freeze. After the freeze starts, a fused quartz rod should be inserted in the thermometer well of the cell to induce a mantle of solid aluminum around the well and provide a liquid-solid interface close to the prt. When the aluminum-point cells were prepared to freeze as outlined above, the equilibrium freezing temperatures of five out of six cells have been found to have a range of 0.51 mK.

The work presented in this paper was performed employing a prt of an R(0 °C) of only about 0.26 Ω with an a-c bridge. The average standard deviations obtained for R(TP) and R(Al) were ±0.14 mK and ±0.17 mK, respectively. However, the values of R(Al) that were obtained included effects of inductive interaction. Therefore, proper correlation with observed resistances at the other fixed points cannot be made. At this low thermometer resistance the temperature sensitivity of d-c resistance measurements employing, for example the Mueller bridge (G–3), is only 1 mK

with 10 mA thermometer current and 10 nV detector sensitivity. The steps of the lowest decade of the Mueller bridge that was available was 10 $\mu\Omega$. The measurements utilizing this Mueller bridge with the above prt would be rather imprecise.[3] A prt of 2.6 or 5 Ω or even slightly higher mounted on a sapphire coil form would permit d-c measurements at about 0.1 mK sensitivity using the Mueller bridge and allow proper correlation of the resistances observed at the various fixed points. The prt should have a helically wound sensor coil for use also with a-c bridges. The comparison measurements at the TP show that the inductive interaction of the prt with its metallic environment would be less if the sensor design were a helical coil instead of the bird-cage type.

The author is grateful to R. E. Michaelis and C. Stanley, Office of the Standard Reference Materials, for providing the aluminum samples for the work; to J. L. Riddle and J. L. Sligh, Temperature Section, for help in assembling the aluminum-point cells and carrying out some of the preliminary freezing-point experiments; to E. I. Klein, Glassblowing Shop, for fabricating the fused quartz cells; and to B. I. Baugher, Scientific Instrument Shop, for "machining" the various components of the furnace.

10. References

[1] Berry, R. J., Platinum resistance thermometry in the range 630–900 °C, Metrologia **2**, No. 2, 80–90 (Apr. 1966).

[2] Brandt, J. L., Properties of pure aluminum, in Aluminum. Vol. **I.** Properties, Physical Metallurgy, and Phase Diagrams, Van Horn, K. R., Editor, 1–30 (American Society for Metals, Metals Park, Ohio, 1967).

[3] Cutkosky, R. D., An a-c resistance thermometer bridge, J. Res. Nat. Bur. Stand. (U.S.) **47C** (Engr. and Instr.), Nos. 1 and 2, 15–18 (Jan.–June 1970).

[4] Evans, J. P., and Burns, G. W., A study of stability of high temperature platinum resistance thermometers, in American Institute of Physics, Temperature, Its Measurement and Control in Science and Industry, Vol. **3**, Part 1, 313–318 (Reinhold Publishing Corp., New York, N. Y., 1962).

[5] Evans, J. P., and Wood, S. D., An intercomparison of high temperature platinum resistance thermometers and standard thermocouples, Metrologia **7**, (No. 3), 108–130 (July 1971).

[6] Furukawa, G. T., Douglas, T. B., and Pearlman, N., Heat capacities, in American Institute of Physics Handbook, pp. 4–105 to 4–118, third edition (McGraw-Hill Book Company, New York, N. Y., 1972).

[7] Furukawa, G. T., Douglas, T. B., Saba, W. G., and Victor, A. C., Heat capacity and enthalpy measurements on aluminum carbide (Al_4C_3) from 15 to 1173 °K. Thermodynamic properties from 0 to 2000 °K, J. Res. Nat. Bur. Stand. (U.S.) **69A** (Phys. and Chem.), No. 5, 423–438 (1965).

[8] Furukawa, G. T., Riddle, J. L., and Bigge, W. R., Investigation of freezing temperatures of National Bureau of Standards tin standards, in Temperature, Its Measurement and Control in Science and Industry, Vol. **4**, Part 1, 247–263 (Instrument Society of America, Pittsburgh, Pa., 1972).

[9] Gmelins Handbuch der Anorganischen Chemie, Achte Auflage, Antimon, System-Nummer 18, Teil B., Lieferung **1** (Verlag Chemie, Berlin, 1943).

[10] Goldsmith, A., Waterman, T. E., and Hirschhorn, H. J., Handbook of Thermophysical Properties of Solid Materials. Vol. **I:** Elements, revised edition, 752 pages (The Macmillan Company, New York, N. Y., 1962).

[11] Hansen, M., Constitution of Binary Alloys, second edition (McGraw-Hill Book Company, New York, N. Y., 1958).

[12] Kasen, M. B., private communication to R. E. Michaelis (OSRM), August 15, 1972.

[13] Kasen, M. B., and Powell, R. L., Report of Investigation, Ultra-Purity Aluminum: RM–1R and RM–1C, private communication, October 27, 1970.

[14] McAllan, J. V., and Ammar, M. M., Comparison of the freezing points of aluminum and antimony, in Temperature, Its Measurement and Control in Science and Industry, Vol. **4**, Part 1, 273–285 (Instrument Society of America, Pittsburgh, Pa., 1972).

[15] McLaren, E. H., and Murdock, E. G., The freezing points of high purity metals as precision temperature standards. III. Thermal analyses on eight grades of zinc with purities greater than 99.99+%, Can. J. Phys. **36**, 585–598 (1958).

[16] McLaren, E. H., and Murdock, E. G., The freezing points of high purity metals as precision temperature standards. V. Thermal analyses on 10 samples of tin with purities greater than 99.99+%, Can. J. Phys. **38**, 100–118 (1960).

[17] McLaren, E. H., and Murdock, E. G., Radiation effects in precision resistance thermometry. I. Radiation losses in transparent thermometer sheaths, Can. J. Phys. **44**, 2631–2652 (1966).

[18] McLaren, E. H., and Murdock, E. G., The freezing points of high-purity metals as precision temperature standards. VIII a. Sb: apparatus, freezing techniques, and ingot morphology, Can. J. Phys. **46**, 369–400 (1968).

[19] McLaren, E. H., and Murdock, E. G., The freezing points of high-purity metals as precision temperature standards. VIII b. Sb: Liquidus points and alloy melting ranges of seven samples of high-purity antimony; temperature-scale realization and reliability in the range 0–631, °C. Can. J. Phys. **46**, 401–444 (1968).

[20] National Bureau of Standards (U.S.), Handbook 102, ASTM Metric Practice Guide, 53 pages (March 1967).

[21] Nesmeyanov, A. N., Vapor Pressure of the Elements (Academic Press, Inc., New York, N. Y., 1963).

[22] Powell, R. L., and Childs, G. E., Thermal conductivity, in American Institute of Physics Handbook, pp. 4–142 to 4–162, third edition (McGraw-Hill Book Company, New York, N. Y., 1972).

[23] Riddle, J. L., Furukawa, G. T., and Plumb, H. H., Platinum resistance thermometry, Nat. Bur. Stand. (U. S.), Monogr. 126, 129 pages (April 1973).

[24] Roeser, W. F., and Lonberger, S. T., Methods of Testing Thermocouples and Thermocouple Materials, Nat. Bur. Stand. (U.S.), Circular 590, 23 pages (Feb. 1958).

[25] Schippers, M., Mikroskopische Untersuchung der Verbindung Al_4C_3 in Gefüge von Gussproben aus Al 99.99 und Al 99.5, Z. Metallk. **51**, 246–248 (1960).

[26] Stull, D. R., and Prophet, H., JANAF Thermochemical Tables, Second Edition, National Standard Reference Data Series—National Bureau of Standards (U.S.), 37, 1141 pages (June 1971).

[27] The International Practical Temperature Scale of 1968. Adopted by the Comité International des Poids et Mesures, Metrologia **5**, (No. 2), 35–44 (April 1969).

[28] Wood, Sharrill D., An investigation of the stability of and insulation leakage in some high temperature resistance thermometers: An interim report, Nat. Bur. Stand. (U.S.), Tech. Note 764, 31 pages (May 1973).

(Paper 78A4–828)

[3] Evans and Wood [5] employed a G–4 model of the Mueller bridge which has 1 $\mu\Omega$ as its lowest decade. Using prt's of the birdcage design, with 0.20 to 0.26 Ω resistance at 0 °C, they give standard deviation of ± 2.2 mK to ± 2.5 mK for the measurements at the antimony point.

538-709 OL - 74 - 4

JOURNAL OF RESEARCH of the National Bureau of Standards—A. Physics and Chemistry
Vol. 78A, No. 4, July–August 1974

Prediction of the Viscosities of "Soda-Lime" Silica Glasses

Kenneth C. Lyon*

Institute for Materials Research, National Bureau of Standards, Washington, D.C. 20234

(March 6, 1974)

Published data are used to develop factors for predicting the viscosity-temperature relationship from the compositions of "soda-lime" type silicate glasses at specific temperatures in the range of 600 to 1300 °C. The effects of Na_2O, K_2O, CaO, MgO, Al_2O_3 and their interactions are evaluated. The influence of minor amounts of BaO, B_2O_3, Li_2O, and F_2, in the temperature range of 700 to 1300 °C, is estimated.

Key words: Composition; Fulcher equation; glasses; soda-lime glasses; viscosity.

1. Introduction

In his review of the subject of the viscosity of glass, Morey [1] [1] points out that this property is of practical importance in all stages of the manufacturing process, particularly with the development and use of automatic glass forming machinery. The glass supply should not only be of constant viscosity, but its viscosity-temperature relationship should be suitable for the forming process and the rate of working. Therefore, he continues, the knowledge of the relation between composition and viscosity and between temperature and viscosity is a matter of importance in glass manufacturing. Numerous investigations of this property, reported in the literature, attest to the interest in the viscosity of glasses. Several of these studies were undertaken to develop an understanding of the nature of glass in the molten state. The sole purpose of many others was to determine the effects of composition and temperature on the viscosities of the glasses studied. Titles of the reports of a number of these investigations are listed under section 8.

The purpose of the investigation reported here is to develop a method for predicting viscosity-temperature relationships from the compositions of silicate glasses of the "soda-lime" type commonly used in the manufacture of glass containers, sheet, and tableware. This investigation is not the first of its kind. The results of previously published studies [2, 3, 4, 5, 6, 7, 8] are generally inadequate in predicting the viscosities of simple alkali-silica glasses or fail to indicate the effects on viscosity of interactions between the components in more complex glasses.

A reliable prediction of glass viscosity is of value because the measurement of the viscosity of a glass at a number of elevated temperatures requires relatively expensive equipment, care, and effort. The glass for the determination has to be melted and homogenized and it should be chemically analyzed. On the other hand, a predicted glass viscosity may be calculated from the results of a chemical analysis, an analysis calculated from raw materials in the batch, or from a hypothetical glass composition.

Prediction of the viscosity-temperature relationship is of increased value if it is necessary to change the composition of a glass being used in a production operation. It may be possible, through prediction, to make the needed change and still maintain the viscous properties characteristic of the glass formerly produced by making compensating changes in glass composition. If such compensation is not possible, the glass technologist will know, by calculation, how the viscous properties have changed and may observe the effect on the process and product.

2. Procedures

All data used in this investigation were taken from published literature. Viscosity is expressed as $\log_{10}$ poise (P). Temperature is given in degrees Celsius (°C).

Discrepancies were found, as anticipated, between the results reported by different authors and laboratories. Results published by Lillie [9, 10], the Owens-Illinois Research Laboratories [11], Poole [12], and Poole and Gensamer [5] were arbitrarily chosen as standards for evaluating the results from other sources.

Interpolation and extrapolation were used to obtain viscosity values corresponding to 600, 700, 800, 900, 1000, 1100, 1200, and 1300 °C for each glass composi-

*Research Associate from the Glass Container Manufacturers Institute, Inc., at the National Bureau of Standards 1972–73. Present address: 317 East Washington, Street, Dunkirk, Indiana 47336.

[1] Figures in brackets indicate the literature references at the end of this report.

tion of interest. The Fulcher equation [13] was used for this purpose. It is

$$\log_{10} \text{viscosity} = A + \frac{B}{T - T_0} \quad (1)$$

in which T is the temperature and A (usually negative), B, and T_0 are constants characteristic of a specific glass composition. The constants were evaluated by least squares [14] treatment of the published viscosity-temperature data. T_0 of eq (1) was found to 1 °C by iteration. The algebraic equivalent of eq (1),

$$T = T_0 + \frac{B}{\log_{10} \text{visc.} - A} \quad (2)$$

was used alternately to evaluate the constants. A was found by iteration to the nearest 0.01 $\log_{10}$ P.

The viscosity values calculated for each temperature level were related to the weight percent composition of the corresponding glasses. Compositions were expressed as functions of the weight percent of components which replace silica in the glass. The development of the empirical equation for calculating viscosity from composition required experimentation in methods of expressing composition and methods of expressing apparent interactions between components. The experimentation advanced from the consideration of two-component alkali-silica glasses to the eventual evaluation of six-component glasses made up of ingredients likely to be found in major amounts in commercial glasses. These ingredients are Na_2O, K_2O, CaO, MgO, Al_2O_3, and SiO_2. The effects of the minor ingredients BaO, B_2O_3, Li_2O, and F_2 were estimated from the differences between the observed viscosities and viscosities calculated on the basis of the major ingredients present. Two-component interactions which seemed to be of significance were evaluated. No attempt was made to evaluate possible three (or more)—component interactions. Standard least-squares regression procedures were used in making the calculations.

3. Results

The empirical equation developed in this investigation to relate the viscosity of a "soda-lime"-silica glass at a specific temperature to its composition is

$$\begin{aligned}\log_{10} \text{poise} = {} & b_1 + b_2 \cdot \%Na_2O + b_3 \cdot \%K_2O + b_4 \cdot \%CaO \\ & + b_5 \cdot \%MgO + b_6 \cdot \%Al_2O_3 + b_7 \cdot \sqrt{\%Na_2K_2O_2}\,^{2} \\ & + b_8 \cdot \%Na_2O \cdot \%CaO + b_9 \cdot \%Na_2O \cdot \%MgO \\ & + b_{10} \cdot \%K_2O \cdot \%CaO + b_{11} \cdot \%K_2O \cdot \%MgO \\ & + b_{12} \cdot \%CaO \cdot \%MgO + b_{13} \cdot (\%CaO)^2 + b_{14} \\ & \cdot (\%MgO)^2 + \ldots b_n \cdot \%N,\end{aligned}$$

where N represents minor ingredients and their interactions.

A summary of components, ranges of composition and data sources for the glasses used in the calculations will be found in appendix A. Appendix B gives an illustrative calculation of viscosity using the predictive factors.

It is to be noted that the constants representing the effects of weight percent component replacing silica are expressed in units of 10 weight percent. This is done to reduce the numerical magnitudes of the products representing interactions and of the second power effects. A soda content of 15.5 percent is thus denoted as 1.55 for purposes of calculation.

The effects on glass viscosity of phosphorous pentoxide [32], zinc oxide [33], strontium oxide [34], and iron oxide [35] may be estimated from published data.

4. Discussion of Procedures

The Fulcher equation (eq (1)) is commonly used to express the glass viscosity-temperature relationship. It has limitations. Macedo and Napolitano [15] comment that, in general, if the data are limited to viscosity values between 10^2 and 10^{12} a good fit can be obtained to the Fulcher equation. A more serious practical problem arises if the equation is used for extrapolation. If the equation is carefully fitted to high temperature data, it will not reliably predict values at lower temperatures, and the reverse, even though the viscosities are in the range of 10^2–10^{12}. This difficulty may be a consequence of the nature of the viscosity-temperature relationship. Plumat [16, 17] argues that the glass viscosity-temperature curve is made up of intersecting curved segments. He illustrates his contention by plotting log viscosity versus reciprocal absolute temperature to show the presence of (nearly) linear segments. The usual viscosity determination has too few data points to illustrate Plumat's concept, but there are three reports [18, 19, 20] which have sufficient determinations for this purpose. It appears, then, that the values predicted by extrapolation could depend on the positions of the measured data points within the several segments of the viscosity-temperature curve to which the equation is fitted. In preparing data for this investigation it was not always possible to avoid extrapolation; however, extended extrapolation was not needed.

The effect of composition on viscosity at constant temperature is analyzed in this study. However, earlier investigators have evaluated the effect of composition on temperatures corresponding to constant viscosity values. This concept offers a direct approach to the practical problem of the effect of composition change on the glass manufacturing process. The practical interest is in temperatures associated with recognized viscosity levels characteristic of the stages in the manufacturing process. More specifically, the interest is in the temperature change or heat removal needed to advance from one stage to the next. The temperatures of interest can be calculated by use of the

[2] This term represents the amount of the hypothetical equimolecular $Na_2O \cdot K_2O$ which could be formed in the glass. It is usually a function of the amount of potash. The amount of soda present could control the amount of the compound theoretically formed in high potash-low soda glasses. The mathematical form provides for a relatively greater effect with low amounts of the second alkali present, diminishing effect as the second alkali is increased, and maximum effect with the two alkalies present in equimolecular concentrations.

TABLE 1. *The effect of replacement of 10 wt. % silica by other components on the $\log_{10}$ viscosity of glasses at 600–1300 °C*

Symbol	Component	Factors							
		600°	700°	800°	900°	1000°	1100°	1200°	1300°
b_1	Intercept	11.7404	8.9040	7.2752	6.1155	5.2559	4.5912	4.0693	3.6486
b_2	Na_2O	−1.4149	−0.9424	−0.8101	−0.7182	−0.6535	−0.6051	−0.5700	−0.5436
b_3	K_2O	−0.8700	−0.6498	−0.4712	−0.3781	−0.3336	−0.3152	−0.3143	−0.3235
b_4	CaO	3.4391	2.0773	1.4369	1.0329	0.7104	0.5395	0.3738	0.2385
b_5	MgO	1.5560	3.3705	3.0888	2.5948	2.1023	1.5678	1.1125	0.7012
b_6	Al_2O_3	1.3377	0.9293	0.6552	0.4982	0.3896	0.3345	0.2880	0.2539
b_7	$\sqrt{Na_2K_2O_2}$ [1]	−0.5996	−0.1548	−0.1052	−0.0690	−0.0323	−0.0138	0.0072	0.0260
b_8	$Na_2O \cdot CaO$	−1.1861	−0.9619	−0.7368	−0.5912	−0.4816	−0.4076	−0.3447	−0.2936
b_9	$Na_2O \cdot MgO$	−1.0317	−1.2709	−1.2973	−1.1189	−0.8889	−0.6438	−0.4180	−0.2089
b_{10}	$K_2O \cdot CaO$	−0.3239	−0.4349	−0.3556	−0.3158	−0.2923	−0.2708	−0.2510	−0.2330
b_{11}	$K_2O \cdot MgO$	−0.4098	−0.6068	−0.5452	−0.3995	−0.2462	−0.0774	0.0669	0.1992
b_{12}	$CaO \cdot MgO$	−1.2973	−1.7221	−1.3761	−1.1431	−0.9721	−0.8381	−0.7307	−0.6417
b_{13}	$(CaO)^2$	−0.2576	−0.1791	−0.2320	−0.2400	−0.2013	−0.2164	−0.1995	−0.1817
b_{14}	$(MgO)^2$	1.2377	−0.3515	−0.4843	−0.5193	−0.5366	−0.4865	−0.4540	−0.4204
No. of Glasses [2]		72	77	77	77	77	77	77	77
Std. Error of Est. [3]		0.1627	0.0568	0.0462	0.0417	0.0370	0.0327	0.0308	0.0315
	$BaO \cdot RO$ [4]		−0.771	−0.650	−0.548	−0.476	−0.418	−0.379	−0.333
	Li_2O		−2.602	−1.952	−1.557	−1.318	−1.175	−1.101	−1.071
	$Li_2O \cdot RO$ [5]		−3.516	−2.728	−2.160	−1.709	−1.336	−1.006	−0.724
	B_2O_3		0.467	−0.446	−0.795	−0.925	−0.984	−0.885	−0.754
	$B_2O_3 \cdot RO$ [5]		−1.075	−0.591	−0.333	−0.169	−0.031	0.050	0.101
	F_2		−4.795	−3.133	−2.284	−1.812	−1.547	−1.390	−1.303

[1] The amount of the equimolecular compound which theoretically could be formed from the Na_2O and K_2O present.
[2] The number of glass compositions, i.e., observations, used in the regression calculations of the factors.
[3] $\sqrt{\frac{\text{Total of variances between calculated and observed results}}{\text{Degrees of freedom}}}$
[4] Alkaline earth oxides, "RO", excluding BaO.
[5] Alkaline earth oxides including BaO.

factors given in table 1 as outlined in appendix B.

The two propositions: (1) viscosity-composition at constant temperature and (2) temperature-composition at constant viscosity are examined in figures 1 and 2. Figure 1 illustrates the effect of composition on the calculated viscosities of soda-silica and potash-silica glasses at three temperatures. Figure 2 shows the effect of composition on temperatures corresponding to three viscosity levels.

If a linear analysis of the relationship between temperature and composition at constant viscosity (fig. 2) is assumed then constraints arise in the choice of constants for the Fulcher Equation when varying composition. This approach would greatly limit the usefulness of the Fulcher Equation and of the constants, b_i, in the empirical relation between concentrations of component oxides and viscosity (sec. 3). The data in figure 2 is insufficient to suggest an appropriate nonlinear relationship, therefore, the approach relating viscosity to composition by a linear function and viscosity to temperature by the Fulcher equation are chosen instead.

Since glass compositions are expressed in terms of weight percent, it is more convenient to relate viscosity to composition expressed in this way than it is to relate viscosity to composition expressed as molecular percentage or ratios of components. Weight percent is based on a unit weight of material. Molecular percent or ratio are based on neither weight nor volume.

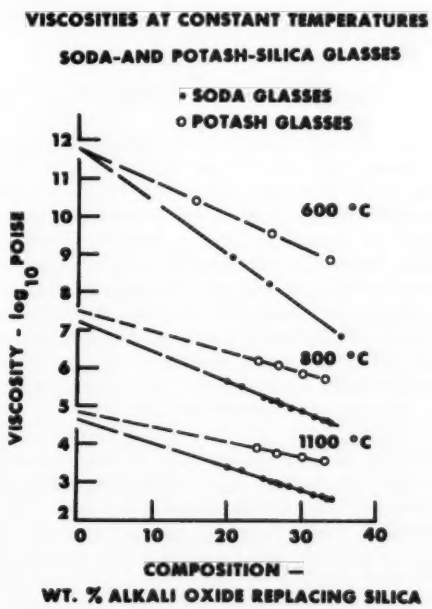

FIGURE 1

Huggins [22] has proposed a method of expressing composition in terms of a unit volume of glass defined

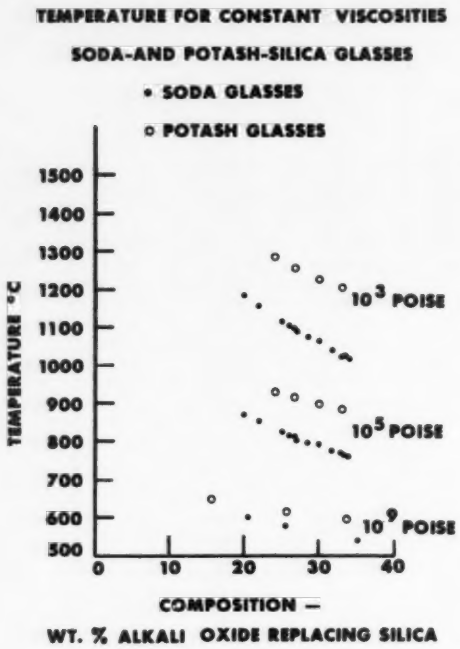

FIGURE 2

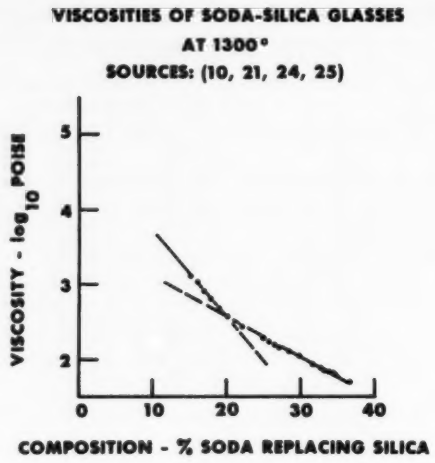

FIGURE 3

by a fixed number of oxygen atoms. This is not a convenient method. The expression of composition as weight percent seems to be satisfactory for the purposes of the present investigation.

5. Discussion of Results

The $\log_{10}$ viscosity-composition relationship for soda-silica glasses appears to be linear in the range of approximately 20–35 percent soda. There is a distinct change of slope at a soda content near 20 percent, as illustrated in figure 3. This is probably due to the miscibility gap in the system. The upper end lies near 20 percent soda. The effect of potash in potash-silica glasses seems to be similar as judged from the relatively few viscosity measurements made on low potash glasses.

A number of interactions between components in the glasses are indicated in table 1. Several authors [4, 5, 11, 12, 23] have either implied, referred to, or illustrated some of these. The expression for the soda-potash interaction maximizes the effect at the equimolecular ratio as indicated by Poole [12]. The soda-lime and soda-magnesia interactions are needed to explain the Poole and Gensamer [5] results. It was assumed that there were similar interactions between potash and these two alkaline earth oxides. The lime-magnesia interaction is indicated by English [23], is illustrated by Owens-Illinois [11] and is implied by Ochotin [4]. A test calculation failed to indicate a maximum effect of this interaction at the dolomite ratio of the oxides. An interaction between lime and alumina illustrated by English [23] could not be confirmed by the results published by Poole and Gensamer [5].

The "Standard Error of Estimate" values (table 1) are large in comparison with the indicated effect of soda, keeping in mind that the soda factors represent the effect of a 10 percent replacement of silica by soda. The magnitude of these "error" values may also be compared with the indicated effect on viscosity of one degree increase of temperature. The latter, listed below, was calculated by differentiation of the Fulcher equation fitted to the mean viscosity values of 77 glasses used in the calculation of the factors of table 1.

Temperature	$-d(\log \text{visc.})/dT$
°C	
600	0.0346
700	.0208
800	.0139
900	.0099
1000	.0074
1100	.0058
1200	.0046
1300	.0038

The factors for barium oxide, lithia, and boric oxide show interactions with "RO". These factors were calculated from glass compositions which contained dolomite. The individual effects of lime and magnesia are not evaluated.

The factors were tested by using them to predict the viscosities of six glasses which had not been included in the calculations leading to the results shown in table 1. The individual glasses are identified by the numbers used in the references from which the data were taken.

These glasses are:

Source Glass No.	[26]		[27]			[28]
	1	2	10	11	330	710
SiO_2	71.24%	70.80%	70.4%	71.8%	69.1%	70.5%
Al_2O_3	1.47	1.82	2.73	2.58	1.61	
CaO	10.81	6.20	10.6	6.01	5.60	11.6
MgO	2.92	4.18	0.62	4.02	4.07	
BaO	0.69	0.78	0.93	0.58	0.16	
Na_2O	12.48	15.80	11.9	12.6	17.7	8.7
K_2O	0.39	0.42	1.18	0.98	0.89	7.7
B_2O_3			0.89	0.85	0.76	
Sb_2O_3						1.1

The results of the predictive calculations are given in table 2.

TABLE 2. *Predicted and interpolated viscosities of six glasses*

Temp. °C	Glass No. 1		Glass No. 2		Glass No. 10	
	$\log_{10}$ Viscosity		$\log_{10}$ Viscosity		$\log_{10}$ Viscosity	
	Predict.	Interpol.*	Predict.	Interpol.	Predict.	Interpol.
700	8.388	8.382	7.770	7.772	8.465	8.365
800	6.475	6.516	6.069	6.113	6.505	6.490
900	5.174	5.214	4.906	4.954	5.196	5.208
1000	4.237	4.260	4.059	4.099	4.260	4.276
1100	3.515	3.526	3.417	3.441	3.557	3.569
1200	2.953	2.944	2.912	2.920	3.017	3.013
1300	2.502	2.473	2.506	2.497	2.588	2.565
	Glass No. 11		Glass No. 330		Glass No. 710	
600					11.319	11.057
700	8.370	8.277	7.328	7.151	8.219	8.134
800	6.557	6.526	5.670	5.640	6.382	6.307
900	5.311	5.301	4.561	4.575	5.118	5.056
1000	4.400	4.398	3.768	3.784	4.201	4.145
1100	3.708	3.703	3.174	3.173	3.488	3.453
1200	3.169	3.153	2.717	2.687	2.933	2.909
1300	2.735	2.706	2.354	2.291	2.484	2.471

*Interpolated from data given in sources.

It is the author's opinion that the differences between predicted and interpolated results shown in table 3 are not serious in view of the several sources of data used in the calculation of the factors and the several sources represented in the tabulation. The results shown for glass No. 710 are of particular interest since this is a standard reference glass for viscosity measurements. It seems reasonable to believe that the consistently higher predicted values may be attributed to the presence of a substantial amount of antimony oxide reported as being in the glass. No predictive factor for the effect of this oxide was developed in this investigation.

In addition to the ranges of composition implied in the summary of appendix A, certain impressions as to applicable limits were formed as the calculations were being made. Table 3 represents a tentative conclusion as to ranges of composition to which the factors may be applied to calculate viscosity. The limits are conservative.

There is no assurance that glass compositions lying within these limits will be free of devitrification or immiscibility effects.

The particular assistance and counsel of G. W. Cleek, L. J. Frolen, A. Napolitano, and G. S. Ross, all of the Institute for Materials Research of the National Bureau of Standards, and of R. A. LeGrand, of the Ball Corporation, is gratefully acknowledged.

TABLE 3. *Suggested limits of glass composition for viscosity prediction*

Component	Range-%
SiO_2	65–80
Na_2O	11–35
CaO	0–14
MgO	0–12
CaO + MgO	0–16
K_2O	0–35
Al_2O_3	0– 8
BaO	0– 5
B_2O_3	0– 4
Li_2O	0– 4
F_2	0– 2

6. Appendix A. Summary of Glasses Used to Calculate 600 °C Factors of Table 1

No. of Glasses	Range of composition (percent)						Source
	SiO_2	Na_2O	K_2O	CaO	MgO	Al_2O_3	
Two-Component Glasses:							
3	79.4–64.8	20.6–35.2					[12]
3	84.3–66.3		15.7–33.7				[12]
Three-Component Glasses:							
6	80.7–64.4	4.6–31.3	3.8–14.3				[12]
7	77.2–61.5	14.2–24.7		3.8–14.3			[5]
8	79.1–62.6	15.0–27.8			3.1–11.7		[5]
4	72.5–65.0	19.8–24.5				5.1–10.2	[5]
Four Component Glasses:							
1	76.1	16.0		4.9	3.0		[5]
10	73.8–64.0	13.8–20.2		4.5–14.4		3.4–10.6	[5]
Five-Component Glasses:							
5	77.4–66.6	12.1–14.6	0.1– 4.4	10.2–12.1		0.2–7.2	[8]
4	70.2–67.5	11.9–15.3		9.8–13.3	0.6– 2.3	4.1– 7.3	[8]
1	69.2	12.7	8.7	9.6	1.7		[8]
Six-Component Glasses:							
20	72.0–59.5	10.5–15.0	0.1– 8.3	8.2–13.0	0.5–6.7	0.2– 6.7	[8]
Mean Composition (percent)	69.4	16.03	3.89	6.46	1.38	2.73	

Summary of Glasses Used to Calculate 700–1300 °C Factors of Table 1

Two-Component Glasses:							
12	80.0–66.2	20.0–33.8					[10,21]
5	76.1–63.4		23.9–36.6				[21]
Three-Component Glasses:							
2	72.0–70.1	26.8–21.1		6.8–8.8			[9,29]
Four-Component Glasses:							
1	71.6	19.3		8.9		0.2	[9]
Five-Component Glasses:							
5	77.4–66.6	12.1–14.0	0.1– 4.4	10.2–12.1		0.2– 7.2	[8]
23	73.8–67.5	11.9–18.0		0.3–13.3	0.1–11.9	0.1–7.3	[8,11,30,31,32]
1	67.2	12.7	8.7	9.6	1.7		[8]
Six-Component Glasses:							
28	73.4–69.7	10.0–15.9	0.1– 8.3	5.9–13.0	0.5– 6.7	0.1– 6.7	[8,31,32]
Mean Composition (percent)	70.4	15.06	3.93	6.63	2.36	1.46	
Other Glasses:			BaO				
8	73.7–69.1	11.1–13.9	1.0– 5.0	4.2– 7.2	2.9– 4.9	0.1– 0.2	[33]
			B_2O_3				
16	74.0–68.6	10.7–16.0	1.0– 5.0	2.9– 7.2	2.1– 4.9	0.1– 0.3	[30]
			Li_2O				
6	73.6–73.2	8.0–14.0	2.1–6.4	6.1– 7.3	4.2– 5.0	0.2	[31]
2	80.6–80.0		19.4–20.0				[21]
			F_2				
3	73.3–71.7	14.4–16.5	1.1– 2.0	6.0– 7.0	4.2– 5.0	0.1– 0.2	[32]

7. Appendix B. Calculation of the Viscosity of a Glass and Its Viscosity—Temperature Characteristics

The method of calculating the viscous properties of a soda-lime glass:

SiO_2	70.61%
Al_2O_3	1.47
CaO	10.81
MgO	2.92
BaO	0.69
B_2O_3	0.42
Na_2O	12.48
K_2O	0.39
Li_2O	0.13
F_2	0.08

will be illustrated.

The first step in the calculation is the division of the percent values by 10. Next, calculate the complete list of component values. These component values are then multiplied by the appropriate predictive factors. The total of these products plus the "intercept" value represents the predicted viscosity. The viscosity corresponding to 900 °C. will be calculated.

Calculation of $\log_{10}$ Viscosity at 900 °C

Component	Component value	Effect on log viscosity
Intercept	1.0	6.1155
Na_2O	1.248	−0.89631
K_2O	.039	−.01475
CaO	1.081	1.11656
MgO	.292	.75768
Al_2O_3	.147	.07324
$\sqrt{Na_2K_2O_2}$	.254	−.01753
$Na_2O \cdot CaO$	1.349	−.79753
$Na_2O \cdot MgO$	.364	−.40728
$K_2O \cdot CaO$	.042	−.01326
$K_2O \cdot MgO$	.011	−.00439
$CaO \cdot MgO$	.316	−.36122
$(CaO)^2$	1.169	−.28056
$(MgO)^2$	.085	−.04414
$BaO \cdot (CaO + MgO)$	.095	−.05206
Li_2O	.013	−.02024
$Li_2O \cdot (CaO + MgO + BaO)$	.019	−.04104
B_2O_3	.042	−.03339
$B_2O_3 \cdot (CaO + MgO + BaO)$	.061	−.02031
F_2	.008	−.01827
Calculated viscosity.....		5.0407

The calculated viscosities for other temperatures are:

700°	8.2028
800	6.3175
1000	4.1234
1100	3.4189
1200	2.8745
1300	2.4382

There are a number of methods which may be used to determine the values of the constants of the Fulcher equation (eq (1)). One of the simpler satisfactory methods is based on the calculated viscosity values for three temperatures. The Fulcher equation is written in the form

$$(-A \cdot T_0 + B) + (\log_{10} \text{Visc.}) \cdot T_0 + T \cdot A = |log_{10} \text{Visc.}) \cdot T$$

Three simultaneous equations representing viscosity-temperature characteristics at 700, 900, and 1300 °C., respectively, are written in this form:

$$(-A \cdot T_0 + B) + 8.203 \cdot T_0 + 700 \cdot A = 5742.1 \quad (700)$$

$$(-A \cdot T_0 + B) + 5.041 \cdot T_0 + 900 \cdot A = 4536.9 \quad (900)$$

$$(-A \cdot T_0 + B) + 2.438 \cdot T_0 + 1300 \cdot A = 3169.4 \quad (1300)$$

The results of the solution of the equations are:

$$T_0 = 280.3$$

$$A = -1.594$$

$$B = 4111.7.$$

These constants may be used in the Fulcher equation in the form of eq (1) to calculate viscosities at other temperatures or in the form of eq (2) to calculate temperatures corresponding to specific viscosities such as those of the "working range" [36].

8. References

[1] Morey, G. W., The Viscosity of Glass, Ch. 5, The Properties of Glass, 2nd ed., 132–165 (Rheinhold, New York, 1954).

[2] Gehlhoff, G. and Thomas, M., Eigenschaften der Gläser in Abhangekeit von der Zusammansetzung. III Die Viskosität der Gläser. Zeitschr f. Techn. Physik **7**, No. 6, 260–278 (1926).

[3] Boow, J., and Turner, W.E.S., The viscosity and working characteristics of glass. Part I–The viscosity of some commercial glasses at temperatures between approximately 500° and 1400°, Jour. Soc. Gl. Tech. **26**, 215–237 (1942).

[4] Ochotin, M. W., Calculation of Viscosity of Commercial Silicate Glasses by the Use of Nomographs, Steklo i Keram. **11**, No. 1, 7–11 (1954) Abstracts: Jour. Soc. Gl. Tech **40**, No. 12, 169A–170A (1956), Glastech. Ber. **29**, No. 6, 253 (1956).

[5] Poole, J. P., and Gensamer, M., Systematic study of effect of oxide constituents on viscosity of silicate glasses at annealing temperatures, Jour. Amer. Ceram. Soc. **32**, No. 7, 220–229 (1949).

[6] Allison, R. S., and Turner, W. E. S., Further investigation upon the influence of boric oxide on the rate of melting of the batch, and on the rate of refining and setting of commercial glasses of the soda-lime-silica type, Jour. Soc. Gl. Tech. **38**, 297–364 (1954).

[7] Knapp, O., Berechnung der Viskosität Ternärer Silikat Gläser aus der Zusammensetzung, Glas-Email-Keramo Technik. **18,** No. 2, 52–59 (1967).
[8] Lakatos, T., Johansson, L. G., and Simmingsköld, B., Viscosity temperature relations in the glass system SiO-Al_2O_3-Na_2O-K_2O-CaO-Mgo in the Composition Range of Technical Glass, Glass. Techn. **13,** No. 3, 88–95 (1972).
[9] Lillie, H. R., Viscosity of glass between its strain point and melting temperature, Jour. Amer. Ceram. Soc. **14,** No. 7, 502–511 (1931).
[10] Lillie, H. R., High temperature viscosities of soda-silica glasses, Jour. Amer. Ceram. Soc. **22,** No. 11, 367–374 (1939).
[11] Owens-Illinois Glass Co., General Research Laboratory, Effect of substituting MgO for CaO on properties of typical soda-lime glasses, Jour. Amer. Ceram. Soc. **27,** No. 8, 221–31 (1944).
[12] Poole, J. P., Low temperature viscosity of alkali silicate glasses, Jour. Amer. Ceram. Soc. **12,** No. 7, 230–233 (1949).
[13] Fulcher, G. S., Analysis of recent measurements of the viscosity of glasses, Jour. Amer. Ceram. Soc. **8,** No. 6, 339–360 (1925).
[14] Legendre, A. M., Nouvelles Méthodes pour la Détermination des Orbites des Cometes., Appendix: Sur la Méthode des Moindres Quarrés, Paris (1805).
[15] Macedo, P. B., and Napolitano, A., Inadequacies of viscosity theories for B_2O_3, Jour. Chem. Phys. **49,** No. 4, 1887–1895, (1968).
[16] Plumat, E., Structure du Verre, Traitment Thermique et Viscosité, Sillicates Industriels **21,** Nos. 10–11, 391–396, 447–457 (1956).
[17] Plumat, E., Relation entre la Viscosité de Verre et sa Structure en Fonction de la Température et de la Composition, Travaux du IV Congres International du Verre, Paris, July, 1956, Group VI Structure, pp. 299–309, Imprimarie Chaux, Paris (1957).
[18] Napolitano, A., and Hawkins, E. G., Viscosity of a standard soda-lime-silica glass, J. Res. Nat. Bur. Stand. (U.S.) **68A** (Phys. and Chem.) No. 5, 439–448 (1964).
[19] Napolitano, A., and Hawkins, E. G., Viscosity of a standard lead-silica glass, Nat. Bur. Stand. (U.S.) Misc. Publ. 206–11, 24 pages (1966).
[20] Napolitano, A., and Hawkins, E. G., Viscosity of a standard borosilicate glass, Nat. Bur. Stand. (U.S.) Spec. Publ. 260–23, 10 pages (1970).
[21] Shartsis, L., Spinner, S., and Capps, W., Density, expansivity and viscosity of molten alkali silicates, Jour. Amer. Ceram. Soc. **35,** No. 6, 155–160 (1952).
[22] Huggins, M. L., Density of silicate glasses as a function of composition, Jour. Optical Soc. Amer. **30,** No. 9, 420–430 (1940).
[23] English, S., The Effect of composition on the viscosity of glass. Part III. Some four component glasses, Jour. Soc. Gl. Tech. **9,** 83–98 (1925).
[24] Preston, E., The Viscosity of soda-silica glasses at high temperatures and its bearing on their constitution, Jour. Soc. Gl. Tech. **22,** No. 90, 45–81 (1938).
[25] Heidtkamp, G. and Endell, K., Ueber die Abhängigkeit der Dichte und det Zahigkeit von temperatur im System Na_2O-SiO_2, Glastech. Ber. **14,** No. 3, 89–103 (1936).
[26] Babcock, C. L., and McGraw, D. A., Application of glass properties data to forming operations, Glass Ind. **38,** No. 3, 137–146, 148–151, 161 (1957).
[27] Robinson, H. A., and Peterson, C. A., Viscosity of recent container glasses, Jour. Amer. Ceram. Soc. **27,** No. 5, 129–138 (1944).
[28] National Bureau of Standards (U.S.), Certificate of Viscosity Values, Standard Sample No. 710, Soda-Lime-Silica Glass, 2pp. Govt. Print. Off. Washington (1962).
[29] Babcock, C. L., Viscosity and Electrical Conductivity ot Molten Glasses, Jour. Amer. Ceram. Soc. **17,** No. 11, 329–342 (1934).
[30] Owens-Illinois Glass Co., General Research Laboratory, Effect of boric oxide on properties of soda-dolomite lime-silica glasses, Jour. Amer. Ceram. Soc. **31,** No. 1, 8–14 (1948).
[31] Owens-Illinois Glass Co., General Research and New Development Division, Effect of K_2O and Li_2O on properties of soda-dolomite lime-silica glasses, Jour. Amer. Ceram. Soc. **33,** No. 6, 181–187 (1950).
[32] Owens-Illinois Glass Co., General Research Laboratory, Effect of fluorine and phosphorous pentoxide on properties of soda-dolomite lime-silica glass, Jour. Amer. Ceram. Soc. **27,** No. 12, 369–372 (1944).
[33] General Research Laboratory, Owens-Illinois Glass Co., Effect of barium and zinc oxide on the properties of soda-dolomite lime-silica glasses, Jour. Amer. Ceram. Soc., **25,** No. 3, 61–69 (1942).
[34] Owens-Illinois Glass Co., General Research Laboratory, Properties of soda-strontium oxide-alumina-silica glasses, Jour. Amer. Ceram. Soc. **31,** No. 1, 1–8 (1948).
[35] Owens-Illinois Glass Company, General Research Laboratory, Effect of iron oxide on properties of soda-dolomite lime-silica glass, Jour. Amer. Ceram. Soc. **25,** No. 14, 401–408, (1942).
[36] American Society for Testing and Materials, Standard definitions of terms relating to glass and glass products, Designation C 162–71, 14 pp. Am. Soc. for Testing and Materials, Philadelphia.

(Paper 78A4–829)

JOURNAL OF RESEARCH of the National Bureau of Standards—A. Physics and Chemistry
Vol. 78A, No. 4, July–August 1974

The System NaCl–$AlCl_3$

Ernest M. Levin

Institute for Materials Research, National Bureau of Standards, Washington, D.C. 20234

and

J. F. Kinney,* R. D. Wells,* and J. T. Benedict

Fairleigh Dickinson University, Teaneck, New Jersey 07666

(March 14, 1974)

The system NaCl–$AlCl_3$ has been restudied by DTA, visual observation, and x-ray diffraction powder techniques for identification of crystalline phases. It was confirmed that the system contains one intermediate compound $NaAlCl_4$ with an incongruent mp of 153 ± 0.5 °C and a region of liquid immiscibility extending from 80.25 to 99.6 mol percent $AlCl_3$ at 191.3 °C, the monotectic temperature.

Key words: Immiscibility; $NaAlCl_4$; phase equilibrium; system $AlCl_3$–NaCl; system NaCl–$AlCl_3$.

1. Introduction

A summary of the pertinent data in previous studies [1–5][1] of the system is given in table 1. In addition, Boud [6] in 1904 reported compound compositions of $3NaCl \cdot AlCl_3$, $NaCl \cdot AlCl_3$, and $NaCl \cdot 2AlCl_3$. The compound $NaAlCl_4$ with an incongruent melting point at ~153 °C seems well established and its crystal structure has been determined [7], using a Weissenberg camera. It is orthorhombic (space group $P2_12_12_1$), with $Z = 4$ and d (x-ray) = 2.00 g/cm³. However, the existence of additional compounds and the occurrence of a stable two liquid region of immiscibility are questionable.

2. Experimental Procedure

The general nature of the diagram was first established with a commercial DTA apparatus[2], using a microholder with Al_2O_3, as a reference material and a 10°/min heating rate. The final diagram (fig. 1) was refined by determining the liquidus and solidus curves by visual observation. The chlorides of aluminum and sodium were obtained as Reagent Grade. The NaCl was analyzed to be 99.7 ± 0.1 percent pure. The $AlCl_3$ was resublimed at 135–150 °C under vacuum from molten $NaCl \cdot AlCl_3$ mixtures containing Al-metal strips [8]. The final purity of $AlCl_3$ was analyzed to be 99.8 ± 0.1 percent. Atomic absorption analysis for Na confirmed a content of < 0.1 percent Na in the $AlCl_3$. To prevent hydration of $AlCl_3$, various mixtures of NaCl and $AlCl_3$ were prepared in glove bags flushed with anhydrous N_2 and sealed under vacuum in Pyrex tubes. Compositions not forming two liquids, i.e., those below 80 mol percent $AlCl_3$, were subjected to three cycles of grinding and sealing in the glove box, followed by heating to promote homogeneity. Samples which had been reground several times appeared pure white in color; but when they were heated to the appropriate invariant temperature of either 153 or 107 °C, they turned sharply to a gray hue.

The two liquid region of the diagram was studied visually by introducing the sealed sample into a nichrome-wound Pyrex tube furnace (40 mm O.D.) insulated by an outer Pyrex tube. Sealed samples with 80 mol. percent $AlCl_3$ and less were studied visually in a silicone oil bath, stirred with a magnetic stirrer. Heat control was accurate enough to permit heating and cooling rates of 6 °C per hour or less. The liquidus temperatures were determined by observing under a magnifying glass the disappearance of tiny crystals approximately 0.5 mm in their largest dimension. Several determinations were averaged, and all temperatures are estimated accurate to ± 0.5 °C. The Chromel-Alumel thermocouple was calibrated using pure Sn (mp 231.89 °C) and the normal freezing and boiling points of water. At times a calibrated Hg thermometer was used also in the oil bath.

*Now with Avon Products Inc., Research and Development Division, Suffern, New York 10901.

[1] Figures in brackets indicate the literature references at the end of this paper.

[2] Certain commercial materials and equipment are identified in this paper in order to adequately specify the experimental procedure. In no case does such identification imply recommendation or endorsement by the National Bureau of Standards, nor does it imply that the material or equipment identified is necessarily the best available for the purpose.

TABLE I. *Phase studies in the system* $NaCl-AlCl_3$

Investigator	Methods of Study	Incong. mp of $NaAlCl_4$	Location of $NaAlCl_4-AlCl_3$ Eutectic		Two Liquid Region		Notes
					Extent	Temp.	
		°C	Mol % $AlCl_3$	Temp. °C	Mol % $AlCl_3$	°C	
Kendall, et al. (1923) [1]	Visual observation in sealed tubes	152	~ 61	115	82.0 − > 99.8	193.5	Compound $XNaCl \cdot YAlCl_3$ under two liquids.
Plotnikov and Shvartsman (1936) [2]	Heating and cooling curves automatically recorded; sealed	—	61	108			Only studied between 50.2 and 80.8 mol % $AlCl_3$.
Shvartsman (1940) [3]	Heating and cooling curves automatically recorded, seal-d	152	61	108	80.8 − 100	190.0	
Cretien and Lous (1943) [4]	Cooling curves in N_2 atm; Chem. analysis	155	65	105	None detected		
Midorikawa (1955) [5]	Cooling curves	154	62	112			Only studied between 48.1 and 70.7 mol % $AlCl_3$.
Present study	DTA; visual observation in sealed tubes; x ray	153 ± 0.5	61.4	107.2	80.25 − 99.6	191.3	

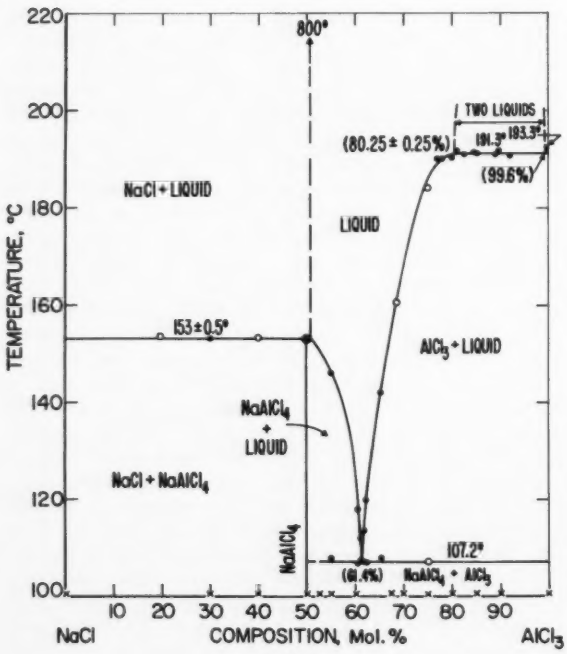

FIGURE 1. *The system* $NaCl-AlCl_3$.

o − Visual observation.
O − DTA.
X − X-ray examination at room temperature.

The solid phases were identified by x-ray diffraction powder techniques, using a dry mount with $Mg(ClO_4)_2$ as desiccant. All compositions could be interpreted in terms of the components NaCl and $AlCl_3$, and one intermediate compound $NaAlCl_4$. The x-ray powder pattern of $NaAlCl_4$ was indexed on the basis of an orthorhombic cell [7], with $a = 10.33$ Å, $b = 9.91$ Å, $c = 6.18$ Å, within a few hundreths Ångstroms of the dimensions reported by Baenziger [7] and Semenenko et al. [9]. Small irregular variations in interplanar spacings with different compositions are attributed to hydration effects rather than to an indication of slight solid solubility of $AlCl_3$ in $NaAlCl_4$.

A two liquid region, as reported by Kendall et al. [1], and Shvartsman [3], was found to exist between a composition of 80.25 ± 0.25 and 99.6 mol percent $AlCl_3$ at 191.3 °C. Two liquids were observed visually to form in several samples containing 80.5 mol percent $AlCl_3$ or greater (fig. 1). In repeated experiments, two liquids were never observed in samples of 80.0 mol percent $AlCl_3$ or less, i.e., 79.5, 77.9, and 75 percent. Atomic absorption analysis for Na in the upper liquid segregated at ~192 °C revealed the composition to be 0.4 mol percent NaCl. The composition of the $AlCl_3$-rich liquid, therefore, is 99.6 mol percent $AlCl_3$.

Several attempts were made to study the closure of the two-liquid dome. Samples of composition 80.6 and 90.2 mol percent $AlCl_3$ were heated in sealed glass tubes to form two liquids. After heating at a rate of 5 °C/day and reaching temperatures of above

210 °C, the tubes burst. The triple point of $AlCl_3$ is reported [10] at 193.3 °C and 2.33 atm.

3. Conclusion

In conclusion, a restudy of the system NaCl–$AlCl_3$ has shown it to contain only one intermediate compound and a definite region of liquid immiscibility. Also, temperatures and compositions of invariant points have been closely defined.

4. References

[1] Kendall, J., Crittenden, E. D., and Miller, H. K., J. Am. Chem. Soc. **45**, 963 (1923); also, Fig. 3107 in Phase Diagrams for Ceramists, published by the Am. Ceram. Soc., Inc. (1969).

[2] Plotnikov, V. O., and Shvartsman, U. I., Western Inst. Chem., Akad. Nauk URSR **3**, 387 (1936).

[3] Shvartsman, U. I., Western Inst. Chem., Akad, Nauk URSR **7**, 1 (1940); also, Fig. 1314 in Phase Diagrams for Ceramists, published by the Am. Ceram. Soc., Inc. (1964).

[4] Chrétien, A., and Lous, E., Compt. Rendu **217**, 451 (1943).

[5] Midorikawa, R., J. Electrochem. Soc. Japan **23**, 72 (1955).

[6] Boud, A., Ann. Chim. Phys. **1**, 8 (1904).

[7] Baenziger, N. C., Acta Cryst. **4**, 216–19 (1951).

[8] Uhr, D., Master's Thesis, 1970, Fairleigh Dickinson Univ., Teaneck, N.J. 07666.

[9] Semenenko, K. N., Surov, V. N., and Kedrova, N. S., Russ. J. Inorg. Chem. (English Transl.) **14**, [4] 481–83 (1969).

[10] Treadwell, W. D., and Terebesi, L., Helv. Chim. Acta **15**, 1053–66 (1932).

(Paper 78A4–830)

JOURNAL OF RESEARCH of the National Bureau of Standards—A. Physics and Chemistry
Vol. 78A. No. 4, July–August 1974

Simultaneous Measurements of Heat Capacity, Electrical Resistivity and Hemispherical Total Emittance by a Pulse Heating Technique: Zirconium, 1500 to 2100 K*

A. Cezairliyan and F. Righini**

Institute for Materials Research, National Bureau of Standards, Washington, D.C. 20234

(February 26, 1974)

Simultaneous measurements of heat capacity, electrical resistivity and hemispherical total emittance of zirconium in the temperature range 1500 to 2100 K by a subsecond duration, pulse heating technique are described. The results are expressed by the relations:

$$C_p = 36.65 - 1.435 \times 10^{-2}\, T + 6.624 \times 10^{-6} T^2$$

$$\rho = 87.95 + 1.946 \times 10^{-2} T$$

$$\epsilon = 0.2031 + 6.362 \times 10^{-5} T$$

where C_p is in $J \cdot mol^{-1} \cdot K^{-1}$, ρ is in $10^{-8}\ \Omega \cdot m$, and T is in K. Estimated inaccuracies of the measured properties are: 3 percent for heat capacity, 2 percent for electrical resistivity and 5 percent for hemispherical total emittance.

Key words: Electrical resistivity; emittance; heat capacity; high-speed measurements; high temperature; thermodynamics; thermophysical properties; zirconium.

1. Introduction

In this paper, application of a pulse heating technique to the simultaneous measurements of heat capacity, electrical resistivity and hemispherical total emittance of zirconium in the temperature range 1500 to 2100 K is described.

The method is based on rapid resistive self-heating of the specimen from room temperature to high temperatures (above 1500 K) in less than one second by the passage of an electrical current pulse through it; and on measuring, with millisecond resolution, such experimental quantities as current through the specimen, potential drop across the specimen, and specimen temperature. Details regarding the construction and operation of the measurement system, the methods of measuring experimental quantities, and other pertinent information, such as the formulation of relations for properties, error analysis, etc. are given in earlier publications [1, 2].[1]

In the following sections of this paper a tabular format is adopted in presenting information on the specimen, measurements, system characteristics, results and errors.

2. Measurements

The details regarding the zirconium specimens used in the present measurements are given in table 1. A summary of the measurement technique and the operational characteristics of the system is given in table 2. The polynomial functions (obtained by the least squares method) that represent the experimental results are given in table 3. The values of properties at 100 degree temperature intervals computed using the functions are given in table 4. The experimental results are presented in the appendix. Each number tabulated in the appendix represents results from over fifty original data points. An estimate of errors in the measured and computed quantities is given in table 5. All values reported in this paper are based on the International Practical Temperature Scale of 1968 [3]. In all computations, the geometrical quantities are based on their room temperature (298 K) dimensions.

*This work was supported in part by the U.S. Air Force Office of Scientific Research.
**Guest scientist from the Istituto di Metrologia "G. Colonnetti" in Torino, under a fellowship from the Consiglio Nazionale delle Ricerche of Italy.

[1] Figures in brackets indicate the literature references at the end of this paper.

TABLE 1. *Specimen information*

No.	Item	Unit	Explanation
1	Substance		Zirconium (polycrystalline).
2	Source[a]		Materials Research Corporation.
3	Purity		99.98%.
4	Impurities		Listed in table 1a.
5	Geometry		Tube made from rod by electro-erosion.
6	Dimensions (nominal)		
	total length	mm	76.2
	effective[b] length	mm	25.4
	outside diameter	mm	6.3
	wall thickness	mm	0.5
	blackbody hole	mm	0.5 × 1 (rectangular).
7	Weight		
	total weight	g	4.312
	effective[b] weight	g	1.425
8	Characteristics		
	atomic weight [4]		91.22
	density[c]	$g \cdot cm^{-3}$	6.53
	resistivity at 293 K	$10^{-8}\Omega \cdot m$	42.8

[a] The supplier is identified in this paper in order to adequately characterize the specimen. Such an identification does not imply recommendation or endorsement by the National Bureau of Standards.

[b] Effective refers to the portion of the specimen between the voltage probes.

[c] Measured value in the present work.

TABLE 1a. *Impurities in the specimen*[a]

(according to the manufacturer's analysis)

Element	C	H	O	N	Al	Fe	Hf	Ni	Si	Ti
ppm	6	3.3	125	2.1	3	30	40	1.5	1.5	1

[a] The total amount of all other detected elements is less than 6 ppm, each element being below 1 ppm limit.

TABLE 2. *Measurement technique and system characteristics*

No.	Item	Unit	Explanation and data
1	General technique		Pulse heating (subsecond).
2	Voltage measurement		Across tungsten knife-edge probes.
3	Current measurement		Across standard resistor (0.001 Ω) in series with the specimen.
4	Temperature measurement		High-speed photoelectric pyrometer [5].
5	Specimen environment		Vacuum ~ 1.3×10^{-3} N·m^{-2} (~ 10^{-5}torr).
6	Power source		Battery bank (14 series-connected 2V batteries, capacity 1100 A·h each).
7	Recording		Digital data acquisition system.
8	Signal resolution		~ 0.01 percent (at full scale).
9	Time resolution	ms	0.4
10	Data processing		Time-sharing computer.
11	Number of specimens		3
12	Number of experiments		12
13	Temperature range	K	1500–2100
14	Temperature subranges	K	I (1450–1680) II (1680–1900) III (1810–2050) IV (1840–2110)
15	Experiment duration	ms	550–680
16	Current pulse length	ms	350–480
17	Imparted power	W	1700–3100
18	Current	A	730–840
19	Rate of current change	A·ms^{-1}	0.08–0.13
20	Heating rate	K·ms^{-1}	2.9–4.8
21	Cooling rate	K·ms^{-1}	0.08–0.3
22	Radiative heat loss (Percent of input power)		2 percent at 1500 K 10 percent at 2100 K

TABLE 3. *Functional representation of results on zirconium*

Heat capacity ($J \cdot mol^{-1} \cdot K^{-1}$)	Resistivity ($10^{-8}\Omega \cdot m$)	Hemispherical total emittance
$C_p = a + bT + cT^2$	$\rho = a + bT$	$\epsilon = a + bT$
$a = 36.65$ $b = -1.435 \times 10^{-2}$ $c = 6.624 \times 10^{-6}$	$a = 87.95$ $b = 1.946 \times 10^{-2}$	$a = 0.2031$ $b = 6.362 \times 10^{-5}$
1500 K < T < 2100 K $\sigma^a = 0.7\%$	1500 K < T < 2100 K $\sigma^a = 0.6\%$	1650 K < T < 2050 K $\sigma^a = 0.9\%$

[a] Standard deviation as computed from the difference between the value of an experimental result (as tabulated in the appendix) and that from the smooth functions reported above.

TABLE 4. *Results on properties of zirconium*

T (K)	C_p ($J \cdot mol^{-1} \cdot K^{-1}$)	ρ ($10^{-8}\Omega \cdot m$)	ϵ
1500	30.03	117.14	[a] 0.299
1600	30.65	119.09	[a] .305
1700	31.40	121.03	.311
1800	32.28	122.98	.318
1900	33.30	124.92	.324
2000	34.45	126.87	.330
2100	35.73	128.82	[a] .337

[a] Extrapolated values.

TABLE 5. *Error analysis (at 2000 K)*

Quantity	Imprecision [a]	Inaccuracy [b]
Temperature	0.5 K	4 K
Voltage	0.03%	0.1%
Current	0.03%	0.1%
Heat capacity	0.7%	3%
Electrical resistivity	0.6%	2%
Hemispherical total emittance	0.9%	5%

[a] Imprecision refers to the standard deviation of a quantity as computed from the difference between the value of the quantity and that from the smooth function obtained by the least squares method. The quantities in the case of temperature, voltage, and current are the individual points measured in a single experiment, and in the case of heat capacity, electrical resistivity, and hemispherical total emittance are the results from all experiments as tabulated in the appendix.

[b] Inaccuracy refers to the estimated total error (random and systematic).

3. Discussion

The differences in the measured properties for the three specimens were within the measurement resolution for the properties, and the final smoothed results (represented by the equations in table 3 and tabulations in table 4) were obtained from the combined data for the three specimens. The heat capacity, electrical

538-709 OL - 74 - 5

resistivity and hemispherical total emittance of zirconium measured in this work are presented and compared graphically with those reported in the literature in figures 1, 2, and 3, respectively. The present results are for temperatures up to 2100 K, which is approximately 30 K below the melting point of zirconium.

The heat capacity results of this work are approximately 1 percent lower than those of Skinner [6] in the overlapping temperature region. Extrapolation of the results of this work to lower temperatures (1200–1400 K) yields values which are 3–6 percent lower than those reported by Coughlin and King [7]. However, too much significance should not be attached to the latter since: (a) the comparison is based on an extrapolation of 100 to 300 K and (b) the constant heat capacity reported by Coughlin and King [7] is not realistic.

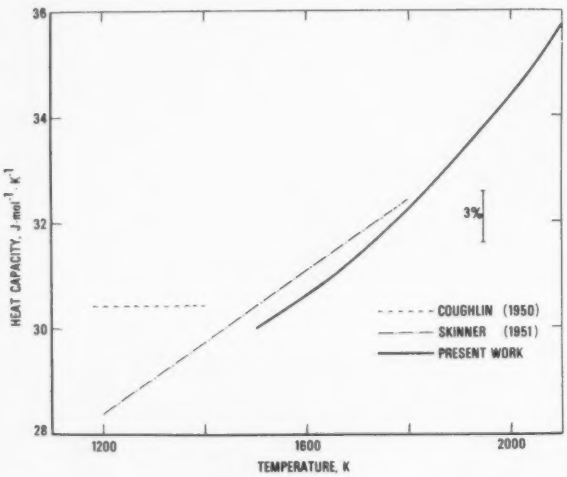

FIGURE 1. *Heat capacity of zirconium reported in the literature.*

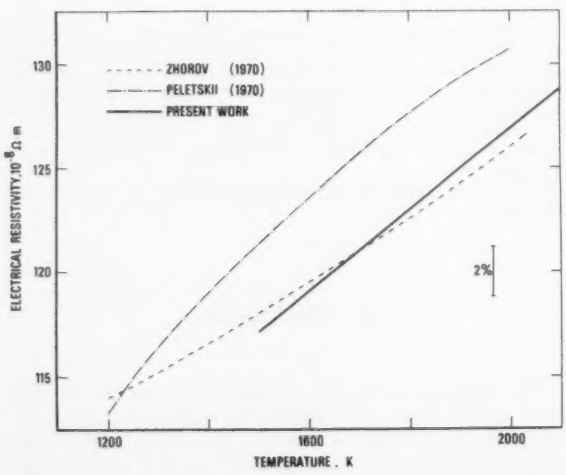

FIGURE 2. *Electrical resistivity of zirconium reported in the literature.*

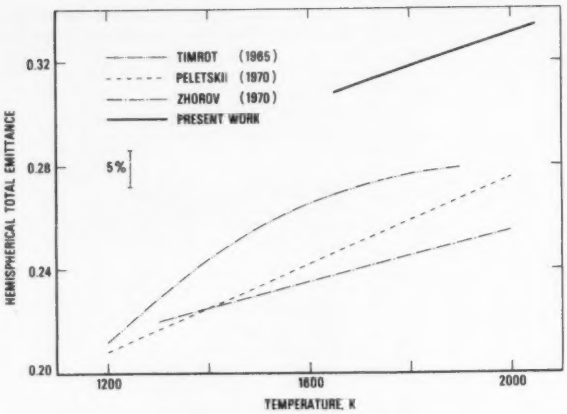

FIGURE 3. *Hemispherical total emittance of zirconium reported in the literature.*

The electrical resistivity results are in reasonably good agreement (maximum difference less than 1 percent) with those of Zhorov [8], and are approximately 3–4 percent lower than those of Peletskii et al. [9], in the overlapping temperature regions.

Zirconium undergoes a solid-solid phase transformation around 1150 K. The measurements of the geometrical quantities of the specimen after a number of experiments indicated permanent distortions (elongation) due to repeated heating and cooling through the transformation point. The reported electrical resistivity results are corrected for the permanent geometrical changes. The magnitude of this correction was about 1 percent. At 293 K, the average electrical resistivity (42.8×10^{-8} $\Omega \cdot$ m) of the three specimens used in this work is within 3.5 percent of the values reported in the literature by Adenstedt [10] (44.1×10^{-8} $\Omega \cdot$ m) and by Powell and Tye [11] (42.2×10^{-8} $\Omega \cdot$ m and 44.3×10^{-8} $\Omega \cdot$ m). Some of the differences in the electrical resistivity values may be due to differences in the chemical composition of the specimens.

The hemispherical total emittance values reported in this work are higher (10–25%) than those reported by Timrot and Peletskii [12], Peletskii et al. [9], and Zhorov [8]. Considerable differences in hemispherical total emittance results of various investigators may be due to differences in specimen surface conditions. Changes in the specimens' surface conditions were noticed during this work, with the initial smooth polished surface changing to an uneven rough surface as the result of repeated heating and cooling through the transformation point. This may partially account for the high emittance values.

The authors express their gratitude to C. W. Beckett for his encouragement of research in high-speed thermophysical measurements and to M. S. Morse for his help with the electronic instrumentation.

4. Appendix

TABLE A-1. *Experimental results on heat capacity of zirconium*

Range	Temperature (K)	Specimen-1		Specimen-2		Specimen-3			
		C_p (J · mol^{-1} · K^{-1})	ΔC_p* (%)	C_p (J · mol^{-1} · K^{-1})	ΔC_p* (%)	C_p (J · mol^{-1} · K^{-1})	ΔC_p* (%)	C_p (J · mol^{-1} · K^{-1})	ΔC_p* (%)
	1500	29.87	−0.52	29.72	−1.03	29.73	−1.00	30.02	−0.02
	1550	30.38	+0.20	30.16	−0.53	30.22	−0.33	30.38	+0.20
I	1600	30.91	+0.86	30.61	−0.11	30.72	+0.25	30.72	+0.25
	1650	31.45	+1.42	31.05	+0.15	31.22	+0.69	31.65	+2.04
	1700	31.54	+0.46	31.10	−0.95	31.32	−0.24	31.32	−0.24
	1750	32.05	+0.72	31.79	−0.10	31.79	−0.10	31.83	+0.03
II	1800	32.57	+0.90	32.22	−0.18	32.25	−0.09	32.36	+0.25
	1850					32.71	−0.18	32.89	+0.37
	1900					33.17	−0.37	33.42	+0.38
	1850	32.66	−0.34	32.42	−1.08				
	1900	33.31	+0.05	33.05	−0.74				
III	1950	33.99	+0.41	33.72	−0.39				
	2000	34.70	+0.74	34.40	−0.12				
	2050	35.44	+1.05						
	1850	32.96	+0.58	32.77	0.00				
	1900	33.21	−0.25	33.02	−0.83				
IV	1950	33.63	−0.66	33.43	−1.26				
	2000	34.25	−0.56	34.01	−1.27				
	2050	35.12	+0.15	34.79	−0.79				
	2100	36.31	+1.62	35.82	+0.27				

*The quantity ΔC_p is percentage deviation of the individual results from the smooth function represented by the pertinent equation in table 3.

TABLE A-2. *Experimental results on electrical resistivity of zirconium*

Range	Temperature (K)	Specimen-1		Specimen-2			Specimen-3		
		ρ ($10^{-8}\,\Omega$ · m)	$\Delta\rho$* (%)	ρ ($10^{-8}\,\Omega$ · m)	$\Delta\rho$* (%)	ρ ($10^{-8}\,\Omega$ · m)	$\Delta\rho$* (%)	ρ ($10^{-8}\,\Omega$ · m)	$\Delta\rho$* (%)
	1500	115.97	−1.02	116.07	−0.93	117.55	+0.34	117.67	+0.44
	1550	117.06	−0.91	117.16	−0.82	118.62	+0.42	118.85	+0.61
I	1600	118.14	−0.81	118.30	−0.67	119.75	+0.54	119.98	+0.74
	1650	119.25	−0.69	119.39	−0.57	120.87	+0.66	121.10	+0.85
	1700	120.36	−0.57	120.50	−0.45	122.00	+0.78	122.00	+0.78
	1750	121.41	−0.50	121.56	−0.38	123.06	+0.85	123.07	+0.86
II	1800	122.50	−0.40	122.57	−0.34	124.10	+0.89	124.10	+0.89
	1850					125.13	+0.93	125.13	+0.93
	1900					126.14	+0.95	126.23	+1.02
	1850	123.60	−0.29	123.61	−0.29				
	1900	124.62	−0.25	124.60	−0.27				
III	1950	125.65	−0.21	125.59	−0.26				
	2000	126.68	−0.16	126.58	−0.24				
	2050	127.71	−0.12						
	1850	123.60	−0.29	123.61	−0.29				
	1900	124.64	−0.24	124.67	−0.21				
IV	1950	125.65	−0.21	125.68	−0.18				
	2000	126.63	−0.20	126.66	−0.18				
	2050	127.61	−0.19	127.62	−0.19				
	2100	128.61	−0.17	128.59	−0.19				

*The quantity $\Delta\rho$ is percentage deviation of the individual results from the smooth function represented by the pertinent equation in table 3.

TABLE A-3. *Experimental results on hemispherical total emittance of zirconium*

Specimen-1			Specimen-2		
Temperature (K)	ϵ	$\Delta\epsilon$ [a] (%)	Temperature (K)	ϵ	$\Delta\epsilon$ [a] (%)
1674.7	0.307	−0.87	1650.5	0.301	−2.37
1680.1	.309	−0.33	1655.5	.304	−1.47
1685.7	.310	−0.12	1660.7	.307	−0.58
1691.4	.312	+0.40	1666.0	.310	+0.28
1697.1	.313	+0.61	1671.4	.312	+0.81
1703.0	.314	+0.80	1676.9	.315	+1.65
1848.8	.320	−0.24	1980.7	.326	−0.96
1856.9	.322	+0.23	1991.0	.327	−0.86
1865.3	.324	+0.68	2001.6	.328	−0.75
1873.7	.325	+0.82	2012.3	.329	−0.65
1882.4	.327	+1.26	2023.3	.329	−0.87
1891.3	.328	+1.39	2034.5	.330	−0.78
2003.3	.330	−0.18			
2014.3	.332	+0.22			
2025.6	.333	+0.30			
2037.1	.334	+0.38			
2048.9	.335	+0.45			
2061.0	.336	+0.52			

[a] The quantity $\Delta\epsilon$ is percentage deviation of the individual results from the smooth function represented by the pertinent equation in table 3.

5. References

[1] Cezairliyan, A., Design and operational characteristics of a high-speed (millisecond) system for the measurement of thermophysical properties at high temperatures, J. Res. Nat. Bur. Stand. (U.S.) **75C** (Eng. and Instr.), No. 1, 7 (1971).

[2] Cezairliyan, A., Morse, M. S., Berman, H. A., and Beckett, C. W., High-speed (subsecond) measurement of heat capacity, electrical resistivity, and thermal radiation properties of molybdenum in the range 1900 to 2800 K, J. Res. Nat. Bur. Stand. (U.S.) **74A** (Phys. and Chem.) No. 1, 65–90 (Jan.–Feb. 1970).

[3] International Practical Temperature Scale of 1968, Metrologia **5,** 35 (1969).

[4] IUPAC Commission on Atomic Weights, Atomic weights of the elements 1969, Pure Appl. Chem. **21,** 91 (1970).

[5] Foley, G. M., High-speed optical pyrometer, Rev. Sci. Instr. **41,** 827 (1970).

[6] Skinner, G. B., Thermodynamic and structural properties of zirconium, Ph.D. Thesis, Ohio State University, 1951.

[7] Coughlin, J. P., and King, E. G., High-temperature heat contents of some zirconium-containing substances, J. Am. Chem. Soc. **72,** 2262 (1950).

[8] Zhorov, G. A., Emissivity of metals of the IVb subgroup at high temperatures, High Temp. **8,** 501 (1970).

[9] Peletskii, V. É., Druzhinin, V. P., and Sobol', Ya. G., Emissivity, thermal conductivity, and electrical conductivity of remelted zirconium at high temperatures, High Temp. **8,** 732 (1970).

[10] Adenstedt, H. K., Physical, thermal and electrical properties of hafnium and high purity zirconium, Trans. A.S.M. **44,** 949 (1952).

[11] Powell, R. W., and Tye, R. P., The thermal and electrical conductivities of zirconium and of some zirconium alloys, J. Less-Common Metals **3,** 202 (1961).

[12] Timrot, D. L., and Peletskii, V. É., The thermal conductivity and integral blackness of zirconium, High Temp. **3,** 199 (1965).

(Paper 78A4–831)

JOURNAL OF RESEARCH of the National Bureau of Standards—A. Physics and Chemistry
Vol. 78A, No. 4, July–August 1974

Measured Enthalpy and Derived Thermodynamic Properties of Crystalline and Liquid Potassium Chloride, KCl, from 273 to 1174 K

Thomas B. Douglas and Ann W. Harman

Institute for Materials Research, National Bureau of Standards, Washington, D.C. 20234

(April 19, 1974)

The enthalpy of KCl relative to that at 273.15 K was precisely measured by drop calorimetry from 273 to 1174 K, and smooth thermodynamic functions were derived for this temperature range. The heat capacities found for the crystalline phase join smoothly the most precise published data for lower temperatures; those for the liquid phase are temperature-independent within the precision of measurement over the 120° range covered. It is concluded that the broad exponential upturn of the heat-capacity curve below the melting point, if attributed to lattice vacancies, indicates a predominance of large vacancy clusters.

Key words: Heat of fusion; high-temperature drop calorimetry; lattice vacancies; muriate of potash; potassium chloride; sylvite; thermodynamic properties.

1. Introduction

The experimental data on potassium chloride reported in this paper were obtained by the authors at the National Bureau of Standards in 1954. Although the results based on an earlier smoothing were incorporated in the various JANAF tables for this substance [23][1], they have not been previously published otherwise. Since the original records were thoroughly annotated and these data appear to be still unexcelled in accuracy for the particular properties they represent, it seemed worthwhile to carry out a complete and careful reanalysis, and to present the results here. The heat capacities can be merged with the precise low-temperature values of Berg and Morrison [4] for the temperature range 2.8–270 K without any compromise of either set of data, and both the JANAF tables [23] and the present paper have chosen to carry out this merging, in order to base the enthalpy on 0 K and to obtain Third-Law entropies, as a firm basis in calculating thermodynamic equilibria involving crystalline or liquid potassium chloride. In fact, even though the small corrections to both pieces of work from the International Practical Temperature Scale of 1948 to that of 1968 (the most recent such scale) have been applied, the present smoothed values differ little from those in the latest JANAF tables (the largest discrepancy amounting to 0.5 percent in the heat of fusion, largely attributable to a different procedure of extrapolating to the melting point). The present authors did not measure the melting point, but have critically selected a value from the literature.

The high practical importance of potassium chloride, not only among the alkali halides but among all inorganic substances, is well known, and stems partly from its fairly high natural abundance, its simplicity of chemical composition, and its chemical stability. There are, however, a number of basic scientific problems in which an accurate knowledge of the high-temperature equilibrium thermal properties of its condensed phases is important and directly applicable. Chief among such problems which motivated the present work are: (1) the abundance and nature of the lattice vacancies in the pure crystal; (2) the thermodynamic properties of solid and liquid solutions containing potassium chloride as one component; and (3) the thermodynamic properties and composition of gaseous potassium chloride. In connection with the third item, one of the present authors concluded twenty years ago that the best available vapor pressures and thermodynamic properties of the solid and liquid were consistent with reasonable electrostatic models of the postulated gas species only if saturated potassium chloride vapor near the melting point contains, in addition to the monomer, KCl, at least 8 mole percent of the dimer, K_2Cl_2. At that time no direct evidence existed for the association of alkali-halide vapors, but the subsequent mass and infrared spectroscopy of other investigators [23] established the truth of this indirect conclusion for potassium chloride.

[1] Figures in brackets refer to literature references at the end of this paper.

2. Sample and Container

A single sample—A.C.S. Reagent Grade potassium chloride from the General Chemical Division of the Allied Chemical & Dye Corporation, New York[2]—was used. The salt was not further purified except by fusing it quickly while contained in platinum (exposed to the atmosphere) to remove any occluded water. Two specimens of this material (each approximately 6.4 g, or 0.086 GFW), subsequently designated "samples 1 and 2", were sealed in cylindrical containers of pure silver ("0.999 fine") for the calorimetric measurements. Each silver container had a mass as close to 12 g as practical, and consisted of a cylinder of $\frac{5}{8}$ in diameter, 0.015 in wall thickness, and approximately 2 in length, with a tight-fitting silver cap sealed in each end by an oxy-gas flame, the final seal being made while the KCl sample was molten. In the subsequent enthalpy measurements each sample was suspended in the furnace by a wire of thermocouple-grade 90 Pt–10 Rh (o.d., 0.015 in) bearing two horizontal thin circular platinum radiation shields and a small hook of 80 Ni–20 Cr, all with controlled masses. The small mass of silver (a few tenths of a mg) lost in such a sealing process was determined by sealing other dry containers having no sample present, and applied as a correction in deducing by difference the exact mass of each sample.

The results of analyzing the sample are recorded in table 1. The qualitative spectrochemical analysis was performed on a typical specimen by the Spectrochemical Analysis Section of the Bureau. Hot KCl is slightly hydrolyzed by such an exposure to moist air as described above; therefore after all the calorimetric measurements on sample 1 (the principal specimen) it was dissolved in CO_2-free water and titrated with standard HCl solution and phenolphthalein, giving (after applying the blanks) the equivalent of 0.04 weight percent of KOH.

TABLE 1. *Chemical and spectrochemical analysis of the sample* [a]

Impurity	Weight percent	Method of analysis
KOH	0.04	Titration with acid
Na	0.001–0.01	Qualitative spectrochemical
Al	0.0001–0.001 (each)	
Ba		
Ca		
Rb		
Si		
Cu	< 0.0001 (each)	
Mg		

[a] In addition B, P, and 44 other metals were sought spectrochemically but not detected.

[2] Mention of a specific commercial organization does not imply recommendation by the National Bureau of Standards of its goods or services.

3. Enthalpy Measurements

3.1. Calorimetric Procedure

The enthalpy of the sample and its container relative to that at 0 °C was measured by "drop" calorimetry, which is described in great detail elsewhere [12]. The particular procedure followed in the present case was briefly as follows. The sample in its container was held in an atmosphere of helium in a vertical silver-core furnace for a time sufficient to allow it to reach the (constant) furnace temperature, and was then dropped into a Bunsen ice calorimeter, which measured its loss of heat (enthalpy) in cooling from the furnace temperature to 0 °C. To account accurately for the heat lost by the container itself, during the drop and to the calorimeter, the measurement was repeated at the same furnace temperature on one or more identical empty containers.[3]

To create a very nearly isothermal environment, the sample or empty container was suspended in the furnace inside a central core of pure silver 10 in long, with o.d. 2 in and wall thickness $\frac{1}{2}$ in. Insulated from this core above and below were two shorter "guard" segments of silver (o.d., also 2 in) controlled by separate heaters to the temperature of the central core. The temperature of the suspended sample or container was taken to be that of the closest portion of the central core. In general, aside from the possible effects of sample composition or indefiniteness of physical state, the measurement of furnace temperature is usually the most serious source of systematic error in high-temperature drop calorimetry. The steps taken toward accurate temperature measurement are outlined in the following section.

3.2. Furnace Thermometry

Up to and including 600 °C (873 K), the furnace temperature was measured by one of two strain-free platinum resistance thermometers (ice-point resistance, approximately 25 ohms) that had been independently calibrated at the Bureau at the ice, steam, and sulfur points on the International Temperature Scale of 1948 (with later conversion to the IPTS–68 [20, 10]). When these thermometers were intercompared in the furnace just before the enthalpy measurements began, their temperature indications were discordant by +0.036° (at 200 °C), −0.035° (at 400 °C), and −0.002° (at 600 °C). The ice-points of both thermometers were periodically redetermined and found not to have changed appreciably. As a precaution against an unsuspected deterioration of the tempering of the thermometer in the furnace, a thermometer reading was always accompanied by a *precise* thermocouple reading.

[3] The preferable use of the same container for these two measurements would have been inconvenient, and is believed unnecessary anyhow because all containers were constructed from adjacent parts of the component materials and because the principal material, silver, has highly reproducible thermal properties when pure and annealed.

Above 600 °C, measurement of the furnace temperature had to rely on thermocouples, these being Pt/90 Pt–10 Rh (0.015-in.-diameter wires). One thermocouple had undergone a standard NBS calibration, and to minimize subsequent changes in its calibration it was used only to calibrate the "working thermocouple" (that used in the enthalpy measurements), by comparison of simultaneous readings when the junctions of both couples were in contact in the center of the furnace. A similar comparison of the "working" thermocouple with the "working" thermometer showed higher temperature readings of the thermocouple (on the basis of its calibration as described above) by 0.26° at 200 °C, 0.10° at 400 °C, and 0.17° at 600 °C. Because the thermometer is the more accurate instrument and there is no monotonic trend in these discrepancies, their mean (0.2°) was subtracted from all thermocouple readings above 600 °C. Otherwise, the graphical smoothing of the thermocouple readings from standard tables (for interpolation purposes) did not compromise any unsmoothed calibration value by more than 0.05°.

Despite the favorable conditions for an isothermal furnace region implied by the dimensions of the silver core (described in sec. 3.1), the structure of the furnace was such as to obviously permit considerable heat conduction out the ends of the core. For this reason "immersion" tests were performed, while the furnace was held at a constant temperature of about 600 °C, to test the temperature gradients around the position of the sample. Raising the thermometer or thermocouple sensing element by one cm raised the temperature reading by 0.0025° or 0.3 °C, respectively; but moving the thermocouple up and down, then rotating, and finally restoring the original level produced no net change. Raising the temperature of the *bottom* silver guard segment by 0.5° produced no effect on the thermometer and thermocouple readings, but raising the temperature of the *top* segment by 1.2° increased the thermometer reading by 0.0075° (the thermocouple *decrease* by 0.05° suggests an error in the test); these small effects are generally not unexpected, since the thermometer and thermocouple leads passed out the top of the furnace core.

3.3. Enthalpy Data

a. Empty Containers

The results of enthalpy measurements on empty containers are given in table 2. The principal series of measurements, designated "1a," was made just before the enthalpy measurements on the potassium chloride samples. Two additional series, "1b" and "2" (on the same and on a new container, respectively), were made several months after the completion of the KCl measurements, and at only three temperatures. The values of individual measurements (unsmoothed, but otherwise fully corrected) are given in the third column, in chronological order for each temperature. However, the heats actually observed have been divided by 0.085554, the number of moles of potassium chloride in sample no. 1. By thus giving the values to be subtracted from those for container-plus-sample on the same basis, the effect of imprecision at a given temperature on the net enthalpy per mole of potassium chloride is directly obvious.

The mean measured empty-container enthalpy for each series at each temperature is given in the fourth column of table 2, and a small largely systematic difference will be noted among the three series at the three temperatures involving all series. It was decided to derive smooth values using the "series 1a" values only, partly because this series was measured closest in time to the potassium chloride samples (tending toward a greater cancellation of instrumental errors), and partly because the container surface in series 1a was believed more comparable to that for the KCl samples. (Each series of empty-container measurements was made at increasing temperatures, except that the highest temperature, 1174 K, was run first, with the belief that this might stabilize most quickly the crystal growth, and hence the radiative emissivity, of the surface.)

The empirical equation derived to represent the smoothed empty-container relative enthalpies from series 1a (in joules per mole of KCl sample No. 1, at temperature T K(IPTS–68) is

$$H_T - H_{273.15} = 37.8035(T-273.15) + 4.6024(10^{-4})\,(T-273.15)^2 + 2.4227(10^{-6})(T-273.15)^3 - 584.84(T-273.15)/T. \qquad (1)$$

Values from eq (1) are given in the fifth column of table 2, and the differences of the mean measured values from these, in the last column.

b. KCl Samples

Table 3 records the enthalpy results on potassium chloride. A second specimen of the salt ("sample No. 2") was measured in a different container at two temperatures (primarily to guard against an appreciable error in the mass of the principal specimen, sample No. 1, that would not otherwise be revealed by inconsistencies in the data). The individual enthalpy measurements are recorded in chronological order for each temperature. For sample No. 1, the liquid range (above 1045 K) was measured first, the crystalline range 373–974 K next, then 1009 K, and finally 1039 K. For sample No. 2 (run shortly after sample No. 1) the two measurements at 1034 K intervened between the second and third at 1009 K.

The container of sample No. 1 proved to be sealed completely tight, and the total mass changed by only about one mg during the whole series of measurements. In sealing sample No. 2, however, a small hole was blown in the top of the container, resulting in an immediate mass loss of 8.6 mg, which was assumed to be half KCl and half molten silver (introducing an

TABLE 2. *Enthalpy data on typical empty containers*

Temperature, T(K) [a]	Container and series	Relative enthalpy, $H_T - H_{273.15}$ (in J per mole of KCl)			
		Measured	Mean measured	Smoothed (eq (1))	Difference
373.15	1a	3,629 3,631	3,630	3,631	−1
473.19	1a	7,346 7,366	7,356	7,353	+3
573.22	1a	11,144 11,140	11,142	11,144	−2
673.23	1a	15,003 15,007	15,005	15,005	0
773.23	1a	18,943 18,952	18,947	18,945	+2
	1b	18,983 18,983	18,983		+38
	2	18,958 18,954	18,956		+11
873.30	1a	22,947 22,981 22,978	22,969	22,976	−7
973.54	1a	27,124 27,115	27,119	27,115	+4
	1b	27,155 27,179	27,167		+52
	2	27,126 27,099 27,097	27,107		−8
1008.64				28,590	
1033.70				29,653	
1038.72				29,866	
1053.76				30,509	
1073.82	1a	31,368 31,376	31,372	31,370	+2
1093.87				32,236	
1133.99				33,985	
1174.10	1a	35,737 35,738 35,755 35,762 35,780	35,754	35,755	−1
	1b	35,824 35,795	35,810		+55
	2	35,727 35,723	35,725		−30

[a] International Practical Temperature Scale of 1968 [20].

uncertainty of 0.04 percent in the net enthalpies for KCl from this sample, owing to the widely different specific heats of these two substances). Furthermore, during the enthalpy measurements on it sample No. 2 steadily lost mass (to a total of 4 mg), which was corrected for on the assumption that minute amounts of KCl had escaped by evaporation.

The thermal values in table 3 (as well as those in table 2) are based on 270.48 J per g of mercury as the ideal calibration factor of the ice calorimeter [12]. The mass of KCl sample No. 1 was 6.3781 g (0.085554 "mol" on the basis of a molecular weight or GFW of 74.551 [2]). The mass of sample No. 2 varied with time from 6.4183 to 6.4141 g, but the gross enthalpies for this sample as recorded in the third column of table 3 have been increased by small amounts (about 0.2 percent) so that their means in the fourth column, as well as those for sample No. 1, may be decreased by the corresponding empty-container values (fifth column of table 2) to give all the mean net molar enthalpies of KCl listed in the fifth column of table 3. All enthalpies in tables 2 and 3 include very small

TABLE 3. *Enthalpy data on samples of potassium chloride (KCl)*

Temperature, T(K)[a]	Sample no.	Relative enthalpy, $H_T - H_{273.15}$ (J mol^{-1})[b]				
		KCl + container		KCl only		
		Measured	Mean measured	Measured	Smoothed[c]	Difference
373.15	1	8,805 8,827	8,816	5,185	5,182	+3
473.19	1	17,884 17,880	17,882	10,529	10,529	0
573.22	1	27,185 27,182	27,183	16,038	16,040	−2
673.23	1	36,714 36,727	36,720	21,715	21,714	+1
773.23	1	46,507 46,497	46,502	27,557	27,560	−3
873.30	1	56,588 56,611	56,599	33,623	33,621	+2
973.54	1	67,154 67,139	67,146	40,032	40,025	+7
1008.64	1	70,963 70,990	70,976	42,386	42,391	−5
	2	70,965 70,958 70,959	70,961	42,371		−20
1033.70	2	73,798 73,787	73,792	44,139	44,133	+6
1038.72	1	(74,727)	----------	(44,861)	44,488	[d](+373)
		(74,649)	----------	(44,783)		[d](+295)
		(74,582)	----------	(44,716)		[d](+228)
		(74,510)	----------	(44,644)		[d](+156)
1053.76	1	102,268 102,228 102,228	102,241	71,731	71,731	0
1093.87	1	106,899 106,923 106,908	106,910	74,674	74,675	−1
1133.99	1	111,631 111,582 111,611	111,608	77,623	77,620	+3
1174.10	1	116,315 116,322	116,318	80,563	80,564	−1

[a] International Practical Temperature Scale of 1968 [20].

[b] Molecular weight ("GFW") = 74.551 [2].

[c] Calculated below 1045 K from eq (2) (crystal), and above 1045 K from eq (3) (liquid).

[d] See discussion in sec. 3.3.b.

corrections for adjustment to a standard mass of each nonsample material (silver, 80 Ni–20 Cr, 90 Pt–10 Rh, and air inside the container). No correction was made for the heat of forming or condensing potassium chloride vapor inside a container, as this heat was calculated not to exceed 0.6 joule per mole of KCl sample [23]. No corrections for furnace temperature were needed, as these temperatures were always constant and within 0.01° of those listed in the tables. Previous tests had shown the time of the sample in the furnace (20 to 80 min) to be adequate for thermal equilibrium; however, at 1054 K the sample was only 9° above the melting point, so to hasten the complete input of the heat of fusion the sample was preliminarily heated at 1094 K for at least 30 min.

For 1039 K the individual net enthalpies for the sample (table 3, fifth column) show a large drift with time which invites separate explanation (see below). The values for the lower temperatures, however, show no drift with time beyond what may be attributed to accidental error, and indicate a heat-capacity curve for the crystal which varies nearly linearly with

increasing temperature except with an accelerated upturn as the melting point is approached. It was found that these data could have been fit satisfactorily by correcting for premelting caused by 0.015 mole percent of liquid-soluble solid-insoluble impurity. However, according to table 1 the only impurities present in comparable abundance are KOH and some sodium salt (presumably NaCl), and the phase diagrams of the KCl-KOH and KCl-NaCl systems [29] show such large solid solubilities (for compositions near pure KCl) as to suggest no premelting at any temperature in table 3. Consequently, the plausible alternative attribution of the above heat-capacity upturn to the effect of lattice vacancies was adopted instead (calling for one or more exponential terms in the enthalpy-temperature function). Moreover, all enthalpy values observed for 1039 K were omitted from the data fit because it is plausible to assume that this near the melting point the sample actually may have undergone extensive premelting which decreased in successive enthalpy measurements: the sample had earlier been fused and rapidly crystallized, and it seems reasonable to assume that the total of 190 min of holding the sample at 1039 K was required for about half the impurity to diffuse into the crystalline KCl. With all premelting ignored in the data fitting, the additive corrections for the impurities would be well within the uncertainties of the final results and were ignored.

Excepting the values for 1038.72 K, the mean corrected unsmoothed relative enthalpy found for potassium chloride at each furnace temperature (from table 3, fifth column) was given equal weight in the method of least squares to derive the coefficients and the exponential argument of the following empirical enthalpy equations (in J mol^{-1} at T K, IPTS–68) for the crystal below the melting point and the liquid above the melting point: [4]

$$\underline{\text{KCl, } T = 273.15 - 1045\text{ K}}: H_T(\text{c}) - H_{273.15}(\text{c}) = 46.5369\,T + 8.1720(10^{-3})T^2 + 9.0725(10^7)\exp(-12300/T) - 13321.3 \quad (2)$$

$$\underline{\text{KCl, } T = 1045 - 1174.10\text{ K}}: H_T(\ell) - H_{273.15}(\text{c}) = 73.3994\,T - 5614.1 \quad (3)$$

Values from eqs (2) and (3) are given in the sixth column of table 3, and the differences of the mean measured values from these, in the last column.

Equations (2) and (3) are based solely on the authors' own data. The final equations recommended to cover these temperature ranges (sec. 4.3) involve small changes to effect a smooth join to good data below room temperature.

[4] The least-squaring of the crystal-state data was actually carried out for fixed values of the exponential argument varying from $-11500/T$ to $-13500/T$ in steps of $-200/T$, the standard deviations not being very sensitive to this argument in this range. On repetition except allowing in the enthalpy a polynomial term in $1/T$, the best fit was inferior to that without this term, and besides, gave a negative coefficient for the $1/T$ term, whereas it was desired to represent all the positive curvature of the heat capacity-temperature curve in the exponential term.

4. Smooth Thermodynamic Functions

4.1. The Melting Point

The authors have not measured the melting point of pure potassium chloride. Nine values reported in the literature are listed later (table 8, sec. 5.1). Of these, the value of Roberts [43] was adopted—because it appears to be based on careful experimental work and because he documented his temperature scale with several fixed-point values, which are compared with those on the International Practical Temperature Scale of 1968 in table 4. Adding 1.7° (interpolated from the last column) to his reported melting point, 770.3° ± 0.5 °C, gives for the adopted melting point 772.0 °C, which may be rounded to 1045 K (IPTS–68).

TABLE 4. *Values of thermometric fixed points on the IPTS–68 and as reported by Roberts*

Fixed point	Value reported by		Difference
	IPTS–68 [20]	Roberts [43]	
	°C	°C	°C
Melting point of ice	0	[a] (0)	0.0
Normal boiling point of water	100	[a] (100)	0.0
Freezing point of lead	327.502	327.3	+0.2
Freezing point of zinc	419.58	419.4	+0.2
Freezing point of aluminum	660.37	658.7	+1.7
Freezing point of gold	1064.43	1062.6	+1.8
Freezing point of palladium	1554.	1551.5	+2.5

[a] Not stated but inferred.

4.2. Joining With Low-Temperature Results

In order to arrive at what they regard as the most reliable formulation of the thermodynamic properties of potassium chloride over the temperature range of their measurements (273–1174 K), the authors carefully examined all available published results at both low and high temperatures (details are given later, in sec. 5.1), and decided to join their values smoothly with those of Berg and Morrison [4], whose measurements of heat capacity cover the range 2.8–270 K. (This compromise led to a small modification of eq (2) up to 373.15 K, noted later.) The decision to give full weight to the low-temperature heat capacities of Berg and Morrison was made because of the following facts about those values. (a) They are of relatively high precision, the (less precise) values of Southard and Nelson [48], Clusius et al. [8], and Strelkov et al. [49] scattering above and below them. (b) They are thoroughly documented in all details pertaining to their accuracy. Their stated estimated accuracy of 0.2 percent (in the range 25–270 K) is supported by agreement of comparably measured heat capacities of Al_2O_3 with the precise values of Furukawa et al. [17]—"excellently" over 78–150 K, though 0.1–0.2 percent higher over 150–270 K. (c) As will presently

be shown, Berg and Morrison's heat capacity-temperature function for KCl may be merged smoothly with the authors' without compromising either set of data.

Using the notation T_1 (ΔT) T_2 for the temperatures from T_1 to T_2 at constant intervals of ΔT, the smooth heat-capacity values of Berg and Morrison are for 2.5, 3, 5 (5) 30 (10) 60 (20) 100 (25) 250, and 270 K. By interpolating their Debye temperatures, the present authors interpolated heat capacities for 45, 55, 65, 70, 75, and 90 K also. In addition, in order to be consistent with the present work, small corrections have been applied to all values derived from their data in order to place the values on the basis of the International Practical Temperature Scale of 1968 [20, 10][5]. The values of heat capacity listed by Berg and Morrison at the three highest temperatures in their table (225, 250, and 270 K), after conversion to IPTS–68, are represented exactly (in J mol^{-1} K^{-1}) by the monotonic equation

$$C_p = 98.9551 - 105.2107/T^{0.13897}. \qquad (4)$$

The temperature derivative of eq (2), based on the authors' data, cannot be expected to represent accurate heat capacities in its lowest interval 273.15 to 373.15 K because there the enthalpy was measured only over the whole interval. However, to merge smoothly the authors' results at still higher temperatures with Berg and Morrison's results below 273.15 K, an empirical polynomial equation was derived for the heat capacity over the temperature interval 270–373.15 K (eq (9) of sec. 4.3). The five coefficients of the equation were determined from C_p and dC_p/dT as given by eq (4) at 270 K and as given by eq (2) at 373.15 K, and from $(H_{373.15} - H_{273.15})$ as given by eq (2). The deviations (in terms of heat capacity) of eqs (2) and (4) from the new equation are plotted in figure 1. Although both eqs (2) and (4) give lower heat capacities than the adopted equation between 305 and 345 K, this results from forcing the new equation to reproduce the (smoothed) measured enthalpy increment, and also it should be noted that the entire curve labeled "Berg and Morrison" is an extrapolation beyond the temperature range of their measurements.

Berg and Morrison's heat capacities were integrated to give the enthalpy and entropy increments over the interval 0–270 K. The major contributions were evaluated from three approximate empirical equations derived to cover the respective temperature ranges 0–20 K, 20–80 K, and 80–270 K with continuity in C_p and dC_p/dT (except for a 15 percent discontinuity in dC_p/dT at 20 K); the minor residual contributions equivalent to the deviations of these equations from the heat-capacity curve were determined graphically. The entropy of KCl(c) is certainly zero at 0 K, and the results are

$$H^\circ_{270} - H^\circ_0 = \int_0^{270} C_p dT = 9934.6 \text{ J mol}^{-1}; \qquad (5)$$

$$S^\circ_{270} = \int_0^{270} (C_p/T)\, dT = 77.490 \text{ J mol}^{-1}\text{K}^{-1}. \qquad (6)$$

The values of eqs (5) and (6) include corrections of -0.4 J mol^{-1} and $+0.004$ J mol^{-1}K^{-1}, respectively, for the conversion to the basis of IPTS–68 [10].

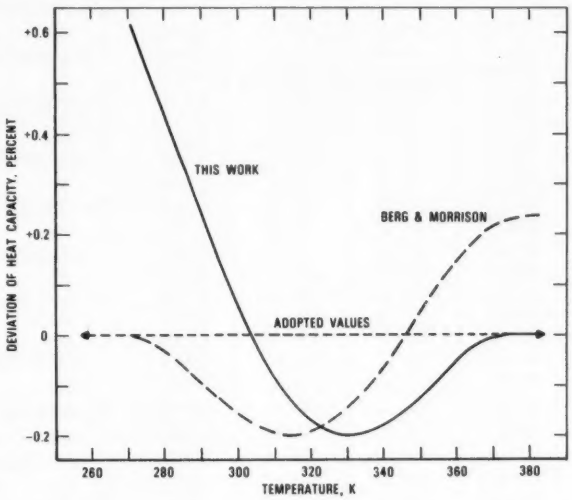

FIGURE 1. *Compromise of KCl heat capacity in the temperature range 270–373.15 K.*

The "Adopted Values" are those given by eqs (9) and (12) or by tables 5 and 6. The curve labeled "This Work" refers to the derivative of eq (2), and the curve labeled "Berg and Morrison" follows eq (4) as an extrapolation of their values [4].

4.3. Final Thermodynamic Functions

After the treatment of the temperature range 270–373.15 K described in sec. 4.2, and using eqs (5) and (6) and the requirement of continuity in enthalpy and entropy to supply the integration constants, the authors derived numerical equations to represent their final values for the common thermodynamic properties of crystalline and liquid potassium chloride from 270 to 1200 K. These numerical equations are given below as eqs (8)–(17). The Gibbs-energy function is then obtainable from the thermodynamic relation

$$-(G^\circ - H^\circ_0)/T = S^\circ - (H^\circ - H^\circ_0)/T. \qquad (7)$$

The values above 1174.10 K involve an extrapolation up to 1200 K of the data on the liquid on which eq (3) is based; otherwise, the equations should be considered applicable only in the respective temperature ranges stated. The energy unit is J mol^{-1} (1 "mole" = 74.551 g), at the temperature T K (IPTS–68). The enthalpy is formulated as that relative to the crystal at 0 K. "ln" signifies the natural logarithm (i.e., to the base e). In general, eight significant figures should be retained in each coefficient of eqs (8)–(10), to avoid loss of significance in the computed thermodynamic functions.

[5] The corrections below 90 K assume that Berg and Morrison [4] adopted the following fixed points of Los and Morrison [31]: normal boiling points of e-H_2 and O_2, 20.273 and 90.190 K, respectively; triple point of O_2, 54.363 K.

KCl(c), 270 − 373.15 K

$$H^\circ - H_0^\circ = 241.29052T - 1.265787640T^2 + 4.100661148(10^{-3})T^3 - 6.5082939(10^{-6})T^4 + 4.08177711(10^{-9})T^5 - 14{,}920.39 \quad (8)$$

$$C_p = 241.29052 - 2.53157528T + 1.23019834(10^{-2})T^2 - 2.60331756(10^{-5})T^3 + 2.04088856(10^{-8})T^4 \quad (9)$$

$$S^\circ = 241.29052 \ln T - 2.53157528T + 6.15099172(10^{-3})T^2 - 8.6777252(10^{-6})T^3 + 5.10222139(10^{-9})T^4 - 894.5502 \quad (10)$$

KCl(c), 373.15 − 1045 K

$$H^\circ - H_0^\circ = 46.5369T + 8.1720(10^{-3})T^2 + 9.0725(10^7)\exp(-12300/T) - 3227.08 \quad (11)$$

$$C_p^\circ = 46.5369 + 1.63439(10^{-2})T + [1.1159(10^{12})/T^2]\exp(-12300/T) \quad (12)$$

$$S^\circ = 46.5369 \ln T + 1.63439(10^{-2})T + 7377[1 + (12300/T)]\exp(-12300/T) - 187.4624 \quad (13)$$

Fusion, 1045 K

$$\Delta H^\circ = 26{,}153.11;\ \Delta S^\circ = 25.0269 \quad (14)$$

KCl(ℓ), 1045 − 1200 K

$$H^\circ(\ell) - H_0^\circ(\mathrm{c}) = 73.3994T + 4480.10 \quad (15)$$

$$C_p^\circ = 73.3994 \quad (16)$$

$$S^\circ = 73.3994 \ln T - 331.3696 \quad (17)$$

Values calculated from eqs (8)−(13) and (15)−(17) are given for round temperatures in table 5 in terms of the joule as the energy unit, and in table 6 in terms of the commonly used "defined thermochemical calorie."

Although table 6 is based on the International Practical Temperature Scale of 1968 and the latest existing JANAF tables for KCl [23] are based on the scale of 1948, the changes resulting from the temperature-scale conversion are quite small in the present case, and it is of interest to ignore these changes and compare the two tables because they are based on the same experimental data. The values of $(H^\circ_{298.15} - H^\circ_0)$ and $S^\circ_{298.15}$ are identical within rounding error, reflecting the agreement in integrating Berg and Morrison's [4] heat capacities. The heat-capacity values of table 6 are higher at 298, 500, 1000, and above 1045 K (liquid) by +0.2, −0.1, +1.5, and −0.3 percent respectively; and the heat of fusion in table 6 is 0.5 percent lower, principally because of the exponential terms in eqs (11) and (12) instead of a simple correction for premelting reflected in the JANAF tables. The Gibbs-energy function (for the same temperatures, and based

TABLE 5. *Thermodynamic functions for potassium chloride (KCL), crystalline and liquid phases (in terms of* ***JOULES*** *per mole)*
(1 mol = 74.551 g; International Practical Temperature Scale of 1968; H_0° refers to the enthalpy of the crystal at 0 K)

T	$H^\circ - H_0^\circ$	C_p°	S°	$-(G^\circ - H_0^\circ)/T$
K	J mol^{-1}	J mol^{-1}K^{-1}	J mol^{-1}K^{-1}	J mol^{-1}K^{-1}
		Crystalline		
270	9934	50.63	77.49	40.70
273.15	10094	50.71	78.08	41.12
280	10442	50.89	79.34	42.04
290	10952	51.16	81.13	43.36
298.15	11370	51.37	82.55	44.41
300	11465	51.42	82.87	44.65
310	11980	51.65	84.56	45.91
320	12498	51.86	86.20	47.14
330	13017	52.04	87.80	48.35
340	13538	52.19	89.36	49.53
350	14061	52.32	90.87	50.69
360	14585	52.45	92.35	51.83
370	15110	52.59	93.78	52.94
380	15637	52.75	95.18	54.04
400	16695	53.08	97.89	56.16
420	17760	53.40	100.49	58.21
440	18831	53.73	102.98	60.19
460	19909	54.06	105.38	62.11
480	20994	54.38	107.69	63.96
500	22085	54.71	109.91	65.75
520	23182	55.04	112.07	67.49
540	24286	55.37	114.15	69.18
560	25397	55.69	116.17	70.83
580	26514	56.02	118.13	72.42
600	27638	56.35	120.03	73.98
620	28767	56.68	121.89	75.50
640	29904	57.01	123.69	76.97
660	31047	57.35	125.45	78.42
680	32198	57.69	127.17	79.83
700	33355	58.03	128.85	81.20
720	34519	58.39	130.49	82.55
740	35691	58.76	132.09	83.87
760	36870	59.14	133.66	85.16
780	38056	59.55	135.20	86.42
800	39252	59.98	136.72	87.66
825	40758	60.57	138.57	89.18
850	42281	61.24	140.39	90.65
875	43821	61.99	142.17	92.10
900	45381	62.85	143.93	93.51
925	46964	63.85	145.67	94.89
950	48574	65.01	147.39	96.25
975	50216	66.37	149.09	97.59
1000	51895	67.96	150.79	98.89
1025	53616	69.82	152.49	100.18
1045	55029	71.52	153.86	101.19
		Liquid		
1045	81183	73.40	178.89	101.19
1050	81550	73.40	179.24	101.57
1100	85219	73.40	182.65	105.17
1150	88889	73.40	185.91	108.61
1200	92559	73.40	189.04	111.90

TABLE 6. *Thermodynamic functions for potassium chloride (KCl), crystalline and liquid phases (in terms of* ***CALORIES*** *per mole)*
(1 cal = 4.1840 J; 1 mol = 74.551 g; International Practical Temperature Scale of 1968; H_0 refers to the enthalpy of the crystal at 0 K)

T	$H^\circ - H_0^\circ$	C_p°	S°	$-(G^\circ - H_0^\circ)/T$
K	cal mol^{-1}	cal mol^{-1}K^{-1}	cal mol^{-1}K^{-1}	cal mol^{-1}K^{-1}
		Crystalline		
270	2374.5	12.101	18.520	9.726
273.15	2412.6	12.120	18.661	9.828
280	2495.8	12.162	18.962	10.048
290	2617.7	12.226	19.390	10.363
298.15	2717.6	12.277	19.729	10.614
300	2740.3	12.288	19.805	10.670
310	2863.4	12.344	20.209	10.972
320	2987.1	12.394	20.602	11.267
330	3111.3	12.437	20.984	11.555
340	3235.8	12.473	21.356	11.838
350	3360.7	12.505	21.718	12.115
360	3485.9	12.535	22.070	12.387
370	3611.4	12.568	22.414	12.653
380	3737.3	12.607	22.750	12.914
400	3990.3	12.685	23.399	13.423
420	4244.8	12.763	24.020	13.913
440	4500.8	12.841	24.615	14.386
460	4758.3	12.919	25.188	14.843
480	5017.5	12.997	25.739	15.285
500	5278.3	13.075	26.271	15.714
520	5540.6	13.154	26.786	16.130
540	5804.5	13.232	27.284	16.534
560	6069.9	13.310	27.766	16.927
580	6336.9	13.388	28.234	17.309
600	6605.4	13.467	28.689	17.681
620	6875.5	13.546	29.132	18.043
640	7147.3	13.625	29.563	18.396
660	7420.6	13.705	29.984	18.741
680	7695.5	13.787	30.394	19.078
700	7972.1	13.869	30.795	19.407
720	8250.4	13.954	31.187	19.729
740	8530.2	14.042	31.571	20.044
760	8812.0	14.134	31.946	20.352
780	9095.7	14.231	32.315	20.654
800	9381.4	14.335	32.676	20.950
825	9741.5	14.476	33.120	21.312
850	10105.4	14.634	33.554	21.666
875	10473.3	14.814	33.981	22.012
900	10846.2	15.020	34.401	22.350
925	11224.7	15.259	34.816	22.681
950	11609.6	15.537	35.226	23.006
975	12002.0	15.863	35.634	23.325
1000	12403.1	16.243	36.040	23.638
1025	12814.6	16.686	36.447	23.945
1045	13152.3	17.093	36.773	24.188
		Liquid		
1045	19403.1	17.543	42.755	24.188
1050	19490.8	17.543	42.839	24.276
1100	20367.9	17.543	43.655	25.139
1150	21245.1	17.543	44.435	25.961
1200	22122.2	17.543	45.181	26.746

538-709 OL - 74 - 6

on either H°_0 or $H^\circ_{298.15}$) is virtually identical for the crystal, and only about 0.01 cal $mol^{-1}K^{-1}$ lower for the liquid in table 6.

5. Discussion

5.1. Comparison with Other Investigators

The investigations measuring the relative enthalpy or heat capacity of potassium chloride (a) below room temperature and (b) above room temperature are outlined in chronological order in table 7. The individual unsmoothed values of enthalpy from most of these investigations, including those of the present authors (table 3), were adjusted to the basis of the International Practical Temperature Scale of 1968 and to the base enthalpy at 273.15 K as well as possible, and are compared with the final smooth values of this paper in figure 2.

TABLE 7. *Reported measurements of the enthalpy or heat capacity of potassium chloride (KCl)*

Authors	Year published	Reference	Temp. range (K)	H or C_p measured?
(a) BELOW ROOM TEMPERATURE				
Nernst	1911	[36]	22–90	C_p
Nernst & Lindemann	1911	[37]	22–90	
Lindemann & Schwers	1913	[30]	22–90	
Southard & Nelson	1933	[48]	17–285	
Keesom & Clark	1935	[25]	2.3–17	
Feodosiev	1938	[16]	86–298	
Clusius et al.	1949	[8]	10–270	
Sayre & Beaver	1950	[45]	69–81	
Keesom & Pearlman	1953	[26]	1–5	
Strelkov et al.	1954	[49]	12–300	
Webb & Wilks	1955	[55]	1–40	
Berg & Morrison	1957	[4]	2.8–270	
Sokolov & Sharpataya	1964	[47]	88–299	
(b) ABOVE ROOM TEMPERATURE				
Plato	1906	[40]	293–999, 1080–1208	H
Russell	1912	[44]	275–317	?
Magnus	1913	[33]	289–823	H
Brönsted	1914	[6]	273–293	?
Lyashenko	1935	[32]	291–1127	H
Popov et al.	1940	[41]	293–923	H
Mustajoki	1951	[35]	334–721	C_p
Skuratov & Lapushkin	1951	[46]	293–933	H
Dworkin & Bredig	1964	[13, 14]	1323–1373	H
Palkin et al.	1965	[39]	296–299	C_p
Bloom & Tricklebank	1966	[5]	300–1123	H
Vasil'kova et al.	1969	[53]	402–1045	H
Leadbetter & Settatree	1969	[27, 28]	314–641	C_p
Marchidan & Ciopec	1970	[34]	400–700	H
Thompson & Flengas	1971	[51]	298–1306	H
Douglas & Harman	1974	This work	273–1174	H

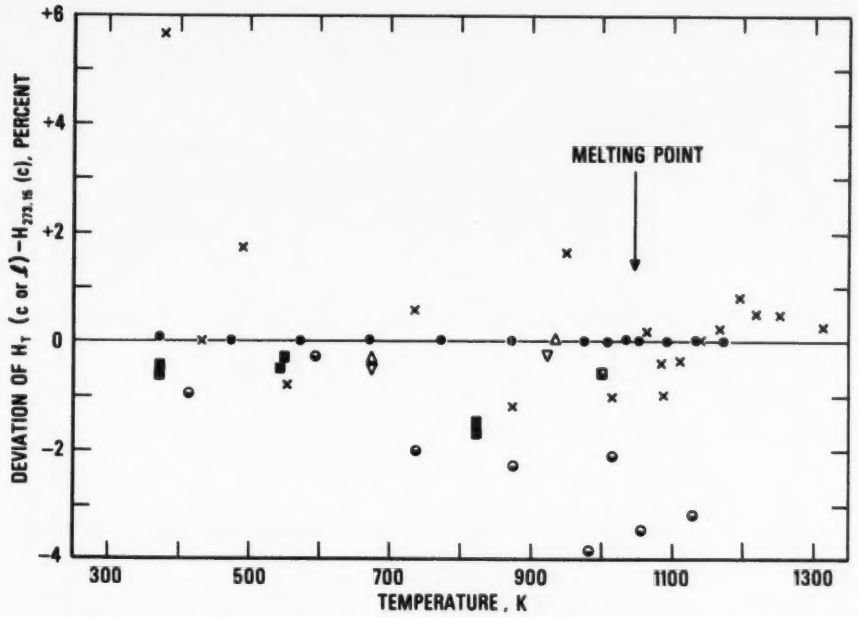

FIGURE 2. *Percentage deviation of KCl unsmoothed relative enthalpy,* $H_T(c \text{ or } \ell) - H_{273.15}(c)$, *of various investigators from those adopted in this paper.*

See fig. 3 for legend of symbols.

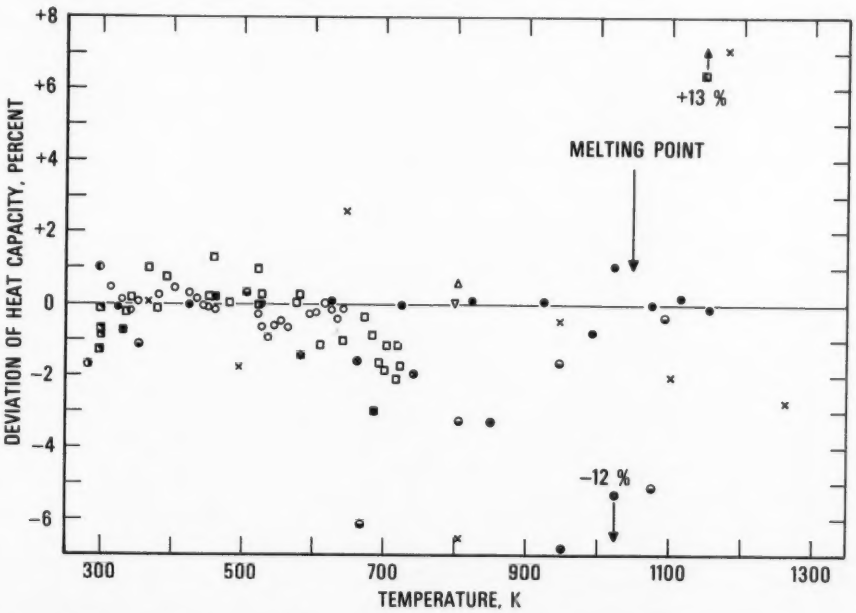

FIGURE 3. *Percentage deviation of unsmoothed heat capacity,* C_p, *of various investigators from those adopted in this paper.*

Base line: Eqs (8)–(17) or tables 5 and 6 (this work).

● : Douglas and Harman	(1974)	This work	□ : Mustajoki	(1951)	[35]
× : Thompson and Flengas	(1971)	[51]	▽ : Popov et al.	(1940)	[41]
○ : Leadbetter and Settatree	(1969)	[27, 28]	◒ : Lyashenko	(1935)	[32]
⊗ : Vasil'kova et al.	(1969)	[53]	◑ : Brönsted	(1914)	[6]
◪ : Palkin et al.	(1965)	[39]	■ : Magnus	(1913)	[33]
◓ : Dworkin and Bredig	(1964)	[13, 14]	◐ : Russell	(1912)	[44]
△ : Skuratov and Lapushkin	(1951)	[46]	◩ : Plato	(1906)	[40]

TABLE 8. *Reported measurements of the melting point and heat of fusion of KCl*

Authors	Year published	Reference	Melting point	Heat of fusion
			°C	*cal mole*$^{-1}$ [b]
Carnelley	1877	[19, 7]	770	
Ramsay	1896	[19, 42]	762	
Jaeger	1914–1915	[19, 21]	771	
Jaeger	1917	[19, 22]	768	
von Wartenberg & Albrecht	1921	[19, 54]	768 ± 3	
Roberts	1924	[43]	[a] 770.3 ± 0.5	
Ginnings & Phipps	1930	[18]	770	
Lyashenko	1935	[19, 32]		6290
Johnson & Bredig	1958	[24]	769.5	
Dworkin & Bredig	1960	[14]		6340
Aukrust et al	1960	[23, 3]	770	[c] 6400
Bloom & Tricklebank	1966	[5]		6200
Vasil'kova et al	1969	[53]		6430
Thompson & Flengas	1971	[51]		6250
Douglas & Harman	1974	This work		6250

[a] See table 4 for values found for thermometric fixed points.

[b] In those cases where defined, 1 cal = 4.184 J.

[c] This is the *calorimetric* value reported. A value derived from phase diagrams also was reported, but is not tabulated here.

A similar comparison of unsmoothed heat capacities above 273 K is shown in figure 3.[6] This comparison includes not only the heat capacities measured directly by some authors, but also the heat capacity corresponding to the difference between the observed relative enthalpies for two adjacent temperatures of measurement,[7] after applying a small correction for curvature when this was significant. The accounting for the curvature correction was done by using the approximate equation [38]

$$C_p = (\Delta H/\Delta T) - [(\Delta T)^2/24][\partial^2 C_p/\partial T^2], \qquad (18)$$

where C_p and $\partial^2 C_p/\partial T^2$ apply at the middle of the temperature interval corresponding to ΔT ($\partial^2 C_p/\partial T^2$ was computed from eq (9) or (12)). The great majority of points in figure 3 fall within 1 percent of the base line, though above 700 K there are fewer investigations and also the scatter is greater.

The reported values for the melting point and heat of fusion found in the literature are summarized in table 8 in chronological order. The heat-of-fusion values range from 1 percent lower to 3 percent higher than the authors' value. Noncalorimetric heat-of-fusion values have been excluded from the table because in general other methods (particularly, derivation from phase diagrams) are less reliable and sometimes misleading.

[6] A few data are omitted from figure 2 (but included in fig. 3) because the temperature intervals covered did not include room temperature. The results of Vasil'kova et al. [53] are represented in figure 3 by selected smoothed values only.

[7] When the temperature interval would otherwise be quite small, individual enthalpies and their temperatures were averaged such that the temperature interval ΔT used would be of the order of that for the authors' data (100°, more or less), so as to make the precision of different investigations more nearly comparable in figure 3.

5.2. Reliability of the Results

The discussion of reliability will be limited to the final values of heat capacity above 273 K and to the heat of fusion (tables 5 and 6, or eqs (9), (12), (16), and (14)). As usual, the limits of absolute accuracy are difficult to ascertain closely, but may be estimated after careful consideration of the identifiable individual sources of systematic error, the measurement precision, and a comparison with high-accuracy results of other investigators.

Several systematic errors prove to be of relatively minor consequence. The furnace temperatures measured only by thermocouple may be in error by amounts up to 0.2°, which corresponds to an error of less than 0.03 percent of the net enthalpy relative to 273 K (and probably also of the heat capacity) of potassium chloride above 873 K. Inconstancy from one container to another of the heat lost during the drop into the calorimeter was estimated to be even less serious. The assumed calibration factor of the ice calorimeter is believed to be accurate to ± 0.01 percent, affecting the relative enthalpy and heat capacity by the same percentage. Although the ambiguity in the mass of KCl sample 2 mentioned in sec. 3.3.b contributes an uncertainty of 0.04 percent to the KCl heat capacity calculated for this sample, the corresponding uncertainty for the sample usually used (sample 1) was estimated to be only 0.005 percent. The sample impurities (table 1) were estimated [23] to cause errors in the heat capacity varying from 0.02 to 0.04 percent (aside from any premelting: see below); however, no such corrections were applied to the data, owing to considerable uncertainty in the applicability of the additivity assumption on which this estimate is based.

The standard deviation of the mean net heat capacity of potassium chloride, as determined from the reproducibility (tables 2 and 3), is 0.2 percent over the liquid range covered, and averages the same over any 100-deg interval in the crystalline range.

The equations given in this paper to represent the enthalpy data for KCl being reported were derived on the assumption that the samples underwent no premelting below the melting point (except for the data at 1038.72 K, which were not included in the fit). Except in a rather short temperature region below the melting point (above 974 K), where the fit is within the precision, this smoothing did not compromise the unsmoothed mean heat capacities for pairs of successive temperatures by more than about 0.1 percent. Yet it was found that the crystal enthalpy data could have been fit almost as well if alternatively the samples were assumed to contain a small amount (empirically assumed to be 0.015 mole percent) of liquid-soluble, crystal-insoluble impurity, with subtraction of the corresponding enthalpies of premelting before the fitting. The results derived from this alternative fitting would correspond to heat capacities of pure KCl different by never more than 0.3 percent below 925 K (or above the melting point, 1045 K), but averaging 2 percent less over the interval 925–1045 K, and almost 5 percent less at 1045 K. As a consequence the heat of fusion would have been 0.5 percent greater than that derived assuming no premelting.

The purity of the samples, while high, was not sufficiently high to rule out unequivocally the possibility of a comparatively small amount of impurity causing premelting to the extents alternatively hypothecated above, and as a consequence the above differences between the two sets of results were retained in considering the reliability of the values derived for pure potassium chloride. Nevertheless, the occurrence of appreciable premelting (except at 1038.72 K, as discussed in sec. 3.3.b) is considered improbable for two reasons. In the first place, the accelerated upturn of the *observed* C_p-versus-T curve below the melting point can be explained by the effect of lattice vacancies whose existence is indicated by other properties (discussed in section 5.3), without the assumption of any premelting; and in the second place available phase diagrams [29] suggest, after use of an earlier analogous treatment [11], solubilities of the known impurities in the KCl (c) too great to cause any melting of the sample at as low a temperature as 1033.7 K (the highest temperature at which accepted enthalpy measurements were made below the melting point). It is true that a small amount (up to about 0.05 mole percent) of silver chloride may have formed according to the reaction

$$4KCl + 4Ag + O_2 + 2H_2O = 4KOH + 4AgCl \qquad (19)$$

when the sample containers were sealed (sec. 3.3.b) and that an early phase diagram of the KCl-AgCl system [29] shows no solid solubility. However, it was estimated that the solidus curve of this system would have to be at least 60 times as steep as the liquidus curve (near 100 percent KCl) for the solidus curve to be crossed at or below 1033.7 K for the present samples, and the ratio of the molar volume of AgCl to that of KCl is not so different from unity that the solid solubility of AgCl in KCl (c) would seem to be actually so small.

On the basis of the foregoing considerations it was estimated that the values adopted in this paper for the heat capacity of KCl (c) are probably not in error by more than amounts varying from 0.2 percent at 273 K to 0.5 percent at 925 K to 5 percent at 1045 K, and with assigned uncertainties of 0.5 percent for the heat of fusion and 0.4 percent for the mean heat capacity of KCl (ℓ) over the range measured (1045−1174 K). However, if there are errors of such magnitude in the heat capacity just below the melting point, they are nearly compensated by a corresponding error of opposite sign in the heat of fusion, so that the enthalpy interval KCl (c) (925 K) to KCl (ℓ) (1045 K) is probably represented accurately to 0.2 percent. These accuracy estimates are consistent with figure 1, according to which the (extrapolated) smoothed heat-capacity values of neither set of observers differ from the adopted values by more than 0.2 percent above 295 K (and Berg and Morrison's estimated accuracy up to 270 K was 0.2 percent). The heat-capacity values of other observers (see fig. 3) were considered too imprecise to aid in assessing the present work.

5.3. Contributions From Lattice Vacancies

In one investigation [50] the results of the thermal analysis of several binary systems and of potassium chloride of different purities were interpreted as indicating that this substance transforms at 753–755 K (presumably at atmospheric pressure) into a polymorphic crystalline modification whose melting point was said to be some 200° lower than that ordinarily encountered (1045 K). This is the only reported evidence of a polymorphic transformation of KCl (except the long-known one to the CsCl-type structure at quite high pressures) of which the authors are aware.

According to Ubbelohde [52], adiabatic elastic constants and linear-thermal-expansion data have been used to convert earlier C_p data on KCl to C_v values which, unlike C_p, were found to show no "premonitory" rise with temperature, within experimental error, below the melting point [15]. The "premonitory" rise of the crystal C_p referred to is clearly shown in figure 4, where the C_p of both crystalline and liquid KCl, as evaluated in the present investigation (eqs (4), (9), (12), and (16)) is plotted against temperature. According to eq (12), the C_p–T curve is very nearly linear from 373 K up to above 700 K, a fact which invites an attempt to interpret quantitatively the upturn of the curve at higher temperatures as represented by the exponential term in the equation. Such an upturn has been found for many crystalline substances, and is too pronounced and too broad to be explainable by premelting (see sec. 5.2), but has generally been accepted as representing the energy needed to create an increasing number of lattice vacancies (or other lattice defects) as the melting point is approached. It may be pointed

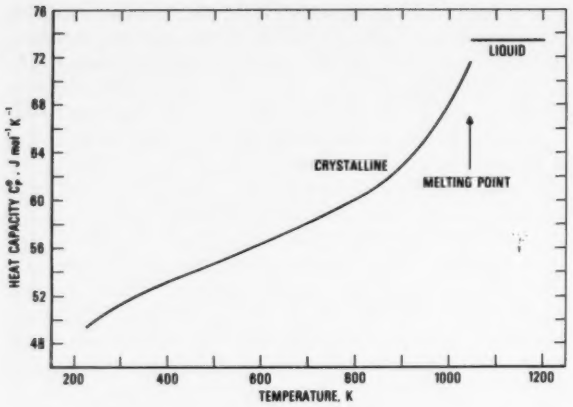

FIGURE 4. *The heat capacity of potassium chloride from 225 to 1200 K.*

The values are given below 270 K by eq (4), and above 270 K by eqs (9), (12), and (16) or by table 5.

out that the cooling of the sample in the ice calorimeter in the present work is believed to be too slow by many orders of magnitude to prevent the maintenance of virtual equilibrium with respect to these vacancies (at least in the high-temperature "intrinsic" region where vacancies (Schottky defects) predominate numerically over lattice-site impurities).

In a pure typically ionic equi-valent salt such as KCl in which interstitial lattice defects are highly unfavorable energetically, there will be equal numbers of cation and anion vacancies which in some important respects simulate a gas of ions. For example, a major energetic effect is a strong Coulombic attraction between vacancies of opposite charge, leading to the extensive formation of vacancy clusters or aggregates (pairs, quartets, etc.). Unless one type of cluster is known to predominate under all conditions of interest, it is appropriate to assume (somewhat arbitrarily at high vacancy concentrations) that for each temperature and pressure there is a definite number of each type of vacancy cluster in thermodynamic equilibrium. Then for each such cluster type (considering isolated cation and anion vacancies as separate types) we can write to a good approximation

$$x_i = g_i \exp(-E_i/RT), \tag{20}$$

and

$$H_i = g_i E_i \exp(-E_i/RT), \tag{21}$$

where x_i and H_i are—per mole (GFW) of salt (KCl)—the number of moles of the vacancy clusters of type i and their enthalpy of formation, respectively; E_i is the energy of formation of one mole of such clusters from perfect crystal; R is the gas constant; and g_i is the degeneracy of the cluster type (in the simplest case, the number of distinguishable orientations). In general, the total enthalpy of vacancy formation will be given by a sum of many terms of the form of eq (21), though at a given temperature only one or two terms may be of appreciable magnitude. Furthermore, taking the *pair* cluster as an example, we may divide these into separate cluster types depending on the pair distance (and consequently on the energy E_i), and this will be approximately equivalent to neglecting all pairs except those with the largest value of x_i.

Comparing the exponential enthalpy term of eq (11), $9.073\ (10^7) \cdot \exp(-12300/T)$ J/mole of KCl, with eq (21) gives from the data of this paper [8]

$$E_i = 1.06 \text{ eV and } g_i = 887. \tag{22}$$

Using these values, eq (20) gives as the vacancy-aggregate concentration, per mole of KCl, a value from 0.001 mole at 900 K to 0.007 mole at 1045 K, the melting point. However, owing to the imprecision of the experimental enthalpy data (small but real), the parameters of eqs (22) cannot be considered to be determined by these data except within wide ranges: allowing a 50 percent greater standard deviation of fit than the best fit, which gave eqs (22), would give a spread from $E_i = 0.97$ eV ($g_i \simeq 400$) to $E_i = 1.18$ eV ($g_i \simeq 3000$). Furthermore, in view of the large magnitudes of the preexponential factor g_i, the interpretation in terms of lattice vacancies only must indicate the importance of large vacancy clusters (see below), and hence the probability that the single empirical exponential term in the enthalpy equation represents a composite of several vacancy types.

Various investigators have employed other methods—particularly ionic conductivity, diffusion with isotopic tracers, charged dislocations, and dielectric relaxation—to measure the concentrations and energies of lattice vacancies in ionic crystals, and we may summarize some results for KCl as given in a fairly recent review [1]. The temperature dependence cited as typical for the first two methods is close to that of eqs (22) (being equivalent to values of E_i from 1.11 to 1.16 eV), but the accompanying preexponential factors cited are much smaller (equivalent to values of g_i from 15 to 44). However, the overall spread of parameter values that have been found for KCl by different methods is very wide. Some of this spread may be due to the wide range of temperatures (from 543 to 1043 K) of the measurements, and some may be due to the customary interpretation of the parameter E_i in eq (20) as half the energy of formation of a mole of vacancy pairs. It may be that at low temperatures where the total vacancy concentration is quite small, this interpretation is valid; and that at high temperatures the electric field involved in such techniques as ionic conductivity effectively dissociates many vacancy clusters which, in the absence of a field, seem to be present during the enthalpy measurements.

One of the authors has used classical ionic-crystal theory (and arbitrary cutoffs) to compute the energy of replacing a single ion of a perfect alkali-halide crystal by another ion of the same charge [9], and the agreement with all comparable calorimetric results was excellent (being within experimental error). In principle, the same approach should be successful in

[8] One eV is equivalent to 9.64867 (10^4) J mol^{-1}.

computing the energies of isolated vacancies and vacancy clusters in potassium chloride, and such computations [9] were begun in the hope of reproducing within a reasonable approximation the empirical parameter values of eqs (22). These computations were soon abandoned, for two reasons. In the first place, calculations involving alternative cutoffs at 2, 4, 6, and 10 independent relaxation parameters (respectively 2, 4, 5, and 8 ion shells surrounding the vacancy) gave isolated-vacancy energies successively decreasing from 2.14 to 1.75 eV, but showing no sign of convergence, a failure possibly caused by the long-range nature (not present in the earlier situation [9]) of the Coulombic potential around the vacancy. In the second place, the indicated extension to vacancy *clusters* would encounter much lower symmetry than for isolated vacancies, and thereby present a problem of great complexity in evaluating the equilibrium relaxation and resulting energy effects of enough ions in the neighborhood of such vacancy clusters.

Very rough estimations did lead to the conclusion, however, that in order to explain the parameters of eqs (22) derived from the authors' enthalpy data—particularly the large multiplicity (value of g_i)—vacancy *pairs* having energies in the range of the stated value of E_i (eqs (22)) would have far too small values of g_i, but that the given parameter values *may* be consistent with a predominance of much larger vacancy clusters (e.g., quadrupoles, octapoles, etc.) for which the number of different geometric arrangements is far greater.

6. References

[1] American Institute of Physics Handbook, 3rd ed. (McGraw-Hill Book Co., New York, 1972), pp. 9–74 to 9–85.
[2] Atomic weights of the elements 1971 (IUPAC Comm. on Atomic Weights), Pure Appl. Chem. **30,** 637–649 (1972).
[3] Aukrust, E., Björge, B., Flood, H., and Forland, T., Ann. N.Y. Acad. Sci. **79,** 830–837 (1960).
[4] Berg, W. T., and Morrison, J. A., Proc. Royal Soc. (London) **A242,** 467–477 (1957).
[5] Bloom, H., and Tricklebank, S. B., Australian J. Chem. **19,** 187–196 (1966).
[6] Brönsted, J. N., Z. Elektrochem. **20,** 555ff (1914).
[7] Carnelley, T., J. Chem. Soc. **31,** 381ff (1877).
[8] Clusius, K. von, Goldmann, J., and Perlick, A., Z. Naturforsch. **4A,** 424–432 (1949).
[9] Douglas, T. B., J. Chem. Phys. **45,** 4571–4585 (1966).
[10] Douglas, T. B., J. Res. Nat. Bur. Stand. (U.S.) **73A** (Phys. and Chem.), No. 5, 451–470 (1969).
[11] Douglas, T. B., and Ditmars, D. A., J. Res. Nat. Bur. Stand. (U.S.) **71A** (Phys. and Chem.) No. 3, 185–193 (1967).
[12] Douglas, T. B., and King, E. G., High Temperature Drop Calorimetry, Chapter 8 in Experimental Thermodynamics Vol. **I** (Butterworths, London, 1968); also in Precision Measurement and Calibration (Heat), D. C. Ginnings, Ed., Nat. Bur. Stand. (U.S.), Spec. Publ. 300, Vol. **6,** 181–219 (1970).
[13] Dworkin, A. S., private communication to JANAF Thermochemical Tables, Dec. 1, 1964. (See also ref. [14].)
[14] Dworkin, A. S., and Bredig, M. A., J. Phys. Chem. **64,** 269–272 (1960).
[15] Enck, F. D., Phys. Rev. **119,** 1873–1877 (1960).
[16] Feodosiev, N., Zhur. Fiz. Khim. (J. Phys. Chem., Russian) **12,** 291ff (1938).
[17] Furukawa, G. T., Douglas, T. B., McCoskey, R. E., and Ginnings, D. C., J. Research NBS **57,** 67–82 (1956) RP2694.
[18] Ginnings, D. C., and Phipps, T. E., J. Amer. Chem. Soc. **52,** 1340–1345 (1930).
[19] Gmelins Handbuch anorg. Chem. System, Verlag Chemie, Berlin, 1938, 22 (K), p. 374.
[20] The International Practical Temperature Scale of 1968, Metrologia **5,** 35ff (1969).
[21] Jaeger, F. M., Akad. Amersterdam Versl. **23,** 360 (1914–1915).
[22] Jaeger, F. M., Z. anorg. Chem. **101,** 185ff (1917).
[23] JANAF Thermochemical Tables, 2nd ed., Nat. Stand. Ref. Data Ser., Nat. Bur. Stand. (U.S.), **37,** 1141 pages, 1971.
[24] Johnson, J. W., and Bredig, M. A., J. Phys. Chem. **62,** 604–607 (1958).
[25] Keesom, W. H., and Clark, C. W., Physica **2,** 698ff (1935).
[26] Keesom, P. H., and Pearlman, N., Phys. Rev. **91,** 1354ff (1953).
[27] Leadbetter, A. J., private communication, July 26, 1967 (see ref. [28]).
[28] Leadbetter, A. J., and Settatree, G. R., Proc. Phys. Soc., London, Solid State Phys. [2] **2,** 385–392 (1969).
[29] Levin, E. M., Robbins, C. R., and McMurdie, H. F., Phase Diagrams for Ceramists, M. K. Reser, Ed. (Am. Ceram Soc., Columbus, O., 1964): KCl-KOH, Fig. 1733 (p. 483); KCl-NaCl, Figs. 1258 and 1259 (p. 376); KCl-AgCl, Fig. 1215 (p. 368).
[30] Lindemann, F. A., and Schwers, F., Physik. Zeit. **14,** 766ff (1913).
[31] Los, J. M., and Morrison, J. A., Canad. J. Phys. **29,** 142ff (1951).
[32] Lyashenko, W. S., Metallurg. **10** [11], 89ff (1935).
[33] Magnus, A., Physik. Zeit. **14,** 5ff (1913).
[34] Marchidan, D. I., and Ciopec, M., Rev. Roum. Chim. **15,** 1177–1180 (1970) (in English) (see Chem. Abstr. **74,** 35358 (1971)).
[35] Mustajoki, A., Ann. Acad. Sci. Fennicae, Ser. A, I, **98,** 7–45 (1951).
[36] Nernst, W., Ann. Physik [4] **36,** 395ff (1911).
[37] Nernst, W., and Lindemann, F. A., Z. Elektrochem. **17,** 817ff (1911).
[38] Osborne, N. S., Stimson, H. F., Sligh, T. S., and Cragoe, C. S., BS Sci. Pap. **20,** 65ff (1925) S501.
[39] Palkin, V. A., Kuz'mina, N. N., and Chernyaev, I. I., Zhur. Neorg. Khim. (J. Inorg. Chem., Russian) **10,** 41–48 (1965).
[40] Plato, W., Zeit. physik. Chem. **55,** 721–737 (1906).
[41] Popov, M. M., Skuratov, S. M., and Nikonova, I. N., Zhur. Obshchei Khim. (J. Gen. Chem., Russian) **10,** 2017–2022 (1940).
[42] Ramsay, W., and Eumorfopoulos, N., Phil. Mag. [5] **41,** 365ff (1896).
[43] Roberts, H. S., Phys. Rev. **23,** 386ff (1924).
[44] Russell, A. S., Physik. Zeit. **13,** 62ff (1912).
[45] Sayre, E. V., and Beaver, J. J., J. Chem. Phys. **18,** 584–594 (1950).
[46] Skuratov, S. M., amd Lapushkin, S. A., Zhur. Obshchei Khim. (J. Gen. Chem., Russian) **21,** 2217–2220 (1951).
[47] Sokolov, V. A., and Sharpataya, G. A., Zhur. Neorg. Khim. (J. Inorg. Chem., Russian) **9,** 1542–1546 (1964).
[48] Southard, J. C., and Nelson, R. A., J. Amer. Chem. Soc. **55,** 4865–4869 (1933).
[49] Strelkov, P. G., Itskevich, E. S., Kostryukov, V. N., and Mirskaya, C. G., Zhur. Fiz. Khim. (J. Phys. Chem., Russian) **28,** 645–649 (1954).
[50] Sumarokova, T. N., and Modestova, T. P., Izv. Akad. Nauk Kaz. SSR, Ser. Khim. Nauk **14,** 26–33 (1964) (Russian); Chem. Abstr. **62,** 3632 (1965).
[51] Thompson, W. T., and Flengas, S. N., Canad. J. Chem. **49,** 1550–1563 (1971).
[52] Ubbelohde, A. R., Melting and Crystal Structure, Oxford Univ. Press, 1965, p. 231.
[53] Vasil'kova, I. V., Podzorov, B. N., and Shapkin, P. S., Zhur. Neorg. Khim. (J. Inorg. Chem., Russian) **14,** 1732ff (1969).
[54] Wartenberg, H. von, and Albrecht, P., Zeit. Elektrochem. **27,** 164ff (1921).
[55] Webb, F. J., and Wilks, J., Proc. Royal Soc. (London) **230A,** 549ff (1955).

[9] Using the justifiable simplification of a single inverse-power repulsive term, consistent with the known lattice energy of a perfect KCl crystal, for the non-Coulombic part of the potential function.

(Paper 78A4–832)

JOURNAL OF RESEARCH of the National Bureau of Standards — A. Physics and Chemistry
Vol. 78A, No. 4, July-August 1974

Publications of the National Bureau of Standards*

Citations with Selected Abstracts

J. Res. Nat. Bur. Stand. (U.S.), **78A** *(Phys. and Chem.)*, No. 3, (May-June 1974), SD Catalog No. C13.22/sec.A:78/3.

Photoionization of CO_2-CO-O_2 mixtures. Formation and reactions of ion clusters, L. W. Sieck and R. Gorden, Jr.

Analysis of low temperature viscosity data for three NBS standard glasses, A. Napolitano, J. H. Simmons, D. H. Blackburn, and R. E. Chidester.

PVT relationships for liquid and glassy poly(vinyl acetate), J. E. McKinney and M. Goldstein.

Correction and extension of van der Poel's method for calculating the shear modulus of a particulate composite, J. C. Smith.

The formation of curved polymer crystals: Polychlorotrifluoroethylene, J. D. Barnes and F. Khoury.

Enthalpy of formation of phosphorus pentachloride; derivation of the enthalpy of formation of aqueous orthophosphoric acid, R. H. Schumm, E. J. Prosen, and D. D. Wagman.

Heat capacities of polyethylene from 2 to 360 K. II. Two high density linear polyethylene samples and thermodynamic properties of crystalline linear polyethylene, S. S. Chang.

The specific heats, C_σ, C_V, of compressed and liquefied methane, B. A. Younglove.

An improved procedure for synthesis of DL-4-hydroxy-3-methoxymandelic acid (DL-"vanillyl"-mandelic acid, VMA), A. J. Fatiadi and R. Schaffer.

Single particle motions in liquids: Qualitative features of memory functions, R. D. Mountain.

The infrared spectra of matrix isolated uranium oxide species, S. Abramowitz and N. Acquista.

J. Res. Nat. Bur. Stand. (U.S.), **78B** *(Math. Sci.)*, No. 2, (Apr.-June 1974), SD Catalog No. C13.22/sec.B:78/2.

Rational equivalence of unimodular circulants, S. Pierce.

How to determine the accuracy of the output of a matrix inversion program, M. Newman.

A conjecture on a matrix group with two generators, M. Newman.

A property of equivalence, M. Newman.

Comments on the discrete matrix model of population dynamics, R. Freese and C. R. Johnson.

Fixed-point solution of plant input/location problems, A. J. Goldman.

A new proof of Pick's theorem, S. Minsker.

**Publications with prices and SD Catalog numbers may be purchased directly from the Superintendent of Documents, U.S. Government Printing Office, Washington, D.C. 20402 (foreign: one-fourth additional). Microfiche copies are available from the National Technical Information Service (NTIS), Springfield, Va. 22151. Reprints from outside journals and the NBS Journal of Research may often be obtained directly from the authors.*

Monogr. 125. **Thermocouple reference tables based on the IPTS-68,** R. L. Powell, W. J. Hall, C. H. Hyink, Jr., L. L. Sparks, G. W. Burns, M. G. Scroger, and H. H. Plumb, Nat. Bur. Stand. (U.S.), Monogr. 125, 410 pages (Mar. 1974) SD Catalog No. C13.44:125, $4.55.

Key words: base metal alloys; noble metal alloys; temperature scale; temperature standards; thermocouples; thermometry.

Revision of the International Practical Temperature Scale requires that there be changes for all accurately tabulated thermophysical values. Revised reference data for thermocouples have been generated in a cooperative program between groups of the National Bureau of Standards in Boulder and Gaithersburg. This Monograph contains tables, analytic expressions, various approximations, and explanatory text. Only the standard letter-designated thermocouples are described: noble metal Types S, R, and B and base metal Types E, J, K, and T. Their appropriate "single-leg" or thermoelement versus Pt-67 values are also included. The new reference data reflect not only revisions in the temperature scale, but also slight changes in the materials themselves and improvements in data fitting methods. The temperature ranges vary for different types, from a low of −270 °C for Type E to a high of 1820 °C for Type B. The main functions and tables are given in terms of Celsius degrees and microvolts. Tables in the appendices represent the data with less precision, in millivolts, and in degrees Fahrenheit as well as Celsius. Approximate quadratic, cubic, and quartic analytic expressions are also given for each thermocouple type in various temperature ranges. Supersedes NBS Circular 561.

SP369. **Soft x-ray emission spectra of metallic solids: Critical review of selected systems and annotated spectral index,** A. J. McAlister, R. C. Dobbyn, J. R. Cuthill, and M. L. Williams, Nat. Bur. Stand. (U.S.), Spec. Publ. 369, 176 pages (Jan. 1974) SD Catalog No. C13.10:369, $1.85.

Key words: alloys; critical review; emission spectra; intermetallic compounds; metals; soft x ray; spectra.

Theory and experimental practice in the field of soft x-ray emission from metallic solids are briefly reviewed, and measurements on a number of systems are critically evaluated and compared with the results of other techniques and theory, with a view to establishing the pertinence of the soft x-ray measurements and indicating specific guidelines for further enhancing their value. In addition, an exhaustive annotated index of measured spectra is provided. Supersedes NBS Monograph 52 in part, for emission spectra only.

SP382. **Hydraulic research in the United States and Canada, 1972,** G. Kulin and P. H. Gurewitz, Eds., Nat. Bur. Stand. (U.S.), Spec. Publ. 382, 340 pages (Jan. 1974) SD Catalog No. C13.10:382, $3.00.

Key words: fluid mechanics; hydraulic engineering; hydraulic research; hydraulics; hydrodynamics; model studies; research summaries.

Current and recently concluded research projects in hydraulics and hydrodynamics for the years 1971-1972 are summarized. Projects

from more than 250 university, industrial, state and federal government laboratories in the United States and Canada are reported.

SP390. **Index of international standards,** S. J. Chumas, Ed., Nat. Bur. Stand. (U.S.), Spec. Publ. 390, 222 pages (Mar. 1974) SD Catalog No. C13.10:390, $5.60.

Key words: analyses; International Commission on Rules for the Approval of Electrical Equipment; International Electrotechnical Commission; International Organization for Standardization; International Organization of Legal Metrology; International Special Committee on Radio Interference; recommendations; specifications; standards; test methods.

This computer-produced Index, based on the Key-Word-In-Context (KWIC) system, contains over 2,700 standards titles of the International Organization for Standardization (ISO), the International Electrotechnical Commission (IEC), the International Commission on Rules for the Approval of Electrical Equipment (CEE), the International Special Committee on Radio Interference (CISPR), and the International Organization of Legal Metrology (OIML).

SP392. **Vibrationally excited hydrogen halides: A bibliography on chemical kinetics of chemiexcitation and energy transfer processes (1958 through 1973),** F. Westley, Nat. Bur. Stand. (U.S.), Spec. Publ. 392, 81 pages (Apr. 1974) SD Catalog No. C13.10:392, $1.30.

Key words: bibliography; chemical kinetics; chemiexcitation; gas phase; halogens; hydrogen; hydrogen halides; laser; quenching; vibrational energy transfer.

A bibliography, a reaction oriented list of references, is provided for published papers and reports containing rate data for reactions of halogen atoms with hydrogen-containing compounds, or of H (D, or T) atoms with halogen-containing compounds to form vibrationally chemiexcited hydrogen halides. The reactions for vibroexcitation of hydrogen halides through unimolecular or photochemical elimination, as well as the processes for vibrational energy transfer between hydrogen halides and various second bodies are also included. In addition, four lists of theoretical papers and a list of critical reviews and bibliographies are provided. Over 300 papers covering 50 types of reactions are listed. The period covered extends from 1958 through 1973.

SP393. **Colorimetry and spectrophotometry: A bibliography of NBS publications January 1906 through January 1973,** K. L. Kelly, Nat. Bur. Stand. (U.S.), Spec. Publ. 393, 54 pages (Apr. 1974) SD Catalog No. C13.10:393, 95 cents.

Key words: bibliography; color; color codes; colorimetry; color measurement; spectrophotometry; vision.

This bibiliography of publications will serve as the key to the large amount of research into color measurement and specification, and color vision carried out by the staff of the National Bureau of Standards (NBS) in colorimetry and spectrophotometry. These 623 publications appeared in NBS publications and outside scientific and technical journals between January 1906 and January 1973. This material has been in constant demand by Bureau members as well as by outside individuals and organizations. The practical value of this wealth of information lies in its ready accessibility to the scientific and technical fraternity by title, by key words or by author, in the Library of Congress and in depository libraries such as large public and university libraries. A short organizational chronology of the colorimetry and spectrophotometry program is included.

SP400-1. **Semiconductor measurement technology. Quarterly report, July 1 to September 30, 1973,** W. M. Bullis, Ed., Nat. Bur. Stand. (U.S.), Spec. Publ. 400-1, 68 pages (Mar. 1974) SD Catalog No. C13.10:400-1, $1.15.

Key words: contact resistance; die attachment; dopant profiles; electrical properties; electronics; gold-doped silicon; hermeticity; metallization; methods of measurement; microelectronics; microwave diodes; mobility; MOS devices; oxide films; photomasks; photoresist; resistivity; resistivity standards; scanning electron microscopy; semiconductor devices; semiconductor materials; semiconductor process control; sheet resistance; silicon; S-parameters; spreading resistance; test patterns; thermal resistance; thermally stimulated capacitance; thermally stimulated current; wire bonds.

This quarterly progress report, twenty-first of a series, describes NBS activities directed toward the development of methods of measurement for semiconductor materials, process control, and devices. Principal accomplishments during this reporting period include (1) extension of the technique for measuring thermally stimulated current and capacitance to include measurements on MOS capacitors, (2) completion of the development of the thermal response method for evaluation of transistor die attachment, (3) analysis of the interlaboratory comparison of transistor scattering parameter measurements, (4) preliminary review of measurement problems in the photolithographic aspects of semiconductor device processing, of problems associated with certain hermeticity testing procedures, and of methods for evaluating metallization step coverage, and (5) initiation of new activity on characterization of oxide films in MOS structures and analysis of diffusion profiles. Results are also reported on spreading resistance, capacitance-voltage, and sheet resistance measurements; the activation energy of the gold acceptor in silicon; evaluation of the base-to-metal contact resistor test structure; metallurgical systems for ultrasonic bonding; burn-out characteristics of fine gold and aluminum bonding wire; transistor thermal resistance measurements; and microwave diode conversion loss measurements. Supplementary data concerning staff, publications, workshops and symposia, standards committee activities, and technical services are also included as appendices.

NSRDS-NBS48. **Radiation chemistry of ethanol: A review of data on yields, reaction rate parameters, and spectral properties of transients,** G. R. Freeman, Nat. Stand. Ref. Data Ser., Nat. Bur. Stand. (U.S.), 48, 43 pages (Feb. 1974) SD Catalog No. C13.48:48, 80 cents.

Key words: chemical kinetics; data compilation; ethanol; G; radiation chemistry; rates; review; spectra.

The yields (G) for products and intermediates formed by irradiation of ethanol, in the solid, liquid and gaseous state, have been compiled and reviewed. Rates of reactions of transient ions and radicals and spectroscopic parameters, including optical and esr spectra, are also included.

BSS49. **Laboratory studies of the hydraulic performance of one-story and split-level residential plumbing systems with reduced-size vents,** R. S. Wyly, G. C. Sherlin, and R. W. Beausoliel, Nat. Bur. Stand. (U.S.), Bldg. Sci. Ser. 49, 53 pages (Mar. 1974) SD Catalog No. C13.29/2:49, 95 cents.

Key words: hydraulic criteria for plumbing; hydraulic test loads; plumbing-vent sizing; reduced-size vents; sanitary DWV systems; secondary ventilation; testing plumbing systems; vents for plumbing.

A laboratory study on one-story and split-level experimental drainage systems where the vents in some cases were varied from one to six pipe-sizes smaller than those presently specified by codes showed satisfactory hydraulic and pneumatic performance under various loading conditions. The research was originally sponsored by the National Association of Home Builders and the National Bureau of Standards and more recently by a program of the Department of Defense through the Tri-Services Investigational Committee on Building Materials. This paper presents criteria recommended for the design and evaluation of systems using reduced-sized vents and a sizing table for one- and two-story systems. The laboratory work also contributed to the development of analytical and test procedures needed for evaluating the application of reduced-size venting to a

broad range of innovative drain-waste-vent designs for buildings of any height.

This work indicates that, in some circumstances, reduced-size venting might be a good alternative to other types of drainage systems for multistory buildings which use either conventional or innovative venting concepts. Because this study involved only a limited number of drainage system designs, it is recommended that ongoing field and laboratory studies be explored if code changes are contemplated to permit the use of smaller vents.

BSS51. **Structural evaluation of steel faced sandwich panels,** J. H. Pielert, T. W. Reichard, and L. W. Masters, Nat. Bur. Stand. (U.S.), Bldg. Sci. Ser. 51, 43 pages (Apr. 1974) SD Catalog No. C13.29/2:51, 90 cents.

Key words: accelerated aging; adhesive bond; ductility; flexural shear; housing systems; local buckling; material variability; moisture conditioning; Operation BREAKTHROUGH; paper honeycomb; structural sandwich; sustained load.

A series of structural evaluation tests performed on components and materials intended for use in one of the Operation BREAKTHROUGH housing systems is described. Four samples of steel faced, paper honeycomb, sandwich panel material and four full size prototype roof panels were evaluated.

The samples of sandwich panel material were used to evaluate the variability of panel material properties and the effect of aging on tensile and shear strength. The roof panels were used to determine the behavior in service considering the effects of adverse environmental conditions on ultimate strength and mode of failure. In addition, the performance of one panel under sustained loading was evaluated.

FIPS PUB28. **Standardization of data elements and representations,** H. S. White, Jr., Nat. Bur. Stand. (U.S.), Fed. Info. Process. Stand. Publ. (FIPS Pub.) 28, 12 pages (1973) SD Catalog No. C13.52:28, 60 cents.

Key words: computers; data elements and representations; data processing systems; Federal Information Processing Standards; management information systems; standards; U.S. Government.

Pursuant to the authority delegated to the Secretary of Commerce by Executive Order 11717 (38 FR 12315, dated May 11, 1973), Subtitle A of Title 15 of the Code of Federal Regulations has been amended to add a new Part 6 which implements the provisions of Section III (f) (2) of the Federal Property and Administrative Services Act of 1949, as amended (79 Stat. 1127). This new Part 6 supersedes and replaces in its entirety the provision of Office of Management and Budget Circular A-86 entitled, "Standardization of data elements and codes in data systems," dated September 30, 1967 which was rescinded by the Director of the Office of Management and Budget on August 29, 1973. Part 6 provides policy and identifies responsibilities of executive branch departments and independent agencies for a government-wide program for the standardization of data elements and representations used in Federal automated data systems. This publication provides a copy of Part 6 and other documents relating to this amendment.

PS59-73. **Prefinished hardboard paneling.** *(ANS A135.5-1973),* K. G. Newell, Jr., Technical Standards Coordinator, Nat. Bur. Stand. (U.S.), Prod. Stand. 59-73, 7 pages (Feb. 1974) SD Catalog No. C13.20/2:59-73, 45 cents.

Key words: hardboard paneling; paneling, hardboard; prefinished hardboard paneling.

This Voluntary Product Standard covers requirements and methods of test for the dimensions, squareness, edge straightness, and moisture content of prefinished hardboard paneling; for the physical properties of the hardboard substrate; and for the finish of the paneling. Methods of identifying products which conform to the requirements of the standard are included.

PS60-73. **Hardboard siding.** *(ANS A135.6-1973),* K. G. Newell, Jr., Technical Standards Coordinator, Nat. Bur. Stand. (U.S.) Prod. Stand. 60-73, 7 pages (Feb. 1974) SD Catalog No. C13.20/2:60-73, 40 cents.

Key words: hardboard siding; siding, hardboard.

This Voluntary Product Standard covers requirements and methods of test for the dimensions, straightness, squareness, physical properties, and surface characteristics of hardboard siding. Definitions of trade terms used and methods of identifying products that comply with the standard are included.

TN594-6. **Optical radiation measurements: The present state of radiometry and photometry,** B. Steiner, Nat. Bur. Stand. (U.S.), Tech. Note 594-6, 56 pages (Mar. 1974) SD Catalog No. C13.46:594-6, 95 cents.

Key words: measurement system; photometry; professional societies; radiometry; standards.

The electro-optics industry and the public that depends on it are part of an informal but influential system for optical radiation measurement. The growth of this industry and of public concerns related technically to it have put severe new strains on this measurement system. The system itself must therefore be analyzed. The state of the art, on which the measurement system depends, is surveyed in terms of basic measurement parameters. The measurement system is analyzed in terms of its three basic components: the flow of physical standards, the generation of procedural standards, and the funding framework. The roles of the professional society and of the Council for Optical Radiation Measurement are reviewed. New requirements of the system are identified. Finally, the methodology of the study is reviewed in detail.

TN594-7. **Optical radiation measurements: Approximate theory of the photometric integrating sphere,** W. B. Fussell, Nat. Bur. Stand. (U.S), Tech. Note 594-7, 39 pages (Mar. 1974) SD Catalog No. C13.46:594-7, 75 cents.

Key words: illuminance distribution; integrating sphere; lamp comparisons; photometric accuracy; photometry; total luminous flux.

An approximate mathematical theory of the photometric integrating sphere is developed. The analysis is accurate to the first order in the ratio of the baffle area to the sphere wall area. The sphere is assumed to be occupied by a circular baffle and a spherical lamp; the centers of the baffle and the lamp lie on a diameter of the sphere. The surfaces of the sphere and the baffle are assumed to reflect in a uniformly diffuse manner. The lamp is assumed to absorb a fraction of the radiation incident upon it, and to transmit (or specularly reflect) the remainder. The luminance distribution at the sphere window is derived for a general source input at any point of the sphere wall. A model lamp illuminance distribution is assumed, and a formula for the fractional error in comparing the total luminous fluxes of two lamps in the integrating sphere, is derived. The physical significance of the formula is described.

TN616. Revised March 1974. **Frequency standards and clocks: A tutorial introduction,** H. Hellwig, Nat. Bur. Stand. (U.S.), Tech. Note 616 (Revised), 72 pages (Mar. 1974) SD Catalog No. C13.46:616 (Rev.), 70 cents.

Key words: cesium beam; clocks (atomic); crystal oscillator; frequency accuracy; frequency stability; frequency standards; hydrogen maser; quartz crystal; rubidium gas cell; timekeeping.

The topic of frequency standards and clocks is treated in a tutorial and nonmathematical way. The concepts of time, frequency stability, and accuracy are introduced. The general physical principles and design features of frequency standards and clocks are described. The design, performance, and limitations of quartz crystal oscillators and atomic devices (cesium, hydrogen, rubidium) are discussed in detail

and critically compared for laboratory devices as well as for devices intended for field usage.

TN647. **Microwave attenuation measurement system (series substitution),** W. Larson and E. Campbell, Nat. Bur. Stand. (U.S.), Tech. Note 647, 28 pages (Feb. 1974) SD Catalog No. C13.46:647, 35 cents.

Key words: attenuation; measurement; rotary-vane attenuator; series substitution.

A dual detection microwave bridge circuit has been incorporated in a series substitution system for the measurement of microwave attenuation devices. The use of an optical rotary-vane attenuator in the system yields practical resolution and stability of 0.00005 dB from zero to 30 dB. The dual detection system has several favorable features: (1) it employs a single microwave source which reduces cost, (2) measurements are obtained without power stabilization of the microwave signal source, and (3) this waveguide configuration enables measurements of attenuation devices at any length with minimum of effort and movement of waveguide components.

The system configuration is convenient for both attenuation difference, and insertion loss measurements from zero to 70 dB over the WR90 waveguide band of 8.2 to 12.4 GHz.

TN649. **The standards of time and frequency in the U.S.A.,** J. A. Barnes and G. M. R. Winkler, Nat. Bur. Stand. (U.S.), Tech. Note 649, 91 pages (Feb. 1974) SD Catalog No. C13.46:649, $1.00.

Key words: astronomical time measurements; clock synchronization; clocks; Coordinated Universal Time (UTC); frequency; frequency standards; International Atomic Time (TAI); International Radio Consultative Committee (CCIR); International Scientific Radio Union (URSI); International Time Bureau (BIH); international time organizations; leap seconds; national time/frequency standards; NBS time and frequency; Precise Time and Time Interval (PTTI); time; time coordination; time interval; time scales; Treaty of the Meter (standards); U.S.A. standard time zones; USNO time and frequency.

This paper describes the national responsibilities for standards of time and frequency in the U.S.A. The National Bureau of Standards (NBS) and the U.S. Naval Observatory (USNO) are the two organizations chiefly involved in distributing accurate and precise time and frequency information within the U.S.A. The NBS is responsible for the "custody, maintenance, and development of the national standards" of frequency and time (interval) as well as their dissemination to the general public. The mission of the USNO includes the "provision of accurate time" for electronic navigation systems, communication, and space technology. This is an integral part of its work concerned with the publication of ephemerides which are used in support of navigation and in the establishment of a fundamental reference system in space.

Both agencies provide the U.S. contribution to the Bureau International de l'Heure (BIH) [International Time Bureau], which has the responsibility of publishing definitive values of Universal Time (UT), International Atomic Time (TAI), and Coordinated Universal Time (UTC).

TN651. **Scattering-matrix description and near-field measurements of electroacoustic transducers,** D. M. Kerns, Nat. Bur. Stand. (U.S.), Tech. Note 651, 40 pages (Mar. 1974) SD Catalog No. C13.46:651, 50 cents.

Key words: electroacoustic transducer measurement techniques; near-field measurement techniques; scattering matrix description of electroacoustic transducers.

Recently developed and successfully applied analytical techniques for the measurement of microwave antennas at reduced distances are "translated" into corresponding techniques for the measurement of electroacoustic transducers in fluids. The basic theory is formulated in scattering-matrix form and emphasizes the use of plane-wave spectra for the representation of sound fields. This theory, in contrast to those based on asymptotic description of transducer characteristics, is suitable for the formulation and solution of problems involving interactions at arbitrary distances. Two new techniques (in particular) are described: One, utilizing deconvolution of planar scanning data, taken with a known transducer at distances d which may be much less than the Rayleigh distance d_R ($\equiv D^2/2\lambda$), provides a means of obtaining complete effective directivity functions, *corrected for the effects of the measuring transducer.* Applicability of a (two-dimensional, spatial) sampling theorem and the "fast Fourier transform" algorithm, which greatly facilitate the necessary computations, is shown. The second technique provides a means of extrapolating received signal as a function of distance (observed with $d \sim d_R$) to obtain on-axis values of effective directivity. Other possible applications are indicated. These techniques rigorously utilize observed output of nonideal (but linear) measuring transducers.

TN803. **A guide to networking terminology,** A. J. Neumann, Nat. Bur. Stand. (U.S.), Tech. Note 803, 29 pages (Mar. 1974) SD Catalog No. C13.46:803, 80 cents.

Key words: computer networks; glossary; telecommunications; teleprocessing; terminology; vocabulary.

A selected set of terms and definitions relating to computer networking is presented in a coherent manner. An introduction gives the rationale for the glossary, defines the scope by a brief tutorial overview, and states the glossary format and conventions. The glossary is arranged alphabetically and contains about 140 definitions and associated terms. The sources of many terms are cited and modifiers indicate the status of definitions. A complete listing of source material is appended.

TN811. **Evaluation of the column connections used in a precast concrete modular housing system,** F. Y. Yokel and T. W. Reichard, Nat. Bur. Stand. (U.S.), Tech. Note 811, 63 pages (Mar. 1974) SD Catalog No. C13.46:811, $1.00.

Key words: building system; column connection; concrete triaxial strength; ductility; neoprene bearing pad; Operation Breakthrough; performance test; precast concrete; structural design.

The column connections used in a housing system employing stacked precast concrete box modules were tested to evaluate their structural performance. The system was proposed for construction in Operation Breakthrough, a research and demonstration program sponsored by the Department of Housing and Urban Development. The system uses innovative structural design concepts, which include: confinement of the concrete in the vicinity of the column bearings by reinforcing ties in order to increase concrete compressive strength; neoprene pads between column bearings in the upper stories; steel-neoprene-steel sandwich in the lower stories; and a grouted dowel through the center of the columns to provide resistance to tension and shear.

The test program included the following: tests to determine the effect of various bearing pads on the load capacity of the connection; tests to determine the load-deformation characteristics of the neoprene pads; a test to determine the performance of a lower-story connection using a steel-neoprene-steel sandwich and a grouted dowel; and tests to evaluate the strength and ductility of the connections when subjected to a shear force. The test results are presented and interpreted and the findings are summarized. Supersedes NBSIR 73-148 (PB 220366/7).

TN812. **Tensile behavior of boron/epoxy-reinforced 7075-T6 aluminum alloy at elevated temperatures,** D. J. Chwirut and G. F. Sushinsky, Nat. Bur. Stand. (U.S.), Tech. Note 812, 31 pages (Mar. 1974) SD Catalog No. C13.46:812, 65 cents.

Key words: aluminum alloy; boron/epoxy; co-cure; composite materials; fabrication process; load-deformation characteristics;

residual stress; rule of mixtures; sandwich specimen; stress-strain curves; tensile properties.

Static tensile tests were performed on specimens of 7075-T6 aluminum alloy, 0° unidirectional boron/epoxy, and 7075-T6 aluminum alloy reinforced on the surface with 0° unidirectional boron/epoxy laminate, at four temperatures up to 300 °F (149 °C). Analytical load-strain curves are formulated for the reinforced-metal specimens using the rule of mixtures, assuming that the longitudinal strains in the composite and the metal remain equal, and taking account of the residual stresses caused by the fabrication process. Two analytical curves are plotted for each reinforced-metal specimen, one based on the measured ply thickness of the composite, and one based on a nominal 0.005-in (0.13-mm) ply thickness. In general, the experimental load-strain curves fall between the two analytical curves for each specimen.

TN817. **Kitchen ranges in fabric fires,** A. K. Vickers, Nat. Bur. Stand. (U.S.), Tech. Note 817, 23 pages (Apr. 1974) SD Catalog No. C13.46:817, 60 cents.

Key words: accidents; burns; FFACTS; flammable fabrics; garments; ignition sources; injuries; kitchen ranges.

Kitchen ranges played a major role in the 1616 fabric accident case histories recorded in the Flammable Fabrics Accident Case and Testing System as of May 1972. They accounted for 214 or 35 percent of the direct garment ignitions in FFACTS. Female victims outnumberd males by 3 to 1; females under 16 and over 65 were particularly heavily represented. Reaching over and leaning against the range caused the majority of the garment ignitions. Shirts, robes, pajamas, nightgowns and dresses were the most frequently ignited garments. Thirty-four victims died from injuries resulting from garment ignitions from ranges; 24 of these fatalities were people over 65 years old.

TN819. **A technical index of interactive information systems,** D. W. Fife, K. Rankin, E. Fong, J. C. Walker, and B. A. Marron, Nat. Bur. Stand. (U.S.), Tech. Note 819, 73 pages (Mar. 1974) SD Catalog No. C13.46:819, $1.20.

Key words: bibliographic systems; computer programs; computer systems; data base; data management; information retrieval; information services; interactive system; query language; software selection; text processing.

This report constitutes a reference to technical features and operational status of interactive information systems, i.e. those providing a "conversational" usage mode to a "non-programmer" through a data terminal device. It is aimed at the ADP service manager, for his use in the state-of-the-art assessments preparatory to a detailed system selection process. It contains an index that describes 46 systems in terms of a list of over 50 technical features plus descriptive, identification, and background information. In addition, there are aids and examples contributing to the intended use of the index.

TN820. **Complete clear text representation of scientific documents in machine-readable form,** B. C. Duncan and D. Garvin, Nat. Bur. Stand. (U.S.), Tech. Note 820, 55 pages (Feb. 1974) SD Catalog No. C13.46:820, 90 cents.

Key words: graphic character sets; information analysis centers; information interchange codes; recording typewriters; scientific computer technology.

Science and technology use a large variety of symbols to represent physical properties, chemical formulas and mathematical expressions.

Data centers that codify and evaluate physical properties need to use this conventional symbolism in their work. It is recommended that these data centers adopt the symbols and terminology specified by the various International Unions both in manual operations and in the creation of machine-readable data bases.

It is demonstrated that these conventional symbols can be produced by modern communications devices that are compatible with the international standard codes for information interchange. A set of characters suitable for representing scientific data and text is presented and proposed as an extension of the ISO information interchange code.

The use of this extended character code by computer oriented data centers at the National Bureau of Standards is described. The equipment needed for this level of performance and criteria for their selection are outlined.

TN821. **Photometric data variability of automotive lighting components,** B. G. Simson and J. Mandel, Nat. Bur. Stand. (U.S.), Tech. Note 821, 15 pages (Mar. 1974) SD Catalog No. C13.46:821, 60 cents.

Key words: Federal Motor Vehicles Safety Standards; interlaboratory test evaluation; motor vehicles; photometric testing; safety standards.

Four automotive lighting components were tested in three commercial testing laboratories to estimate the degree of photometric data repeatability and reproducibility. The laboratories used the photometric testing techniques required by Federal Motor Vehicle Safety Standard No. 108. The precision of this test method was placed in a range of about 10 percent coefficient of variation. However, this value should be considered more as an indication of existing conditions than as a predictive parameter.

TN822. **A review of Federal and military specifications for floor coverings,** W. C. Wolfe, Nat. Bur. Stand. (U.S.), Tech. Note 822, 99 pages (Apr. 1974) SD Catalog No. C13.46:822, $1.50.

Key words: carpets; floor coverings; government; performance; procurement; specifications; standards; tests; user needs.

In this manual, which is organized so as to aid ready reference, requirements and test methods in Federal and military specifications for flooring, or floor coverings are combined, indexed and reviewed. The manual covers carpet, resilient flooring, monolithic surfacings or seamless flooring, and polyurethane coatings related to seamless flooring. It also covers all serviceability requirements except those relating to flammability, fire safety and acoustical properties.

Physical and material requirements in Federal specifications for floor coverings are considered in separate sections. Military specifications for monolithic surfacings and Federal specifications for floor coverings and polyurethane coatings are summarized in comprehensive tables. Under each physical requirement, comments indicate whether it is a quality control or a performance requirement. Each comment is followed by a list of those Federal specifications which include the requirement and a brief description of the criteria and test methods in the specifications. Comments on materials requirements relate to their adequacy and applicability to the product for which they were written. Finally, recommendations are made for improvements in performance requirements which should be considered for inclusion in future flooring and floor covering specifications.

TN823. **Cryogenic Physics Section, summary of activities 1973,** R. J. Soulen, Jr., Ed., Nat. Bur. Stand. (U.S.), Tech. Note 823, 23 pages (Mar. 1974) SD Catalog No. C13.46:823, 60 cents.

Key words: Josephson junctions; noise thermometer; nuclear orientation; paramagnetism; superconductivity; temperature.

This report summarizes the research activities of the Cryogenic Physics Section which specifically relate to thermometry. The topics range from superconductive fixed points to nuclear orientation thermometry, as well as Josephson junction noise thermometry and paramagnetism.

TN824. **A laboratory study of some performance characteristics of an aluminum oxide humidity sensor,** S. Hasegawa, L. Greenspan, J. W. Little, and A. Wexler, Nat. Bur. Stand. (U.S.), Tech. Note 824, 28 pages (Mar. 1974) SD Catalog No. C13.46:824, 65 cents.

Key words: aluminum oxide sensor; humidity; humidity sensor; hygrometer; measurement of frost points; moisture measurement; water vapor measurement.

A laboratory study was made of the performance of aluminum oxide humidity sensors over a range of ambient temperatures from + 20 °C to − 60 °C encompassing dew points from + 18 °C to frost points of − 100 °C. Information was obtained on such characteristics as sensitivity, hysteresis, temperature effect, pressure-altitude effect and short-term and long-term repeatability. The sensors were found to be capable of detecting frost points as low as − 100 °C at ambient temperatures of − 40 °C and − 60 °C. It is estimated that the total uncertainty inherent in these sensors is approximately 4 °C.

TN826. **Cost-benefit analysis of computer graphics systems,** I. W. Cotton, Nat. Bur. Stand. (U.S.), Tech. Note 826, 47 pages (Apr. 1974) SD Catalog No. C13.46:826, 90 cents.

Key words: computer graphics; cost-benefit analysis; cost-effectiveness; economics; performance evaluation.

This report assesses the state-of-the-art in cost benefit analyses of computer graphics systems and suggests an approach for developing improved methodology. Cost-benefit analyses are distinguished from analyses of system performance in that the latter are directed at optimizing system performance at a given level of investment, while the former are directed at justifying the investment itself.

Computer graphic system design alternatives are first outlined. Then methods of analyzing the performance and costs of computer systems in general and graphic systems in particular are discussed. With this information it is shown how cost-effectiveness analyses may be performed. The next crucial step is to conduct benefit analysis, an ill-defined art. The results of benefit analysis must be combined with cost-effectiveness analysis in order to perform the desired cost-benefit analysis.

An experimental methodology is suggested for better performing benefit analyses of computer graphic systems. A more rigorous formulation of the cost-benefit procedure is then outlined. No attempt is made in this report to actually perform such an analysis.

NBSIR 73-152. **Measurement of transit time and related transistor characteristics,** D. E. Sawyer, G. J. Rogers, and L. E. Huntley, 131 pages (Oct. 1973). Order from NTIS as AD 914258.

Key words: delay time; electronics; high-frequency probes; Sandia bridge; scattering; S-parameters; transistors; vector voltmeter.

Two instruments for transistor delay-time measurements, the vector voltmeter and Sandia bridge, were analyzed and comparative measurements were made on several types of commercial and two special transistors. It was found that extraneous pickup at the measurement frequency can cause large errors in measured delay time. A technique for minimizing these errors was developed and verified for the Sandia bridge by removing the frequency dependence of delay force, probe tip protrusion and lateral motion (skating) with loading were recorded for special probe assemblies to be used in an automatic wafer prober for measurements on transistors in custom-designed integrated circuit wafers. The data is used to assist in adjusting the probers. A technique was developed for determining the effects of the probe assemblies on transistor measurements made from 0.1 to 2.0 GHz. Each probe assembly may be represented by an equivalent circuit consisting of three unknowns; these unknowns are determined by making impedance measurements at the input connectors with the probe tips contacted by combinations of open circuits, short circuits, and resistors of known value. Arrays of such terminations were successfully fabricated and characterized. An S-parameter interlaboratory testing program was developed. The plan calls for six of each of three types of transistors to be measured by participants at frequencies from 0.11 to 2.0 GHz. Additionally, a 10-dB attenuator and R-C networks on TO-72 headers are to be circulated to pinpoint measurement discrepancies.

NBSIR 73-180. **Testing of the NBS clinical microcalorimeter,** E. J. Prosen and R. N. Goldberg, 31 pages (Apr. 1973). Order from NTIS as COM 74-10139.

Key words: clinical chemistry; clinical microcalorimetry; microcalorimeter; NBS microcalorimetry; testing of microcalorimeter.

The NBS Clinical Microcalorimeter has been tested for stability, sensitivity, ease of operation, and accuracy. The accuracy was tested by means of electrical calibration and the determination of the heat of neutralization of HCl(aq) with NaOH(aq). The heat of this reaction agrees with the best literature value within the precision of the calorimeter. The precision is about 0.6 percent when measuring about 50 mJ of heat of chemical reaction. The accuracy is estimated as 1 percent. The precision of electrical energy determination is about 0.4 percent for energies of from 1 to 1400 mJ.

NBSIR 73-199. **Experimental and analytical studies of floor covering flammability with a model corridor,** W. Denyes and J. Quintiere, 115 pages (May 1973). Order from NTIS as COM 74-10129.

Key words: flame spread; floor covering materials; model corridor; scaling laws; test method.

An experimental model corridor facility was designed, constructed, and instrumented. The facility examines flame spread over floor covering materials in a small scale corridor under a forced air flow condition. A gas burner flame serves as the ignition source.

A study was made of the factors influencing flame spread in the model corridor. These factors included energy release rate of the ignition source, air velocity, and model corridor geometry. Twenty-six carpet materials and 5 other floor covering materials were studied in the model corridor, and 369 flame spread runs were conducted.

It was found that flame spread behavior in the model corridor generally involves either a rapidly accelerating flame front which propagates the full 8 foot length of the test section ("flameover"), or involves a decelerating flame front which results in extinction a short distance from the ignition source. Radiant heating of the floor material due to hot products of combustion heating the ceiling is a significant factor in causing flameover. Carpet assembly was found to affect flame spread more significantly than pile fiber type.

The data have been analyzed to determine quantitatively the effects of the factors influencing flame spread. Scaling relationships have been presented to attempt to extrapolate the model corridor results to full scale corridor fires.

Finally a procedure has been suggested for using the facility in a floor covering flammability test method. The procedure is based on determining the minimum energy input rate to cause flameover.

NBSIR 73-200. **A model corridor for the study of the flammability of floor coverings,** W. Denyes and J. W. Raines, 40 pages (May 1973). Order from NTIS as COM 74-10478.

Key words: air flow, energy input; flameover; flame spread; floor covering flammability; model corridor; test repeatability.

A program was carried out to develop a laboratory test method that would measure the flame propagation characteristics of floor covering materials. A facility was designed which included a floor mounted specimen in a rectangular cross-sectional duct having a forced supply of air and a gas burner ignition source. The effects of variations in duct size, ignition source, and air flow were studied. Factors influencing repeatable test results were explored. Flame spread was measured by an observer and temperature and heat flux measurements were recorded on an electronic digital data acquisition system.

NBSIR 73-234. **Drapery and curtain fires—data element summary of case histories,** A. K. Vickers, 28 pages (July 1973). Order from NTIS as COM 74-10128.

Key words: burns; case histories; curtains; death; draperies; FFACTS; fires; flammable fabrics; houses; standards; statistical data.

A preliminary examination of 1,567 computerized case histories from the NBS Flammable Fabric Accident Case and Testing System has found 77 incidents in which curtains and draperies were involved in fires. This report is a summary of information relating to these 77 incidents, and includes the location of incidents, ignition sources, personal injury, fabrics involved and personal characteristics of victims. Fifteen people died from these fires and 32 others were injured. Curtains or draperies were the first fabric item to ignite in 28 of 55 curtain and drapery incidents in which the ignition source is known.

NBSIR 73-280. **Thermodynamics of chemical species important to rocket technology,** T. B. Douglas and C. W. Beckett, 109 pages (Jan. 1, 1973). Order from NTIS as COM 74-10549.

Key words: associated vapors; graphite; heat capacity; molybdenum; molybdenum pentafluoride; niobium; radiance temperature; spectral emittance; surface roughness; thermodynamic properties.

The enthalpy of high-purity molybdenum was accurately measured 273-1173 K, and joined smoothly to lower-temperature (German) and higher-temperature (NBS) results to give thermodynamic functions 273-2100 K. The heat capacity of a grade of Poco graphite was measured by a subsecond-duration pulse-heating technique 1500-3000 K (estimated inaccuracy, 3% or less). Based largely on earlier NBS IR and Raman spectroscopy, ideal-gas thermodynamic functions for MoF_5 were generated and are tabulated for 0-6000 K. Three alternative classical-thermodynamic or quasi-chemical treatments are developed for deriving thermodynamic properties from vaporization data on partially associated vapors, with calculations to illustrate experimental-error propagation for one treatment. A subsecond-duration pulse-heating technique was applied to niobium metal to measure its change in normal spectral emittance and radiance temperature at and near its melting point (wavelength, 650 nm), studying dependence on solid-state roughness (0.1 to 0.95 μm).

NBSIR 73-281. **Thermodynamics of chemical species important to rocket technology,** T. B. Douglas and C. W. Beckett, 122 pages (July 1, 1973). Order from NTIS as COM 74-10550.

Key words: electrical resistivity; iron; molybdenum pentafluoride; partly associated vapors; solid-state transformations; solution calorimetry; specific heat; spectral emittance; transition alloys; vapor pressure.

Using a subsecond-duration transient technique, the specific heat, electrical resistivity, and hemispherical total emittance were simultaneously measured 1500-2800 K for iron and the alloy 80Nb-10Ta-10W (estimated uncertainties: 3%, 0.5-1%, and 3% for the respective properties). Comparisons are made with generalized approximations. At the gamma-to-delta transformation of iron (about 1680 K), the temperature, heat of transformation, specific heat, spectral emittance, and electrical resistivity were measured, thereby demonstrating the feasibility of the technique for solid-solid transformations. Two other alloys were likewise measured. Solution calorimetry involving several thermochemical steps (including oxidation by XeO_3 in aqueous HF) gave the standard heat of formation of MoF_5(c). A new static vapor-pressure method, after verification to 1 percent by I_2 and MoF_6, and after modifications to deal with the necessarily added MoF_6, gave the vapor pressure of MoF_5 at 393 K and indicated (using also earlier NBS transpiration data) 85-90 mole percent of monomer in the saturated vapor.

NBSIR 73-294. **Cost sharing as an incentive to attain the objectives of shoreline protection,** H. E. Marshall, 70 pages (Dec. 1973). Order from NTIS as COM 74-10541.

Key words: beach erosion control; cost sharing; economics; efficiency; equity; incentives; shoreline protection.

The nation's shorelines are being eroded by high winds and waves. Nonfederal interests have traditionally received Federal help in the form of cost sharing for protective structures. This study provides the Army Corps of Engineers with an evaluation of alternative cost-sharing rules for shoreline protection with respect to efficiency, equity, and administrative feasibility.

Existing cost-sharing rules are described for hurricane, beach erosion, and emergency protection. The present cost-sharing system appears to induce local interests to choose (1) costly techniques of protection, e.g., engineering rather than management techniques, and (2) overbuilt projects in terms of the efficient scale.

It is concluded that the Association Rule, which requires local beneficiaries of shoreline protection to share in all of the costs of a project purpose in the proportion that local benefits bear to national benefits at the margin, should be applied to all shoreline protection programs. All techniques of protection should be subject to the same percentage cost-sharing rule. It is also concluded that *all* categories of project costs should have the same percentage cost share apply to them. Finally, Federal cost sharing might be used as an incentive to encourage local interests to comply with minimum land use requirements that would prevent shoreline damages.

NBSIR 73-297. **Fracture and deformation of alumina,** S. M. Wiederhorn, 14 pages (July 31, 1973). Order from NTIS as AD 772066.

Key words: electron microscopy; fracture; mechanical properties; plastic deformation; sapphire; sodium chloride.

This report summarizes work conducted during the past eight years on the fracture and deformation of ceramic materials. Accomplishments discussed in this report include: an elucidation of fracture process of aluminum oxide and sodium chloride; the development of techniques to study the deformation of aluminum oxide during abrasion; and the development of techniques for measuring fracture mechanics parameters on ceramic materials.

NBSIR 73-351. **Thermal conductivity standard reference materials from 6 to 280 K: VI. NBS sintered tungsten,** J. G. Hust, 58 pages (Jan. 1974). Order from NTIS as AD 775367.

Key words: cryogenics; electrical resistivity; Lorenz ratio; Seebeck effect; standard reference material; thermal conductivity; transport properties; tungsten.

Thermal conductivity, electrical resistivity, Lorenz ratio, and thermopower data are reported for two specimens of NBS sintered tungsten for temperatures from 6 to 280 K. Variability of this tungsten was studied by means of electrical resistivity and residual resistivity measurements on 39 specimens. These data indicate a material variability of about ± 10 percent in thermal conductivity at helium temperatures. Above 90 K variation in thermal conductivity is only about ± 1 percent. To reduce the uncertainty caused by specimen variation at low temperatures, characterization by residual electrical resistivity data is described. By this procedure the low temperature uncertainty is reduced to about ± 3 percent.

NBSIR 73-405. **Use of organic coatings on the interior surfaces of equestrian statues at Memorial Bridge Plaza,** F. Ogburn, 9 pages (Nov. 1973). Order from NTIS as COM 74-10131.

Key words: bronze statuary; organic coatings; restoration; statues.

The equestrian statues at Memorial Bridge Plaza in the District of Columbia are bronze castings. The exterior finish is subject to corrosion processes associated with pores and cracks in the castings. The interior surfaces are subjected to high humidity and condensation. Detrimental corrosion is expected only at discontinuities in the plated coatings on the exterior surfaces. Painting of interior surfaces has been recommended, but the need for painting is not clear. The NCP is advised to keep the statues under close observation till the fall of 1974 and then reconsider their course of action.

NBSIR 73-412. **The incidence of hazardous material accidents during transportation and storage,** W. A. Steele, D. Bowser,

and R. E. Chapman, 40 pages (Nov. 1973). Order from NTIS as COM 74-10512.

Key words: accidents; hazardous material; storage of hazardous material; transportation of hazardous material.

This report is one of a series describing background research concerning the incidence of abnormal loading. The report is organized in terms of modes of hazardous material transportation and storage. These modes—pipeline, water, motor vehicle, and railroad transportation systems—are addressed in four sections with Storage Systems discussed in a fifth. The sections depend on the amount of available data, rather than the risk involved in an accident. A summary of the results is presented in the last section. On the whole, there is little empirical evidence to substantiate a threat to buildings from hazardous materials transport. However, trends in volumes shipped in proximity to structures of interest raises the prospect of future incidents.

NBSIR 73-414. **Building and evaluation of a polluted air delivery system,** G. P. Baumgarten and F. W. Ruegg, 36 pages (Apr. 1974). Order from NTIS as COM 74-10866.

Key words: air pollution; critical flow; laminar flow; nozzle; porous plug; sulfur dioxide concentration.

The building and evaluation of a prototype SO_2 polluted air delivery system (PADS) is discussed. The delivery system was built to deliver sulfur dioxide (SO_2) in air at a rate of 5 liters per minute with design concentrations by volume of 1.0, 0.1 and 0.01 parts per million. It consists of a diluent air delivery system utilizing a critical flow sonic nozzle and three separate concentrated SO_2 in air flow systems utilizing laminar flow porous plugs, one plug for each desired output concentration. The delivery system is contained in a dispatch case and the two gases are delivered to it from pressurized containers through detachable supply lines. Prospective use by unskilled technicians dictated simplicity and durability and compactness.

By maintaining specific upstream pressures on the critical flow nozzle and the laminar flow porous plugs of 45 and 12 psig respectively, the prototype PADS produced average output concentrations of 0.76, 0.100 and 0.003 parts per million of SO_2 in air based on concentration measurements with an NBS calibrated analyzer. The expected output concentrations were 0.98, 0.105 and 0.010 respectively, based on flow calibrations of the individual components. The uncertainty of the output concentration is estimated to be about ± 10 percent.

NBSIR 73-416. **Report on meeting of ISO/TC 6/SC 5 testing methods and quality specifications for pulp,** W. K. Wilson, J. H. Schulz, C. E. Brandon, and J. L. Borstelmann, 69 pages (Nov. 16, 1973). Order from NTIS as COM 74-10511.

Key words: ISO recommendations; pulp; pulp, testing methods; testing methods for pulp.

The ninth meeting of ISO/TC 6, Paper, SC 5, Testing Methods for Pulp, was held in Madrid, Spain, November 2-8, 1973. Over 30 delegates from 11 countries discussed methods for testing of pulp and, to some extent, paper. Methods were agreed upon for the determination of saleable mass of flash dried pulp, disintegration of pulp, laboratory beating of pulp, preparation of laboratory sheets, and measurement of ISO brightness of pulp. It was agreed that ISO Recommendations for determination of saleable mass of pulp in lots, determination of dry matter content, and determination of trace metals in pulp should be revised. Plans were made to continue studies of methods for the determination of viscosity, aqueous extraction, dirt and shives, total sulphur content, saleable mass of unitized lots of pulp, statistical evaluation of number of sample bales, preparation of laboratory sheets, and fiber classification and drainability.

NBSIR 73-424. **A study of young children's pull-apart strength (an addendum to NBSIR 73-156—a study of the strength capabilities of children ages two through six),** W. C. Brown, C. J. Buchanan, and J. Mandel, 17 pages (Apr. 1974). Order from NTIS as COM 74-10867.

Key words: children; children's strength; pull-apart; safety; strength; test methods; toys; toy safety.

The Child Pull-Apart Strength Study was conducted to provide information which can be used to develop reliable and realistic standards and test methods for children's toys. The study was conducted with over 500 children in the Washington Metropolitan area, and included both black and white children from varying economic and social backgrounds.

The pull-apart test device used is a prototype model designed and constructed at the National Bureau of Standards. This test device was designed to measure the force that children can exert when pulling an object apart.

The results of the pull-apart strength study are consistent with those obtained in the previous child strength study which dealt with twisting, pulling, pushing, and squeezing (NBSIR 73-156). The study provided quantitatively precise and useful information about the effects of age and sex on the pull-apart strength capability of children ages two through six. The results are exhibited in tables of averages, standard deviations, coefficients of variation, and 95th and 5th percentiles.

NBSIR 74-430. **Chemical kinetics data survey VII. Tables of rate and photochemical data for modelling of the stratosphere (revised),** D. Garvin and R. F. Hampson, 104 pages (Jan. 1974). Supersedes NBSIR 73-203. Order from NTIS as COM 74-10724.

Key words: atmospheric chemistry; chemical kinetics; data evaluation; energy transfer; gas phase; high temperature air chemistry; ion-molecule reactions; optical absorption cross sections; photochemistry; quantum yield; rate constants.

Chemical kinetic and photochemical data for gas phase reactions pertinent to the chemistry of the stratosphere are presented in four tables. These tables give recommended values and also cite recent experimental work. They give data in the following subject areas: chemical reactions and photochemistry of neutral species, energy transfer reactions, high temperature air reactions, and ion-molecule reactions.

NBSIR 74-432. **1972 international activities center for building technology,** C. C. Raley, 68 pages (Aug. 1973). Order from NTIS as COM 74-10751.

Key words: cooperative programs; foreign visitors; information exchange; international building technology; international organization memberships; professional interaction.

This report summarizes the Center for Building Technology's 1972 international activities including formal cooperative programs, exchange programs, special projects, international organization memberships, foreign guests at CBT, and CBT foreign travel.

NBSIR 74-444. **A review of natural stone preservation,** G. A. Sleater, 40 pages (Dec. 1973). Order from NTIS as COM 74-10548.

Key words: air pollution; historic structures; laboratory evaluation; natural weathering; stone decay; stone preservation.

With increased interest in stone preservation, it is desirable to know what causes stone to decay, and what materials can be used to preserve stone. This review covers the following topics: causes of stone decay, including faults in the stone, salts, natural weathering factors, air pollution, living organisms, and most importantly, water action; various materials that have been used to preserve stone, including paints, waxes, oils, inorganic chemical surface treatments and impregnants, silicones, siliconates, and synthetic organic polymers; methods of evaluating stone preservatives. Field and laboratory procedures for testing stone preservatives, the cleaning of stone, a glossary, and a bibliography are given in appendices.

NBSIR 74-455. **Abstracts of papers on testing and analysis of flammable fabrics October 1972 to October 1973,** J. F. Krasny, 27 pages (Mar. 1974). Order from NTIS as COM 74-10865.

Key words: burn injuries; carpets; clothing; fabrics; fire retardants; flammability testing.

This collection of abstracts covers papers on textile flammability testing and analysis of flame retardant fibers and finishes, for the period October 1972 to October 1973. It is hoped that this collection will facilitate research in this area in which there has been great interest in connection with the introduction of fabric and garment flammability standards by the Federal and several state governments. Similar collections appear in the Proceedings of the Annual Meetings of the Information Council on Fabric Flammability, available from the Council, Room 510, 1457 Broadway, New York, N.Y. 10036.

NBSIR 74-464. **The Shirley Highway Express-Bus-On-Freeway Demonstration Project—second year results,** J. T. McQueen, R. F. Yates, and G. K. Miller, 87 pages (Nov. 1973). Order from NTIS as COM 74-10785.

Key words: bus transit; busway operations; commuter travel behavior; express bus-on-freeway operations; project evaluation; transit operations.

This report contains: (a) A review of the performance of the Shirley Highway Express-Bus-On-Freeway Demonstration Project between 1969 and 1973; (b) A description of the methodology and data use to estimate project measures of effectiveness; (c) A discussion of factors considered in commuter mode choice decision making.

This column lists all outside publications by the NBS staff, as soon after issurance as practical. For completeness, earlier references not previously reported may be included from time to time.

Allan, D. W., Glaze, D. J., Machlan, H. E., Wainwright, A. E., Hellwig, H., Barnes, J. A., Gray, J. E., **Performance, modeling, and simulation of some cesium beam clocks,** *Proc. 27th Annual Symp. on Frequency Control, Philadelphia, Pa., June 12-14, 1973,* pp. 334-346 (Electronic Industries Association, Washington, D.C. 1973).

Key words: atomic clock; atomic clock modeling; atomic clock noise; atomic clock performance; atomic time scale accuracy; comparison of atomic time scales; comparison of frequency standards; frequency calibration; frequency drift; simulation of clock performance.

With the availability of a new primary frequency standard, NBS-5 at the National Bureau of Standards, we have been able to evaluate with greater confidence than in the past the performance characteristics of the commercial cesium beam clocks used in the AT(NBS) atomic time scale. Two other techniques have also been employed to evaluate a clock's performance, viz., interclock comparisons and comparisons with other national laboratories.

Utilizing the above performance data we have constructed models for the behavior of cesium beam atomic clocks. Based on these models and appropriate optimization procedures, algorithms have been developed to generate an atomic time scale, AT(NBS), from the ensemble of standards available to us. The model is shown to well fit both individual clocks as well as clock ensembles. This modeling provides a direct opportunity for clock data simulation. Simulation techniques are developed and applied in the testing of some diagnostic tests for frequency and/or time steps. The results are very encouraging as a new effort for even better clock modeling.

Rate calibrations of AT(NBS), UTC(NBS), TAI, and other national time scales are given with reference to NBS-5, and these are compared with other past primary cesium beam frequency standards. TAI was measured as too high in rate by 12 ± 5 parts in 10^{13}.

Allan, D. W., Gray, J. E., Machlan, H. E., **The National Bureau of Standards atomic time scales: Generation, dissemination, stability, and accuracy,** *IEEE Trans. Instrum. Meas.* **IM-21,** No. 4, 388-391 (Nov. 1972).

Key words: AT(NBS); clock dispersion; clock ensemble; frequency and time standards; International Atomic Time; Loran-C; model of clock stability; optimum time prediction; precision and accuracy of timing; time coordination, synchronization, and dissemination; UTC(NBS).

The independent atomic time scale at the National Bureau of Standards AT(NBS), is based upon an ensemble of continuously operating cesium clocks calibrated occasionally by an NBS primary frequency standard. The data of frequency calibrations and interclock comparisons are statistically processed to provide nearly optimum time stability and frequency accuracy. The long-term random fluctuation of AT(NBS) due to nondeterministic perturbations is estimated to be a few parts in 10^{14}, and the present accuracy is inferred to be 1 part in 10^{12}.

A small coordinate rate is added to the rate of AT(NBS) to generate UTC(NBS): this small addition is for the purpose of maintaining synchronization within a few microseconds of other international timing centers. UTC(NBS) is readily operationally available over a large part of the world via WWV, WWVH, WWVB, and telephone; also via some passive time transfer systems, e.g., Loran-C and the TV line-10 system; and also experimentally via satellite and WWVL. The precision and accuracy of these dissemination systems will be discussed.

Allan, D. W., **Statistical modeling and filtering for optimum atomic time scale generation,** (Proc. Frequency Standards and Metrology Seminar, Quebec, Canada, Aug. 30-Sept. 1, 1971), Paper in *Proceedings of the Frequency Standards and Metrology Seminar,* pp. 388-410 (Quantum Electronics Laboratory, Laval University, Quebec, Canada, 1972).

Key words: clock stability model; frequency calibration; frequency stability; international time scale; time scale accuracy; time scale stability.

Statistical models for the fractional frequency fluctuations in atomic clocks, clock ensembles, and some of the propagation media are developed. Using these models, near optimum time prediction algorithms are employed to generate time for a clock ensemble or for a set of laboratories' time scales. An example using data from the BIH Circular D bulletin is illustrated and the results compared with IAT.

Accuracy and uniformity problems are considered in light of the CCDS June 1970 recommendations. A model for an evaluable primary frequency standard is developed as well as for a time scale (flywheel frequency standard). It is shown that under certain conditions the accuracy of a time scale can be better than the accuracy of the primary standard for the current calibration, if there is a sufficient number of independent past calibrations. A method of simultaneously achieving accuracy and uniformity is discussed.

Aminadav, N., Selig, H., Abramowitz, S., **Raman spectrum of F_3NO gas,** *J. Chem. Phys.* **60,** No. 1, 325-326 (Jan. 1, 1974).

Key words: gas; ONF_3; Raman spectroscopy; thermodynamic properties; vibrational analysis.

The Raman spectrum of gaseous F_3NO has been observed allowing a definite vibrational assignment. The thermal functions have been computed using this assignment and previous microwave and electron diffraction data.

Andrews, J. R., **Inexpensive laser diode pulse generator for optical waveguide studies,** *Rev. Sci. Instrum.* **45,** No. 1, 22-24 (Jan. 1974).

Key words: fiber optics; GaAs; impulse; laser; optics; picosecond; pulse; waveguide.

538-709 OL - 74 - 7

An inexpensive GaAs laser diode pulse generator is presented. This generator has found application in the evaluation of optical pulse dispersion in glass fiber optical waveguide studies. It is capable of producing optical impulses as narrow as 110 psec at a wavelength of 0.9 μ and a pulse repetition rate of 50 kHz. With a slight modification, it may be used to produce optical pulses of considerably longer duration at reduced repetition rates.

Armstrong, G. T., **Recent developments in calorimetry and thermochemistry at the National Bureau of Standards,** (Proc. Plenary Lectures of 8th Symp. on Calorimetry and Thermal Analysis, Okayama, Japan, Nov. 1972), Paper in *Calorimetry, Thermometry and Thermal Analysis* **6,** 51-60 (Kagaku Gijitsu-Sha, Tokyo, Japan, 1973).

Key words: calorimetry; microcalorimetry of biological processes; standard reference materials for calorimetry; thermochemistry; thermodynamic data.

The thermochemistry work at the National Bureau of Standards provides standard reference data for the National Measurement System both in the form of critical compilations of work done elsewhere and also in the form of new measurements of key substances. A new electrolyte thermodynamic data center has been formed. On-going compilations of the properties of inorganic compounds are being systematized in the form of a catalog of thermochemical quantities. New measurements on organic halogen, nitrogen, and sulfur compounds are extending the range of certified standard reference materials for calorimetry.

A new program on the microcalorimetry of biological processes has shown the applicability of calorimetry to practically important problems of clinical chemistry, and has resulted in improvements in the accuracy of microcalorimetric measurements.

Arp, V. D., Clark, A. F., Flynn, T. M., **Superconducting levitation of high speed vehicles,** *Transp. Eng. J.* **99,** No. TE4, 873-885 (Nov. 1973).

Key words: fatigue life; magnetic properties; materials; refrigeration; superconducting magnets; suspension; transportation; urban transportation.

The current status (December 1972) of worldwide research on high speed ground transportation techniques is reviewed. Particular attention is given to studies of magnetic levitation using superconducting magnets, including comparison with alternative magnetic techniques and with air suspension systems. Superconducting levitation appears to be a strong contender in the U.S. Department of Transportation hopes to select in the late 1970's the best of the possible levitation techniques for subsequent advanced development. Cryogenic engineering research needed in support of major development of a superconducting levitated system is identified.

Barnes, I. L., Garner, E. L., Gramlich, J. W., Machlan, L. A., Moody, J. R., Moore, L. J., Murphy, T. J., Shields, W. R., **Isotopic abundance ratios and concentrations of selected elements in some Apollo 15 and Apollo 16 samples,** (Proc. 4th Lunar Science Conf., March 5-8, 1973, Houston, Tex.), *Geochimica et Cosmochimica Acta, Suppl. 4,* **2,** 1197-1207 (1973).

Key words: chromium; isotopic ratios; lead; model ages; nickel; potassium; rubidium; strontium; thorium; uranium.

The elements Pb, U, Th, Rb, Sr, K, Cr, and Ni have been determined on a series of Apollo 15 and 16 rocks and soils. The elements U, Rb, Cr, and Ni show isotopic abundances identical with those of terrestrial materials in both types of samples but the $^{39}K/^{41}K$ ratio is fractionated by about 1 percent in the soils and the extreme reversed discordancy of the Pb-U-Th ages in the Apollo 16 soils indicated that lead has also been fractionated in these.

The breccia 60335,36 has concordant Pb-U-Th model ages of 4075 MY and the basalt 15495,59 shows one slightly discordant age of around 4480 MY. The Rb-Sr model ages are in good agreement with the Pb-U-Th model ages.

Beehler, R. E., **Recent progress on atomic frequency standards,** (Proc. 1972 Precision Electromagnetic Measurement Conf., Boulder, Colo., June 26-29, 1972), Paper in *CPEM Digest,* pp. 166-167 (IEEE, Inc., New York, N.Y., June 1972).

Key words: atomic frequency standards; cesium beam standards; hydrogen masers; rubidium standards.

A brief summary is presented of a paper reviewing progress achieved in the development of atomic frequency standards during recent years. Particular emphasis is placed on cesium, rubidium, and hydrogen maser standards.

Bennett, H. S., **Two-electron *U* centers in ionic crystals: Point-ion models,** *Phys. Rev. B* **6,** No. 10, 3936-3940 (Nov. 15, 1972).

Key words: BaF_2; CaF_2; CdF_2; ionic polarization; KCl; Mollwo-Ivey relations; NaCl; point-ion potential; SrF_2; *U* centers

The Hartree-Fock-Slater (HFS) equations for the two-electron orbitals about a proton located substitutionally at an anion site have been solved numerically in the point-ion lattice potential. The lattice relaxation of the nearest-neighbor ions is included in the model. The five lowest-lying *U*-center states for NaCl, KCl, CdF_2, CaF_2, SrF_2, and BaF_2 have been calculated within the framework of the above model. It is found that the low-lying singlet states have the following order for increasing values of the energy: $^1S(1s, 1s)$, $^1P(1s, 2p)$, and $^1S(1s, 2s)$. The energy levels for the triplet states $^3S(1s, 2s)$ and $^3P(1s, 2p)$ lie between the energy levels for the $^1S(1s, 1s)$ and $^1P(1s, 2p)$ states. The ordering of the triplet states depends upon the host crystal and the lattice relaxation. In some cases, these triplet states may be degenerate or very nearly so. In addition, the extent to which the peak energies of the *U* bands obey Mollwo-Ivey relations is given for the alkali halides and for the alkaline-earth fluorides. The predictions based upon the numerical HFS wave functions are compared with the predictions based upon past variational wave functions and with experiment.

Berger, H. W., **Polarography. Constant-current coulometry. Differential thermal analysis,** Parts 10.7, 10.8 and 10.9 in *Paint Testing Manual,* Gardner/Sward, 13th Edition, G. G. Sward, Ed., *Amer. Soc. Testing Mater. Spec. Tech. Publ.* **500,** pp. 556-563 (1972).

Key words: coulometric titration; coulometry; differential thermal analysis; diffusion current; dropping mercury electrode, half-wave potential; polarography.

Polarography is an instrumental method of analysis based on the evaluation of current-voltage curves that are obtained during the electro-reduction or oxidation of a chemical compound. The limiting current is diffusion controlled and is a function of concentration. The half-wave potential is the voltage at one-half the diffusion current and is characteristic of the reaction occurring. The dropping mercury electrode, used in polarography, has the particular advantage of being constantly renewed.

Constant current coulometry is a highly accurate analytical technique based on Faraday's Law and involves measuring the number of coulombs (current × time) that pass through a chemical cell. Coulometric titrations can be performed by electrogenerating the necessary titrant in situ.

Differential thermal analysis is used for identifying or measuring the physical and chemical changes that occur in materials as they are heated or cooled. The temperature of a test sample is compared to an inert reference and the differential temperature is recorded. Exothermic and endothermic temperature changes are related to chemical reactions or physical transformation.

Blunt, R. F., Candela, G. A., Forman, R. A., **Effect of γ irradiation on the magnetic properties of ruby,** *J. Appl. Phys.* **44,** No. 4, 1753-1755 (Apr. 1973).

Key words: aluminum oxide; chromium; color centers; magnetic susceptibility; radiation damage; ruby.

The magnetic susceptibilities of ruby samples (Cr^{3+} in α-Al_2O_3) were measured before and after Co^{60} γ irradiation. Within the experimental error the magnetic susceptibility was found to be unchanged by the irradiation. The degree of microwave saturation possible for the Cr^{3+} spin system, when at the resonance condition for complete saturation, showed a marked decrease after irradiation. Together, these results indicate that the γ irradiation has changed the resonance condition for approximately 10-15 percent of the Cr^{3+} in a 0.05 wt% Cr_2O_3 sample. A likely inference is that the oxidation state of at least 99 percent of the chromium is unaltered, and that less than 10 ppm Cr has valence differing from three in the irradiated sample. These experiments are in essential agreement with other experiments on ruby.

Bower, V. E., **Determination of the Faraday by means of the iodine coulometer,** (Proc. 4th Int. Conf. on Atomic Masses and Fundamental Constants, Teddington, England, Sept. 6-10, 1971), Paper in *Atomic Masses and Fundamental Constants,* J. H. Sanders and A. H. Wapstra, Eds., pp. 516-520 (Plenum Press, London, England, 1972).

Key words: coulometry; Faraday; fundamental constants.

This paper describes briefly the work now in progress at NBS on the determination of the Faraday by means of the iodine coulometer. Results obtained to date are compared with a recent determination of the Faraday by means of the silver coulometer and with an adjusted value of the same constant derived from recent determinations of the gyromagnetic ratio of the proton and proton magnetic moment in nuclear magnetons.

Brennen, W., Brown, R. L., **Measurements on the nitrogen atom and pressure dependences of the visible nitrogen afterglow intensity in a nitrogen carrier using EPR,** *J. Chem. Phys. Letters to Editor* **52,** No. 9, 4910-4911 (May 1, 1970).

Key words: atom recombination; energy transfer; Lewis-Rayleigh afterglow; N-atoms; N_2 first positive bands; nitrogen afterglow.

The relative visible nitrogen afterglow intensity in a N_2 carrier was measured as a function of pressure and N-atom concentration using EPR detection over a range 0.12 to 75 torr. The specific intensity $I/[N]^2$ was found to be independent of pressure and [N], within the experimental uncertainty.

Brown, D. W., Florin, R. E., Wall, L. A., **The effect of dilute fluorine on certain fluoropolymers,** *Appl. Polym. Symp. No. 22,* 169-180 (1973).

Key words: crosslinking; fluorine; fluoropolymers.

Various fluoropolymers were exposed to 5 percent fluorine in helium at 25 °C and one atmosphere. About 10-100 percent as many fluorine molecules were charged as monomer units in each polymer. Certain polymers degraded as shown by decreases in their intrinsic viscosities. Degrading polymers had the structures

$$\begin{pmatrix}CH_2CF\\CF_3\end{pmatrix}, \begin{pmatrix}CH_2CF\\CF_3\end{pmatrix}(C_2F_4)\ (1{:}4),$$

$$\begin{pmatrix}CHFCH\\CF_3\end{pmatrix}, \begin{pmatrix}CH_2CH\\C_3F_7\end{pmatrix}, \begin{pmatrix}CF_2CF{=}CFCF\\CF_3\end{pmatrix},$$

and

$$\begin{pmatrix}CF_3\\CH_2C\\CF3\end{pmatrix}(C_2F_4)\ (1{:}4).$$

The intrinsic viscosity of polyperfluoropropene was not changed. Other polymers cross-linked, as shown by formation of gel. These had the structures

$$\begin{pmatrix}CH_2CH\\CF_3\end{pmatrix}, \begin{pmatrix}CH_2CH\\CF_3\end{pmatrix}(C_2F_4)\ (1{:}2),$$

$$\begin{pmatrix}CH_2CH\\C_3F_7\end{pmatrix}(C_2F_4)\ (1{:}3), \begin{pmatrix}CH_2CH\\C_6F_5\end{pmatrix}, \begin{pmatrix}CF_2CF\\C_6H_5\end{pmatrix}$$

and

$$\begin{pmatrix}CF_2CF\\C_6F_5\end{pmatrix}$$

In homopolymers the greater the hydrogen content the more likely the polymer was to crosslink, suggesting that crosslinking proceeds via abstraction of hydrogen atoms. However, an increased content of tetrafluoroethylene in copolymers also was associated with greater crosslinking or reduced degradation. Viton and a copolymer of 3,3,3-trifluoropropene gave highly crosslinked materials. The vulkanizates of Viton are quite resistive to stress relaxation at 250 °C in air. Those of the trifluoropropene copolymer are very unstable.

Brown, D. W., Lowry, R. E., Wall, L. A., **Radiation-induced polymerization at high pressure of *cis*- and *trans*-1,3,3,3-tetrafluoropropene in bulk and with tetrafluoroethylene,** *J. Polym. Sci. Part A-1,* **11,** 1973-1984 (1973).

Key words: copolymerization; high pressure; polymerization; radiation; tetrafluoroethylene; tetrafluoropropene.

The radiation-induced polymerization of *cis*- and *trans*-1,3,3,3-tetrafluoropropene in bulk and with tetrafluoroethylene was studied at pressures between 5000 and 15000 atm and temperatures between 21 and 100 °C. At 10^3 rad/hr the homopolymerization rates range from about 10^{-4} to 1 percent/hr. The activation enthalpy and volume are about 8 kcal/mole (33 kJ/mole) and -10 cm^3/mole, respectively, for both isomers. The *cis* isomer polymerizes about twice as rapidly as the *trans* isomer. The latter freezes in the experimental range of temperature and pressure; the polymerization rate is very low in solid phase. Polymer intrinsic viscosities increase with polymerization pressure and decrease with polymerization temperature; the largest value obtained was 0.23 dl/g. In the copolymerizations all reactivity ratios favor incorporation of tetrafluoroethylene by factors of 6-16. The preference is stronger when the *trans* isomer is used.

Brown, R. L., **Effects of N-atom concentration, pressure, and carrier composition on some first positive band intensities in the yellow nitrogen afterglow,** *J. Chem. Phys.* **52,** No. 9, 4604-4617 (May 1, 1970).

Key words: energy transfer; first positive N_2 bands; Lewis-Rayleigh afterglow; nitrogen afterglow; nitrogen atoms; vibrational relaxation electronic quenching.

Absolute intensities of seven N_2 1st positive bands with $\nu' = 6$-12 were measured as a function of carrier pressure, carrier composition, and N-atom concentration in the range 4.5-0.06 torr. For an Ar carrier large pressure-dependent shifts in the $B\ ^3\Pi_g$ vibrational distribution to higher levels were observed below 4 torr; similar but much smaller shifts were also found for N_2 and He carriers. With Ar, reducing the N-atom concentration shifted the vibrational distribution to lower levels. Changes in carrier composition produced large pressure dependent changes in the absolute and relative band intensities. An attempt was made to fit the results to a model involving vibrational relaxation and electronic quenching in $B\ ^3\Pi$. While qualitatively successful, this model could not account quantitatively for the observed relative intensity changes over the whole pressure range for which data are available and, in addition, implied physically unreasonable vibrational relaxation rates. It is suggested that the observed changes in the $B\ ^3\Pi_g$ vibrational distribution below 4 torr may arise from vibrational relaxation in some precursor state.

Camarda, H. S., ***P*-wave neutron strength-function measurements and the low-energy optical potential,** *Phys. Rev. C* **9,** No. 1, 28-37 (Jan. 1974).

Key words: function; mass number; neutrons; optical potential; *R*-matrix; strength; time-of-flight.

Using the National Bureau of Standards electron linac and underground time-of-flight facility, precise average neutron-transmission measurements have been made in the energy range 1 keV $\leq E \leq$ 600 keV on the elements As, Br, Nb, Rh, Ag, In, Sb, I, La, Ho, Au, and Th. The samples were "thick" in that the *s*-wave self-protection had to be accounted for at low energies. However, the samples were still sufficiently thin that any errors introduced by neglecting *p*-wave self-protection were negligible. The average *R*-matrix theory was employed in the analysis and the $l=0$ scattering length R' and the *p*-wave strength function S_1 were extracted from the data. The behavior of S_1 vs mass number A in the region of the $3P$ maximum was found to vary smoothly with no evidence of any splitting of the resonance. Using Moldauer's optical potential, which fits the $l=0$ data well, the behavior of S_1 vs A was calculated. The predicted behavior was found to differ significantly from experiment. In particular, experiment indicates S_1 peaks at a lower mass number and that the maximum is stronger than indicated by the calculations. When the constants of the potential were changed in order to reproduce the observed behavior of S_1, a significant discrepancy with the $l=0$ data resulted. The results presented here imply an orbital angular momentum dependence of the low-energy optical potential.

Chang, S-S., **Thermal relaxation and glass transition in polyethylene,** *J. Polym. Sci.*, No. 43, 43-54 (1973).

Key words: annealed; crystallinity; glass transition; polyethylene; relaxation; temperature drifts.

Thermal relaxations in the glass transition region can be observed as spontaneous temperature drifts of the sample under adiabatic conditions. Upon the heating of a quenched glass, positive drifts are observed reaching a peak at some temperature just below its T_g. An annealed glass produces a peak in the negative drift at temperatures just above its T_g. Heat capacity measurements have been made on three linear polyethylene samples having 71 to 96 percent crystallinity and on one branched polyethylene sample, in an adiabatic calorimeter from 2 to 360 K. In all four samples, temperature drifts were detected with peaks occurring around 235-240 K. The temperature of the peaks is not significantly affected by the degree of crystallinity. However, the magnitude of the peaks decreases as the crystallinity is increased.

Cohen, G. G., Alexandropoulos, N. G., Kuriyama, M., **Relation between x-ray-Raman and soft-x-ray-absorption spectra,** *Phys. Rev. B* **8,** No. 12, 5427-5431 (Dec. 15, 1973).

Key words: energy transfer; lithium; momentum transfer; x-ray absorption; x-ray inelastic scattering.

A spectrum of x-ray inelastic scattering of copper $K\alpha_1 K\alpha_2$ radiation scattered by metallic lithium through $2\theta = 115°$ was obtained. (These conditions correspond to a momentum transfer $k = 6.87 \times 10^{10}$ m^{-1}.) The spectrum is compared quantitatively to an experimental soft-x-ray-absorption spectrum of lithium. This comparison serves as an experimental verification of the relation between x-ray-Raman spectra and soft-x-ray-absorption spectra. The method renders possible the study of solid-state effects via x-ray Compton-Raman experiments without *ad hoc* assumptions concerning the wave functions of the inner electrons. Also presented is some evidence of the failure of a random-phase approximation and the impulse approximation in the region under investigation.

Costrell, L., Ed., **CAMAC—organization of multi-crate system,** (AEC Committee on Nuclear Instrument Modules), *AEC Report No. TID-25876,* 42 pages (U.S. Atomic Energy Commission, Washington, D.C., Mar. 1972).

Key words: CAMAC; computer interfacing; control systems; instrumentation; instrumentation standards; nuclear instrumentation; standards.

CAMAC is a design for modular equipment systems used on-line with digital processors and computers and incorporates a comprehensive data transfer highway (Dataway). This extension to the CAMAC specifications defines a Branch Highway and a standard Crate Controller for communication between a system controller or computer and as many as seven crates. The specification has been developed by the ESONE Committee of European Laboratories and has been endorsed by the U.S. AEC Committee on Nuclear Instrument Modules (NIM Committee). Except for pages i-vii and page 30A, this report is identical to Euratom Report EUR 4600e dated October 1971. AEC Report TID-25877 constitutes a supplement to and is to be used in conjunction with this report. The basic CAMAC specifications are defined in AEC Report TID-25875.

Costrell, L., **Highways for CAMAC systems—a brief introduction,** *IEEE Trans. Nucl. Sci.* **NS-21,** No. 1, 870–875 (Feb. 1974).

Key words: CAMAC; computer interfacing; control systems; instrumentation; instrumentation standards; nuclear instrumentation; standards.

The interconnection between CAMAC crates and between the crates and a computer is called the CAMAC highway. The purpose of this paper is to present a brief summary of CAMAC highway configurations to put in perspective the highway papers that follow and to serve as a starting point for the panel discussion on CAMAC highways.

Cowan, D. O., LeVanda, C., Collins, R. L., Candela, G. A., Mueller-Westerhoff, U. T., Eilbracht, P., **Mössbauer and magnetic susceptibility studies of biferrocenylene (II, III) picrate,** *J. Chem. Soc. Chem. Commun.*, pp. 329-330 (1973).

Key words: biferrocenylene (2,3) picrate; magnetic susceptibility; Mössbauer.

Mössbauer and magnetic susceptibility studies of biferrocenylene (II, III) picrate show that extensive donor-acceptor interactions occur in this mixed-valence molecule which result in fractional oxidation states for the iron atoms.

Currie, L. A., DeVoe, J. R., **The isotope separator as a tool for low-level radioassay and trace activation analysis,** (Proc. Symp. on Nuclear Techniques in Measurement and Control of Environmental Pollution, Salzberg, Austria, Oct. 26-30, 1970), Paper in *Nuclear Techniques in Environmental Pollution,* pp. 183-190 (International Atomic Energy Agency, Vienna, Austria, 1971).

Key words: activation analysis; iodine; mass separation; physical-radiochemical separation.

Determinations of environmental radioactivity and of low-level products of nuclear activation are frequently limited in sensitivity because of isotopic contamination. Sensitivity may be limited by radioisotopes because of interfering radiations and by stable isotopes because of decreased specific activity. To overcome these limitations, electromagnetic isotope separation, which is applicable to most elements, has been investigated as a complement to radiochemical separation and decay scheme resolution. An added advantage of mass separation in environmental studies is the physical separation of a diluting radioisotope—radioisotope dilution being desirable because of the possibility of unknown initial amounts of stable isotopes.

The characteristics of the relatively new class of laboratory isotope separators having moderately large beam currents, 1-5 mA, are particularly suitable, for they include reasonable throughput (~mg/h), yield (~10%) and resolution (~10^3). Isotope separation was investigated in connection with the neutron activation analysis of trace

quantities ($\sim 10^9$ atoms) of iodine. The mass-separation step was found to be essential because of the production of interfering iodine fission products—even when uranium contamination was as low as 1 ppm. A particularly important result of our investigation was the absence of any detectable blank effect from prior separations. In addition, it has been shown that for certain problems electromagnetic separation, when combined with a high efficiency radiation detector, is far more sensitive and selective than a high resolution detector without mass separation.

Dehl, R. E., **NMR second moment of rotator-phase polycrystalline n-$C_{19}H_{40}$,** *J. Chem. Phys. Letters to Editor* **60,** No. 1, 339-340 (Jan. 1, 1974).

Key words: molecular rotation; NMR second moment; n-nonadecane; paraffin; rotator phase; wideline NMR.

The proton NMR second moment of polycrystalline n-$C_{19}H_{40}$ in the rotator phase at 25 °C was measured for several spectra of the as-received ("98.5%") and the solution-recrystallized paraffin. The average second moment of the as-received paraffin (0.060 $(mT)^2$) was considerably lower than that of the recrystallized paraffin (0.076 $(mT)^2$), indicating the importance of chemical purity in obtaining accurate second moments of paraffins. The results for the recrystallized paraffin were significantly lower than Andrew's theoretical prediction (0.088 $(mT)^2$), but significantly higher than the value predicted by Olf and Peterlin (0.064 $(mT)^2$). Because of these discrepancies, the theoretical NMR second moment of the "rotator" paraffin was reevaluated, using exact calculations of the most important dipolar contributions and estimates of the smaller terms. The calculated and observed values were thus found to differ by only 4 percent. The NMR second moment is consistent with simple rotation or large-amplitude oscillation of the chains about their long axes.

Dehl, R. E., **The effect of salts on the nmr spectra of D_2O in collagen fibers,** *Biopolymers* **12,** 2329-2334 (1973).

Key words: collagen; D_2O in collagen; deuterium nmr; $MgCl_2$ in collagen; $MgSO_4$ in collagen; wideline nmr.

The effects of two salts, $MgCl_2$ and $MgSO_4$, on the wide-line nmr spectrum of D_2O in oriented, undenatured collagen fibers have been examined at four different D_2O contents. $MgCl_2$ was found to decrease the nmr doublet splitting, as compared with equal quantities of pure D_2O, while the major effect of $MgSO_4$ was to inhibit the adsorption of D_2O without significantly affecting its nmr spectrum. The results, together with a few observations of KCl and LiCl solutions, indicate that even fairly high concentrations of salt have only small effects on the nmr spectrum of D_2O in fibrous collagen. It is considered unlikely that either "two-state" or "structured-water" models can satisfactorily account for the D_2O-nmr doublet spectrum or the effects of salts on it, over the entire range of observed D_2O content.

Diamond, J. J., Calvano, N. J., **Ballistic resistance of police body armor,** *NILECJ-STD-0101.00,* 10 pages (U.S. Department of Justice, Law Enforcement Assistance Administration, National Institute of Law Enforcement and Criminal Justice, Washington, D.C., Mar. 1972).

Key words: armor (wearable); ballistic deformation; ballistic penetration; body armor; bullet proof vests.

This standard establishes performance requirements for ballistic penetration, and methods of test for ballistic penetration and deformation of police body armor intended to protect the torso against small arms gunfire. Standards are established for armors intended to provide three levels of protection: Armors protective against .30-06 armor piercing rifle fire, armors protective against .357 magnum revolver fire, and armors protective against .22 long rifle high velocity rifle fire.

Diamond, J. J., Weissler, P. G., **Hearing protectors for use on firing ranges,** *NILECJ-STD-0102.00,* 11 pages (U.S. Department of Justice, Law Enforcement Assistance Administration, National Institute of Law Enforcement and Criminal Justice, Washington, D.C., Mar. 1973).

Key words: earmuffs; earplugs; firing range noise; gunfire noise; hearing protectors.

This standard establishes performance requirements and methods of test for wearable devices used to protect the auditory system against the gunfire noise on firing ranges. The test method described measures hearing protection by psychoacoustic tests on human subjects, that is, the real-ear protection at threshold of audibility. It is based on ANSI Standard Z24.22-1957.

Douglas, W. M., Johannesen, R. B., Ruff, J. K., **Reactions of coordinated ligands. II. μ-oxo-bis(difluorophosphineiron tetracarbonyl),** *Inorg. Chem.* **13,** No. 2, 371-374 (1974).

Key words: carbonyl compounds; coordination compounds; fluorophosphine; iron carbonyl; nmr; nuclear magnetic resonance.

Reaction of $Fe(CO)_4PF_2Br$ with potential sources of the oxide ion (*e.g.*, Ag_2O, Cu_2O, etc.) yielded the new complex compound, $Fe(CO)_4PF_2OPF_2Fe(CO)_4$. A more convenient preparation of this material involved the use of $AgMnO_4$ instead of the metal oxides. The ^{31}P and ^{19}F nmr parameters for the complex were obtained by analysis of the spectra as a AA′XX′-X″X‴ spin system.

Dragoo, A. L., Paule, R. C., **Ultrapure materials: Containerless evaporation and the roles of diffusion and Marangoni convection,** (Proc. 12th Aerospace Sciences Meeting, Washington, D.C., Jan. 30-Feb. 1, 1974), *AIAA Paper No.* **74-209,** pp. 1-8 (American Institute of Aeronautics and Astronautics, New York, N.Y., 1974).

Key words: Al_2O_3; complex equilibria; convective-diffusion; evaporative rate; purification (evaporative); solutal-capillary; thermal capillary convection; vacuum vaporization.

Contamination from containers is a major problem in preparing ultrapure refractory materials. Space with its zero gravity and its high vacuum offers an opportunity for containerless purification of these materials. The evaporation of impurities from a melt will involve many complex chemical equilibria. Thermodynamic calculations have been modified to describe these equilibria when impurities in the melt evaporate into vacuum. The contributions of diffusion and Marangoni convection to mass transfer rates in the bulk liquid have been estimated. Calculations for the evaporative purification of molten alumina are given.

Dragoo, A. L., **Diffusion,** Chapter IV in *Beryllium: Physico-Chemical Properties of Its Compounds and Alloys, Atomic Energy Review Special Issue,* O. Kubaschewski, Ed., No. 4, pp. 173-175 (International Atomic Energy Agency, Vienna, Austria, 1973).

Key words: chemical interdiffusion; grain-boundary diffusion; intrinsic diffusion; lattice diffusion; self-diffusion; tracer diffusion.

The tracer diffusion coefficient, the self-diffusion coefficient, the intrinsic diffusion coefficient and the interdiffusion coefficient are briefly described. Grain boundary and lattice (volume) diffusion are contrasted. The frequency factors (D_0) and activation energies (Q) are tabulated for diffusion in the borides, carbides, and oxides of Be, Hf, Mo, Nb, Ta, Th, Ti, and Zr and for diffusion of C, N, and O in these metals. The purity of the solvent media, the preparation and properties of the samples, the method, the type of diffusion coefficient measured and the temperature range are also specified.

Dragoo, A. L., **Diffusion,** Chapter IV in *Tantalum: Physico-Chemical Properties of Its Compounds and Alloys, Atomic Energy Review*

Special Issue, O. Kubaschewski, Ed., No. 3, pp. 131-133 (International Atomic Energy Agency, Vienna, Austria, 1972).

Key words: chemical interdiffusion; grain-boundary diffusion; intrinsic diffusion; lattice diffusion; self-diffusion; tracer diffusion.

The tracer diffusion coefficient, the self-diffusion coefficient, the intrinsic diffusion coefficient and the interdiffusion coefficient are briefly described. Grain boundary and lattice (volume) diffusion are contrasted. The frequency factors (D_0) and activation energies (Q) are tabulated for diffusion in the borides, carbides, and oxides of Be, Hf, Mo, Nb, Ta, Th, Ti, and Zr and for diffusion of C, N, and O in these metals. The purity of the solvent media, the preparation and properties of the samples, the method, the type of diffusion coefficient measured and the temperature range are also specified.

Evans, A. G., Fuller, E. R., **Crack propagation in ceramic materials under cyclic loading conditions,** *Met. Trans.* **5,** 27-33 (Jan. 1974).

Key words: ceramics; cyclic failure; relation to static failure; slow crack growth; tension/compression; time to failure.

An analysis is presented which enables crack propagation rates under cyclic loading conditions to be predicted from static slow crack growth parameters. A comparison of the predicted times to failure under cyclic conditions with available measured failure times, for several ceramic materials at ambient temperatures, suggests that there is no significant enhancement of the slow crack growth rate due to cycling. This is verified in a series of measurements of slow crack growth rates under static and cyclic conditions.

Evans, A. G., Linzer, M., **Failure prediction in structural ceramics using acoustic emission,** *J. Amer. Ceram. Soc.* **56,** No. 11, 575-581 (Nov. 1973).

Key words: acoustic emission; ceramics; failure prediction; fracture.

Crack propagation in a typical structural ceramic (porcelain) is accompanied by acoustic emission. Two types of emission are detected. The first type is caused by slow growth of the fracture-initiating flaw; the emission rate depends primarily on crack velocity. Failure prediction using this source of emission can be effective, however, only if low-level emission, which may be related exclusively to crack growth, can be detected. The second source of emission, which occurs during bulk stressing, is the cracking associated with second-phase particles (quartz particles in porcelain) as a result of the combined action of the applied stress and local thermal and mechanical stresses. An analysis for predicting emission rates is developed and forms the basis for using this source of acoustic emission in failure prediction.

Fanconi, B., **Low-frequency vibrational spectra of some homopolypeptides in the solid state,** *Biopolymers* **12,** 2759-2776 (1973).

Key words: far infrared spectroscopy; interchain hydrogen bonding; low frequency vibrations; polypeptides; Raman spectroscopy.

Low-frequency Raman and far-infrared spectra of polyglycine, poly-L-alanine, and poly-L-valine have been measured. The Raman spectra exhibit an intense band near 100 cm^{-1} for these homopolypeptides. Lattice calculations of the polyglycines are used to assign the intense Raman band to a rotatory lattice mode. For homopolypeptides in the β conformation, an infrared band is observed whose frequency varies inversely with the square root of the mass of the peptide repeating unit. This infrared band is assigned to the hydrogen bond stretching lattice vibration.

Farabaugh, E. N., Parker, H. S., Armstrong, R. W., **Skew-reflection x-ray microscopy of the vapor-growth surface of an Al_2O_3 single crystal,** *J. Appl. Crystallogr.* **6,** Part 6, 482-486 (Dec. 1973).

Key words: Al_2O_3; Berg-Barrett; single crystal; skew reflection; vapor growth; x-ray diffraction microscopy.

The most commonly used geometry for the Berg-Barrett x-ray microscopy uses the zero-layer reflections as described by Newkirk. It can be shown that non-zero-layer reflections, skew-plane reflections, can be used equally well to obtain x-ray micrographs. The analysis of the stereographic representation of the skew-reflection geometry demonstrates the many usable reflections and gives the conditions for minimum image distortion. In these x-ray micrographs the contributions to diffraction contrast from shadowing and subboundaries can be identified. An estimate of the height of steps occurring on the crystal surface can also be made.

Feldman, A., Horowitz, D., Waxler, R. M., **Mechanisms for self-focusing in optical glasses,** *IEEE J. Quantum Electron.* **QE-9,** No. 11, 1054-1061 (Nov. 1973).

Key words: absorption coefficient; damage threshold; electrostriction; electrostrictive self-focusing; Kerr effect; laser damage; nonlinear index of refraction; self-focusing; thermal self-focusing.

The relative contributions of the Kerr, electrostrictive, and thermal effects to the self-focusing thresholds of borosilicate crown glass, fused silica, and dense flint glass have been estimated from an analysis of damage-threshold data for linearly polarized and circularly polarized radiation. The measurements were made with a Nd:glass laser operating in the TEM_{00} mode with a temporal pulsewidth of 25 ns. The Kerr effect appears to be the largest effect. The thermal effect is also significant. The electrostrictive effect is smallest. Reasonable values of the absorption coefficient are calculated from the thermal contribution. The results are in qualitative agreement with the work of others.

Field, B. F., Finnegan, T. F., Toots, J., **Volt maintenance at NBS via $2e/h$: A new definition of the NBS volt,** *Metrologia* **9,** No. 4, 155-166 (1973).

Key words: Josephson effect; standard cell; tunnel junction; voltage comparator; voltage standard.

This paper describes in detail the procedures, methods and measurements used to establish a new definition of the U.S. legal volt via the ac Josephson effect. This new definition has been made possible by the use of thin film tunnel junctions (capable of producing 10 mV outputs) and high accuracy voltage comparators. The Josephson junction is used as a precise frequency-to-voltage converter with e conversion factor equal to $2e/h$. A series of measurements of $2e/h$ have been carried out at NBS referenced to the as-maintained unit of emf based on a large group of standard cells. Measurements made at regular intervals over a one year period (1971 to 1972) indicate that the mean emf of this group of standard cells has decreased about 4 parts in 10^7. Primarily to remove the effects of this drift, on July 1, 1972 a new as-maintained unit was defined by choosing a value of $2e/h$ consistent with the existing unit of emf. The adopted value of $2e/h$ is 483593.420 GHz/V_{NBS}. The precision (one standard deviation) with which the new unit of emf can be maintained with the present techniques and apparatus is about 2 parts in 10^8. The accuracy of the present system is estimated to be 4 parts in 10^8. Comparisons of $2e/h$ systems at different national laboratories have been limited by uncertainties associated with the physical transfer of standard cells. In order to determine the relative agreement of the various $2e/h$ systems with precision better than 1 or 2 parts in 10^7, it appears desirable to compare $2e/h$ systems directly by transporting one of them.

Frommer, M. A., Shporer, M., Messalem, R. M., **Water binding and irreversible dehydration processes in cellulose acetate membranes,** *J. Appl. Polym. Sci.* **17,** 2263-2276 (1973).

Key words: adsorption of water; cellulose acetate; dehydration; free induction decay; freezing of water; irreversible processes; membranes; NMR; porous membranes.

The relative amounts of freezing and nonfreezing water in various water-wet cellulose acetate (CA) membranes were determined by NMR techniques, from the initial heights of the water component in the free induction decay (NMR intensity). The results suggest that (1) a significant fraction of the water in various wet CA membranes does not freeze, probably because of strong interaction with the polymer; (2) the relaxation times T_2 of the nonfreezing water are of the order of milliseconds indicating that they are still highly mobile compared with ice; (3) all the water contained in dense CA films or in membranes equilibrated at relative humidity of 0.93 does not freeze upon cooling the membranes from room temperature to − 60 °C; (4) the amounts of nonfreezing bound water in membranes is higher than the total amount of water absorbed from liquid water by a dense film of the same polymer. However, the amounts of nonfreezing water in various CA membranes as calculated from the "relative NMR intensities" is substantially lower than those calculated from DSC melting endotherms by assuming the heat of fusion of water in membranes to be identical to that of pure water. Various possible reasons for this discrepancy are discussed. Measurements on the first desorption-adsorption cycle of *wet* CA membranes have also been performed. They suggest that during the first dehydration process, irreversible changes are induced in the structure of the membrane which result in a significantly lower accessibility of the polymer to interact with water. The extent of these irreversible changes in membrane structure is dependent on the details of the dehydration process being more pronounced at higher temperatures.

Gallagher, A., Lewis, E. L., **Determination of the vapor pressure of rubidium by optical absorption,** *J. Opt. Soc. Amer.* **63,** No. 7, 864-869 (July 1973).

Key words: rubidium; vapor pressure.

The vapor pressure of rubidium was determined in the neighborhood of 330 K from measurements of optical absorption of the resonance lines. A narrow-line source was used and a full analysis of the line profiles was done. Measurements of resonance-broadening depolarization give another check on the Rb vapor pressure in the 430-K range, assuming that theoretical cross section is correct. The results are very close to the analytic compromise previously suggested by Nesemeyanov.

Galy, J., Roth, R. S., **The crystal structure of $Nb_2Zr_6O_{17}$,** *J. Solid State Chem.* **7,** 277-285 (1973).

Key words: anion excess fluorite; crystal structure; $Nb_2Zr_6O_{17}$; square anti-prism.

$Nb_2Zr_6O_{17}$ is orthorhombic, space group *Ima*2, with $a = 40.91$, $b = 4.93$, $c = 5.27$ Å. The asymmetric structural unit contains one octahedron, three sevenfold coordinated ions, and one square antiprism, and its relations to the fluorite and ZrO_2 structures are discussed. Variations in compositions can be accounted for by increasing or decreasing the number of sevenfold coordinated ions in the structure.

Gebbie, K. B., Steinitz, R., **On spatial variations in the intensity of chromospheric H_α,** *Astrophys. J.* **188,** No. 2, 399-406 (Mar. 1, 1974).

Key words: features observed in H_α; H_α filtergrams; lateral contrasts in intensity; profile variation mechanism.

We investigate the formation of patterns in H_α spectroheliograms and filtergrams. Introducing a *source-sink-control diagram*, we conclude that the H_α line source function in the quiet solar chromosphere is indirectly controlled by the photospheric radiation fields in the Balmer and Paschen continua. We demonstrate that in producing the observed patterns, horizontal spatial variations in the shape of the absorption profile are extremely effective compared to changes in the source and sink terms. Applying this mechanism, we compute asymptotic values for the contrasts and visibilities in chromospheric H_α.

Geist, J., Blevin, W. R., **Chopper-stabilized null radiometer based upon an electrically calibrated pyroelectric detector,** *Appl. Opt.* **12,** No. 11, 2532-2535 (Nov. 1973).

Key words: ac power measurements; electrically calibrated radiometer; pyroelectric detector; radiometer; radiometry.

In this paper we will describe a new type of radiometric system that combines the high-accuracy characteristics of electrical calibration and null detection with the noise and background discrimination of chopper-stabilized, synchronous detection. We start by outlining those characteristics required for high accuracy and those required for good noise discrimination. Next we show that these requirements are mutually inconsistent for certain types of detectors (thermopiles), but that they can all be well satisfied by electrically-calibrated pyroelectric detectors. Then we discuss the special requirements for a chopper-stabilized null radiometer, including wave-form independent, lock-in detection, and lastly we describe the performance of a system that we have constructed.

Geist, J., Schmidt, L. B., Case, W. E., **Comparison of the laser power and total irradiance scales maintained by the National Bureau of Standards,** *Appl. Opt.* **12,** No. 11, 2773-2776 (Nov. 1973).

Key words: intercomparison; irradiance scale; laser power scale.

The paper describes an intercomparison of the instrument used to realize and maintain the NBS laser power and energy scale with the instrument used to realize and maintain the upper end of the NBS total irradiance scale. The intercomparison was conducted by performing simultaneous measurements of the average power from a cw krypton laser with both instruments. The procedure and apparatus of the comparison are described. The measured difference between the two instruments was well within the ~ 1.5 percent limit of error associated with the intercomparison.

Geltman, S., Teague, M. R., **Atomic absorption of ultra intense laser radiation,** *J. Phys. B: At. Mol. Phys. Letter to Editor* **7,** No. 1, L22-L27 (1974).

Key words: atoms; free-free absorption; ultra-intense laser radiation.

We derive an expression for the rate of absorption by an atomic system (bound or free) of radiation from an ultra intense laser beam. The absorption characteristics are radically different from those of conventional weak-field absorption theory.

Glaze, D. J., Hellwig, H., Jarvis, S., Jr., Wainwright, A. E., Allan, D. W., **Recent progress on the NBS primary frequency standard,** *Proc. 27th Annual Symp. on Frequency Control, Philadelphia, Pa., June 12-14, 1973,* pp. 347-356 (Electronic Industries Association, Washington, D.C., 1973).

Key words: cesium beam standard; Doppler effect; frequency accuracy; frequency stability; power shift; primary frequency standard.

The design of NBS-5 is discussed in detail including its relation to previous NBS primary cesium beam frequency standards. The application of pulsed microwave excitation, and the use in the accuracy evaluation of frequency shifts due to known changes in the exciting microwave power are discussed. Significant changes in the measured atomic velocity distribution with the beam alignment are reported and compared with measured Ramsey patterns. Stabilities of 3×10^{-14} for one-day averaging are reported and data on accuracy are given. Preliminary results give an evaluated accuracy of 2×10^{-13} with indications that this figure may be improved in the future.

The bias-corrected frequency of NBS-5 agrees to within 1×10^{-13} with the value obtained with NBS-III in 1969 which is preserved in the rate of the NBS Atomic Time Scale.

Goldberg, R. N., Armstrong, G. T., **Microcalorimetry: A tool for biochemical analysis,** *Med. Instrum.* **8,** No. 1, 30-36 (Jan.-Feb. 1974).

Key words: analytical chemistry; bacterial identification; biochemistry; cellular processes; clinical chemistry; enzyme activity; immunochemistry; medical instrumentation; microcalorimetery; thermochemistry.

In order for the application of heat measurements to analysis and clinical chemistry to be feasible, three requirements must be met: (1) specificity of reaction, (2) knowledge of the thermochemistry involved, and (3) adequate instrumentation. Instrumentation requirements are met by devices known as heat conduction microcalorimeters. Some of the principles underlying these instruments are reviewed. The current status of microcalorimetry regarding requirements of sensitivity, sample volume, accuracy, reproducibility, and speed is considered. A brief review of analytical applications that have utilized microcalorimetry is given. These applications include assays for enzymes and substrates, bacterial identifications, and investigation of cellular processes. The advantages and disadvantages of the method as well as possibilities for future development are considered.

Goldman, A. J., **Approximate localization theorems for optimal facility placement,** *Transp. Sci.* **6,** No. 2, 195-201 (May 1972).

Key words: facility location; optimal location.

The problem is that of locating a flow-receiving facility in a region, so as to minimize the weighted sum of distances between sources and facility. It is shown here that if a subregion S both generates "sufficiently much" of the region's total flow, and admits entry via specified "gate" points without "too much" circuity, then (a) S contains at least one "near-optimal" location for the facility, and (b) no strictly optimal location can lie "too far" from S.

Goldman, A. J. **Minimax location of a facility in a network,** *Transp. Sci.* **6,** No. 4, 407-418 (Nov. 1972).

Key words: facility location; network theory; optimal location.

The problem is that of locating a facility in a network N so as to minimize the largest of its distances from the vertices of N. A method is given that either solves the problem, or else reduces it to an analogous problem for a single "cyclic component" of N. When N is acyclic (a tree), a very efficient solution algorithm results. Partial analogs of these results are given for a "weighted-distance" extension of the problem.

Goldman, D. T., Logan, D. A., **Solid wastes—a technological assessment,** *Chem. Eng. Progr.* **69,** No. 9, 33-35 (Sept. 1973).

Key words: engineering education; solid waste disposal; technology assessment.

A technology assessment is performed on the problem of the disposal of municipal refuse. Various alternative methods are considered including proposed methods for the utilization of solid waste. The identification of those affected by the various alternatives and an evaluation of the impacts these alternatives have on the affected parties are presented. The conclusions of this simple assessment is that sanitary landfills is the most desirable form of presently available disposal methods. For the future, new methods for the utilization of solid waste are required.

Haber, S., **Numerical evaluation of multiple integrals,** *SIAM Rev.* **12,** No. 4, 481-526 (Oct. 1970).

Key words: best integration formulas; diophantine approximation; Gaussian quadrature; integration; Monte Carlo; multiple integration; multiple quadrature; numerical analysis; numerical integration; optimal formulas; quadrature.

This paper is an expository survey of the main methods that have been developed for numerical evaluation of multiple integrals. Among the approaches discussed are: the Monte Carlo method and its generalizations; number-theoretical methods, based essentially on the ideas of diophantine approximation and equidistribution modulo 1; the functional analysis approach, in which the quadrature error is regarded as a linear functional and one attempts to minimize its norm; and the classical approach of designing formulas to be exact for polynomials of high degree while using as few values of the integrand as possible. Most of the research in this field is quite recent.

Halford, D., **Infrared-microwave frequency synthesis design: Some relevant conceptual noise aspects,** (Proc. Frequency Standards and Metrology Seminar, Quebec, Canada, Aug. 30-Sept. 1, 1971), Paper in *Proceedings of the Frequency Standards and Metrology Seminar,* pp. 431-466 (Quantum Electronics Laboratory, Laval University, Quebec, Canada, 1972).

Key words: Allan variance; base units; fast linewidth; frequency multiplication; infrared frequency metrology; Josephson effect; linewidth; methane frequency standard; phase noise; unified standard.

Extremely accurate and precise frequency synthesis into the infrared and visible radiation regions will allow new vistas of metrology. Frequency and time measurements are the basic operations which will be affected, and impact is expected in such diverse areas as length standards and metrology, spectroscopy, timekeeping, communications, and relativistic tests. In addition the set of independent base units of measurement may change, and the speed of light may become a conventional (defined) quantity. The attainment of the desired high accuracy and precision will be easiest and cheapest if there is careful optimization of the synthesis design aspects involving noise. When frequencies in the terahertz region are considered, the linewidth of the signal becomes an important parameter. Due to the low-frequency-divergence of the instability of good signal sources, the concept of the *fast linewidth* becomes of particular importance. Some of the properties and importance of the *fast linewidth* in system design are discussed in this paper.

Halford, D., Shoaf, J. H., Risley, A. S., **Spectral density analysis: Frequency domain specification and measurement of signal stability,** *Proc. 27th Annual Symp. on Frequency Control, Cherry Hill, N.J., June 12-14, 1973,* pp. 421-431 (Electronic Industries Association, Washington, D.C. 10006).

Key words: amplitude fluctuations; cross-spectral density; frequency domain; frequency noise; modulation noise; noise specification and measurement; oscillator noise; phase noise; radio frequency power spectral density; script $\mathscr{L}$(f); script $\mathscr{M}$(f); script $\mathscr{N}$; sidebands; signal stability; spectral density.

Stability in the frequency domain is commonly specified in terms of spectral densities. The spectral density concept is simple, elegant, and very useful, but care must be exercised in its use. There are several different but closely related spectral densities, which are relevant to the specification and measurement of stability of the frequency, phase, period, amplitude, and power of signals. Concise, tutorial descriptions of useful spectral densities are given in this survey. These include the spectral densities of fluctuations of (a) phase, (b) frequency, (c) fractional frequency, (d) amplitude, (e) time interval, (f) angular frequency, and (g) voltage. Also included are the spectral densities of radio frequency power and its two normalized components, Script $\mathscr{L}$(f) and Script $\mathscr{M}$(f), the phase modulation and amplitude modulation portions, respectively. Some of the simple, often-needed relationships among these various spectral densities are given. The use of one-sided spectral densities is recommended. The relationship to two-sided spectral densities is explained. The concepts of cross-spectral densities, spectral densities of time-dependent spectral densities, and smoothed spectral densities are discussed.

Hastie, J. W., Hauge, R. H., Margrave, J. L., **Infrared spectra of matrix-isolated species in the gallium-fluorine system,** *J. Fluorine Chem.* **3,** 285-291 (1973/74).

Key words: aluminium; fluorides; gallium; infrared spectra; matrix isolation.

The species GaF_3, GaF, AlF_3, AlF and $(AlF)_2$ have been isolated in inert-gas matrices and their infrared absorption spectra obtained over the range 33-4000 cm^{-1}. The following techniques were used to generate these species; (i) co-deposition of Ga or GaF and molecular F_2 or F atoms with an excess of inert gas; (ii) Knudsen cell effusion and matrix isolation of the vapors over GaF_3, GaF_3 + Ga and GaF_3 + Al.

Hellwig, H., Jarvis, S., Jr., Halford, D., Bell, H. E., **Evaluation and operation of atomic beam tube frequency standards using time domain velocity selection modulation,** *Metrologia* **9,** No. 3, 107-112 (1973).

Key words: atomic beams; cavity phase shift; cesium beam; frequency accuracy; frequency standard; pulsed excitation; second-order Doppler shift; velocity distribution.

Pulsed excitation of atomic and molecular beam devices with separated Ramsey-type interaction regions allows the observation of signals due to very narrow atomic velocity groups. The theoretical background of this method is discussed. Experimental operation of a near mono-velocity cesium beam tube is demonstrated. The velocity distribution of a commercial cesium beam tube is obtained using the pulse method. The normal Ramsey pattern of this beam tube is calculated from the velocity distribution and compared with the measured Ramsey pattern. The pulse method allows the direct determination of the cavity phase shift and of the second-order Doppler correction in beam devices. The pulse method thus shows promise for the evaluation of existing laboratory as well as commercial cesium beam tubes with respect to these effects.

Hellwig, H., Bell, H. E., **Some experimental results with an atomic hydrogen storage beam frquency standard,** *Metrologia* **8,** 96-98 (1972).

Key words: atomic hydrogen beam; dispersion; frequency stability; frequency standard; hydrogen maser.

A frequency standard is described in which a quartz crystal oscillator is locked to the hydrogen hyperfine transition using the dispersion of this resonance. The hydrogen storage beam apparatus closely resembles a hydrogen maser with a low-Q cavity below oscillation threshold. Cavity pulling can be reduced to a point where environmental temperature fluctuations limit the stability mainly via the second-order Doppler effect. Locking to the dispersion feature of the resonance eliminates the need for frequency modulation in order to find line-center. The stability of the frequency standard was measured against crystal oscillators and cesium beam frequency standards; stabilities of 4×10^{-13} were recorded for sampling times of 30 seconds and of 3 hours.

Hellwig, H., Jarvis, S., Jr., Glaze, D. J., Halford, D., Bell, H. E., **Time domain velocity selection modulation as a tool to evaluate cesium beam tubes,** *Proc. 27th Annual Symp. on Frequency Control, Philadelphia, Pa., June 12-14, 1973,* pp. 357-366 (Electronic Industries Association, Washington, D.C., 1973).

Key words: atomic beams; cavity phase shift; cesium beam; frequency standard; pulsed excitation; second-order Doppler shift; velocity distribution.

Pulsed excitation of atomic and molecular beam devices with separated Ramsey-type interaction regions allows the observation of signals due to very narrow atomic velocity groups. The theoretical background of this method is discussed. Experimental operation of a near mono-velocity cesium beam tube is demonstrated. The velocity distribution of a commercial cesium beam tube and of the primary laboratory standard NBS-5 are obtained using the pulse method. The normal Ramsey patterns are calculated from the velocity distribution and compared with the measured Ramsey patterns. The pulse method allows the direct determination of the cavity phase shift and of the second-order Doppler correction in beam devices. Velocity distributions obtained via the pulse method allow the use of microwave power shift results for accuracy evaluations. These aspects as well as the effects of modulation and different velocity distributions are discussed in detail. The pulse method thus shows promise for the evaluation of existing laboratory as well as commercial cesium beam tubes with respect to these effects.

Howell, B. F., Margolis, S., Schaffer, R., **Residual fluorescence as an index of purity of reduced nicotinamide adenine dinucleotide,** *Clin. Chem.* **19,** No. 11, 1280-1284 (1973).

Key words: alcohol dehydrogenase; fluorescence studies; nicotinamide adenine dinucleotide; optical rotation.

Determination of fluorescence remaining after reduced nicotinamide adenine dinucleotide (NADH) has reacted with excess acetaldehyde in the presence of alcohol dehydrogenase (EC 1.1.1.1) is useful as a criterion of NADH purity when used in conjunction with other methods for determining purity such as the rate of reaction, the ratio of ultraviolet absorbances at 260 nm and 340 nm, the color, and the chromatographic homogeneity of the preparation. Measurement of residual fluorescence monitors the enzymatically inactive material which absorbs at 340 nm. The specific optical rotations of NADH at several wavelengths are also reported.

Huie, R. E., Herron, J. T., Davis, D. D., **Absolute rate constants for the addition and abstraction reactions of atomic oxygen with 1-butene over the temperature range 190-491 K,** *J. Phys. Chem.* **76,** No. 23, 3311-3313 (1972).

Key words: abstraction reactions; addition reactions; atomic oxygen; reaction kinetics; 1-butene.

Using the technique of flash photolysis-resonance fluorescence, absolute rate constants have been measured for the reaction of ground-state atomic oxygen with 1-butene over the temperature range 190-491 K. With a measured precision of 3-5 percent at each temperature, it was found that the data could not be fit by a single straight line. It was concluded that the curvature in the Arrhenius plot was due to concurrent abstraction and addition reactions, the former process representing approximately 15 percent of the total reaction at 300 K and 39 percent at 500 K. The rate expressions derived were $k_{addition} = (3.7 \pm 1.8) \times 10^{-12}$ exp(− 50 ± 210 cal mol^{-1}/RT) cm^3 $molecule^{-1}$ sec^{-1} and $k_{abstraction} = (1.6 \pm 0.9) \times 10^{-11}$ exp(− 1970 ± 430 cal mol^{-1}/RT) cm^3 $molecule^{-1}$ sec^{-1}.

Johnson, C. R., **Gersgorin sets and the field of values,** *J. Math. Anal. Appl.* **45,** No. 2, 416-419 (Feb. 1974).

Key words: D-stable matrix; diagonal; doubly stochastic matrix; field of values; Gersgorin circles; numerical radius; positive definite; spectrum.

Two links are drawn between two well-known inclusion sets for the characteristic roots of a complex matrix: the field of values and the Gersgorin circles. An application is made to the theory of D-stable matrices.

Kaufman, V., Artru, M-C., Brillet, W-U L., **Revised analysis of the $2p^5 3s$, $3p$, $3d$, and $4s$ configurations of triply ionized aluminum (Al IV),** *J. Opt. Soc. Amer.* **64,** No. 2, 197-201 (Feb. 1974).

Key words: aluminum; energy levels; spectra; ultraviolet; wavelengths.

The spectrum of triply ionized aluminum (Al IV) was observed between 700 and 2200 Å. About 60 new lines have been identified as transitions between the $2p^5 3s$, $3p$, $3d$, and $4s$ configurations. The ground-state combinations have been remeasured (124-161 Å). Ener-

gies and designations are given for all levels of these configurations, and several changes and additions to the previous analysis have been made. Results of calculations of these configurations are included to support the level identifications. An isoelectronic comparison is discussed.

Kayser, B., Lipkin, H. J., Meshkov, S., **Tests of higher symmetries,** *Phys. Rev. D* **8,** No. 11, 4193-4198 (Dec. 1, 1973).

Key words: cross sections; reactions; Regge pole; SU(3); symmetry breaking; trajectory.

Model-independent cross-section relations predicted by unbroken SU(3) symmetry, and some predicted by $SU(6)_{W,strong}$, are compared with experiment. The relations are found to be satisfied, apart from deviations which follow, in every case, the pattern and rough size of symmetry breaking expected from Regge-pole exchange. Interestingly, this Regge symmetry breaking diverges with increasing energy. It is argued that this behavior, though contrary to intuition, is reasonable.

Kelleher, D. E., Wiese, W. L., **Observation of ion motion in hydrogen Stark profiles,** *Phys. Rev. Lett.* **31,** No. 24, 1431-1434 (Dec. 10, 1973).

Key words: Balmer; broadening; dynamic; ion; plasma; Stark.

We have measured the central part of the Balmer H_β or D_β line in similar stabilized arc plasmas, but of different chemical compositions. We have found an ion-motion effect which appears to scale with the inverse square root of the reduced mass of the radiator-perturber system and which, for H_β at least, essentially removes one of the largest remaining discrepancies between experiment and Stark-broadening theory.

Kessler, K. G., **Absolute measurements of differential cross sections for electron scattering at intermediate energies (50-500 eV),** *Comments At. Mol. Phys.* **1,** No. 3, 70-72 (Aug.-Sept. 1969).

Key words: differential cross sections; elastic cross sections; electron scattering.

Technological improvements in the design and construction of electron impact spectrometers now make possible more reliable absolute measurements of elastic and inelastic differential cross sections for the scattering of electrons by atoms and molecules. Cross sections can now be determined with an imprecision of 5 percent or less, depending upon the degree to which systematic errors are brought under control.

Kranbuehl, D. E., Verdier, P. H., Spencer, J. M., **Relaxation of fluctuations in the shape of a random-coil polymer chain,** *J. Chem. Phys. Letter to Editor* **59,** No. 7, 3861-3862 (Oct. 1, 1973).

Key words: lattice-model polymer chains; Monte Carlo; polymer chain dynamics; relaxation times.

The relaxation times of deviations from spherical symmetry of random-coil polymer chains in dilute solution have been investigated by dynamical Monte Carlo studies of lattice-model chains without excluded volume. The deviations are found to persist for times of the order of the longest relaxation times of the internal motions of the chains.

Kuriyama, M., Early, J. G., Burdette, H. E., **Fluid flow effects on crystalline perfection,** (Proc. 12th Aerospace Sciences Meeting, Washington, D.C., Jan. 30-Feb. 1, 1974), *AIAA Paper No. 74-204,* pp. 1-10 (American Institute of Aeronautics and Astronautics, New York, N.Y., 1974).

Key words: copper single crystals; crystal perfection; dislocations; fluid flow; thermal convection; x-ray topography.

In the absence of gravity, thermal convection, i.e., convection induced by gravity acting on density differences in the melt, would be expected to be negligible. Fluid flow in the melt, including thermal convection, probably affects the perfection of crystals grown from the melt. At present, the relationship between crystal growth conditions, in particular, fluid flow conditions, and the degree of crystal perfection has not been well established for metals. It is, therefore, highly desirable to document the perfection of crystals grown from the melt in terms of directly controllable process parameters, before one even begins to analyse the fluid flow conditions in the melt in terms of thermodynamical variables. In this paper, optimum solidification parameters for the production of highly perfect copper crystals by Czochralski growth are sought along with documentation of crystal imperfections under various growth conditions. A vital part of research of this type is the assessment of crystal perfection. X-ray techniques which do not in their application produce defects and which allow the characterization of imperfections in single crystals are chosen to assess crystal perfection. The properties of crystals grown from the melt are anticipated to vary over a large range, since the growth conditions, especially the fluid flow conditions, are deliberately changed. The x-ray techniques employed ranged from ordinary Laue photography through Borrmann topography to double-crystal scanning diffractometry, thus allowing crystals with a wide variation in perfection to be studied. As a set of controllable solidification parameters, the rotation of the seed and of the melt and the diameter of the bottle-neck are chosen. X-ray diffraction topographs are analysed along with the data obtained from rocking curve measurements. Tables of growth conditions and quantitative data of rocking curve widths are presented.

Kurylo, M. J., **Kinetics of the reactions $OH(v=0)+NH_3 \rightarrow H_2O+NH_2$ and $OH(v=0)+O_3 \rightarrow HO_2+O_2$ at 298 K,** *Chem. Phys. Lett.* **23,** No. 4, 467-471 (Dec. 15, 1973).

Key words: ammonia; kinetics; OH radical; ozone; stratosphere.

The rate constants for the reactions $OH(X^2\Pi, v=0)+NH_3 \xrightarrow{k_1} H_2O+NH_2$ and $OH(X^2\Pi, v=0)+O_3 \xrightarrow{k_2} HO_2+O_2$ were measured at 298 K by the flash photolysis resonance fluorescence technique. The values of the rate constants thus obtained are $k_1=(4.1\pm0.6)\times10^{-14}$ and $k_2=(6.5\pm1.0)\times10^{-14}$ in units of cm^3 $molecule^{-1}$ sec^{-1}. The results are discussed in terms of understanding the dynamics of the perturbed stratosphere.

Laughlin, D. E., Cahn, J. W., **The crystal structure of the metastable precipitate in copper-based copper-titanium alloys,** *Scr. Met.* **8,** 75-78 (1974).

Key words: coherency; copper-titanium; $D1_a$; electron diffraction; $L1_2$.

Knight and Wilkes recently reported that the metastable ordered phase which forms by precipitation from copper-rich copper-titanium binary alloys is of the type $L1_2$. This note shows that this indexing is incorrect, and that the previously assigned structure of $D1_a$ is fully consistent with all experimental findings.

Ledbetter, H. M., Naimon, E. R., **Relationship between single-crystal and polycrystal elastic constants,** *J. Appl. Phys.* **45,** No. 1, 66-69 (Jan. 1974).

Key words: Debye temperature; elastic constants; lattice-vibrational properties; polycrystal; single crystal; Voigt-Reuss-Hill.

A new method is given for computing effective polycrystalline elastic constants from single-crystal elastic coefficients. Agreement with observation is good. The method is based on the assumed equivalence of the lattice-vibrational properties of single crystals and polycrystals of the same material; single-crystal and polycrystal Debye temperatures are equated. Present predictions of polycrystal elastic moduli differ significantly from those of most other averaging methods by being lower than the familiar Voigt-Reuss-Hill results.

Lee, P. H., Broida, H. P., Braun, W., Herron, J. T., **Direct observation of vibrationally excited hydrogen produced by colli-**

sional energy transfer from electronically excited sodium, rubidium, caesium, and mercury, *J. Photochem.* **2,** 165-172 (1973/74).

Key words: absorption spectra; apparatus and method; energy transfer; gases; kinetics of reaction; photochemistry; vacuum u.v.

Hydrogen has been vibrationally excited by direct energy transfer from electronically excited sodium, rubidium and caesium, and mercury. The vibrational excitation of the $B^1\Sigma^+_u \leftarrow X^1\Sigma^+_g$ transitions in hydrogen was detected by absorption of the vacuum u.v. radiation from a low pressure molecular hydrogen lamp.

Lenzi, M., McNesby, J. R., Mele, A., Xuan, C. N., **Collisional deactivation of $NH_2(\tilde{A}^2A_1)$,** *J. Chem. Phys.* **57,** No. 1, 319–323 (July 1, 1972).

Key words: ammonia; fluorescence; Jovian; vacuum ultraviolet.

$NH_2(\tilde{A}^2A_1)$ was produced by photolysis of ammonia in the vacuum ultraviolet. Deactivation rates of this radical were measured by the quenching of fluorescence in NH_3, CH_4, H_2, N_2, He, Ne, Ar, Kr, Xe. An estimate of the lifetime of spontaneous radiative decay of 0.8×10^{-5} sec is suggested. Application of the results to the dynamics of the Jovian atmosphere is reported.

Levin, E. M., Benedict, J. T., Sciarello, J. P., Monsour, S., **The system K_2SO_4-Cs_2SO_4,** *J. Amer. Ceram. Soc.* **56,** No. 8, 427-430 (Aug. 1973).

Key words: Cs_2SO_4; density K_2SO_4-Cs_2SO_4 solid solutions; equilibrium diagram Cs_2SO_4-K_2SO_4; hexagonal solid solutions; K_2SO_4; phase diagram Cs_2SO_4-K_2SO_4; polymorphism Cs_2SO_4-K_2SO_4 solid solutions; solid solutions.

The phase diagram for the system K_2SO_4-Cs_2SO_4 was determined by using DTA for melting relations and DTA and high-temperature x-ray diffractometry for subsolidus relations. At the solidus the system shows complete solid solubility, with a minimum at 940 °C and 50 mol% Cs_2SO_4. Orthorhombic K_2SO_4 and Cs_2SO_4, the stable low-temperature forms, show mutual solid solubility and form a eutectoid at 50 mol% Cs_2SO_4 and 430 °C, the lowest temperature of stability of the high-temperature hexagonal solid-solution phase. Isothermal plots of the *a* and *c* dimensions of this hexagonal phase vs composition show large positive deviations from linearity for *c*. These deviations are interpreted on the basis of the crystal structure of $KNaSO_4$ with a similar unit cell.

Lyon, G., **Syntax-directed least-errors analysis for context-free languages: A practical approach,** *Commun. ACM* **17,** No. 1, 3-14 (Jan. 1974).

Key words: arbitrary input strings; context-free grammars; dynamic programming; parsing.

A least-errors recognizer is developed informally using the well-known recognizer of Earley, along with elements of Bellman's dynamic programming. The analyzer takes a general class of context-free grammars as drivers, and any finite string as input. Recognition consists of a least-errors count for a corrected version of the input relative to the driver grammar. The algorithm design emphasizes practical aspects which help in programming it.

Madey, T. E., Yates, J. T., Jr., Erickson, N. E., **ESCA study of fractional monolayer quantities of chemisorbed gases on tungsten,** *Chem. Phys. Lett.* **19,** No. 4, 487-492 (Apr. 15, 1973).

Key words: carbon monoxide; ESCA; monolayer; oxygen; photoyields; sensitivity; tungsten.

X-ray photoelectron spectroscopy (ESCA) has been used in a study of CO and O_2 chemisorbed on a polycrystalline tungsten sample. Working under ultrahigh vacuum conditions, the surface was cleaned and then covered with known monolayer and fractional monolayer quantities of adsorbed CO and O_2. The O(ls) and C(ls) spectral features were detected, and the influence of an adsorbed layer on the tungsten spectral features was determined. A chemical shift of 3.4 eV in the O(ls) line from chemisorbed CO is related to the different modes of bonding of CO to tungsten. A model calculation of the photoelectron yields expected from an adsorbed monolayer is in good agreement with the experimental results.

Mandel, J., Lashof, T. W., **Interpretation and generalization of Youden's two-sample diagram,** *J. Qual. Technol.* **6,** No. 1, 22-36 (Jan. 1974).

Key words: collaborative reference programs; interlaboratory tests; test method evaluation; Youden diagram.

Youden's two sample diagram is a useful method for certain types of interlaboratory comparisons of test results. Generally, points in the plot fall within an elongated ellipse, the major axis of which makes a 45° angle, approximately, with the x, y axes. Occasionally it happens that the axes are not the bisectors of the coordinate axes. This paper (1) examines more closely the assumptions underlying the Youden diagram and presents a more general method of interpreting it and (2) generalizes the diagram to situations where the two samples do not have the same level and/or the axes of the ellipse definitely do not bisect the coordinate axes.

Mauer, F. A., Hubbard, C. R., **Evaluation of the energy dispersive powder diffraction method for the determination of quartz in dust samples,** (Proc. Roundtable Discussion on Analytical Techniques for Quartz, Cincinnati, Ohio, Dec. 6-7, 1972), Paper in *Analytical Techniques for Quartz*, pp. 17-23 (National Institute for Occupational Safety and Health, American Conference of Governmental Industrial Hygienists, Cincinnati, Ohio, Jan. 1974).

Key words: analytical methods; industrial hygiene; quartz; silicosis; x-ray diffraction.

An energy dispersive powder diffractometer was assembled and used to determine the amount of quartz on six silver membrane filters, such as those used in sampling airborne dust. The amount of quartz, which varied from 24 to 531 μg, was also determined by weighing. The results obtained indicate that the overall uncertainty in the weight of quartz obtained by the energy dispersive x-ray method is at least 50 μg. The method, therefore, does not meet the National Institute for Occupational Safety and Health requirement for a practical lower limit of detection of 20 μg and an analytical range of 20 μg to 4 mg.

Mazur, J., Guttman, C. M., McCrackin, F. L., **Monte Carlo studies of self-interacting polymer chains with excluded volume. II. Shape of a chain,** *Macromolecules* **6,** No. 6, 872-874 (Nov.-Dec. 1973).

Key words: asymmetry of polymer configurations; excluded volume; principal moments; radius of gyration; self-interacting polymer chains.

The principal moments of the squared radius of gyration of polymer chains with excluded volume were computed for chains on the simple cubic and face-centered cubic lattices. The moments were ordered for each configuration by their magnitude, then averaged over a large number of chain configurations and divided by the squared radius of gyration to yield shape factors of the chain. These shape factors were found to be independent of chain length for long chains. The shape factors showed that the instantaneous shape of a polymer chain is very asymmetrical. With increasing interaction energy between the segments of the chains, the chains became less asymmetrical; at the Θ point the shape factors became equal to those of the random coil as previously calculated by Šolc and Stockmayer. The relative variations of the principal moments were also calculated. The largest principal moments were found to have the largest relative variations.

Mazur, J., Rubin, R. J., **Average span of self-avoiding walks on the simple cubic lattice,** *J. Chem. Phys. Letters to Editor* **60,** No. 1, 341-342 (Jan. 1, 1974).

Key words: polymer chains; ratio method; self-avoiding walks; span.

In a recent publication, Bellemans concluded that the average span of a self-avoiding walk has a different asymptotic dependence on the number of steps than does the root-mean-square end-to-end distance. In this paper, we reanalyse Bellemans' data and show that there is no basis for his conclusion.

McAlister, A. J., Cuthill, J. R., Dobbyn, R. C., Williams, M. L., **Soft x-ray study of the *d*-bands in $AuAl_2$,** (Proc. Int. Conf. on Band Structure Spectroscopy of Metals and Alloys, Strathclyde, Glasgow, Scotland, Sept. 26-30, 1971), Paper in *Band Structure Spectroscopy of Metals and Alloys,* D. J. Fabian and L. H. Watson, Eds., pp. 191-203 (Academic Press, London, England, 1973).

Key words: Au; $AuAl_2$; *d*-bands; emission spectrum; $N_{6,7}$; soft x-ray.

The $N_{6,7}$ soft x-ray emission spectrum (5d to 4f transition) of Au in $AuAl_2$ has been measured. This work, together with the x-ray photoemission results of Chan and Shirley, shows the *d*-bands to be distributed over a range of approximately 4 eV, with maxima at 5.0 and 7.1 eV below the Fermi level. These results raise some questions about the interpretation of the Al L emission spectrum from the compound, which appeared to offer strong confirmation of nonrelativistic band calculations of the electronic structure of $AuAl_2$, and again raise the possibility of *d*-band participation in the strong coloring of the compound, an effect which the Al emission spectrum and nonrelativistic band calculations appeared to exclude.

McCarter, R. J., **A new technique for thermal analysis of vapor-producing reactions,** *J. Appl. Polym. Sci.* **17,** 1833-1846 (1973).

Key words: differential thermal analysis; DTA; kinetics; pyrolysis; TGA; thermal analysis; thermal degradation; thermogravimetric analysis.

An apparatus was developed for measuring the rate at which vapors are evolved during the thermal degradation of materials and thereby deriving the kinetics of such reactions. Requisite to the operating scheme of the apparatus is the provision of a high-temperature zone to convert condensable or tarry vapors into noncondensable form. The apparatus yields a direct measure of reaction velocity, rather than the integrated indication obtained with thermogravimetric analysis. This simplifies the identification and calculation of kinetic parameters. Increases in sensitivity and operating range are also achieved. Flexibility in operation is obtained that permits the separate recording of reactions that tend to overlap. Although the apparatus principally has been operated using a combustible gas indicator to meter the evolved vapors, a number of options are available for the latter function, including flowmeters and various continuous gas analyzers. The applicability of the method appears promising.

McCrackin, F. L., Mazur, J., Guttman, C. M., **Monte Carlo studies of self-interacting polymer chains with excluded volume. I. Squared radii of gyration and mean-square end-to-end distances and their moments,** *Macromolecules* **6,** No. 6, 859-871 (Nov.-Dec. 1973).

Key words: excluded volume; Monte Carlo; polymer solution; radii of gyration; theta point.

Random walks that are not allowed to intersect themselves were generated on the simple cubic and face-centered cubic lattices and used as a model of a linear polymer chain in dilute solution with excluded volume and attractive energies between chain elements. The mean-square end-to-end distances and mean squared radii of gyration and their moments were computed for chain lengths up to 2000 segments and for a wide range of attractive energies. The partition functions of the chains were also computed. The attractive energy required for a given property of the chain to be the same as the given property of a random coil, the θ point, was investigated. The required attractive energy depended slightly on the particular property chosen for comparison, so rather than a unique θ point, a narrow range of θ points was found.

McDaniel, C. L., **Phase relations in the systems Na_2O-IrO_2 and Na_2O-PtO_2 in air,** *J. Solid State Chem.* **9,** 139-146 (1974).

Key words: compounds; dissociation; Na_2O-IrO_2 system; Na_2O-PtO_2 system; phase relations.

The equilibrium phase relations for the Na_2O-IrO_2 and Na_2O-PtO_2 systems were determined in air using the quenching technique. The Na_2O-IrO_2 system contains two stable compounds $Na_2O{\cdot}IrO_2$ and $2Na_2O{\cdot}3IrO_2$, which dissociate at 1235 and 1040 °C, respectively. The Na_2O-PtO_2 system contains three compounds: $Na_2O{\cdot}PtO_2$, metastable $2Na_2O{\cdot}3PtO_2$, and $Na_xPt_3O_4$ ($0 \leq x \leq 1$). Their dissociation temperatures are 890, 710, and 810 °C, respectively. Indexed x-ray diffraction powder patterns for $Na_2O{\cdot}IrO_2$ and $2Na_2O{\cdot}3IrO_2$ are given.

Merris, R., Newman, M., **An explicit isomorphism with applications to inequalities for matrix functions,** *J. Algebra* **25,** No. 3, 468-474 (June 1973).

Key words: central idempotents; group algebras; irreducible representations; matrix functions.

Inequalities for matrix functions are derived in a uniform way for an explicit isomorphism.

Mielenz, K. D., **Eureka!** *Appl. Opt.* **13,** No. 2, A14 and A16 (Feb. 1974).

Key words: Archimedes; Buffon; burning mirrors; feasibility; history of optics; Second Punic War; solar energy.

In view of the recently renewed controversy whether Archimedes could have used mirrors to defer the attacking Roman fleet during the siege of Syracuse in the Second Punic War, it is pointed out that the feasibility of this has been demonstrated by Buffon in 1747. Additional facts are presented which also suggest that the use of burning mirrors could have presented a serious threat to the blockading Romans.

Morrissey, B. W., Stromberg, R. R., **The conformation of adsorbed blood proteins by infrared bound fraction measurements,** *J. Colloid Interface Sci.* **46,** No. 1, 152-164 (Jan. 1974).

Key words: blood proteins; infrared bound fraction; protein adsorption; protein conformation.

The likelihood that surface-induced blood coagulation results from specific protein-material interactions has led to a study of the conformation of adsorbed blood proteins. Infrared difference spectroscopy was used to determine the bound fraction, i.e., the fraction of carbonyl groups of an adsorbed molecule directly interacting with the surface, of serum albumin, prothrombin, and fibrinogen *in situ.* Measurements were carried out on individual proteins as a function of the amount adsorbed, time of absorption, pD, and ionic strength using a silica surface.

The results obtained for serum albumin and prothrombin indicate that the internal bonding of these globular proteins is sufficient to prevent changes in the structure while adsorbed, even at low surface population. The bound fraction of fibrinogen increases with increasing adsorbance, suggesting possible interfacial aggregation. The conformation of all three proteins was found to be independent of the time of adsorption, although major differences in the rates of adsorption were observed.

Studies of cross-linked and denatured serum albumin have provided information on the conformational changes concomitant with

adsorption of the native protein. Qualitatively, such changes, if they occur, are small. This conclusion is supported by computer simulation studies of lysozyme adsorption. Studies of the effect of pD and ionic strength on the adsorbance and bound fraction of serum albumin show that caution must be exercised when identifying the plateau adsorbance of a protein isotherm with a close-packed monolayer.

Mount, G. H., Linsky, J. L., Shine, R. A., **One- and multi-component models of the upper photosphere based on molecular spectra. I: The violet system of CN (0,0),** *Solar Phys.* **32,** No. 1, 13-30 (Sept. 1973).

Key words: best-fit model; carbon abundance; molecular spectra; upper photosphere.

Spectroheliograms taken in the CN(0,0) violet band near λ3883 Å show very small scale network and cell structures with high contrast. The bandhead itself, which is a broad feature due to overlap of several CN lines, allows the diagnostic simplicity of a continuum since motions, magnetic fields, and broadening mechanisms are unimportant. We have obtained spectroheliograms in the bandhead and center-to-limb photoelectric spectra of CN(0,0) at Kitt Peak National Observatory. From the photoelectric spectra and a detailed analysis of the formation of the CN(0,0) spectrum we derive a best-fit one-component upper photospheric model differing from that of the HSRA and recommend a change in solar carbon abundance from the HSRA value of $\log A_c = 8.55$ to $\log A_c = 8.25$. From the calibrated spectroheliograms we consider a multi-component model to account for the observed fine structure intensity variations.

Mozer, B., De Graaf, L. A., Le Neindre, B., **Neutron-diffraction studies in liquid ^{4}He,** *Phys. Rev. A* **9,** No. 1, 448-459 (Jan. 1974).

Key words: condensate fraction; density and temperature; liquid helium; neutron diffraction; pair correlation and three-atom correlation function; structure factor.

Structure factors of liquid helium have been determined from neutron-diffraction measurements of high statistical accuracy. Diffraction measurements were performed out to momentum transfers of 7 $Å^{-1}$ for three different densities of liquid helium at a constant temperature above the helium λ transition and at a nearly constant temperature below the λ transition for the same three densities. Statistically significant differences in the structure factors are observed as the density is varied at constant temperature and for temperatures above and below the λ transition at constant density. The radial pair-correlation functions have been calculated from the liquid-structure factors. The structure factors or the related radial pair-correlation functions can be used to obtain information about three-atom correlations in liquid helium above and below the λ transition from a construction of their isothermal density derivative. The temperature dependence of the constant-density structure factors or their derived pair-correlation functions can also be used to test a current theoretical estimate of the condensate fraction in liquid helium.

Naimon, E. R., **Elastic constants of the perovskite $RbMnF_3$ using a Born model,** *Phys. Rev. B* **9,** No. 2, 737-740 (Jan. 15, 1974).

Key words: Born-Mayer repulsion; Born model; elastic constants; electrostatic interactions; perovskite; $RbMnF_3$.

The elastic constants of $RbMnF_3$ were calculated using a Born model, which consists of electrostatic and Born-Mayer repulsive interactions. This model has two adjustable parameters; these were determined from the equilibrium volume and one of the three second-order elastic constants. Calculated third-order elastic constants agreed reasonably well with experiment. Also calculated were the electrostatic contributions to the first-, second-, and third-order elastic constants of the cubic perovskite structure for several values of ionic charge. Relationships of these constants to those of the NaCl- and CsCl-type structures are given.

Newbury, D. E., Yakowitz, H., Yew, N. C., **Observation of magnetic domains in nickel using the scanning electron microscope,** *Appl. Phys. Lett.* **24,** No. 2, 98 (Jan. 15, 1974).

Key words: bitter patterns; contrast mechanisms; magnetic domains; nickel; scanning electron microscopy; transformer alloy.

Scanning electron microscope (SEM) observation of magnetic domains in a polycrystalline pure nickel sheet was made possible through the use of a 50-kV accelerating potential. The contrast was unobservable in an SEM capable of only a 30-kV accelerating potential.

Newman, M., **Symmetric completions and products of symmetric matrices,** *Trans. Amer. Math. Soc.* **186,** 191-201 (Dec. 1973).

Key words: fields; principal ideal rings; symmetric completion; symmetric matrices; unimodular matrices.

We show that any vector of n relatively prime coordinates from a principal ideal ring R may be completed to a symmetric matrix of $SL(n, R)$, provided that $n \geq 4$. The result is also true for $n = 3$ if R is the ring of integers Z. This implies for example that if F is a field, any matrix of $SL(n, F)$ is the product of a fixed number of symmetric matrices of $SL(n, F)$ except when $n = 2$, $F = GF(3)$, which is a genuine exception.

Olsen, P. T., Driscoll, R. L., **Determination of γ_p' at the National Bureau of Standards,** (Proc. 4th Int. Conf. on Atomic Masses and Fundamental Constants, Teddington, England, Sept. 6-10, 1971), Paper in *Atomic Masses and Fundamental Constants,* J. H. Sanders and A. H. Wapstra, Eds., pp. 471-484 (Plenum Press, London, England, 1972).

Key words: fine structure constant; gyromagnetic ratio of proton; nuclear induction; precision solenoid.

The gyromagnetic ratio of the proton, γ_p' is one of our most important fundamental physical constants. (The prime indicates that the protons are in a spherical sample of pure H_2O.) Not only is it used for calibration purposes in nuclear magnetic resonance experiments, but it plays a crucial role in determining the fine structure constant from the measurement of 2e/h via the ac Josephson effect. Additionally the continued measurement of γ_p' can be used to monitor as-maintained units of current.

The precision of γ_p' measurements at the National Bureau of Standards (NBS) has improved significantly since the early measurements of the 1950's, from several parts per million (ppm) to the present 0.1 to 0.2 ppm. Current efforts are now being directed towards improving the present 3 to 4 ppm accuracy of the experiment by an order of magnitude. It is the purpose of this paper to briefly report the progress being made in this direction. First, a general discussion of the experiment is given, including (a) use of the method of nuclear induction to determine the precession frequency; (b) a description of a new and improved series of pitch measurements using a laser interferometer; (c) a discussion of the effect of the change in original winding tension on the effective diameter of the windings; and (d) an analysis of the effect of the finite susceptibility of the solenoid and water sample support structure on the calculated magnetic field. All of the known corrections to the field are then summarized, and finally, a brief analysis of the uncertainties in the experiment is given along with a value for γ_p'.

Penn, D. R., **An improved Anderson model,** *Phys. Rev. B* **9,** No. 3, 839-843 (Feb. 1, 1974).

Key words: adsorbates on metal surfaces; density of states; impurity wave function; magnetic impurities; phase shift; reformulation of the Anderson model.

The Anderson model has been very successful in the study of (magnetic) impurities in metals and has also proved useful for atoms adsorbed on metal surfaces. The model as originally formulated is phenomenological in that the position and width of the resonant impurity state cannot be calculated within the context of the model even in the absence of correlation effects. Anderson and McMillan and also Kanamori have proposed theories which are more quantitative. We show that the results of both theories follow from very simple assumptions. Moreover, we show that for the case of a free-electron-like metal and a spherical impurity potential both theories will give a correct density of states for the metal plus impurity if the wave function associated with the impurity is chosen properly. This is particularly important for the theory of Kanamori where the use of a non-Hermitian Hamiltonian raises questions about its validity. The best choice for the impurity wave function requires it to be energy dependent, unlike that one which appears in the usual Anderson model. However, it is shown that an energy-independent wave function can be chosen such that the Anderson-McMillan and Kanamori theories will yield a good density of states.

Perlstein, J. H., Ferraris, J. P., Walatka, V. V., Jr., Cowan, D. O., Candela, G. A., **Electron transport and magnetic properties of new highly conducting TCNQ complexes,** (Proc. 18th AIP Conf. on Magnetism and Magnetic Materials, Denver, Colo., Nov. 28-Dec. 1, 1972), Paper in *Magnetism and Magnetic Materials*, C. D. Graham, Jr., and J. J. Rhyne, Eds., No. 10, 1494-1498 (American Institute of Physics, New York, N.Y., 1973).

Key words: electron transport; magnetic properties; metallic; TCNQ complexes.

Single crystals of the 1:1 complexes tetrathiafulvalinium tetracyanoquinodimethane (TTF-TCNQ) and tetrathianaphthacinium tetracyanoquinodimethane (TTN-TCNQ) have been synthesized and the electron transport properties and magnetic susceptibility have been measured from 2 K to room temperature. For TTN-TCNQ, σ at room temperature is $1\Omega^{-1}$ cm^{-1}. For TTF-TCNQ, σ at room temperature along the long axis ($\sigma_{\|}$) is in the range $192\text{-}652\Omega^{-1}$ cm^{-1} depending on sample whereas perpendicular to the long axis $\sigma_{\perp}$ is $1\Omega^{-1}$ cm^{-1}. The conductivity remains metallic down to 66 K in both directions whereupon a continuous metal to insulator transition occurs. The activation energy in the insulating state is 0.0062 eV. The transition is associated with a small hysteresis between the heating and cooling curves suggesting a possible structural change. In the metallic region, $\rho_{\|}$ follows a T^2 dependence whereas $\rho_{\perp}$ follows a T^{+1} behavior. The magnetic susceptibility is diamagnetic below 20 K becoming increasingly more paramagnetic with increasing T even in the metallic region. It is suggested that spin disorder scattering may account for the anomalous temperature dependence of $\rho_{\|}$.

Piermarini, G. J., Block, S., Barnett, J. D., **Hydrostatic limits in liquids and solids to 100 kbar,** *J. Appl. Phys.* **44,** No. 12, 5377-5382 (Dec. 1973).

Key words: diamond-anvil pressure cell; glass transition pressures; hydrostaticity; pressure gradients; pressure measurements; ruby fluorescence.

The hydrostatic properties of the materials methanol, isopropyl alcohol, water, sodium chloride, silver chloride, and the binary mixtures pentane-isopentane and methanol-ethanol have been determined in the diamond-anvil pressure cell up to 180 kbar by line-broadening and line-shift measurements of the sharp R_1 ruby fluorescence line. A liquid mixture 4:1 by volume of methanol:ethanol remains hydrostatic to almost 100 kbar at room temperature. This mixture exceeds the hydrostatic limit of the previous generally accepted fluid, 1:1 pentane:isopentane which has a hydrostatic limit of about 70 kbar. Silver chloride and water (ice VII) are better than sodium chloride as pressure-transmitting media, but do not even qualitatively approach hydrostatic conditions much above 70 kbar. The stress sensitivity level of the ruby limits the extent to which slight deviations from hydrostatic conditions can be determined in solid systems and suggests the qualitative nature of the method in characterization of quasihydrostatic states. The equilibrium freezing pressure of methanol at 24 °C was redetermined to be 35.8 ± 0.8 kbar.

Rains, T. C., Epstein, M. S., Menis, O., **Automatic correction system for light scatter in atomic fluorescence spectrometry,** *Anal. Chem.* **46,** No. 2, 207-210 (Feb. 1974).

Key words: atomic fluorescence spectrometry; automatic correction; electrodeless discharge lamp; light scatter; standard reference material.

Light scattering of incident radiation by solvent droplets and unvaporized solute particles in the flame is a major interference in atomic fluorescence spectrometry (AFS). A technique for the automatic correction of light scatter is described which increases the speed and accuracy of analysis. The light from an electrodeless discharge lamp and a 150-W xenon lamp is alternately passed through the flame. The resulting signal from the multiplier phototube is fed to a lock-in amplifier which corrects for the contribution of the light scattering to the fluorescence signal. The principles of the technique and apparatus for making the automatic correction are described. To accomplish this correction, scatter of the incident radiation from the electrodeless discharge and xenon lamps is balanced initially while aspirating a 1 percent lanthanum solution. The method has been applied to the determination of 0.11 and 0.26 μg Cd/gram in SRM's Orchard Leaves and Liver, respectively, without any prior separation or preconcentration.

Raveché, H. J., Mountain, R. D., **Structure studies in liquid ^{4}He,** *Phys. Rev. A* **9,** No. 1, 435-447 (Jan. 1974).

Key words: condensate fraction; ground state wave function; neutron diffraction; pair correlation function; triplet correlation function; ^{4}He.

We investigate, using neutron-diffraction data, several properties of the local atomic structure in liquid ^{4}He, both above and below the superfluid transition. Distinguishing features of the pair-correlation function are summarized and the diffraction data are employed to investigate a proposed form for the condensate fraction as a function of temperature. The pair-correlation function is used to examine an inequality that gives an upper bound that is close to the observed values, and also to examine the use of approximate integral equations for the ground-state wave function. Triplet correlations and closure approximations are studied from the isothermal density derivative of the pair-correlation function. The results suggest that, analogous to the pair-correlation function, the triple-correlation function shows a temperature dependence that is not observed in simple classical fluids.

Richmond, J. C., **A standard for night vision devices for law enforcement,** (Proc. of the Society of Photo-Optical Instrumentation Engineers, San Diego, Calif., Aug. 27-29, 1973), Paper in *Image Intensifiers: Technology, Performance, Requirements and Applications*, A. D. Schnitzler and M. W. Klein, Eds., **42,** 109-115 (1974).

Key words: contrast transfer function; distortion; flare; image intensifiers; law enforcement; light equivalent background; light induced background; night vision; optical gain.

A draft Standard for Passive, Hand-Held Night Vision devices has been developed for the Law Enforcement Standards Laboratory of the National Bureau of Standards. This Standard is now being circulated for comment prior to adoption as a Standard of the National Institute of Law Enforcement and Criminal Justice of the Law Enforcement Assistance Administration of the Department of Justice.

The paper mentions some of the philosophy behind the standard, lists the performance requirements and describes briefly the test procedures for (A) focus adjustment, curvature of field and distortion

of the eyepiece lens, (B) optical gain, optical gain stability, light equivalent background, light induced background, luminance of output screen, luminance uniformity, cathode and screen quality, contrast transfer function, distortion and flare of a night vision device complete with objective lens, but with the eyepiece removed, and (C) for resistance to vibration, high and low temperature storage, operation and thermal shock and humidity of night vision devices complete with both objective and eyepiece lenses, and (D) boresight adjustment, click movement and resistance to mechanical shock of night vision devices intended for use as rifle sights.

Risley, A. S., **The Josephson junction as applied to the measurement of the frequencies of several laser lines,** (Proc. Frequency Standards and Metrology Seminar, Quebec, Canada, Aug. 30-Sept. 1, 1971), Paper in *Proceedings of the Frequency Standards and Metrology Seminar,* pp. 325-328 (Quantum Electronics Laboratory, Laval University, Quebec, Canada, 1972).

Key words: harmonic generation; Josephson junction; laser frequencies; methane; microwave frequency stability.

The Josephson junction has been applied to the measurement of laser frequencies as high as 3.8 THz by direct multiplication from an X-band source. An attempt is being made to extend this technique to frequencies as high as 10.7 THz.

Roberts, R. W., **Energy research: Scientists seek to ease the pinch,** *The Futurist* **VIII,** No. 1, 19-22 (Feb. 1974).

Key words: buildings; conservation, energy.

In this period of energy shortage, intensive research and development efforts are required for the development of viable alternatives to traditional energy sources. During the inevitable lag time between energy need and new supply, conservation measures can do much to reduce the energy gap. This is especially true in buildings, where vast amounts of energy are currently wasted. Various NBS programs bearing on the design and operation of more energy efficient buildings are summarized.

Rowe, J. M., Livingston, R. C., Rush, J. J., **Neutron quasielastic scattering study of SH^- reorientation in rubidium hydrosulfide in the intermediate temperature trigonal phase,** *J. Chem. Phys.* **59,** No. 12, 6652-6655 (Dec. 15, 1973).

Key words: neutron scattering; orientational disorder; phase transition; reorientation; residence time; rubidium hydrosulfide; vibration amplitude.

The reorientation of $(SH)^-$ ions in the trigonal phase of RbSH has been investigated by neutron quasielastic scattering at 373 and 393 K. The quasielastic peaks show a distinct two-component (elastic and broadened) structure, the behavior of which is used to establish that the ions are reorienting between two equilibrium sites (presumably by 180° flips along the trigonal axis) with average times between reorientation of 5.4 ± 0.4 psec and 4.0 ± 0.4 psec at 373 and 393 K. Mean square amplitudes of hydrogen vibration are determined from the momentum transfer dependence of the total intensity, and found to be higher than that found in the high temperature fcc phase, even though the rate of reorientation is an order magnitude faster in the cubic phase.

Scavennec, A., Nahman, N. S., **A simple passively mode-locked CW dye laser,** *IEEE J. Quantum Electron.* **QE-10,** No. 1, 95-96 (Jan. 1974).

Key words: DODCI; dye laser; laser; mode-lock; picosecond; rhodamine 6 G.

The operation of a simple passively mode-locked 5800-Å dye laser is reported. A single active medium, solution of rhodamine 6 G and diethyloxadicarbocyanine iodide (DODCI) in glycol flowing as an unconfined liquid film, is used for the simultaneous production of gain and nonlinear absorption.

Sharman, L. J., Tovey, H., Vickers, A. K., **Current status and national priorities for flammable fabric standards,** *Proc. 6th Annual Meeting of Information Council on Fabric Flammability, New York, N.Y., Dec. 7, 1972,* pp. 265-306 (Information Council on Fabric Flammability, New York, N.Y., May 1, 1973).

Key words: blankets; children's sleepwear; fabric fires; fabric flammability standards; FFACTS; fire injuries; flammable fabrics; flammability standards priorities; garment flammability; garments; sampling plans; upholstered furniture.

The present status (calendar year 1972) of flammability standards issued by the Department of Commerce is described. During 1972, a sampling plan was developed for the Standard for the Flammability of Children's Sleepwear, DOC FF 3-71. The Standard was reissued with this plan included. A Flammability Standard for Mattresses was also issued. Work is in progress on a proposed flammability standard for blankets and flammability test methods for upholstered furniture. The approaches used in development of the standard and the current status of the work are discussed.

The results of a recent analysis of information available to the Fire Technology Division, National Bureau of Standards, on the relative need for specific flammability standards for wearing apparel are discussed. The system used for developing "candidate priorities" for standards is briefly described. A list of high priority garment types is presented, along with examples of compilations of data from the NBS-Flammable Fabrics Accident Case and Testing System (F-FACTS) and other sources supporting the placement of the individual garment types on the list.

Shumaker, J. B., **A spectroscopic study of equilibrium in nitrogen arcs,** *J. Quant. Spectrosc. Radiat. Transfer* **14,** 19-26 (1974).

Key words: arc plasma; equilibrium; LTE; nitrogen.

Nitrogen arc measurements of the intensity of the 4915 Å – 4935 Å NI doublet and of the 3995 Å NII line show that local thermodynamic equilibrium cannot be assumed in nitrogen arcs at electron densities below 1×10^{17} cm^{-3}. Below this point, the results suggest that gas and electron temperatures differ significantly and that ground states are overpopulated with respect to upper electronically excited states.

Simmonds, M. B., **Using the semiconductor junction in quantum interference devices,** *J. Appl. Phys.* **45,** No. 1, 366-368 (Jan. 1974).

Key words: Josephson junctions; quantum interference; SQUID.

We have fabricated small-area tunnel junctions of a lead-tellurium-lead structure. These have been used in conjunction with bulk superconductors to make hybrid interference devices. We have successfully operated these devices at bias frequencies of 30 MHz, 300 MHz, and 10 GHz.

Straty, G. C., Goodwin, R. D., **Dielectric constant and polarizability of saturated and compressed fluid methane,** *Cryogenics* **13,** No. 12, 712-715 (Dec. 1973).

Key words: dielectric constant; methane; polarizability.

Accurate measurements of the dielectric constant of methane have been made on the saturated liquid from near the triple point to 188 K and on the compressed fluid along selected isotherms from 100 K to 300 K and at pressures to 345 bar. The data are combined with accurate densities to obtain the molar polarizability and its dependence on density and temperature. The density range examined extends to nearly three times the critical density. The molar polarizability is found to increase initially with density and then decrease in qualitative agreement with theoretical predictions and the behaviour of other fluids.

Thrower, P. A., Nagle, D. C., Horton, W. S., **The anisotropy of pyrolytic graphite,** *J. Appl. Crystallogr.* **6,** Part 5, 347-351 (Oct. 1973).

Key words: magnetic susceptibility; orientation function; perferred orientation; pyrolytic graphite.

Two proposed expressions, $I_1(\phi)=\cos^m \phi$ and $I_2(\phi)=(1+b^2 \sin^2 \phi)^{-1}$, for the orientation function, $I(\phi)$, of pyrolytic graphites have been shown analytically to give quite different values for the Bacon anisotropy factor (BAF) for oriented materials. BAF values derived from the angle of half-maximum intensity using $I_1(\phi)$ are within 20 percent of numerically calculated values for the BAF range 10-90, whereas values obtained using $I_2(\phi)$ are smaller by as much as a factor of twenty. The effect of sample preparation on such measurements has been found to be negligible. Diamagnetic-susceptibility measurements on the graphites investigated validated the calculated BAF values in that the derived single-crystal susceptibilities were in reasonable agreement with known values. BAF values calculated *via* $I_2(\phi)$ produced unacceptable paramagnetic values parallel to the basal plane. It is suggested that $I_1(\phi)$ be used for rapid BAF determinations; although numerical calculation is preferred, the difficulty of measuring $I(\phi)$ at large ϕ, for highly oriented materials, may make the full numerical procedure impracticable and this approximate procedure the more desirable.

Verdier, P. H., **Monte Carlo studies of lattice-model polymer chains. III. Relaxation of Rouse coordinates,** *J. Chem. Phys.* **59,** No. 11, 6119-6127 (Dec. 1, 1973).

Key words: excluded volume; lattice-model polymer chains; onte Carlo; polymer chain dynamics; relaxation times.

The relaxation of the seven lowest Rouse coordinates for simple lattice models of polymer chains of up to 64 beads, with and without excluded volume, is studied by simulation on a digital computer. The similarity between the relaxation of the lattice-model chains without excluded volume and that of a statistical-bead model, noted in previous studies of end-to-end length, is confirmed and examined in greater detail. The effect of excluded volume in slowing down the relaxation of the Rouse coordinates is examined, and a simple picture is suggested which accounts qualitatively for the results obtained. The nonnormal coordinate nature of the Rouse coordinates for chains with excluded volume is demonstrated by their nonexponential autocorrelation functions. However, the results suggest that for each chain length, there is a unique longest internal relaxation time, corresponding to an internal coordinate closely resembling the lowest Rouse coordinate.

Wampler, R. H., **Some recent developments in linear least-squares computations,** (Proc. Computer Science and Statistics 6th Annual Symp. on the Interface, University of California, Berkeley, Calif., Oct. 16-17, 1972), Paper in *Proceedings of the Computer Science and Statistics Sixth Annual Symposium on the Interface,* M. E. Tarter, Ed., 94-110 (Western Periodicals Co., North Hollywood, Calif., Oct. 1972).

Key words: analysis of variance; computer programs; Gram-Schmidt orthogonalization; Householder transformations; ill-conditioned test problems; iterative refinement; least squares computations; linear equations; OMNITAB; regression; rounding errors; statistics.

The results of an evaluation of linear least-squares computer programs (Wampler (174, 175)) are briefly summarized. Subsequent work, including problems encountered, to provide a more accurate least-squares routine for the OMNITAB II program is discussed. In this connection, the comparative results of running a number of ill-conditioned problems on OMNITAB II and two other reliable programs are presented. A bibliography of the recent literature on least-squares analysis has been prepared with special emphasis on the computational aspects of obtaining least-squares solutions.

Weiss, A. W., **Correlation in excited states of atoms,** *Advan. At. Mol. Phys.* **9,** 1-46 (1973).

Key words: correlation; energy levels; oscillator strengths; spectroscopy; wave functions.

This article reviews the current status of work on electron correlation in excited states of light atoms through approximately $Z=20$. The primary orientation is towards *ab initio* correlation calculations, so that semiempirical methods are not discussed except insofar as they relate directly to the correlation problem. Furthermore, the discussion is restricted to the effects of correlation on only two properties, namely energies and oscillator strengths. After a brief statement and description of the correlation problem in general, we concentrate on 1) methods currently employed to attack excited state correlation, and 2) a description of some of the results obtained so far which appear to be peculiar to excited states.

Since most excited state correlation calculations have relied on the multiconfiguration expansion, this method is described at some length. For convenience the variety of such approaches are classified according to the choice of zeroth order, or reference state, starting point, which may be the Hartree-Fock, Hartree-Fock-Slater, or statistical model. Allowing the reference state orbitals to relax in the field of the virtual configuration leads to the multiconfiguration self-consistent field approximation, and this method is described as well. The charge expansion scheme and the pair correlation approach are also discussed from the standpoint of providing a framework for analyzing much of the results which have been obtained.

Some of the more striking effects of excited state correlation are related to the readjustment of energy levels along an isoelectronic sequence. Not only are there anomalies associated with level crossings, but the asymptotic degeneracy effects predicted by the charge expansion theory appear, very often, to persist along an entire sequence. One of the large correlation corrections in the ground state involves orbital polarization, and this also happens with excited states, where it can often be understood as a series perturbation phenomenon. Series perturbations represent a large and important correlation correction not only for the series but for the perturbing state as well. These effects are all discussed by way of examples. Finally, some discussion is given of the role of pair correlations in excited states.

Wiese, W. L., **Experimental studies of the Stark broadening of hydrogen lines,** (Proc. VI Yugoslav Symp. and Summer School on the Physics of Ionized Gases, Miljevac by Split, Yugoslavia, July 16-21, 1972), Paper in *Physics of Ionized Gases,* M. V. Kurepa, Ed., pp. 559-596 (Institute of Physics, Beograd, Yugoslavia, 1972).

Key words: atomic line shapes; critical review; hydrogen lines; plasma sources; Stark broadening.

Recent experimental investigations on the Stark broadening of hydrogen lines by high density plasma sources are critically viewed. The principal requirements for accurate Stark broadening experiments are discussed, and plasma sources, line profile measurements, and diagnostic techniques are reviewed in detail. The most recent experimental results are presented, compared with theory, and their significance for future theoretical work on Stark broadening is pointed out.

Wiese, W. L., **Regularities in atomic oscillator strengths,** (Proc. VI Yugoslav Symp. and Summer School on the Physics of Ionized Gases, Miljevac by Split, Yugoslavia, July 16-21, 1972), Paper in *Physics of Ionized Gases,* M. V. Kurepa, Ed., pp. 627-649 (Institute of Physics, Beograd, Yugoslavia, 1972).

Key words: atomic oscillator strengths; perturbation theory; regularities; systematic trends.

A review of the recently detected regularities and systematic trends among atomic oscillator strengths is presented. The quantum mechanical background for the existence of these regularities is discussed and, in particular, the relationship between oscillator strengths and nuclear charge as derived from perturbation theory is derived in detail. All regularities are illustrated by some typical graphical or tabular examples.

U. S. GOVERNMENT PRINTING OFFICE : 1974 O - 538-709

SJRA UNIVE300UA R 1
UNIVERSITY MICROFILMS INC
ATTN SERIALS SECTION
300 NORTH ZEEB RD
ANN ARBOR MI 48106

UNITED STATES
GOVERNMENT PRINTING OFFICE
PUBLIC DOCUMENTS DEPARTMENT
WASHINGTON, D.C. 20402

OFFICIAL BUSINESS
PENALTY FOR PRIVATE USE, $300

U.S. DEPARTMENT OF COMMERCE
POSTAGE AND FEES PAID
COM-375

U.S.MAIL

JOURNAL OF RESEARCH of the National Bureau of Standards
A. Physics and Chemistry

Vol. 78A, No. 4 July–August 1974

Contents

Page

The glass transition temperature of monodispersed polystyrenes and their binary mixtures. Leo A. Wall, Roestamsjah, and Mary H. Aldridge. 447

A method of measuring the solubilities of hydrocarbons in aqueous solutions. Robert L. Brown and Stanley P. Wasik. 453

Theoretical and experimental Compton scattering cross sections at 1.12 MeV in the case of strongly bound K-shell electrons. P. N. Baba Prasad and P. P. Kane. 461

Standardization of ^{60}Co and ^{137}Cs gamma-ray beams in terms of exposure. T. P. Loftus and J. T. Weaver. 465

Investigation of freezing temperatures of National Bureau of Standards aluminum standards. George T. Furukawa. 477

Prediction of the viscosities of "soda-lime"-silica glass. Kenneth C. Lyon. 497

The system NaCl-$AlCl_3$. Ernest M. Levin, J. F. Kinney, R. D. Wells, and J. T. Benedict. 505

Simultaneous measurements of heat capacity, electrical resistivity and hemispherical total emittance by a pulse heating technique: zirconium, 1500 to 2100 K. A. Cezairliyan and F. Righini. 509

Measured enthalpy and derived thermodynamic properties of crystalline and liquid potassium chloride, KCl, from 273 to 1174 K. Thomas B. Douglas and Ann W. Harman. 515

Publications of the National Bureau of Standards. 531

Library of Congress Catalog Card Number: 62–37059

For sale by the Superintendent of Documents, U.S. Government Printing Office, Washington, D.C. 20402. (Order by SD Catalog No. C 13.22/sec.A:78/4). Single copy price varies. Subscription price: $17.00 a year; $4.25 additional for foreign mailing.

UNITED STATES GOVERNMENT PRINTING OFFICE, WASHINGTON : 1974